



**HAL**  
open science

# Development of steering law for On Orbit Servicing operation

Sofiane Kraïem

► **To cite this version:**

Sofiane Kraïem. Development of steering law for On Orbit Servicing operation. Physics [physics]. Institut Supérieur de l'Aéronautique et de l'Espace (ISAE), 2022. English. NNT: . tel-04117430

**HAL Id: tel-04117430**

**<https://hal.science/tel-04117430>**

Submitted on 5 Jun 2023

**HAL** is a multi-disciplinary open access archive for the deposit and dissemination of scientific research documents, whether they are published or not. The documents may come from teaching and research institutions in France or abroad, or from public or private research centers.

L'archive ouverte pluridisciplinaire **HAL**, est destinée au dépôt et à la diffusion de documents scientifiques de niveau recherche, publiés ou non, émanant des établissements d'enseignement et de recherche français ou étrangers, des laboratoires publics ou privés.



# THÈSE

En vue de l'obtention du

## DOCTORAT DE L'UNIVERSITÉ DE TOULOUSE

Délivré par :

Institut Supérieur de l'Aéronautique et de l'Espace

---

**Présentée et soutenue par :**  
**Sofiane KRAIEM**

le lundi 16 mai 2022

**Titre :**

Development of steering law for On Orbit Servicing operation

Développement de lois de pilotage pour le service en orbite

---

**École doctorale et discipline ou spécialité :**

EDSYS : Automatique et Robotique

**Unité de recherche :**

Équipe d'accueil ISAE-ONERA ACDC

**Directeur(s) de Thèse :**

Mathieu ROGNANT (directeur de thèse)

Yves BRIERE (co-directeur de thèse)

**Jury :**

M. Yves BRIERE Enseignant Chercheur ISAE-SUPAERO - Co-directeur de thèse

M. Benoit CLÉMENT Professeur ENSTA Bretagne - Rapporteur

M. Vincent DUBANCHET Ingénieur Thalès Alenia Space Cannes - Examinateur

Mme Helene EVAIN Docteure CNES - Examinatrice

M. Paolo GASBARRI Professeur Université de Rome La Sapienza - Examinateur

M. David HENRY Professeur Université de Bordeaux - Rapporteur

M. Mathieu ROGNANT Ingénieur de recherche ONERA - Directeur de thèse

M. Jurek SASIADEK Professeur Carleton University - Examinateur



# Abstract

Space manipulators allow to respond to a variety of problems in future space exploitation and exploration such as on-orbit deployment, active debris removal or servicing operations. However, a difficulty to autonomously control space manipulator systems arise with large and light structures presenting flexible behavior. Flexible dynamics remain a challenging topic as its modeling may present a first difficulty while the different coupling with the manipulator may deteriorate the control quality. This thesis addresses design and control problems related to autonomous space manipulator equipped with kinetic moment exchange devices for spacecraft rotation control when dealing with system internal disturbances, model uncertainties and measurement errors. The modeling of rigid-flexible dynamics of a multi-body system remains a challenging task, and a first contribution of this work is a generic modeling tool to derive kinematic and dynamic of a rotation-free-floating Space Manipulator System (SMS) with flexible appendages. This analysis led to the main contribution of this thesis, namely the implementation and the design of such control scheme for On-Orbit Servicing operations. Thanks to the model, proposed control include the non-measurable states (i.e flexibility) in the system decoupling and linearization, and the steering laws established are based on Nonlinear Dynamic Inversion (NDI) framework where observers are introduced to improve the quality of linearization. In a first implementation an Extended State Observer (ESO) have been involved to estimate flexible dynamics. Then, in a second time, the modeling uncertainties and measurement errors have been handled by the addition of a Nonlinear Disturbance Observer (NDO). Inter-dependencies between observers and control dynamics have motivated a simultaneous computation of their gains to improve system stability and control performances. This point has been achieved by the resolution of Linear Matrix Inequalities (LMI) to guarantee stability with an appropriate Lyapunov function. In order to highlight the interest of the proposed scheme and validate our approach in a realistic environment, extensive tests of an on-orbit space telescope assembly use-case have been performed on a high-fidelity simulator.



# Résumé

Les manipulateurs spatiaux permettent de répondre à une variété de problèmes dans les futures exploitations et explorations spatiales, tels que le déploiement en orbite, l'élimination active des débris ou les opérations de maintenance. Toutefois, il est difficile de contrôler de manière autonome les systèmes de manipulateurs spatiaux dans le cas de structures légères et de grande taille présentant alors un comportement flexible. La dynamique flexible représente un défi, premièrement par sa modélisation et secondement les couplages avec le manipulateur peuvent détériorer la qualité du contrôle. Cette thèse aborde les problèmes de conception et de contrôle d'un manipulateur spatial autonome équipé de dispositifs d'échange de moment cinétique pour le contrôle de la rotation d'un vaisseau spatial lorsqu'il est confronté à des perturbations internes au système, des incertitudes de modèle et des erreurs de mesure. La modélisation de la dynamique rigide-flexible d'un système multi-corps reste une tâche difficile, et une première contribution de ce travail est un outil de modélisation générique pour dériver la cinématique et la dynamique d'un manipulateur spatial flottant dont les rotations sont contrôlées et en présence d'appendices flexibles. Cette analyse a conduit à la contribution principale de cette thèse, à savoir l'implémentation et la conception d'une loi de contrôle pour les opérations de maintenance en orbite. Grâce au modèle, la commande proposée inclut les états non mesurables (i.e. les modes flexibles) dans le découplage et la linéarisation du système, et les lois de pilotage établies sont basées sur l'inversion dynamique non linéaire où des observateurs sont introduits pour améliorer la qualité de la linéarisation. Dans une première mise en œuvre, un observateur d'état étendu a été utilisé pour estimer la dynamique flexible. Puis, dans un deuxième temps, les incertitudes de modélisation et les erreurs de mesure ont été traitées par l'ajout d'un observateur de perturbations non linéaires. Les interdépendances entre les observateurs et la dynamique de contrôle ont motivé un calcul simultané de leurs gains afin d'améliorer la stabilité du système et les performances de contrôle. Ce point a été atteint par la résolution d'inégalités matricielles linéaires pour garantir la stabilité obtenue à l'aide d'une fonction de Lyapunov appropriée. Afin de mettre en évidence l'intérêt du schéma proposé et de valider notre approche dans un environnement réaliste, des tests approfondis d'un cas d'utilisation de l'assemblage d'un télescope spatial en orbite ont été réalisés sur un simulateur haute-fidélité.



# Acknowledgments

I would like to start by giving thanks to my thesis supervisors, Mathieu Rognant and Yves Brière with whom it was a great pleasure to work with and learn from. The time you dedicated for me, your pedagogy and your kindness really helped me grow professionally. I really enjoyed working among you in this supportive and motivating environment. I also would like to give a special thanks to David Henry and Benoit Clément for the time taken to review this thesis and provide relevant feedbacks to improve its content. Likewise, I would like to thank Paolo Gasbarri for presiding the thesis jury, Jurek Sasiadek, H el ene Evain and Vincent Dubanchet for their interest in this work and the productive discussions.

I am also grateful to Jean-Marc Biannic for the time he took, his advice and its contribution to improve this work. I give thanks to Daniel Alazard and Christophe Louembet for their general advice and for the time they took to participate in my thesis committee. I am also acknowledging to Christelle Cumer for her huge kindness and for the help she provided.

As unbelievable as it can sound but during the thesis there is also some moments of fun and relaxation and I would like to give a heartfelt thank you to the people whom I share those moments with me. At ISAE-Supaero, I really enjoyed the game times even if I rarely won any of those games. So thanks to Alice, F elix, Florent, Guilia, Ilyes, Jason, Louis, Thomas, Val erian and everyone else who joined. On the ONERA side I also enjoyed spending time where I met hardworking and interesting people such as Arthur, Cl ement, F elix, Gustav, Julio, Lucien, Pierre-Julien to work and share a laugh and a special thanks to the people whom I had the chance to share at a moment the office with: David, Franca, Guido, Milo, Sovanna, Waly, William.

Finally I want to thank my family for their support over the years and my brother for his help in the reviewing of my English.





# Remerciements

I would like to start by giving thanks to my thesis supervisors, Mathieu Rognant and Yves Brière with whom it was a great pleasure to work with and learn from. The time you dedicated for me, your pedagogy and your kindness really helped me grow professionally. J'ai vraiment apprécié de travailler parmi vous dans cet environnement motivant. Je tiens également à remercier tout particulièrement David Henry et Benoit Clément pour le temps qu'ils ont consacré à la relecture de cette thèse et pour les commentaires pertinents qu'ils ont formulés afin d'en améliorer le contenu. J'aimerais également remercier Paolo Gasbarri pour avoir présidé le jury de thèse, Jurek Sasiadek, Hélène Evain et Vincent Dubanchet pour leur intérêt dans mes travaux et les discussions productives.

Je suis également reconnaissant envers Jean-Marc Biannic pour le temps qu'il a consacré, ses conseils et sa contribution à l'amélioration de ce travail. Je remercie Daniel Alazard et Christophe Louembet pour leurs conseils généraux et pour le temps qu'ils ont pris afin de participer à mon comité de suivi de thèse. Je remercie également Christelle Cumer pour son immense gentillesse et pour l'aide qu'elle m'a apportée.

Aussi incroyable que cela puisse paraître, il y a aussi des moments de plaisir et de détente pendant la thèse et je tiens à remercier chaleureusement les personnes qui ont partagé ces moments avec moi. A l'ISAE-Supaero, j'ai beaucoup apprécié les pauses-jeux, même si je n'ai que très rarement gagné. Merci donc à Alice, Félix, Florent, Guilia, Ilyes, Jason, Louis, Thomas, Valérian et tous les autres avec qui j'ai partagé un moment de pause et de détente. Du côté de l'ONERA, j'ai également apprécié de passer du temps où j'ai rencontré des personnes travailleuses, intéressantes et avec lesquelles on rigole bien comme Arthur, Clément, Félix, Gustav, Julio, Lucien, Pierre-Julien... et un grand merci aux personnes avec qui j'ai eu la chance de partager à un moment le bureau: David, Franca, Guido, Milo, Sovanna, Waly, William.

Enfin je tiens à remercier ma famille pour leur soutien au cours de ces années et mon frère pour son aide dans les moments de relectures de mon anglais.

*To my parents,*

# Contents

<b>Table of Acronyms</b>	<b>xix</b>
<b>Introduction</b>	<b>1</b>
<b>1 Literature overview</b>	<b>5</b>
1.1 Overview of Space Manipulator Systems through the years . . . . .	6
1.2 Modeling of Space Manipulator System . . . . .	14
1.3 Control methods of Space Manipulator Systems . . . . .	21
1.4 Summary and identified area of improvements . . . . .	27
<b>2 Development and validation of analysis and simulation tools</b>	<b>29</b>
2.1 Developing analysis and simulation tools for SMS <sup>1</sup> . . . . .	30
2.2 Modeling of a rigid multi-body free-floating SMS . . . . .	33
2.3 Modeling of flexible rotation-free-floating SMS . . . . .	48
2.4 Matlab-Simulink simulation and analysis tools . . . . .	57
2.5 Chapter conclusions . . . . .	71
<b>3 Steering law for SMS in presence of flexible appendages</b>	<b>73</b>
3.1 Areas of improvements . . . . .	74
3.2 Interest of a common base and manipulator control . . . . .	82
3.3 Joint-space control of an SMS with flexible appendages . . . . .	92
3.4 Base and manipulator control of an SMS with flexible appendages . . . . .	100
3.5 Illustration of the proposed methods . . . . .	103
3.6 Chapter conclusions . . . . .	115

---

<sup>1</sup>Space Manipulator System

---

<b>4</b>	<b>Robust joint-space control for rotation-free-floating SMS</b>	<b>117</b>
4.1	Robust control challenges . . . . .	118
4.2	Control strategy . . . . .	120
4.3	Illustration of the proposed method . . . . .	133
4.4	Chapter conclusions . . . . .	164
	<b>Conclusion</b>	<b>167</b>
<b>A</b>	<b>Detail of Convective matrix evaluation</b>	<b>171</b>
A.1	Base-derivative of inertia matrices . . . . .	171
A.2	Joint-derivative of inertia matrices . . . . .	175
<b>B</b>	<b>Simple SMS study case</b>	<b>181</b>
	<b>Bibliography</b>	<b>210</b>

# List of Figures

1	Engineering Test Satellite VII "KIKU-7" (ETS-VII), (credit: JAXA) . . . . .	2
2	Astronaut Stephen K. Robinson attached to the Canadarm 2 from its feet (credit: NASA) . . . . .	2
3	Astronaut Leroy Chiao operating the Canadarm 2 from the ISS <sup>2</sup> in the Destiny module (credit: NASA) . . . . .	2
1.1	Astronaut Thomas Pesquet during a solar array installation spacewalk (credits: NASA) . . . . .	7
1.2	Astronauts Musgrave and Hoffman install corrective optics during the first servicing mission of HST (credits: NASA) . . . . .	7
1.3	Three ISS crew members capturing Intelsat VI (credits: NASA) . . . . .	7
1.4	Photography of the deployed SRMS (credits: usspaceshuttle) . . . . .	7
1.5	Robonaut 1A et 1B (credits: NASA) . . . . .	8
1.6	Thomas Marshburn teleoperating Robonaut with virtual reality equipment (credits: NASA) . . . . .	8
1.7	Replica of the first artificial Earth' satellite, Sputnik 1 exposed in Washington,D.C (credit NASA <sup>3</sup> ) . . . . .	9
1.8	Illustration of the space debris distribution orbiting around the Earth, (credit ESA <sup>4</sup> ) . . . . .	9
1.9	Illustration of the ETS-VII spacecraft (credit NASDA) . . . . .	10
1.10	Illustration of the ENVISAT spacecraft capture by a space-tug (credit ESA) .	10
1.11	Illustration of the Orbital Express mission . . . . .	11
1.12	Illustration of the experimental satellite mission Restore-L, (credits: NASA) .	11
1.13	Illustration of the Robotic Servicing of Geosynchronous Satellites (RSGS) mission, (credits: DARPA <sup>5</sup> ) . . . . .	11
1.14	Distinction between on-orbit assembly and servicing paradigms, [PJ18] . . . .	13

---

<sup>2</sup>International Space Station

<sup>3</sup>National Aeronautics and Space Administration

<sup>4</sup>European Space Agency

<sup>5</sup>Defense Advanced Research Projects Agency

1.15	Two-link manipulator and its end-effector VM, [VD87] . . . . .	18
1.16	A three-link space manipulator and its DEM, [LXB98] . . . . .	18
2.1	Denavit-Hartenberg parameters . . . . .	34
2.2	Illustration of a SMS <sup>6</sup> with $n_r$ reaction-wheels and a $n_m$ -DoF <sup>7</sup> s manipulator	45
2.3	Example of a flexible satellite . . . . .	48
2.4	Illustration of a rotation-free-floating SMS equipped with $n_r$ reaction-wheels, a $n_m$ -DoFs manipulator and $n_p$ flexible appendages . . . . .	54
2.5	Description of the Simulink model . . . . .	57
2.6	Examples of SMS modeled with the proposed Matlab tools, on the left a SMS composed of a 3-DoFs manipulator, 3 reaction-wheels and 2 flexible solar arrays, on the right a modeled version of the PULSAR telescope use-case <a href="https://www.h2020-pulsar.eu/">https://www.h2020-pulsar.eu/</a> . . . . .	59
2.7	Visual of the illustrative SMS used for tool validations . . . . .	60
2.8	Upper subplots represent the input torques, $\tau_{r_{in}}$ (left) and $\tau_{m_{in}}$ (right); Lower subplot represents the evolution of the torque error signal $\epsilon_\tau$ (2.73) . . . . .	62
2.9	Upper figures represents the input torques $\tau_{q_{in}}$ ( $\tau_{r_{in}}$ on the left and $\tau_{m_{in}}$ on the right); Lower figures correspond to the control performances with the desired velocities in the red full-line and the measured velocities in the blue dash-line . . . . .	63
2.10	Left subplots represent the system's angular momentum and right subplots the linear momentum. Sub-figures in first row respectively represent the base momentum, in second row the reaction-wheels momentum, in third row the manipulator momentum and in fourth row the total momentum . . . . .	64
2.11	Comparison between singular values of direct linear models: on the left SDT <sup>8</sup> models and on the right models linearized from our tools [Cum+21] . . . . .	65
2.12	Comparison between eigenvalues of direct linear models: on the left SDT models and on the right models linearized from our tools <a href="https://www.h2020-pulsar.eu">https://www.h2020-pulsar.eu</a> . . . . .	66
2.13	Upper subplot represent the control torques $\tau_{q_{in}}$ ; Lower subplot illustrates the evolution of the torque error signal $\epsilon_\tau$ (2.76) . . . . .	67

---

<sup>6</sup>Space Manipulator System

<sup>7</sup>Degree of Freedom

<sup>8</sup>Satellite Dynamic Toolbox

2.14	Listing of system's works evolutions (2.82); Left side subplots represent from top to bottom works derived from: the inertial, convective forces and the external control torques powers; Right side subplots represent from top to bottom works derived from: the inertial, convective and potential forces . . . . .	70
2.15	Lost work (2.83) for the SMS motions obtained with input control torques represented in Figure 2.13 . . . . .	71
2.16	Flexible mode velocities $\dot{\eta}$ for the input torques represented in Figure 2.13 . . . . .	71
3.1	Block diagram of classical control approach in the literature . . . . .	76
3.2	Illustration of the SMS desired motion. Left to right the initial, the mid-configuration and the final configurations . . . . .	78
3.3	Manipulator's joints control performances, measured velocities (full-line) and desired velocities (dashed-line) . . . . .	79
3.4	Upper subplot is the measured reaction-wheels' joint velocities second subplot represents the base angular velocity and lower subplot is the flexible modes velocities . . . . .	80
3.5	Dissipated work (2.83) during the complete motion with a fixed base attitude . . . . .	81
3.6	Variation of the joint contribution to the base motion ( $\mathcal{K}_{\omega_0}^m$ ) plotted in $\mathcal{R}_{sat}$ <sup>9</sup> for the initial reaction-wheels (left) and the second actuators configuration (right) . . . . .	89
3.7	Evolution of the end-effector normalized manipulability indices, $\mu_{\mathbf{r}_{EE}}^N$ , plotted in $\mathcal{R}_{sat}$ for the initial reaction-wheels (left) and the second actuators configuration (right) . . . . .	90
3.8	Evolution of the end-effector normalized manipulability indices, $\mu_{\mathbf{r}_{EE}}^N$ , with a fix base attitude constraint plotted in $\mathcal{R}_{sat}$ for the initial reaction-wheels (left) and the second actuators configuration (right) . . . . .	91
3.9	Block diagram of the proposed joint control method . . . . .	92
3.10	Block diagram of the proposed base-manipulator control method . . . . .	100
3.11	Illustration of the SMS task: the initial configuration (left), the mid-task configuration (middle) and the final configuration (right) . . . . .	105
3.12	Evolution of system variation for a given task, upper subplot represents the evolution of the relaxation term $\rho_1$ and the lower subplot represents $\rho_2$ 's evolution	106

---

<sup>9</sup>Satellite frame



3.13	Manipulator's joints measured velocities and control performances; upper subplot is the measured manipulator's joint velocities and lower subplot is the relative tracking error . . . . .	108
3.14	Reaction-wheels measured velocities and control performances; upper subplot is the reaction-wheels' joint velocities and lower subplot is the relative tracking error . . . . .	109
3.15	Detail of the computed torque (3.38) highlighting interests of including unmeasured states in the NDI <sup>10</sup> . . . . .	110
3.16	Upper subplot represents base angular velocities; Lower subplot represents the flexible vibration $\dot{\eta}$ . . . . .	111
3.17	Manipulator's joints measured velocities and control performances; upper subplot is the measured manipulator's joint velocities and lower subplot is the relative tracking error . . . . .	112
3.18	Upper subplot is the measured reaction-wheels' joint velocities second subplot represents the base angular velocity and lower subplot is the flexible modes velocities . . . . .	113
3.19	Detail of the computed torques (3.63) for the four reaction-wheels . . . . .	114
3.20	Dissipated work (2.83) during the complete motion . . . . .	115
4.1	Block diagram of the proposed joint space control method . . . . .	120
4.2	Spacecraft component overview (elements are detailed in tables 4.1 and 4.2), <a href="https://www.h2020-pulsar.eu">https://www.h2020-pulsar.eu</a> . . . . .	133
4.3	Stowed view (left) and end-effector closeup (right) of CAESAR arm, <a href="https://www.h2020-pulsar.eu">https://www.h2020-pulsar.eu</a> . . . . .	136
4.4	Snapshot after the assembly of the upper inner ring, <a href="https://www.h2020-pulsar.eu">https://www.h2020-pulsar.eu</a> . . . . .	137
4.5	Snapshots after the two first pre-assembly operations, <a href="https://www.h2020-pulsar.eu">https://www.h2020-pulsar.eu</a> . . . . .	137
4.6	Snapshot after the lower inner ring assembly, <a href="https://www.h2020-pulsar.eu">https://www.h2020-pulsar.eu</a> . . . . .	138
4.7	Snapshots of the four consecutive pre-assembly operations, <a href="https://www.h2020-pulsar.eu">https://www.h2020-pulsar.eu</a> . . . . .	139
4.8	Final view of PULSAR, <a href="https://www.h2020-pulsar.eu">https://www.h2020-pulsar.eu</a> . . . . .	140

---

<sup>10</sup>Nonlinear Dynamic Inversion

4.9	Evolution of relaxation terms for each tasks of the PULSAR scenario . . . . .	141
4.10	Evolutions of all the manipulator's joints for each $t_i \in \mathcal{T}_{2T}$ ; the dotted-line represents the desired velocity $\dot{q}_{m_d}$ and the full-lines correspond to each $\dot{q}_m$ for each task . . . . .	144
4.11	Evolutions of all the manipulator's joints for each $t_i \in \mathcal{T}_{3T}$ ; the dotted-line represents the desired velocity $\dot{q}_{m_d}$ and the full-lines correspond to each $\dot{q}_m$ for each task . . . . .	145
4.12	Evolutions of all the manipulator's joints for each $t_i \in \mathcal{T}_{4T}$ ; the dotted-line represents the desired velocity $\dot{q}_{m_d}$ and the full-lines correspond to each $\dot{q}_m$ for each task . . . . .	146
4.13	Evolutions of all the reaction-wheels' joints for each $t_i \in \mathcal{T}_{2T}$ ; the dotted-lines represent the desired velocities $\dot{q}_{r_d}$ and the full-lines correspond to each $\dot{q}_r$ for each task . . . . .	147
4.14	Evolutions of all the reaction-wheels' joints for each $t_i \in \mathcal{T}_{3T}$ ; the dotted-lines represent the desired velocities $\dot{q}_{r_d}$ and the full-lines correspond to each $\dot{q}_r$ for each task . . . . .	148
4.15	Evolutions of all the reaction-wheels' joints for each $t_i \in \mathcal{T}_{4T}$ ; the dotted-lines represent the desired velocities $\dot{q}_{r_d}$ and the full-lines correspond to each $\dot{q}_r$ for each task . . . . .	149
4.16	Illustration of the manipulator control performances; For each manipulator joints the relative tracking error $\dot{\epsilon}_{tc}(\dot{q}_i)$ of each $t_i \in \mathcal{T}_{2T}$ on the left, for each $t_i \in \mathcal{T}_{3T}$ on the middle, for each $t_i \in \mathcal{T}_{4T}$ on the right . . . . .	150
4.17	Illustration of the reaction-wheels control performances; For each reaction-wheels the relative tracking error $\dot{\epsilon}_{tc}(\dot{q}_i)$ of each $t_i \in \mathcal{T}_{2T}$ on the left, for each $t_i \in \mathcal{T}_{3T}$ on the middle, for each $t_i \in \mathcal{T}_{4T}$ on the right . . . . .	151
4.18	Represent the feedback control torques ( $\mathbf{M}^\diamond \mathbf{v}$ ) evolution for lower sub-figures illustrate the linearizing torques evolution for $i \in \mathcal{T}_{2T}$ . . . . .	153
4.19	Illustrate the linearizing torques ( $\mathbf{D}^\diamond \dot{\mathbf{q}}$ ) evolution for $t_i \in \mathcal{T}_{2T}$ . . . . .	154
4.20	Illustrate the evolution of the estimated disturbance torques ( $\mathbf{D}_x^\diamond \mathbf{x}_e + \hat{\boldsymbol{\tau}}_d$ ) for $\mathcal{T}_{2T}$ . . . . .	155
4.21	Represent the feedback control torques ( $\mathbf{M}^\diamond \mathbf{v}$ ) evolution for $i \in \mathcal{T}_{3T}$ . . . . .	156
4.22	Illustrate the linearizing torques ( $\mathbf{D}^\diamond \dot{\mathbf{q}}$ ) evolution for $t_i \in \mathcal{T}_{3T}$ . . . . .	157
4.23	Illustrate the evolution of the estimated disturbance torques ( $\mathbf{D}_x^\diamond \mathbf{x}_e + \hat{\boldsymbol{\tau}}_d$ ) for $\mathcal{T}_{3T}$ . . . . .	158

---

4.24	Represent the feedback control torques ( $\mathbf{M}^\diamond \mathbf{v}$ ) evolution for $t_i \in \mathcal{T}_{4T}$ . . . . .	159
4.25	Illustrate the linearizing torques ( $\mathbf{D}^\diamond \dot{\mathbf{q}}$ ) evolution for $t_i \in \mathcal{T}_{4T}$ . . . . .	160
4.26	Illustrate the evolution of the estimated disturbance torques ( $\mathbf{D}_x^\diamond \mathbf{x}_e + \hat{\boldsymbol{\tau}}_d$ ) for $\mathcal{T}_{4T}$ . . . . .	161
4.27	Represent the evolution of the flexible mode velocities, $\dot{\boldsymbol{\eta}}$ , for $\mathcal{T}_{2T}$ . . . . .	162
4.28	Represent the evolution of the flexible mode velocities, $\dot{\boldsymbol{\eta}}$ , for $\mathcal{T}_{3T}$ . . . . .	163
4.29	Represent the evolution of the flexible mode velocities, $\dot{\boldsymbol{\eta}}$ , for $\mathcal{T}_{4T}$ . . . . .	164
B.1	Two configurations of the simple SMS used for illustrations . . . . .	181

# List of Tables

3.1	Physical parameters of the considered SMS <sup>11</sup> . . . . .	89
3.2	Detail of the SMS' physical properties . . . . .	104
3.3	Flexible modes' physical properties . . . . .	104
4.1	Spacecraft sub-components, <a href="https://www.h2020-pulsar.eu">https://www.h2020-pulsar.eu</a> . . . . .	134
4.2	Spacecraft sub-components, <a href="https://www.h2020-pulsar.eu">https://www.h2020-pulsar.eu</a> . . . . .	135
4.3	LMI <sup>12</sup> resolution times according to the size of $\mathcal{T}$ . . . . .	140
4.4	Values of $\rho_1(t_i)$ . . . . .	142

---

<sup>11</sup>Space Manipulator System

<sup>12</sup>Linear Matrix Inequality



# Nomenclature

## List of Acronyms

<b>ISS</b>	International Space Station
<b>NDI</b>	Nonlinear Dynamic Inversion
<b>ESO</b>	Extended State Observer
<b>GEO</b>	Geostationary-Earth Orbits
<b>LEO</b>	Low-Earth Orbits
<b>OOS</b>	On-Orbit Servicing
<b>ADR</b>	Active Debris Removal
<b>DoF</b>	Degree of Freedom
<b>CoM</b>	Center of Mass
<b>LMI</b>	Linear Matrix Inequality
<b>JAXA</b>	Japan Aerospace Exploration Agency
<b>CSA</b>	Canadian Space Agency
<b>ESA</b>	European Space Agency
<b>NASA</b>	National Aeronautics and Space Administration
<b>DLR</b>	Deutsches Zentrum für Luft- und Raumfahrt, German Center for Air and Space-flight
<b>CNES</b>	Centre national d'études spatiales
<b>DARPA</b>	Defense Advanced Research Projects Agency
<b>OSAM-1</b>	On-orbit Servicing, Assembly, and Manufacturing 1
<b>MPC</b>	Model Predictive Control
<b>GSFC</b>	Goddard Space Flight Center
<b>DH</b>	Denavit-Hartenberg
<b>DCM</b>	Direction cosine-matrix
<b>TITOP</b>	Two Inputs-Two Outputs Port Model

---

<b>ROS</b>	Robot Operating System ( <a href="https://www.ros.org">https://www.ros.org</a> )
<b>SDT</b>	Satellite Dynamic Toolbox
<b>SPART</b>	Spacecraft Robotics Toolkit
<b>SMS</b>	Space Manipulator System
<b>VM</b>	Virtual Manipulator
<b>DEM</b>	Dynamically Equivalent Manipulator
<b>GJM</b>	Generalised Jacobian Matrix
<b>ESO</b>	Extended State Observer
<b>DO</b>	Disturbance Observer
<b>NDO</b>	Nonlinear Disturbance Observer
<b>LFT</b>	Linear Fractionated Transfer
<b>AOCS</b>	Attitude and Orbit Control System
<b>SMT</b>	Segmented Mirror Tile
<b>XML</b>	eXtensible Markup Language

## List of Notations

$\mathbb{R}$	Real numbers
$\mathbb{N}$	Natural numbers
$\mathcal{S}_i$	Solid i
$\mathcal{A}_i$	Joint i
$\mathcal{R}_i$	$\mathcal{S}_i$ 's Cartesian body frame
$\mathcal{R}_{ine}$	Inertial frame
$\mathcal{R}_{sat}$	Satellite frame
$\mathcal{I}_i$	Inertia of solid i
$m_i$	mass of solid i
$\mathbf{t}_i$	twist of solid i
$\boldsymbol{\omega}_i$	Angular velocity of solid
$\dot{\mathbf{r}}_i$	linear velocity of solid

---

$\mathbf{q}$	Generalized joint pose-variable
$q_m$	Manipulator's joint pose-variable
$q_r$	Reaction-wheel's pose-variable
$\eta$	Flexible mode displacement variable
$\mathcal{T}$	Kinetic energy
$\mathcal{P}$	Potential energy
$\mathcal{L}$	Lagrangian
$\tau$	Torque
$\tau_m$	Manipulator's joints' control torque
$\tau_r$	Reaction-wheels' control torque
$\tau_0$	Base control torque
$\tau_{ext}$	External torque





# Introduction

Robotic systems are predicted to a bright future in the variety of applications in the space exploitation and exploration. Notably, space manipulator systems provide advantageous solutions to reduce humanized flight missions. Refueling or more generally servicing a satellite, on-orbit deployment and active debris removal are few examples of applications that could benefit from the use of space manipulators. However, the need of developing autonomous control of the robotic systems arises as one of the main challenge.

For space exploitation and exploration, structures too large to be self-deployed are more and more common such as space stations and telescopes. The ISS<sup>13</sup> is the principal example of robotic systems key role in the expansion of a space structure. The Canadian space agency (CSA<sup>14</sup>) has wildly contributed to the improvement of robotic technologies through the years. In terms of in-space assembly, the first version of the Canadarm on the space shuttle helped for the installation of the docking module of the MIR space station in 1995 [Hil+01] and the second version of the Canardarm is still used for assembly purposes and extended the scope of robotic utilizations. Besides assembly, assisting astronauts in extra-vehicular activities as well as inspecting, maintaining and repairing are the current applications of the Canadarm 2. Moreover, the increase number of space objects, in activity or not, has raised a concern as it threatens the future launches. Two approaches are considered to improve the actual situations. First the de-orbiting of space debris, for which manipulator systems provide safest and sustainable solutions over the different methods considered (e.g. harpoon capture, drag augmentation, propulsion de-orbiting removal method) [ZLW20]; [Bie+21]. The second approach aims at extending the lifespan of a defective satellite. The Hubble Space Telescope is the most iconic servicing mission in which robotic manipulator were assisting astronauts in four successful missions in 1993, 1997, 1999 and 2002 [Tat98]. Through the aforementioned examples of SMS<sup>15</sup> use, one main advantage proposed by space robots is the versatility.

Nevertheless, space manipulators have been mostly tele-operated either from the ground, the space shuttle or the space station. However, time-delay communications represent one major problem to safely and precisely operate a manipulator for deployment, servicing or capture scenarios [Pen02]. Early studies have started to develop autonomous control technologies to perform challenging operations. The first demonstration mission without a crew was the Engineering Test Satellite No. 7 (ETS VII) in 1997, which allowed to experimentally validate technologies to proceed to both tele-operated and autonomous manipulator's tasks [Oda00]. From the promising results, improving autonomous control technologies has remained an open study subject to fulfill the full potential of space robotics used in space exploitation.

---

<sup>13</sup>International Space Station

<sup>14</sup>Canadian Space Agency

<sup>15</sup>Space Manipulator System



Figure 1 – Engineering Test Satellite VII "KIKU-7" (ETS-VII), (credit: JAXA)



Figure 2 – Astronaut Stephen K. Robinson attached to the Canadarm 2 from its feet (credit: NASA)



Figure 3 – Astronaut Leroy Chiao operating the Canadarm 2 from the ISS in the Destiny module (credit: NASA)

The main remaining difficulties identified to improve the autonomous technologies are the following [FA+14]:

- The safe and reliable docking with a target presenting unknown physical properties (i.e. mass, inertia, velocities). Concerning the ADR<sup>16</sup>, tumbling objects are to be captured and means to first estimate the target's states in the approach phase are one area to be improved [PMK12]. Secondly, stabilizing the uncontrolled malfunctioning satellite offers considerable challenges to safely absorb the grasping contact forces, as illustrated with the studies developed for the ENVISAT spacecraft de-orbiting effort [Est+20]. The methods that were developed to reduce the undesired motions from the capture impact are mainly based on path-planning strategies, MPC<sup>17</sup> or impedance control.

<sup>16</sup>Active Debris Removal

<sup>17</sup>Model Predictive Control

Rybus and al. [RSS16] established a control scheme of the manipulator system based on a path-planning that optimizes the use of actuators while restraining the end-effector velocity in the capture phase. This preliminary work has later been extended with the introduction of a nonlinear MPC [RSS17]. Such methods rely on the modeling of the SMS and a relative knowledge of the target states and physical properties which make them challenging to be developed.

- To make space more sustainable, extension of mission lifespan not only can be provided by OOS<sup>18</sup> missions but also with a reduced use of fuel-consuming actuators. The use of electrical actuators are now mostly considered and could offer new control possibilities for SMS applications [Wil+18]. One difficulty of the control of a robotic manipulator installed on a mobile base is to consider all the couplings. Actively controlling the base during a manipulator task is essential to insure the precision of its motions as well as maintaining a fixed spacecraft orientation for communication purposes. Colmenarejo and al. [Col+18] established a robust control scheme, based on an  $H_\infty$  synthesis for a separate manipulator and base's thrusters in order to cancel undesired couplings in the system.
- An additional difficulty is related to the large and light structure, notably considering in-space assembled spacecraft. With elements such as antennas, solar arrays or sun-shields, flexible behaviors are nearly unavoidable. Meng and al. [Men+17] studied the coupling between the end-effector motions and the flexible appendages after developing a model to describe the equations of motions of an SMS with flexible solar arrays. They established a coupling factor to adapt path-planning and control strategies. With a following study, these coupling factors are considered to reduce the influence of the end-effector on the vibrations during the pre-capture phase [Men+18]. However, these studies carry strong hypothesis to include the flexible dynamics. For this reason, the consideration of flexible appendages in an SMS have been made for simple applications. Hirano and al. [Hir+13] developed a simple dynamics model to develop active vibrations control. Such methods are viable for small satellites but extendable with difficulty for current spacecraft too large to be self-deployed. To compensate for the challenging modeling, robust control strategies have been considered. Wu and al [Wu+18a] established an  $H_\infty$  synthesis for a control coupled with a nonlinear observer in order to deal with unknown external disturbances and evaluate their influence on the manipulator.
- Another area of improvement concerns the possibility of performing different tasks during a mission of an SMS. The concept of space-tug has raised interest as it fully benefits of the robotic systems to fulfill different needs of OOS [Ale+16]. Nonetheless, performing tasks that significantly differ will require robust control strategies to consider system variations.

To summarize, this last years the interest to develop autonomous control of SMS and improve the technologies to use robotic systems in the space exploitation have not ceased to increased. Since the experimental tests of the ETS VII mission, new challenges have appeared.

---

<sup>18</sup>On-Orbit Servicing

Rotation-free-floating SMS, which corresponds to a robotic manipulator system with a base actuated with moment exchange devices, have yet to be widely studied to develop their potentially interesting features. Moreover, with light elements constituting the large space structure, the needs of introducing modeling tools is required to describe the equations of motions of a rotation-free-floating SMS with flexible appendages. In addition, a need of high fidelity simulation tools is required to develop and validate the control laws proposed as well as deeply analyzing robotic systems.

In that matter, this study aims at providing the necessary tools for the control of a rotation-free-floating SMS with flexible appendages to perform OOS operations.

In order to develop control schemes, the methodology followed is resumed as:

1. Chapter 1 provides an overview of the use of SMS through the years and the control challenges with a literature review. This chapter aims at establishing the scope of this study and identifying the improvement areas.
2. Prior to introducing control schemes, chapter 2 establishes kinematic and dynamic models to describe the equations of motions of a rotation-free-floating SMS with flexible appendages. Two contributions result from this chapter. First, a formalism to integrate the flexible dynamics of appendages and secondly a Matlab-Simulink simulation tools that allows to perform analysis and time-domain simulations of a studied robot.
3. In chapter 3, a common control of the base and manipulator is discussed. With novel kinematic indices, it becomes possible to quantify the different actuators' influences to perform a given task. Besides allowing to pre-design an SMS or develop path-planning methods, such indices motivate and justify the interest to introduce a common base-manipulator control. Then, for OOS operations, based on an NDI<sup>19</sup> scheme a steering law for an SMS with flexible appendages is developed. To insure high performances, an ESO<sup>20</sup> is additionally designed such that un-measured states are included in the system linearization. A simultaneous control and observer gains synthesis is proposed through an LMI<sup>21</sup> resolution to satisfy a precise velocity control and insure stability of the closed-loop system.
4. With the promising results obtained in chapter 3, the following chapter extends the proposed control scheme with robustness criteria, such as variations of the system's mass distribution, modeling uncertainties, measurement errors. Thus, the joint-space control law developed in chapter 4, is based on the similar NDI-ESO structure with an additional NDO<sup>22</sup> to take into account modeling and measurement errors. A new common observers and control gains synthesis is proposed and performed with an LMI resolution to satisfy the robustness of the method. Then the control is validated through extensive simulations performed on an actual in-orbit deployment scenario of a space telescope.

---

<sup>19</sup>Nonlinear Dynamic Inversion

<sup>20</sup>Extended State Observer

<sup>21</sup>Linear Matrix Inequality

<sup>22</sup>Nonlinear Disturbance Observer

# Literature overview

---

## Sommaire

<b>1.1 Overview of Space Manipulator Systems through the years . . . . .</b>	<b>6</b>
1.1.1 Background . . . . .	6
1.1.2 Active Debris Removal . . . . .	8
1.1.3 On-Orbit Servicing . . . . .	10
1.1.4 On-Orbit Deployment . . . . .	12
1.1.5 Next steps of improvements . . . . .	13
<b>1.2 Modeling of Space Manipulator System . . . . .</b>	<b>14</b>
1.2.1 Control classification . . . . .	14
1.2.2 Modeling of a rigid Space Manipulator System . . . . .	16
1.2.3 Modeling of flexible appendages . . . . .	19
<b>1.3 Control methods of Space Manipulator Systems . . . . .</b>	<b>21</b>
1.3.1 Early studies . . . . .	21
1.3.2 Control method to reduce manipulator coupling disturbances on the base	21
1.3.3 Base disturbances control . . . . .	25
<b>1.4 Summary and identified area of improvements . . . . .</b>	<b>27</b>

---

Space manipulator systems (SMS<sup>1</sup>) refer in this chapter to one or multiple DoF<sup>2</sup> robotic arm(s) that operate from a spacecraft base to perform a wide range of orbital applications. After providing a general review of SMS' evolution through the last forty years, modeling and control methods are enumerated to highlight current limitations and sources of improvements. This chapter aims at introducing the motivations of this research study and introduces the contributions to future SMS applications.

---

<sup>1</sup>Space Manipulator System

<sup>2</sup>Degree of Freedom

## 1.1 Overview of Space Manipulator Systems through the years

### 1.1.1 Background

Since November 13<sup>th</sup> 1981 and the second mission of the space-shuttle Colombia, the Shuttle Remote Manipulator System, also known as Canadarm, has inaugurated forty years of space manipulator missions. This 6-DoF robotic manipulator with a deployed length of 15.2m has been developed by the Canadian Space Agency (CSA<sup>3</sup>) to fulfill over its thirty years of exploitation ninety missions. Among the most famous ones, the servicing of the Hubble space telescope [Lyn+07] or the installation of the docking module of the MIR space station in 1995 [Hil+01]. Canada has notably contributed over the years to the development of technologies that diversify the scope of space manipulators' possibilities. Beside the Space Shuttle, Canadian manipulators have been made to perform satellite rendez-vous and servicing missions [Sal+05] but their main contribution is the Space Station Mobile Servicing System (MSS) that provides the assets to assemble, transport, inspect and repair payloads in orbit. The MSS' main elements are the Space Station Remote Manipulator System (SSRMS), the Mobile Base System (MBS) and the Special Purpose Dexterous Manipulator (SPDM). The SSRMS is a longer and more performing version of the Canadarm entitling it Canadarm 2 and present on the ISS<sup>4</sup> since 2001. Thanks to the mobile platform it can be deployed along the entirety of the ISS and with the SPDM a number of tasks requiring precision are made possible. Improvement of mobility are obtained with the different grasping points that permit a relocation of the manipulator.

Both Canadarms are perfect illustrations of the usefulness of SMS to improve and facilitate space exploitation and exploration. Human risk factor is one of the first reasons for the development of SMS. From the tragic loss of Columbia in 2003, the Canadarm has allowed to reduce risks by performing inspections of the Space Shuttle before proceeding to re-entry. From a general stand point, Canadarms have assisted astronauts in their extra-vehicular missions and also reduced their numbers by performing the repetitive maintenance tasks of the ISS. Likewise, Canadarms have largely contributed to in-space assemblies of space stations. On-orbit assembly is a major aspect of space exploitation for which SMS has proven its efficiency and feasibility. An other asset of SMS is the capture of spacecraft or payloads. For instance, Canadarm 2 is regularly used for the berthing of the different transfer vehicles.

---

<sup>3</sup>Canadian Space Agency

<sup>4</sup>International Space Station

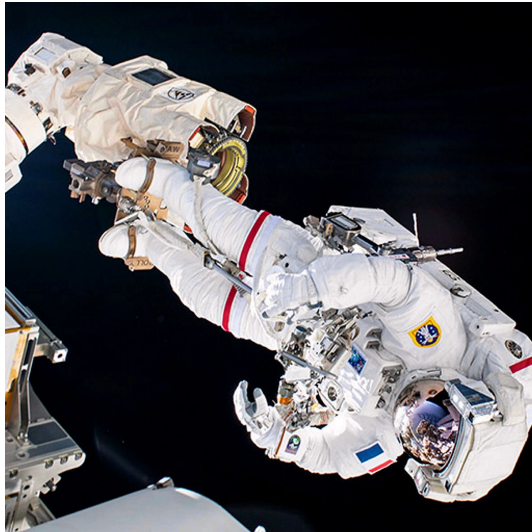


Figure 1.1 – Astronaut Thomas Pesquet during a solar array installation spacewalk (credits: NASA)



Figure 1.2 – Astronauts Musgrave and Hoffman install corrective optics during the first servicing mission of HST (credits: NASA)

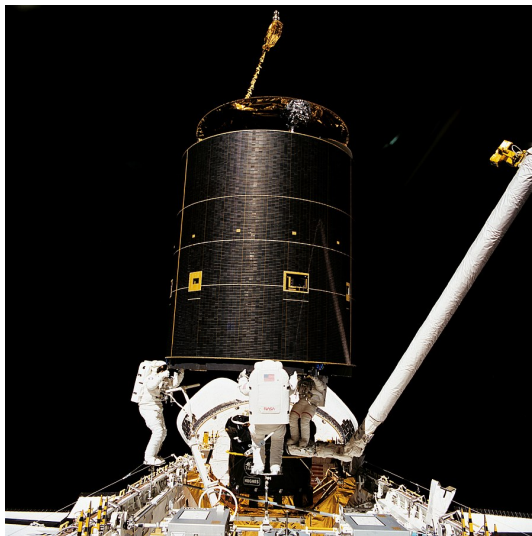


Figure 1.3 – Three ISS crew members capturing Intelsat VI (credits: NASA)



Figure 1.4 – Photography of the deployed SRMS (credits: usspaceshuttle)

The interest in SMS have gone beyond Canadian frontiers, in particular, for the ISS expansion. The Japanese spatial agency, JAXA<sup>5</sup>, and the European one, ESA<sup>6</sup>, have added their own manipulator system to the space station. The European Robotic Arm (ERA) has allowed the assembly of the Russian module and remains used for inspection and maintenance operations in addition to assist astronauts in extra-vehicular missions [Did+01]. Regarding the Japanese Experiment Module Remote Manipulator System (JEMRMS), its first purpose

<sup>5</sup>Japan Aerospace Exploration Agency

<sup>6</sup>European Space Agency



was to assist during experiments on the Japanese module, Kibo [SW01].

To emphasize on the purpose of reducing human risks and humanized flight, robotic systems have been studied and considered to perform tasks instead or with astronauts. In that respect, humanoid robots have been made such as DLR<sup>7</sup>'s Justin or NASA<sup>8</sup>-DARPA<sup>9</sup>'s Robonaut I and II. They are aiming at assisting astronauts during extra-vehicular operations and more generally perform highly repetitive tasks instead of astronauts. In that regard they are equipped with two manipulators disposed on their torso<sup>10</sup> [Blu+03]; [Dif+12].

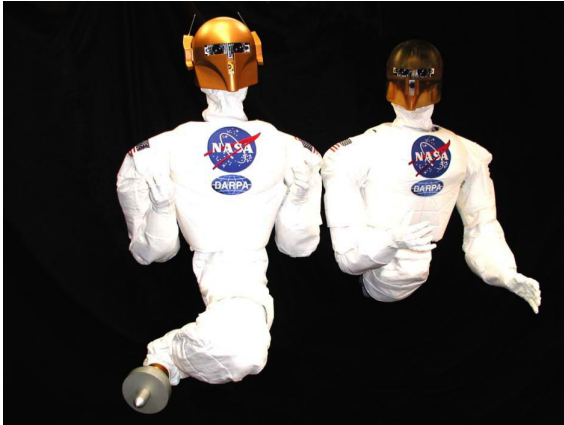


Figure 1.5 – Robonaut 1A et 1B (credits: NASA)

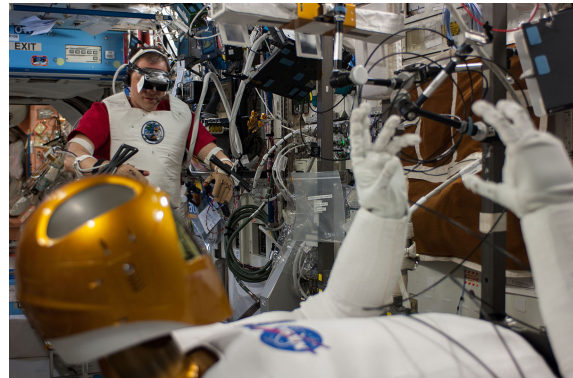


Figure 1.6 – Thomas Marshburn teleoperating Robonaut with virtual reality equipment (credits: NASA)

The various uses for robotic systems gathered on the ISS illustrate three major fields of space exploitation and exploration, namely capture of payloads, on-orbit assembly and maintenance or servicing [Acq09]. To highlight the importance and usefulness of SMS in these fields, further examples are presented within this section.

### 1.1.2 Active Debris Removal

Beside capturing payloads or transfer vehicles, SMS have widely been thought of to answer the space debris mitigation objectives. Since 1957 and the beginning of space exploitation with the launch of the Sputnik telescope, space debris are more present than satellites in activity. In 1978, Donald J. Kessler raised an alarm bell, with the "Kessler syndrom" on the risk of exponential rise of space debris in LEO<sup>11</sup> caused by a chain reaction of collisions [KCP78]. To give an idea of the current situation, the following figures may help. During approximately more than sixty years of space activity, more than 5.300 launches for 42.000 orbiting objects,

<sup>7</sup>Deutsches Zentrum für Luft- und Raumfahrt, German Center for Air and Space-flight

<sup>8</sup>National Aeronautics and Space Administration

<sup>9</sup>Defense Advanced Research Projects Agency

<sup>10</sup>[http://www.esa.int/Enabling\\_Support/Space\\_Engineering\\_Technology/Driving\\_a\\_robot\\_from\\_Space\\_Station](http://www.esa.int/Enabling_Support/Space_Engineering_Technology/Driving_a_robot_from_Space_Station)

<sup>11</sup>Low-Earth Orbits

which half are regularly tracked by the US Space Surveillance Network in GEO<sup>12</sup>, only 1.200 correspond to active satellites. The size of those objects varies from millimeters to the size of a bus as for instance the ENVISAT spacecraft. According to NASA removing 1% of the space debris or five moderate risk debris per year would be sufficient to stabilize their numbers in LEO [Lew+12]. Different solutions have arisen such as the use of tether-based methods, drag sail or laser-based methods [Cas11]; [Bra+13]; [MK19]; [SGG16], however space manipulators present the safest solution [Bie+21] and versatility [Bon18].

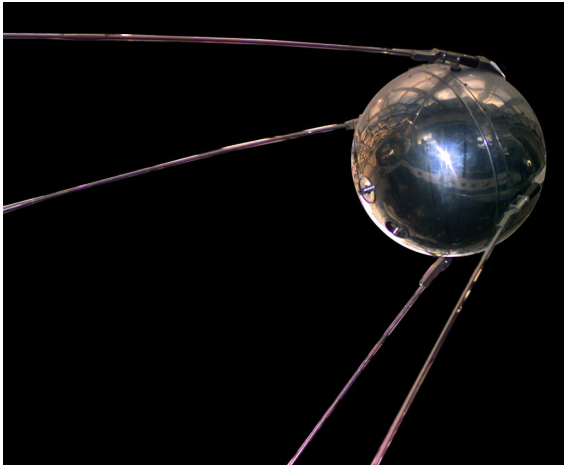


Figure 1.7 – Replica of the first artificial Earth’ satellite, Sputnik 1 exposed in Washington,D.C (credit NASA)



Figure 1.8 – Illustration of the space debris distribution orbiting around the Earth, (credit ESA)

Early studies and experiments have shown feasibility of capturing cooperative targets to initiate active debris removal technology development. In 1997, the Engineering Test Satellite VII (ETS-VII) was launched by JAXA, formerly the National Space Development Agency of Japan (NASDA), in order to perform demonstration experiments to illustrate docking maneuvers with a robotic manipulator [Oda00]. Those experiments aimed at evaluating the improvement made since the SRMS as well as studying different tele-operation solutions and possibility of autonomous capture. Those seminal works have been followed by the study of tumbling targets management. A possible origin for a space debris large enough to be de-orbited may be a loss of actuators control or a collision leading to the tumbling of the space debris. An experimental mission planned for 2025 aiming at demonstrating technologies for autonomously removing Ariane rocket bodies, entitled Active Grabbing & Orbital Removal for Ariane (AGORA) mission [Kum+15] will allow to reach an important step in space manipulator technology. Indeed the grasping of non-cooperative debris require high performing visual technologies to safely proceed at the capture phase, as not only no grasping feature are available but also an estimation of the relative dynamics is needed. Adapted stabilization strategies can then be based on adapting the target dynamics and ensure stability and safety [Jan+15]. Moreover the robotic manipulator and the servicer’s base control need to be complementary for the target to be captured which presents some dynamics that may differ from

<sup>12</sup>Geostationary-Earth Orbits

what is expected in the mission analysis [Ell19]. The Control and Management of Robotics Active Debris Removal (COMRADE) project has been developed by ESA with, in particular, the functionality of stabilizing both the servicer and the malfunctioning satellite to safely realize ADR<sup>13</sup> [Col+20].



Figure 1.9 – Illustration of the ETS-VII spacecraft (credit NASDA)

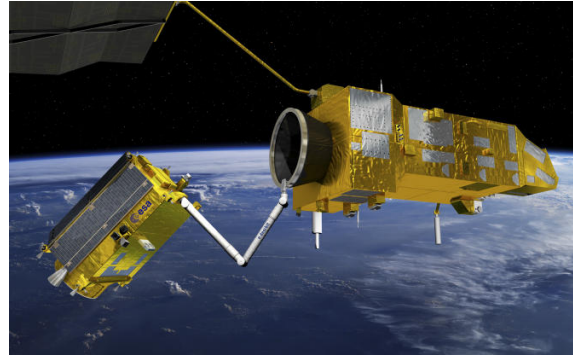


Figure 1.10 – Illustration of the ENVISAT spacecraft capture by a space-tug (credit ESA)

### 1.1.3 On-Orbit Servicing

Before reaching the necessity of removing spacecraft from orbits of interest, maintenance solutions and repairing operations have been proposed. Indeed, satellites may observe a shortening of their lifespan simply because of a malfunctioning device or an obsolete payload. The concept of space-tug, which consists of a spacecraft along with the help of an SMS, performs orbit transfers and servicing tasks, has appeared as an interesting alternative to the different ADR solutions as it gives possibility of servicing or repairing a satellite instead of de-orbiting it [Bon18]. The DLR has been developing such a concept to deal with near end-life satellites and has planned a demonstration mission, the Deutsche Orbitale Servicing Mission (DEOS). It will perform first the capture of a non-cooperative satellite with the servicer's manipulator. Then after a servicing application, the satellite will be finally de-orbited [Rei+11]. The de-orbiting of ENVISAT has been studied by Airbus and their partners to be performed with a similar concept. Dealing with large and tumbling satellites, the detumbling phase of the client satellite remains challenging and space-tug allows to use the servicer's actuators to carry out maneuvers in that matter [Est+20]. Space robots have a key future and a role to play in the lifespan extension and enhancement of on-orbit space structures.

After the five servicing missions of the Hubble space telescope to extend its lifespan where SMS were used as an assistance of astronauts [Tat98] and the experimental tests of capturing cooperative targets with the ETS-VII mission or even the assembly of the ISS, studies have been pursued to improve capturing and servicing technologies [Li+19b]. In 2007, the Orbital

---

<sup>13</sup>Active Debris Removal

Express mission established by DARPA and NASA aimed at developing a safe and cost-effective approach to autonomously service satellites in orbit. This demonstration mission allowed to illustrate progress obtained to autonomously capture the client satellite with the help of vision based technologies [Fri08]. Predefined tasks were defined and supervised from the ground to complete the realization of the refueling mission. DARPA is also contributing on the improvement of servicing technologies for instance with the Spacecraft for the Universal Modification of Orbits (SUMO), a low-cost flight demonstration to help demonstrate autonomous servicing operations with a robotic manipulator [Bos+04]. One other DARPA project is the Robotic Servicing of Geosynchronous Satellites (RSGS) program, they expect to demonstrate the reliability, feasibility and usefulness of a robotic servicing in GEO over several years. As illustrated with the DEXTRE, SMS with appropriate end-effector offer sufficient versatility to successfully perform different missions and adapt to the servicing operations required.

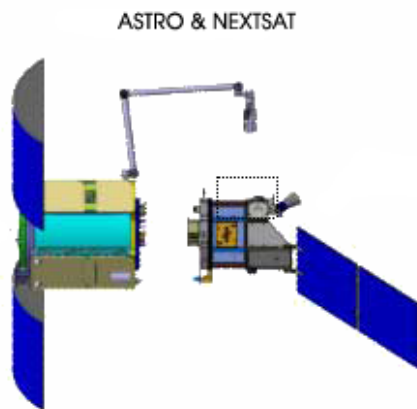


Figure 1.11 – Illustration of the Orbital Express mission

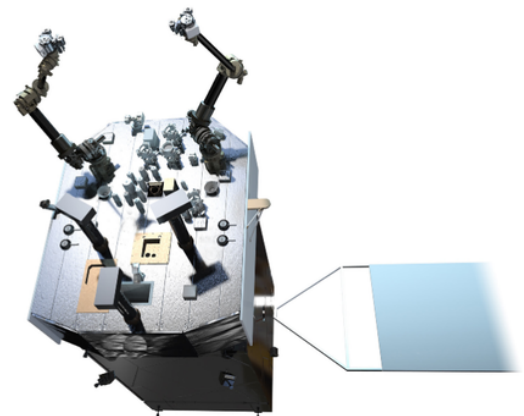


Figure 1.12 – Illustration of the experimental satellite mission Restore-L, (credits: NASA)

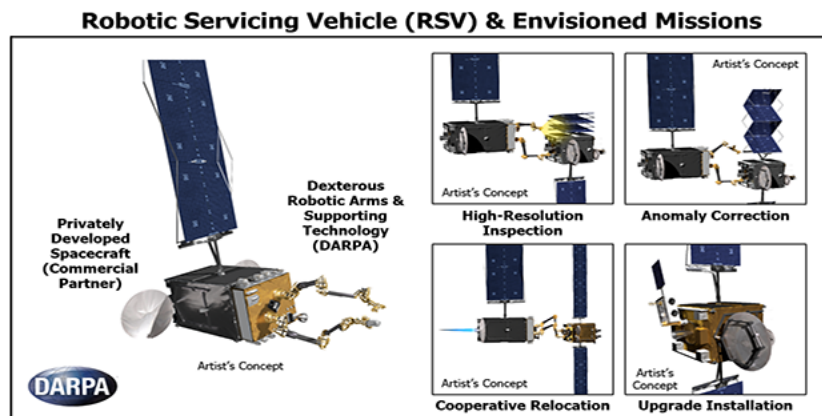


Figure 1.13 – Illustration of the Robotic Servicing of Geosynchronous Satellites (RSGS) mission, (credits: DARPA)

On-orbit servicing also consists in refueling missions. In that purpose, the ISS manipulator has been updated for refueling missions and expand servicing possibilities [Gef+15]. This Robotic Refueling Mission has tested different technologies of hardware for different kind of satellites with some success in the two first phases while the third phase has encountered loss of methane. Currently, NASA is preparing the launch of the OSAM-1<sup>14</sup>, previously known as Restore-L, with the ambition of autonomously refueling a US government satellite. The success of such a mission would be one giant leap for domestic servicing industries.

Another side of the servicing aspect is the inspection of the space structures. Beside the Canadarms and the safety inspection procedures before re-entry [Gil+04], mobile manipulators have been considered [Xu+94]. For instance, the Skyworker prototype aimed at performing inspections for structures assembly [Sta+01].

Servicing missions are various which require versatile solutions. It thus highlights the growing interest of SMS to efficiently and durably pursue space exploitation and exploration [Li+19b].

#### 1.1.4 On-Orbit Deployment

Recent and future of space exploitation is writing itself with large infrastructures and spacecrafts. In the past, space stations have benefited from the use of SMS to constantly expand and upgrade on-board technologies [FA+14]. Now space structures could also benefit from SMS to reduce the launch constraints. The difference between on-orbit assembly/deployment and on-orbit servicing can be summed up in either the mission's purpose. The objective of assembly/deployment missions are to expand the space structure while servicing operations will aim at increasing a satellite's lifespan or modify its use. Different SMS strategies are considered to deploy space structures on-orbit, either using an embedded manipulator or the one on a servicer satellite. However the generalization of using robotic methods to deploy or expand space infrastructures reside in the standardization of SMS features [PJ18]. The DLR is developing the Compliant Assistance and Exploration SpAce Robot (CAESAR) in that way. It is a manipulator system that provides the necessary flexibility to perform different manufacturing and human assistance missions [Bey+18].

Besides space stations, space telescopes are perfect examples of future structures in need of means to deploy in their working orbit. For instance, the PULSAR telescope<sup>15</sup> allows to illustrate the benefit of using a robotic manipulator to deploy the mirror too large to be self-deployed [Rog+19]. The deployment of space antennas with the help of the satellite's manipulator system have likewise been studied [Li+19a] as it offers more versatility in the launch configuration options. In the ambition of facilitating and diversifying launches packing options, the Archinaut in-space manufacturing technology has been proposed. It will allow to extend on-orbit structure deployment possibilities. Archinaut aims at deploying a wild range of space structures in order to simplify on-orbit assemblies [Kug+17].

---

<sup>14</sup> On-orbit Servicing, Assembly, and Manufacturing 1

<sup>15</sup><https://www.h2020-pulsar.eu>

Through the DARPA Phoenix program, cellularized satellite architectural unit, or satlet, have been put in place in order to improve the degree of modularity in space structure assembly [Mel+15]. With the help of SMS, those modular systems can provide low-cost solutions to satellite construction and deployment as well as versatility for redefining mission objectives [Hen14].

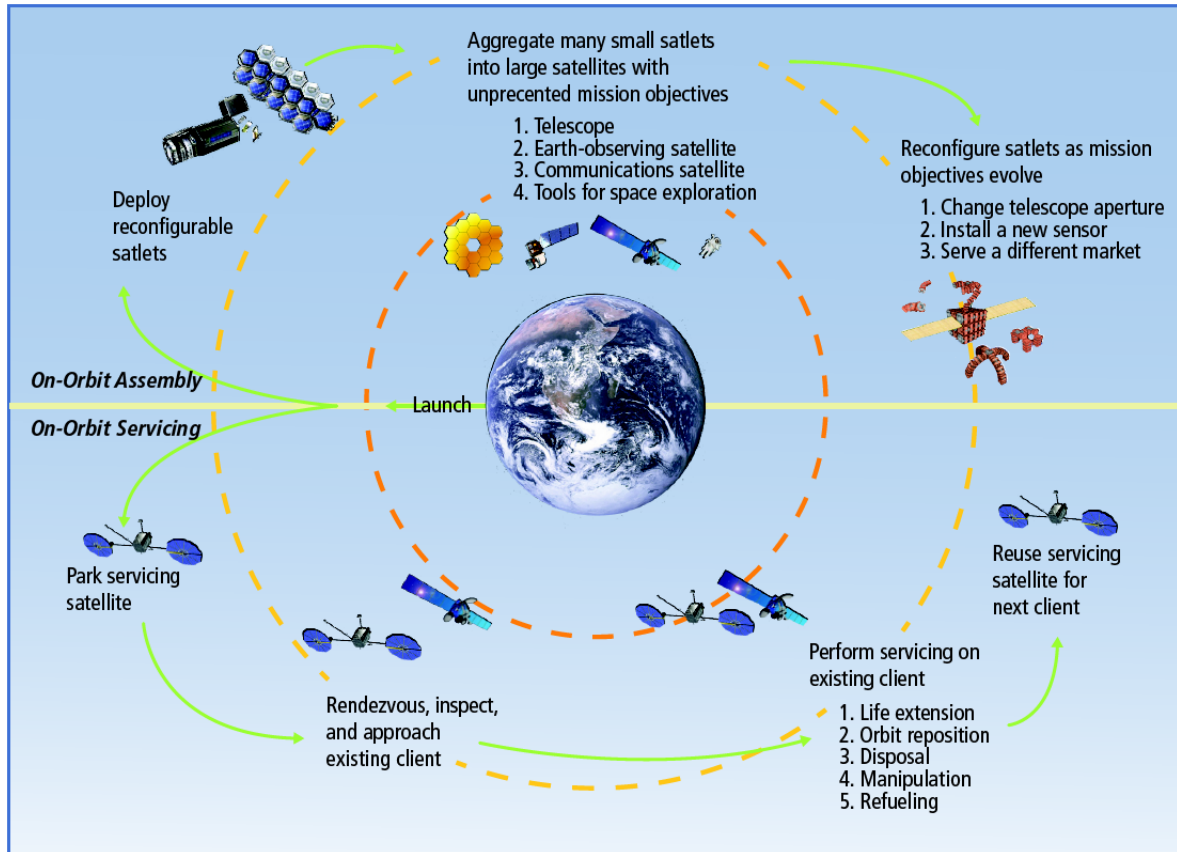


Figure 1.14 – Distinction between on-orbit assembly and servicing paradigms, [PJ18]

### 1.1.5 Next steps of improvements

Space manipulators' interest has ceased to increase through the years as they offer versatility and allow to answer the current turnovers in space exploitation and exploration. However, SMS technologies still require to be improved in order to be viable solutions. One major improvement needed is the autonomous control of systems to perform capture and servicing tasks. Most of the SMS presented have been tele-operated from ground stations or remotely controlled from the Space Shuttle or the ISS. The main issue is the communication delays that can be observed, as it can be illustrated with the Robot Technology Experiment (ROTEX) that took flight in 1993 with the Shuttle Columbia. The ROTEX consisted in experimentally demonstrating tele-operation technologies from both the Shuttle and from ground stations [Hir+94]. With regard to the ground control, delay compensations of up to 7 seconds have

been a key to the success of the predefined demonstrating tasks [HLF94]. In most cases for LEO applications, delays between five and ten seconds have to be taken into account [Pen02] which may be critical for capture missions or to manipulate payload through restrained manipulator workspaces. Furthermore, with large and light structures, internal flexible vibrations may occur with the manipulation of a payload in a servicing or deployment mission.

These undesired disturbances negatively impact the control performances of the manipulator. To ensure stability and mission success, improvements in autonomous control are mandatory. A first requirement to develop such control strategies is to have an accurate modeling of the SMS to describe the behaviors of robots evolving on-orbit. As further expanded upon in the following sections, the modeling difficulties are in the integration of the flexible elements that are subject to numerous hypotheses. Another point of consideration is the coordinate control of both satellite's base and manipulator to perform on-orbit tasks. It could bring efficiency in capture or deployment scenario as well as insuring safe operations [Li+19b].

## 1.2 Modeling of Space Manipulator System

Space manipulator are evolving in free-falling mode which means that, at the opposite of a ground-based manipulator, every motion has an immediate opposite reaction on the floating satellite base. In this section, we try to review the different modeling methods that allow to obtain the kinematics and dynamics of such systems in function of their control mode. In space robotics, the kinematics refer to velocities while the dynamics are employed for system's accelerations.

### 1.2.1 Control classification

Umetani and al.[UY89] and Dubowski and al. [DP93] have proposed to distinguish space manipulator control whether the satellite base is controlled or not. The choice is justified and based by the consideration of linear and angular momentum in the system. When the satellite's base is actively controlled with reaction-jets, the SMS control mode is then referred as free-flying. It corresponds to a control mode in which the momentum is by definition not preserved as base actuators induce an external torque/force to the overall system. On the other hand, if the base is let free of any control, the system is then considered as free-floating which defines a control mode that ensure momentum conservation if in addition no external forces/torques are applied on the system.

A deeper analysis on the control modes has been proposed by Wilde and al. [Wil+18] according on the choice of actuators to control spacecraft's base motions. The discussion, based on the momentum, separates actuators that generate external forces/torques (i.e. typically reaction-jet thrusters) and the ones that does not (i.e. control-moment gyroscopes, reaction-wheels).

**Conserved momentum:** When space manipulators are composed of rigid links and are neither subject to external forces or torques, the total momentum remains conserved. By decomposing the kinematic momentum into a linear and an angular contribution, two sub-modes of free-floating control can be derived [Wil+18]: the floating and the rotation-free-floating.

The floating mode will define an under-actuated control mode for which the 6-DoFs of the base spacecraft are let free of any control and only the manipulator's DoFs are actuated. In that case, each manipulator motion has a direct impact on the base motions. It is a straight interpretation of the conservation of the overall system momentum conservation. For some applications it will lead to the main difficulty of the manipulator's control and in some cases it is the basis of strategies to adjust base attitude/pose controlling the manipulator's joints. Spacecraft orientations are modified or impacted in presence of torque driven actuators in the manipulator which often correspond to revolute joints. The 3 spacecraft linear DoFs may be controlled with a manipulator's prismatic joints that will modify the system center-of-mass in consequence of the changes obtained with the revolute joints.

The second sub-mode is the rotation-free-floating. In this mode, the spacecraft base's rotations are controlled with actuators providing internal torques. Typically, using momentum exchange devices, such as reaction-wheels or control-moment gyroscopes, will maintain the momentum conservation by only affecting the angular kinematic moment. The three linear DoFs remain uncontrolled in this sub-mode.

In the continuation of this document free-floating and floating modes will be comparable while rotation-free-floating and free-floating will designate the same control mode. Likewise no distinction between kinematic momentum and system's momentum is made, as for such system its expression is obtained in function of the system's velocities.

**Unconserved momentum:** Momentum conservation holds as long as no external forces/torques are being applied on the system. Similarly to the floating mode, a division of the free-flying control mode can be made in function of the actuators that are present and that will affect or not the angular and/or linear momentum of the system.

One can define as rotation-free-flying, or rotation-flying, a space manipulator that is actively controlled and for which the base has its three linear DoFs controlled by external torques while the three angular DoFs are either activated by internal torques or let free of any control. The control of rotations by external torques can be obtained with reaction-jet thrusters that produce a total null force. In that control mode, only the linear kinematic moment is conserved.

When the linear DoFs of the spacecraft are, in addition to the manipulator, actuated by external forces, the SMS is said to be translation-free-flying controlled. Reaction jet-thrusters may be used at the condition that they provide a total null torque. Moreover, if momentum exchange devices are used to control the angular spacecraft DoFs, the system remains translation-free-flying or translation-flying. This control sub-mode thus refers to a



system for which only the angular kinematic moment is conserved.

A last sub-mode can be defined as flying in order to refer to SMS with a base fully actuated by external forces and torques. With this last mode, system momentum is time-varying.

**Precision on the external disturbances** As those considerations are made for rigid SMS and subject to no external forces/torques, it is worth noting the control mode classification holds with the usual approximations developed in space manipulator control literature. For a space manipulator evolving in a free-fall environment, it will be assumed that the gravitation attraction, the environmental forces (solar radiation-pressure) and atmospheric actions are neglected allowing to study the system as an isolated one. This discussion allows to define an oriented frame centered in the CoM<sup>16</sup> of the spacecraft in respect to an inertial coordinate system [Wil+18].

### 1.2.2 Modeling of a rigid Space Manipulator System

The modeling of an SMS consists of developing the dynamics and kinematics of a system composed of one or multiple kinematic chains sharing a common moving base. In terms of space robotics the dynamic model of the system defines the equations of motions expressed in function of the accelerations, forces and torques. In addition a kinematic model refers to the relation of the manipulator joint state and end-effector expressed in the Cartesian space, which corresponds to the satellite frame ( $\mathcal{R}_{sat}$ <sup>17</sup>). Moreover, evaluating the system from the accelerations and forces/torques is defined as the forward kinematics/dynamics and reciprocally the evaluation of the system inertia and moment is referred as the inverse kinematics/dynamics. In the contrary of Earth manipulators, the end-effector position in the inertial frame ( $\mathcal{R}_{ine}$ <sup>18</sup>) not only depends on the manipulator's geometry and the joints' configurations but also on the system's inertia distribution. These results to the inverse and forward kinematic problem being also a dynamic one [FA+14].

In a general way, the recursive Newton-Euler and the Lagrangian methods are the two main solutions to derive the equation of motions for a multi-body system [Wit07]; [XK12]. The Newton-Euler formulation is derived by an interpretation of the Newton's Second law of Motion. With a recursive approach, each forces and moments acting on each bodies are enumerated to obtain the equations of motions. As elaborated by Lindberg and al. [LLZ93], the expression of the dynamic model is obtained in function of the joints' forces/torques displacements by eliminating the constraint forces acting between adjacent bodies with geometric properties. The Lagrangian approach bases itself on a work and energy description of the system's bodies using a set of generalized coordinates. It presents the advantage of providing a simpler and systematic computation method. Moreover, the resulting dynamic model expression is established in a more compact form as work-less forces and constraint forces are

---

<sup>16</sup>Center of Mass

<sup>17</sup>Satellite frame

<sup>18</sup>Inertial frame

not taken into account but only kinetic and potential energies are [Bru+10]. Though, the dynamics model is similarly expressed in function of the manipulator's joints torques/forces displacements. In comparison the Newton-Euler method presents a more complex way of deriving the equations of motions, however its main advantage relies in the recursivity of its approach. By expressing for each body all the forces/torques applied, in particular the ones between adjacent bodies, the Newton-Euler formulation provides the possibility of elaborating plug-in methods to derive a multi-body system forward dynamic model [ACT08]. Likewise, this method is well suited when all the forces/torques are known to describe the system's motions in both an inertial frame and a Cartesian coordinate system.

In the contrary of ground-base manipulator, an SMS presents the particularity of developing dynamic singularities in addition to kinematic ones. A dynamic singularity occurs when the base is deprived of an attitude control system (i.e. a free-floating SMS) and the lack of a means to compensate for the manipulator's motions will lead to the impossibility of moving its end-effector in some directions [PD93]. This free-floating common constraint is a direct consequence of the conservation of momentum from which the system dynamics are obtained. Both linear and angular momentum equations are expressed in function of the system's velocities, however only the linear one presents a holonomic constraint. Such a constraint can be described by an equation relating the coordinates (and time) of the system. As the linear momentum equation corresponds to the motion of the CoM of the system, it can also be represented with the CoM's positions instead of its velocities. Therefore, it implies its integrability and thus yields to a holonomic constraint. On another hand, the angular momentum cannot be represented by an integrable equation leading to a non-holonomic constraint [NM90]. Those constraints transpose the fact that for free-floating manipulators, the dynamic couplings between the manipulator and the base make the end-effector pose dependent on the manipulator's trajectory and likewise on its velocities.

An overview of methods to apprehend and take into account the dynamic coupling between orientation and position of the manipulator's end-effector and the spacecraft's base of a free-floating SMS has been detailed by Flores-Abad and al. [FA+14]. Additionally, as developed in Siciliano and al. [Sic+09] a manipulator placed on a mobile platform can be modeled as a terrestrial robotic manipulator which as motivated original studies. In the pioneer work of Longman and al. [Lon90], methods to solve the kinematics and dynamics problem have been proposed. With the time function of the joint's history for a fixed base, the end-effector's relative position to the spacecraft is firstly established. Secondly, with the angular momentum conservation the angular and inertial position of the satellite are asserted. With this method, they were able to obtain a feasible solution for the inverse kinematics problem of both end-effector and spacecraft's base attitude. It has also provided an important analysis result, the manipulator's workspace is a sphere which its radius is monotonically decreasing in function of the manipulator's mass. Beside this work, other methods have been later developed to tackle the inverse kinematics/dynamics problem whose difficulty resides in the addition of inertial parameter resolutions. From the different existing methods developed to obtain the equations of motions for a free-floating manipulator, the focus is placed on three major ones:

- The first one, proposed by Vafa and Dubowsky [VD87], is the Virtual Manipulator

method. It consists of an idealized mass-less kinematic chain whose base is fixed in the inertial frame and whose end-effector coincide with the studied manipulator one. When no external forces/torques apply on the system, the CoM is fixed in the inertial frame and the VM<sup>19</sup> and space manipulator share the same kinematics and dynamics properties. Thus, the VM is employed to develop the kinematics/dynamics model of the space manipulator without describing the equations of motions of the three DoFs of the base. This idealized mass-less model allows to analyze the system in simulation but cannot be physically built.

- To overcome the possibility of experimentally developed equivalent ground-base manipulator, Liang and al. [LXB97] introduced the DEM<sup>20</sup> approach. Similarly to the VM, the first joint is a passive revolute one, the orientation of each joint is similar to the studied manipulator and the links have the same lengths. In addition to modeling or solving the inverse kinematics/dynamics problem, the VM and DEM approaches are employed for workspace analysis [FA+14].
- As the study of kinematics model without any external forces/torques corresponds to the study of the end-effector motions in an inertial frame, the Jacobian matrix is used to describe the translation and rotation of the manipulator in function of the joint angular positions. Umetani and al. [UY89] have then proposed a GJM<sup>21</sup> to solve the inverse kinematic problem. In addition to the joint's angles, the GJM includes the inertia parameters and therefore depends not only on the manipulator kinematics but likewise on the dynamics. The GJM allows to consider the dynamic singularities of a free-floating space manipulator which makes this approach interesting for non-holonomic path-planing [NM90] or to develop control strategies when base and manipulator coupling are a concern [Nen+99].

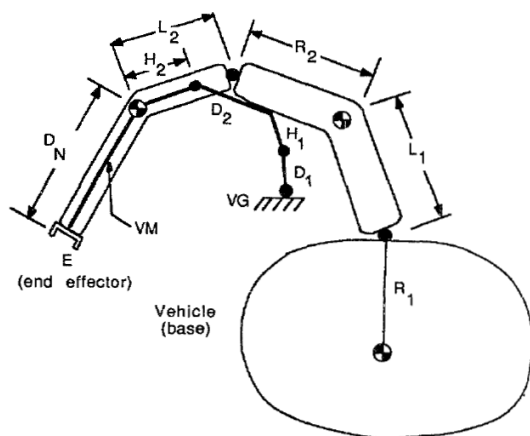


Figure 1.15 – Two-link manipulator and its end-effector VM, [VD87]

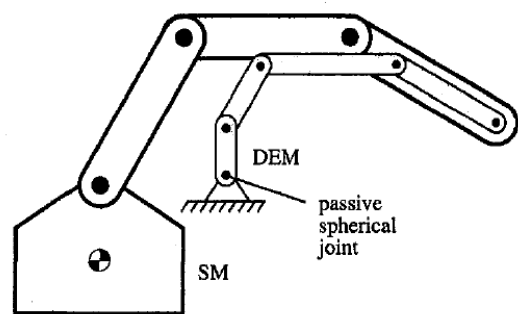


Figure 1.16 – A three-link space manipulator and its DEM, [LXB98]

<sup>19</sup>Virtual Manipulator

<sup>20</sup>Dynamically Equivalent Manipulator

<sup>21</sup>Generalised Jacobian Matrix

**Extension with Multi-kinematic chains:** The presence of a second manipulator provides more flexibility in the control and stabilization of the global SMS. Beside the classical Lagrangian and Newton-Euler approaches, two modeling methods have been developed to synthesize the kinematics model of a multi-arm SMS [FA+14]. The two methods are the Barycentric Vector Approach and the Direct Path Method whose implementation have been compared by Moosavian and Papadopoulos [MP98].

The Barycentric Vector Approach is based on the study of the overall system's CoM and a set of body-fixed vectors. The CoM is used as a representative point for the system linear motions and the vectors are used to obtain the geometric configuration of the system and its mass distribution. This approach leads to the decoupling of the linear and angular motions from the dynamics equations when no external forces/torques apply to the system.

The Direct Path Method, likewise considered a representative point for the system linear motions, however it can be chosen differently from the CoM. The Direct Path Method is better suited for modeling multi-manipulator systems in presence of external forces/torques (i.e. free-flying SMS). In comparison of the two methods, it provides simpler term equations and less computation are required [MP98].

Multiple manipulators have the particularity and the possibility of presenting closed and open kinematic chains. The computation of the dynamics may change from the open to the closed kinematic chain and reciprocally. With such considerations, Nakamura and Yamane [NY00] have proposed a general algorithm to compute the dynamics of both closed and open kinematics without switching modeling methods. In addition, Newton-Euler approaches allow to easily connect and close kinematic chains as such based modeling methods develop for each body the forces/torques applied [ACT08].

### 1.2.3 Modeling of flexible appendages

Flexible appendages are and will be nearly present in all spacecrafts and satellite structures. Solar arrays, sun-shields or even antennas are sources of flexible behaviors and more generally all light and large elements may exhibit flexible dynamics. An appropriate modeling of these dynamics is required to develop control strategies as illustrated by the Hubble telescope attitude control which has suffered from a poor flexible modeling [Fos+95]. Space robots systems and from a general standing, dynamic couplings between the different elements composing the spacecraft need to be considered in a control strategy such that stability is insured. If there is no means to cancel vibrations resulting from a maneuver of the manipulator or environmental disturbances [ZCG17] then the loss of system controllability may be unavoidable as the problem is an under-actuated one. For this reason, flexible dynamics modeling is a key to SMS control improvements and remains a challenging task with the complexity of space structures.

With a manipulator control purpose, first modeling approaches have been considering simple model. As a first approach, the flexible beam model has been considered in a planar problem [ZM10] and later developed to integrate coupling with the rest of the system with

Hamilton's principle [Hir+13]; [Liu+18]. These models are suitable for small satellites and appendages for basic control applications. Moreover, as most of flexible modeling methods, the appendages dynamics are based on generalized damped spring/masses systems. These formulations are written as a second order state representation involving mass, damping and stiffness matrices of the coupled rigid-flexible system [Hen+16]; [HAS19].

In order to consider several flexible appendages connected to a rigid hub, multi-body modeling approach have been developed. Those approaches offer the possibility of developing independent model of each bodies and then connect them to the rest of the structure. Recursive formulations have been introduced early based on variational and vector calculus [BH87]; [KH88]. Deformation modes are employed to represent the relative elastic deformation of each body, then adding the positions, velocities and accelerations of each joints, equation motions are recursively obtained with the system graph definition. In most cases, the flexible properties of a body is obtained from a Finite Element Method (FEM) [Lik72].

A first finite element based approach to establish multi-body models is with the Finite Element-Transfer Matrix method [LP60]. Associating a transfer function for each body of the system to describe its state on both connection point, the system model is obtained by the multiplication of these transfer functions. This approach is limited to tree-like structures modeling [RZZ14]. However, one drawback of FEM is the important number of flexible DoF with which a method can be developed in order to reduce DoF [Dok72]. Moreover considering restraining assumptions the studies on the spacecraft rotations or the amplitude of vibrations, a reduction of the overall number of flexible DoF can be obtained. With a Rayleigh–Ritz discretization the system's impedance matrix can be evaluated [SA08] and according to the considered deformations, suitable discretization methods apply [JL21].

A second finite element modeling method is the Component Modes Synthesis [Hin75] that provides the advantage of condensing the matrix representation of each body [Yu+16]. Similarly, from effective mass/inertia matrix [Imb79] or impedance matrix [Pas87] modeling method, the construction of a spacecraft model can be obtained with individual body properties and parameters and constructed body-by-body [ACT08]. With a similar modeling technique, Guy and al. [Guy+14] have proposed a generic and systematic multi-body modeling method to obtain with a Linear Fractional Transformation a spacecraft model that considers system uncertainties suitable for simulation and control validation. Likewise with the dual quaternion formalism, a Linear Fractional Transformation of the COMRADE satellite and its flexible solar arrays and the presence of propellant sloshing have been developed for similar control purposes [Hen+21]. An extension of these works to consider complex and multiple interconnections between the bodies composing the structure have been developed [San+18]. In a context of ADR, a recursive multi-body modeling approach has the advantage of including the target dynamics as a new manipulator link with respect to the existing topology [Xu+14].

In addition to the rigid coupling existing between the different SMS elements, studying the influence of flexible appendages may benefit to the control strategies. A coupling index has been proposed by Meng and al. [Men+17] to relate mutual effects and indirect ones between the end-effector and flexible appendages. Adapted manipulator motions can then be defined

to reduce vibrations before the capture of flexible targets [Men+18]. Studying the influence of a flexible target to be served by an SMS likewise with flexible appendages, allow pre-sizing of the mission spacecraft. Under restrictive motion assumptions, the Lagrangian formalism can be developed to obtain the servicer and the towed satellite with their respective flexible elements such that criterion on target's mass allow to dimension the servicer [AY15].

## 1.3 Control methods of Space Manipulator Systems

### 1.3.1 Early studies

With the diversity of OOS<sup>22</sup> missions, SMS control requires to overpass different challenges to perform autonomous tasks. A first control difficulty resides in the effects of coupling between manipulator's end-effector and its base. Early control methods have been developed to move the manipulator while minimizing its impact on the base motions. For a free-floating satellite, the objective is to maintain system's controllability while for a free-flying robot it allows to avoid an overuse of base actuators. Longman and al. [LLZ87] have introduced SMS kinematics to develop joint adjustment to account for base motions in the manipulator's control. A trajectory planing was introduced by Dubowsky and Torres [DT91], based on an Enhanced Disturbance Map that provides manipulator motions with relatively low spacecraft disturbances. With the GJM introduced by Umetani and Yoshida and based on the angular conservation momentum [UY87], resolved motion rate and acceleration control based method have been developed to take into account the dynamic interaction between manipulator and satellite base [UY89]; [Par+93]. When momentum conservation hypotheses are not applicable, the GJM approach has been extended to compute a manipulator trajectory to capture a tumbling satellite [SB08]. From the manipulator Jacobian expression Nenchev and al. [NYU96] have proposed a reaction-null space control method to decouple a free-floating manipulator and its base dynamics, and later extended the proposed method decoupling control tasks to simplify dynamics expressions in the control law [Nen+99]. An adaptive version of reaction null-space control has been studied to include dynamic modeling uncertainties for a free-floating SMS [Xu+13]. Likewise, with the fixed-base model of the manipulator, DEM, adaptive control approaches can be assessed to perform joint space control [PO04].

### 1.3.2 Control method to reduce manipulator coupling disturbances on the base

Later studies have pursued the development of control laws to reduce undesired manipulator impacts on its base which will be operating on-orbit. In particular for ADR applications, the impact caused by the capture of a target creates a disturbance torque on the manipulator with a direct influence on the servicer base. In that way ADR studies have improved manipulator control methods resulting in lowering the influence of end-effector contact dynamics and

---

<sup>22</sup>On-Orbit Servicing

minimizing the target momentum. An extension of the reaction-null space control method has been proposed by Jin and al. [Jin+17] with the introduction of a reaction torque to create a base reaction-less and dynamic singularity-free control of a free-floating manipulator.

**Momentum accumulation:** Most of the proposed Jacobian based approaches consider an initial system linear and angular momentum null. If initially the overall momentum is non-null, it will accumulate during the servicing mission and will affect the manipulator's dynamics as a Centrifugal/Coriolis force. The direct consequence of this additional force/torque is the end-effector that cannot remain in a given position. A reaction-null space control method with a bias momentum approach has been put in place by Dimitrov and Yoshida [DY04] to benefit of the initial angular momentum in the pre-impact capture phase. Moreover, for multi-arms SMS, a momentum redistribution approach offers efficient moment reduction during the capture of a target presenting an unknown angular momentum [Zha+17]. Another approach, proposed by Nanos and al. [NP17], consists in tackling the non-zero angular momentum of a free-floating spacecraft as a fixed-base terrestrial robot that requires gravitational compensation. However these approaches constrain the manipulator workspace. A workspace adjustment has been proposed by Nanos and Papadopoulos [NP11] to immunize the end-effector of the accumulating angular momentum of the free-floating SMS. Likewise, impedance control can include the momentum in the feedback linearization similarly to an external force [NY06]. Nevertheless, to avoid the exact feedback linearization of a torque control law of a free-floating SMS, an appropriate coordinate transformation allows to remove the disturbances induced by the momentum [Gio+16]. Additionally to avoid the computation of the Jacobian and globally solving the inverse kinematic problematic, a dynamic formulation of the SMS has been proposed by Zhou and al [ZLW19] in which the end-effector is considered as a virtual base. The Lagrange multipliers method is employed to analytically obtain the joint's control torque such as the end-effector follows a desired trajectory while minimizing its base perturbations.

Free-flying robots benefit from a minimization of base disturbances as their rejection are done with fuel-consuming actuators which consequently impacts the missions' lifespan. In that purpose, fuel efficient control methods have been proposed. An early study has established an optimal control algorithm based on the Pontryagin's maximum principle to minimize the fuel consumption of a free-flying spacecraft equipped with jet thrust mechanism [Sak99]. Giordano and al. [GGAS17] came forth with an extraction of the accumulated momentum with the base actuators by decomposing external and internal forces to let the end-effector deal with only internal ones. The momentum of a grasped object causes a manipulator's workspace shift which can be tackled with a control of the system CoM, which corresponds to the center of the maximum reachable workspace. Giordano and al. have proposed simultaneous control methods of the system CoM and end-effector to efficiently use the thrusters [GCAS18]; [GOAS19].

**Detumbling strategies:** Docking maneuver remains a challenging control task and in particular when the manipulator and the target present a non-null differential energy. Con-

sidering tumbling, or non-cooperative, targets have raised interests in ADR applications. A first strategy developed to reduce the impact of grasping is the impedance control of the end-effector. Nakanishi and al. [NY06] proposed such a method to limit the contact force impact on the free-floating manipulator and avoid both spacecrafts to push each other. Impedance control is equivalent to a mass-damper-spring system fixed at a point in space. Yoshida and al. [Yos+04] emphasized on the dynamic conditions to satisfy a safe grasping that depend on the inertial property of the chaser spacecraft or the impedance control. The main objective of an impedance control is to obtain smaller inertial characteristics of the servicer compared to the target's one. It results on the chaser that will not significantly deflect the target. However impedance control may present two main difficulties. Firstly, the drift of the chaser is relatively fast and switching from a base control to the manipulator may be frequent [GCAS18]. In consequence, approaches considering the accumulated momentum may be more appropriated [GGAS17]. Secondly, these approaches require dynamics estimations of the target properties to be properly developed, as established in [CUFA20]; [FA+20].

Adaptive control may present a solution to the estimation difficulties. As proposed by Nguyen and al. [NHS11], during and after the capture of an unknown target adaptive algorithm may provide reaction-less motion of the chaser's base. Without target dynamics information, their proposed method, based on a recursive least square algorithm, allows to adapt the unknown parameters to safely capture the target. The detumbling of a non-cooperative object, or the operation to bring it at a state of rest, has been studied by Aghili [Agh09b] who suggested a first optimal control that aims at minimizing the detumbling time while ensuring the interaction torque between the manipulator and target under a defined value. From the Pontryagin's principle, an optimal path-planning problem is solved to ensure the condition on the interaction torque. The detumbling, during the post-grasping phase, is obtained with a coordination control for a combined system of the space robot and the target satellite. It aims at dumping the initial velocity of the tumbling satellite. In a more recent study from the same author, the optimal detumbling control strategy has been extended to achieve momentum dissipation of the grasped non-cooperative target in time and/or energy efficiency way while considering forces/torques limitations [Agh20]. It was also improved by Dubanchet and al. [Dub+15], who proposed  $H_\infty$  to compute a manipulator and base controllers suitable for on-board processors.

Moreover, to deal with the model's uncertainties of the target, Gangapersaud and al. [GLR19] preferred the use of force control to detumble the target without requiring target inertial parameters. Wang and al. [Wan+18a] developed the dynamics of the target and the SMS so that a coordination controller can be put forward. Optimal detumbling and path-planning are obtained with quartic Bézier curves and an adaptive differential evolution algorithm with detumbling time constraints. As proposed by Aghili [Agh09a], a coordination control allows the manipulator to track a defined path while dumping the initial velocity of the target and synchronously control the chaser's base attitude. Likewise, in the debris removal mission e.Deorbit the chaser's rotational and linear DoFs and the manipulator are simultaneously controlled with a robust  $H_\infty$  control solution to safely detumble a large debris [Col+20]; [Fau+22].



**Path-planning approaches:** Without considering a specific SMS application or an OOS task, path-planning approaches allow in a general way to develop methods for: reducing a manipulator's influence on its base, optimizing the workspace with collision avoidance considerations, efficiently using actuators. Papadopoulos and al. [Pap92] have studied the non-holonomic property of free-floating manipulators to obtain singularity-free paths, as the dynamic singularities are path dependent. A reachable workspace is defined such that a Cartesian space planning method allows to obtain manipulator's motions to control the base orientation. This work has later been extended to develop a path planning method that simultaneously provides end-effector and spacecraft attitude control only with the manipulator's joints control [PTN05]. Path-planning methods aiming at reducing the manipulator's impact on the rest of the SMS have been studied for various applications. In capture scenarios, adaptive reaction null space methods have been widely developed for free-floating manipulators as it avoids the use of base actuators [YDH19]. More generally, methods based on the GJM have allowed to reduce the free-floating base disturbances during the capture contact. As proposed by Hu and al. [HW18] the impacts are considered in their developed generalized mass Jacobian matrix. Then it allows to introduce a base attitude disturbance ellipsoid used to define the impact direction and minimizing the base attitude disturbances in the control strategy. Moreover, developing path-planning methods allow to reduce the impact of the grasping. As established by Zhang and al. [Zha+20], the manipulator's path is obtained with a particle swarm optimization so that the contact has low influence on the base. Similarly, Yang and al. [Yan+19] developed a strategy to synchronize the manipulator's end-effector of the servicer and the target that reduces the relative motions. Likewise, optimizations with multiple constraints have been developed to include a reduction of coupling influences actuators limits or the system's velocities. These optimizations result in appropriate manipulator trajectories that can be adapted according to the servicing application [LY20]. Trajectory optimizations also provide the advantage of a reduce use of available actuators, as developed in [RSS17].

Furthermore, momentum accumulation or external forces may impose an unwanted end-effector motion. Therefore it may require a solution for the inverse kinematic when the manipulator is in a near singularity configuration as it could saturate its actuators. In order to avoid dynamic singularities, Nanos and al. [NP15] studied Cartesian trajectory planning of free-floating SMS such as for a given end-effector trajectory an initial manipulator configuration is defined resulting in non-singular configurations during end-effector motion. The proposed method advantageously allows to consider initial angular momentum. Wang and al. [Wan+18b] benefit of the manipulator's redundancy which offers infinite solutions for the inverse kinematics problem to optimize trajectories. With null-space vectors, they use Bézier curves to represent the joints' trajectories while minimizing their range and rate or consider singular-free trajectories. Likewise, additional constraints as adding minimizing base disturbance and collision avoidance criteria can be included. A more recent study proposed by Shao [Sha+21] tackles the singular avoidance problem introducing a nonsingular terminal sliding surface with a terminal sliding mode controller. It also provides quick convergence time. Considering free-flying robots, Seddaoui and al. [SS19] proposed a common trajectory planning for collision-free and singularity-free paths with fuel-consumption optimization constraints. Fuel consumption, that also goes hand in hand with the mission's lifespan of a free-flying SMS, can be tackled by adding additional constraints in the path-planning optimization problem

as proposed by Breger and al. [BH08]. Their solution is to solve a non-convex problem formulation to reduce by two the fuel consumption of the satellite from a convex formulation of the problem. Similarly, adding constraints on actuator capacity and end-effector in the optimization allows to compute manipulator's trajectories such that the impact with the target to be captured can be done in an energy-efficiently way and without collision [Lam10].

### 1.3.3 Base disturbances control

In-space robots are affected by multiple disturbances that mainly impact the spacecraft base attitude control. Two categories of perturbations can be identified. The external ones such as atmospheric drags, gravitational fields and solar radiations that induce external torques and forces on the global system. And the internal ones such as flexible vibrations and perturbations from couplings in the system. They either extend the modeling formulation or transposes physical constraints as the kinetic momentum expression. In this section the emphasis will be placed on the internal disturbances which is a rising problematic with the current and future space structures that mostly exhibit flexible behaviors. Moreover, the study is restrained to flexible elements outside the manipulator's kinematic chain.

**Active control:** As illustrated with the Hubble space telescope attitude control degradation due to the flexible solar arrays[Fos+95], early studies have shown interest in flexible disturbances control. When the application is enabling the possibility of active vibration suppressions, different actuators have been studied and proposed. A first approach is the use of an active joint between the flexible appendage and the rigid hub. Hirano and al. [Hir+13] proposed a virtual joint model to actively control the flexible appendage and reject the vibrations due to the coupling with the manipulator. As flexible deformation are generally not-measurable, an estimation of the flexible states is included in the control law with a force/torque sensor between the hub and the appendage. Likewise, Ataei and al. [Ata+20] studied the use of elastic connection between the flexible appendage and the rigid satellite base. Boundary controllers are then designed to ensure asymptotic stability of the satellite attitude control without accurate system modeling. In a second study, in which no manipulator is considered, permanent magnet synchronous motors are used to actively reduce the flexible modes during the assembly of solar arrays [Guo+20].

Another method to actively reject flexible disturbances is the use of piezoelectric actuators positioned on the appendage [HM05]. Such methods assume available sensors to measure deformations. However, when flexible modes are not measurable, state observers are developed in the control law structure [CYL17]. Otherwise the placement of piezoelectric actuators and sensors has been studied by Angeletti [Ang+21] in order to perform precise pointing of the base attitude without reaching flexible deformation thresholds.

Different strategies have considered the use of control moment gyroscopes distributed on the flexible structures. Hu and Zhang [HZ16] have developed an adaptive controller for vibration suppression in addition to a nonlinear controller that provides desired control input

for large angles of the three-axis attitude maneuvers. Likewise, Jia and al. [Jia+17] have proposed a two controller strategy for a flexible manipulator with control moment gyroscopes. They first decouples the system dynamics as a slow and fast subsystem in order that the flexible displacement correspond to the fast subsystem and the manipulator's rigid motion to the slow one. Moreover, decomposing the flexible dynamics in a fast subsystem also aims at reducing the not-measurable states, as developed in the singular perturbation method detailed in [YGC19].

**Passive control:** Active control offers answers to simple systems exhibiting flexible behaviors, however they remain hardly implementable considering the large structures in future SMS applications. As a first approach to avoid the excitation of the flexible modes, input control torque can be filtered. Chu and al. [CC12] proposed an adaptive disturbance rejection filter combined with an optimal input shaping control law to identify and adapt the disturbance rejection. An adaptive notch filter is additionally developed with the closed-loop system dynamics.

As the main difficulty to control free-floating robot lies in the couplings, different studies have developed control strategies based on the quantification of the undesired system couplings. For instance, the relation between manipulator and sloshing of a fuel-tank has been studied by Rackl and al. [RGL18] while Meng and al. [Men+17] proposed coupling indices between flexible appendages and manipulator motions. With these last coupling indices, a hybrid control method for vibration rejection has been formulated by the same authors [Men+18].

Furthermore, other disturbances may apply on SMS which require different control strategies. As discussed in [Cao+20] external disturbances also impact the system such that system modeling becomes difficult to deploy active control methods. Besides the unknown external perturbations, modeling of the SMS with or without flexible appendages may be challenging. For those reasons, robust control methods have been employed to perform accurate manipulator and base control. Studies have tackled model uncertainties with  $H_\infty$  controllers. As established in [FTST06], additionally to the nonlinear  $H_\infty$  a complementary neural network has been developed to compensate for model inaccuracies as well as rejecting external disturbances. Zhongyi and al. [ZFY08] developed a disturbance observer in the system decoupling. The observer is developed with the VM approach in order to include model uncertainties which are considered as lumped disturbances in the joint space. Likewise, Qiao and al [QWY19] proposed the use of a disturbance observer to deal with vibrations of flexible appendages while a  $H_\infty$  controller is defined as such to compensate for SMS's modeling uncertainties. Moreover,  $H_\infty$  synthesis allows to consider parametric variations with LFT<sup>23</sup> representation. Colmenarejo and al. [Col+20] tackled flexible uncertainties with such methods as in order to perform capture tasks in presence of flexible appendages. Zhang and al. [Zha+15] developed an adaptive trajectory tracking control for free-floating SMS. The proposed control method, allows to consider both parametric and non-parametric uncertainties as well as un-

---

<sup>23</sup>Linear Fractionated Transfer

known bounded external torques. Chu and al. [CCS12] extended the combined DO<sup>24</sup> and a feedback control method with a fuzzy logic system to tune parameters online to improve perturbation rejections. Zhou and al. [ZZZ17] incorporated a linear switching surface in the controller design to deal with dynamic uncertainties in their proposed tracking control method for free-floating robots.

**Use of base actuators:** The lifespan of a mission is one criterion for future spacecrafts and in that purpose alternative to jet-thrusters are studied. Electrical actuators are then favored for the spacecraft attitude control. Giordano and al. [Gio+20] proposed a common control of thrusters and reaction-wheels such that only the critical moment of the capture of a non-cooperative target are tackled with the thrusters. Reaction-wheels are also considered as electrical kinetic moment exchange devices allowing to control the spacecraft base during manipulator motions without affecting the mission lifespan. Shi and al [SKK16] have developed the dynamic model of an SMS with reaction-wheels to propose a controller robust to model uncertainties in order to maintain the spacecraft attitude. To overcome reaction-wheel torque limitations, Li and al. [LLW13] have discussed the interest of single gimbal control moment gyroscopes during manipulator motions as they provide higher control torques than reaction-wheels. Likewise, Wu and al. [Wu+18b] have considered the combination of reaction-wheels and control moment gyroscopes to maintain the satellite platform fixed during manipulator operations. Developing a null-motion between actuators allows to deal with saturation of reaction-wheels and the inherent geometric singularity of gyroscopes. Antonello and al. [AVT19] have discussed the different coordinate control methods to control both manipulator and its base. With the recursive Newton-Euler approach control moment gyroscopes are incorporated in the SMS dynamics and discussion are made based on the additional use of thrusters or not.

## 1.4 Summary and identified area of improvements

SMS have shown an increasing interest in space exploitation and exploration during these last decades, however remaining substantial improvements are required to consider them as serious solutions. A first improvement consists in developing autonomous space robots to perform highly repetitive tasks and allowing to reduce manned-missions. However, difficulties to develop control laws arise with the complex modeling of space structures. Indeed, flexible appendages are frequent in satellites and space structures which required to be taken into account in SMS studies. As space manipulators operate in free-falling environments, the different coupling between each elements that composed the system have to be considered in the control applications. Besides coupling between manipulator and its base that either is controlled or let free of rotation and drift, the manipulator system motions are inducing flexible vibrations for which it is difficult to implement active control.

With the literature review, we identified the following axis of improvement:

---

<sup>24</sup>Disturbance Observer

- Development of analysis and simulation tools in order to represent and study the behavior of SMS with flexible appendages.
- Defining SMS control laws such that a manipulator can precisely perform on-orbit servicing tasks in presence of disturbances induced by flexible appendages. Include base actuators to attenuate the base disturbances due to different system couplings and external perturbations.
- Consideration of a first robustness criterion due to modeling uncertainties and sensors' measurement errors.
- Consideration of a second robustness criterion on the inertia distribution changes. SMS are inclined to proceed to different operations which leads to system variations. These variations are mostly inertia ones and according to system's velocities couplings of the different SMS's elements may required to be considered.

# Development and validation of analysis and simulation tools

---

## Sommaire

---

<b>2.1</b>	<b>Developing analysis and simulation tools for SMS<sup>1</sup></b>	<b>30</b>
2.1.1	Problem statement and challenges	30
2.1.2	Modeling objectives	32
<b>2.2</b>	<b>Modeling of a rigid multi-body free-floating SMS</b>	<b>33</b>
2.2.1	Introduction of Denavit-Hartenberg notations	34
2.2.2	Velocities and accelerations	38
2.2.3	Multi-body system dynamics	41
2.2.4	Dynamics of a rotation-free-floating SMS	45
<b>2.3</b>	<b>Modeling of flexible rotation-free-floating SMS</b>	<b>48</b>
2.3.1	Modeling hypothesis	48
2.3.2	Modeling of a rigid-flexible multi-body system	50
<b>2.4</b>	<b>Matlab-Simulink simulation and analysis tools</b>	<b>57</b>
2.4.1	Simulator functionalities	57
2.4.2	Validation and performances of the developed simulation tools	59
2.4.3	Example of possible analysis with modeling tools	67
<b>2.5</b>	<b>Chapter conclusions</b>	<b>71</b>

---

<sup>1</sup>Space Manipulator System

## 2.1 Developing analysis and simulation tools for SMS with flexible appendages

### 2.1.1 Problem statement and challenges

#### 2.1.1.1 Problematic of the study

The objective of the study is to develop steering laws for space manipulator systems performing OOS<sup>2</sup> operations. An SMS defines a system composed of at least one satellite base and one robotic manipulator. The study will put the focus on rotation-free-floating SMS with a unique manipulator. Such robotic systems have shown growing interest to perform multiple and various tasks. As defined in the previous chapter, rotation-free-floating or free-floating system refers to an SMS from which the satellite's three rotational DoF<sup>3</sup>s are actively actuated by electrical actuators. In this work, reaction-wheels are selected. Moreover, in an objective of not impacting the mission's lifespan the three linear DoFs of the base, often controlled with reaction-jet actuators, will not be actively actuated in this study. Therefore, adapting multi-body modeling formalism to integrate and describe space manipulators dynamics with reaction-wheels in the satellite base is a first concern of the study.

As identified in the previous literature overview, flexible appendages will be systematically present in application involving SMS. The flexible modeling raises a second focus on the study as it remains challenging. As active control is difficult to conceive, the flexible modeling could bring significant advantages in the control design process. Thus, deriving the dynamics model of a rotation-free-floating SMS with flexible appendages would provide new control approaches adapted to intern disturbances.

An SMS evolves in a free-falling environment leading to multiple coupling within the overall system. Studying and evaluating those couplings is necessary to ensure stability and feasibility of manipulator motions to perform a given task. Developing means to analyze couplings and more generally to evaluate and study feasible motions and configurations that can possibly achieve an SMS is another focus of development in this work. Besides, the tools are introduced such that control laws can be developed and validated with time-domain simulations.

To summarize, tools of analysis and simulations for rotation-free-floating SMS with flexible appendages have been elaborated and are described in this chapter so that control and analysis problematics can be introduced.

---

<sup>2</sup>On-Orbit Servicing

<sup>3</sup>Degree of Freedom

### 2.1.1.2 Modeling of rigid SMS

SMS modeling refers to the derivation of both a dynamic and kinematic model of the robot. A kinematic model gives the relations between the manipulator's joint state and the end-effector in the satellite frame. A dynamic model provides the system's equations of motions in terms of accelerations, forces and torques. A particularity of space robots is the inverse/forward kinematic problem that likewise is a dynamic one [FA+14]. In that matter, different modeling strategies have been developed in function of the SMS applications.

Early studies have focused on performing manipulator maneuvers without moving the satellite base. Additionally to that objective, path-planning approaches have considered singular-free motions. Another particularity of space robots is the possibility of reaching dynamic singularities. A dynamic singularity corresponds to a configuration where the system controllability is lost. Therefore, initial modeling approaches have been established such as the focus was on developing a feasible manipulator motion resulting in a low impact on the base rotations. The VM<sup>4</sup> and DEM<sup>5</sup> modeling methods respectively introduced by Vafa and Dubowsky [VD87] and Liang and al. [LXB97], provided modeling methods inspired by ground-base manipulators. In both approaches, a fixed satellite base is considered to develop a kinematic/dynamic model for control purposes and workspace analysis. A third approach, introduced by Umenati [UY89], is the GJM<sup>6</sup>. Based on a conservation of the kinetic momentum initially null, the GJM allows to express the relation between the manipulator's end-effector and the joints in the Cartesian space. Such expressions are employed for workspace analysis, path-planning and end-effector control for free-floating SMS.

Nevertheless, these first approaches are advantageous for simple manipulator systems and are less adapted to provide solutions to actual robots for which multiple kinematic-chains may be considered. Two main modeling methods are then developed to obtain a kinematic/dynamic model of SMS: the Newton-Euler and the Lagrangian formalism. The Newton-Euler approach, which is a direct interpretation of Newton's second law, formulates that the dynamic model by considering for each body of the system the force and moment applied. The recursivity of the method is a first advantage for its implementation [VL+16]. Moreover, the independent consideration of each body allows more flexibility in the modeling process and leads to the possibility of developing plug-in approaches [ACT08]. Thus, for instance closed-kinematic chains and additional elements connected to the end-effector can be studied. The Lagrangian formalism provides a simpler and systematic modeling method based on the energies and works present in the system. Regarding energies of a space robot, only the kinetic ones are considered which allows by developing a Lagrangian approach to obtain an easier method to derive a dynamic model [Wil+18]. It provides as well a discussion on the system momentum which may be used as a control development start. With rigid systems and assuming no external interactions, the momentum conservation is a means of state parameters estimation to retrieve the physical properties of the SMS [CLNP17].

---

<sup>4</sup>Virtual Manipulator

<sup>5</sup>Dynamically Equivalent Manipulator

<sup>6</sup>Generalised Jacobian Matrix



In this way, it is a common strategy to model a rigid multi-body system evolving in a free fall environment by initiating a Lagrangian formalism. In this chapter, the integration of base actuators is based on the consideration of additional kinematic chains. In that matter, the energetic approach of the Lagrangian formalism provides a simple method to include additional elements to the overall SMS.

### 2.1.1.3 Modeling of flexible appendages

To take an analogy with ground-base robotic manipulators, usual control methods are based on an accurate modeling to linearize and decouple actuators from each other. In that philosophy, integrating the flexible dynamics onto the rigid one developed with a Lagrangian approach would be a notable starting point to develop efficient SMS steering laws.

Nonetheless, flexible modeling represents a challenging task considering the complexity of space structures. From a finite element method, flexible displacement DoFs can be described with a second order transfer function corresponding to a generalized damped spring/masses system. This representation often involves a large number of DoFs which is a primary concern when modeling a spacecraft with flexible elements. Multiple methods have been established to reduce the number of flexible DoFs [LP60]; [Dok72]; [SA08]; [JL21].

With a reduced flexible model for the appendages, integration to the overall rigid SMS is the main challenge. Studies have considered simplistic models based on a flexible beam with a mass at its end such as couplings between the appendage and the satellite base [Hir+13]; [Liu+18]. Newton-Euler approaches are adapted to integrate flexible dynamics as for each body a force/moment is listed so that a connection between two bodies is made with summing forces and torques on the junction. Such methods have been put forward by different authors [RZZ14]; [San+18]. Nevertheless, a drawback of the methods developed in the literature is the consideration of linearized model. Such modeling allows the elaborations of control laws, however it may reduce analysis and simulation applications as linearization are mainly assumed with base velocity limitations.

## 2.1.2 Modeling objectives

Regarding the new needs in SMS uses, different improvements of existing modeling tools are required. A first area of improvements is the need of new control methods of SMS to perform various and longer operations during their exploitation time. In this study, the focus is made on rotation-free-floating spacecrafts on which base rotations are controlled with reaction-wheels. With a preferred Lagrangian formalism, these actuators are included in a multi-body and multi-kinematic chains of a rigid system to describe kinematics/dynamics of rotation-free-floating SMS.

Furthermore integrating flexible bodies raises the main challenges. For control purposes, linear models have been used to synthesized control gains. However, such modeling techniques

lead to develop robust control strategies as hypothesis and uncertainties may be numerous. To be able to limit modeling constraints and hypothesis, in this present work a Lagrangian approach is developed to include SMS's flexible appendages dynamics onto the multi-body rigid ones.

The developed modeling tools should firstly give the possibility of creating fine analysis of a rotation-free-floating SMS with flexible appendages. For this matter, the formalism to derive a kinematic/dynamic model is first detailed based on a Lagrangian approach and with the help of the DH<sup>7</sup> parameters. At the conclusion of this first non-trivial contribution tools to analyze and study the behavior of flying and floating SMS with flexible appendages are introduced. Developed on Matlab-Simulink kinematic and dynamic functions are established to obtain respective direct and inverse models. With Simulink models, time-domain simulations are possible. Discussions on the uses and performances of this tools are provided in the following chapter. The chapter concludes on an illustration of the possible analysis that can be formed with the present tools.

## 2.2 Modeling of a rigid multi-body free-floating SMS

In this section, the rigid multi-body kinematics and dynamics are developed with the objective of describing the behavior of free-floating and free-flying space robots. As previously defined, a kinematic model is the expression of a manipulator's end-effector angular and linear velocities in function of its joints' pose expressed in the robot's frame. The Differential kinematics, or system's dynamic model, is the expression of the relations between accelerations, forces and torques of the system's states. As the Lagrangian formalism provides a simpler and systematic method to derive an SMS dynamic model, in this section the study of a rigid multi-body system with multiple kinematic chains is developed with this approach. Then an extension of the Lagrangian formalism is developed to integrate the flexible dynamics of the SMS appendages. First a general formalism is detailed, based on the Denavit-Hartenberg convention [KK86], to obtain a recursive computation method to derive the dynamics of the multi-kinematic chains robot with a common base. As established by Rocha and al. [RTD11], one of the advantages of the DH convention is the use of a minimal number of the kinematic chain parameter to fully describe its kinematic model.

From the obtained general kinematic/dynamic modeling method, a discussion is developed to adapt it for rotation-free-floating SMS. More particularly for a one-manipulator robot with reaction-wheels to control the spacecraft base rotations.

---

<sup>7</sup>Denavit-Hartenberg

## 2.2.1 Introduction of Denavit-Hartenberg notations

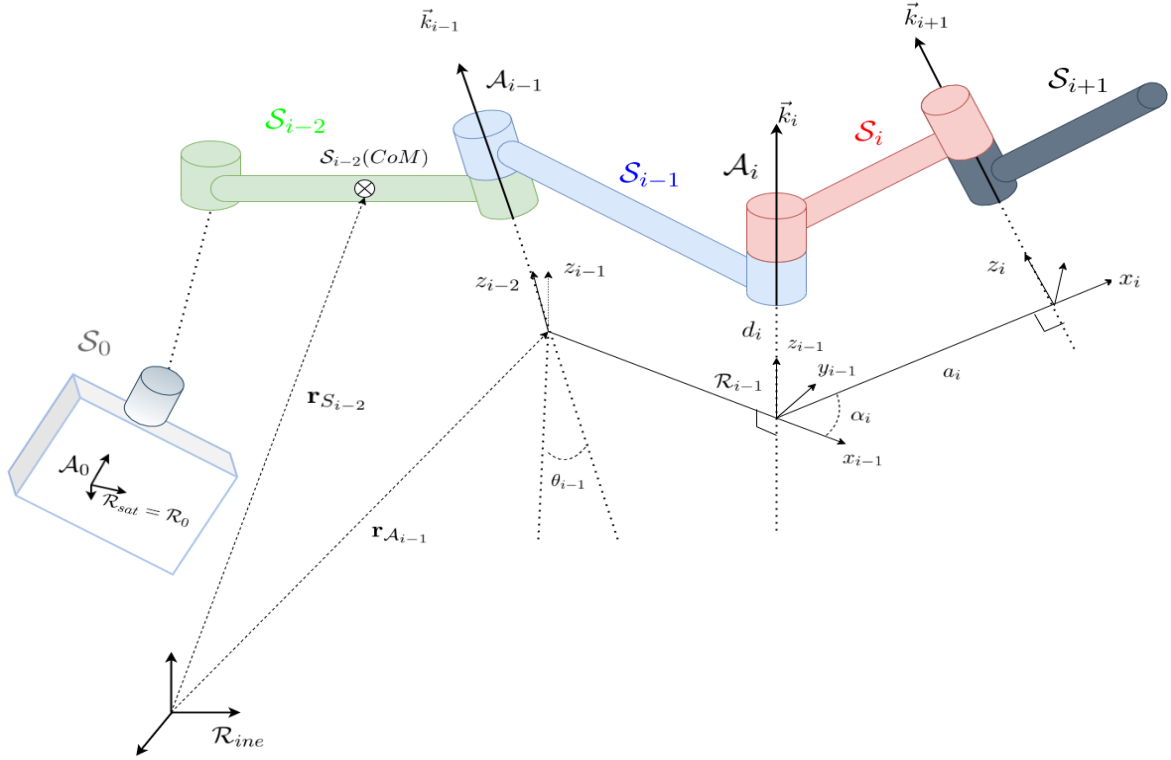


Figure 2.1 – Denavit-Hartenberg parameters

**Reference frames and coordinate transformations** As illustrated with Figure 2.1, a kinematic chain is a series of rigid bodies inter-connected by a joint with one or less DoF. For that reason the DH convention is well suited to develop a kinematic model with a reduced number of four parameters. These parameters are defined for each body with a specific frame that is associated with it, as visualized with Figure 2.1. Therefore a recursive formulation of the kinematic model can be established. Before introducing the DH parameters' identification method, one will define the construction of the multi-kinematic chain system with the following notations. The base is defined as the first rigid solid of the system and referred as  $S_0$ . From the robot's base,  $n_q$  more solids (or links) are considered, with  $n_q \in \mathbb{N}$ . It is assumed that the last solid of a unique kinematic chain system is the  $n_{EE}^{th}$ . In particular, for a single kinematic chain  $n_q = n_{EE}$ . To ease the reading such notations are abusively conserved for multiple kinematic chains with more than one link, the subscript  $EE$  will refer to the last solid of a kinematic chain with more than one DoF. The notation  $S_i$  is used to refer at the  $i^{th}$  solid such that  $i \in [1, n_q]$ . Between the bodies  $S_{i-1}$  and  $S_i$  a connecting joint, denoted  $A_i$ , is either considered fixed, prismatic or revolute. Moreover, for each joint and solid, a Cartesian body frame,  $\mathcal{R}_{i-1} = (O_{i-1}, \vec{x}_{i-1}, \vec{y}_{i-1}, \vec{z}_{i-1})$ , is associated in respect to the following steps:

- The axis  $\vec{z}_{i-1}$  is defined along the axis of joint  $A_i$

- The origin  $O_{i-1}$  corresponds to the intersection between  $z_{i-1}$  and the normal to  $z_{i-2}$  and  $z_{i-1}$  that carries  $\vec{x}_{i-1}$
- The vector  $\vec{y}_{i-1}$  is deduced from the following cross product  $\vec{x}_{i-1} = \vec{z}_{i-1} \times \vec{x}_{i-1}$
- The first Cartesian frame  $\mathcal{R}_0 = (O_0, \vec{x}_0, \vec{y}_0, \vec{z}_0) = \mathcal{R}_{sat}$  is defined such that  $\vec{z}_0$  is along the axis of  $\mathcal{A}_1$ ,  $\vec{x}_0$  and  $\vec{y}_0$  are arbitrarily chosen
- The last frame  $\mathcal{R}_{n_{EE}} = (O_{n_{EE}}, \vec{x}_{n_{EE}}, \vec{y}_{n_{EE}}, \vec{z}_{n_{EE}})$  is defined such that  $\vec{x}_{n_{EE}}$  is normal to the axis of  $\mathcal{A}_{n_{EE}}$ ,  $\vec{z}_{n_{EE}}$  and  $\vec{y}_{n_{EE}}$  are arbitrarily chosen

Then the four DH parameters are defined with these referential frames such as:

- $d_i$  is the distance between  $x_{i-1}$  and  $x_i$  along axis  $\vec{z}_{i-1}$ , it corresponds to a prismatic DoF
- $\theta_i$  is the rotation around  $\vec{z}_i$  between  $\vec{x}_{i-1}$  et  $\vec{x}_i$ , it corresponds to a rotational DoF
- $a_i$  is the distance between  $z_{i-1}$  and  $z_i$  along axis  $\vec{x}_i$ , it corresponds to the common normal of  $\vec{z}_i$  and  $\vec{z}_{i-1}$
- $\alpha_i$  is the rotation around  $\vec{x}_i$  between  $\vec{z}_{i-1}$  and  $\vec{z}_i$

Moreover, the geometry of the SMS with respect to an inertial frame,  $\mathcal{R}_{ine}$ <sup>8</sup>, can be described with the position vector,  $\mathbf{r}_{\mathcal{A}_i} \in \mathbb{R}^{3 \times 1}$ , of each joint  $\mathcal{A}_i$  and the position vector of each CoM<sup>9</sup>,  $\mathbf{r}_{\mathcal{S}_i} \in \mathbb{R}^{3 \times 1}$ , of link  $\mathcal{S}_i$  ( $i \in [0, n_q]$ ). One will note that the choice of considering CoM simplifies the derivation of the kinematic model. With the DH parameters, homogeneous transformations can be defined to recursively express the pose and orientation of the  $i^{th}$  link or joint. For that purpose, the matrix  $\mathbf{T}_{\mathcal{A}_{i-1}, \mathcal{A}_i}$  is introduced as a homogeneous transformation matrix between the frames  $\mathcal{R}_{i-1}$  and  $\mathcal{R}_i$  which applies a rotation and a translation from the first frame to the second. Denoting  $\mathbf{T}_{trans}^x(d)$  a translation matrix along axis  $\vec{x}$  of a distance  $d$  and  $\mathbf{T}_{rot}^x(\theta)$  a rotational matrix around axis  $\vec{x}$  of an angle  $\theta$ , the matrix  $\mathbf{T}_{\mathcal{A}_{i-1}, \mathcal{A}_i}$  is then defined with the DH parameters as:

$$\mathbf{T}_{\mathcal{A}_{i-1}, \mathcal{A}_i} = \mathbf{T}_{trans}^{z_{i-1}}(d_i) \mathbf{T}_{rot}^{z_{i-1}}(\theta_i) \mathbf{T}_{trans}^{x_i}(a_i) \mathbf{T}_{rot}^{x_i}(\alpha_i) \quad (2.1)$$

---

<sup>8</sup>Inertial frame

<sup>9</sup>Center of Mass

with the details of translation and rotational matrices given by:

$$\mathbf{T}_{trans}^{z_{i-1}}(d_i) = \begin{bmatrix} 1 & 0 & 0 & 0 \\ 0 & 1 & 0 & 0 \\ 0 & 0 & 1 & d_i \\ 0 & 0 & 0 & 1 \end{bmatrix} \quad (2.2a)$$

$$\mathbf{T}_{rot}^{z_{i-1}}(\theta_i) = \begin{bmatrix} \cos(\theta_i) & -\sin(\theta_i) & 0 & 0 \\ \sin(\theta_i) & \cos(\theta_i) & 0 & 0 \\ 0 & 0 & 1 & 0 \\ 0 & 0 & 0 & 1 \end{bmatrix} \quad (2.2b)$$

$$\mathbf{T}_{trans}^{x_i}(a_i) = \begin{bmatrix} 1 & 0 & 0 & a_i \\ 0 & 1 & 0 & 0 \\ 0 & 0 & 1 & 0 \\ 0 & 0 & 0 & 1 \end{bmatrix} \quad (2.2c)$$

$$\mathbf{T}_{rot}^{x_i}(\alpha_i) = \begin{bmatrix} 1 & 0 & 0 & 0 \\ 0 & \cos(\alpha_i) & -\sin(\alpha_i) & 0 \\ 0 & \sin(\alpha_i) & \cos(\alpha_i) & 0 \\ 0 & 0 & 0 & 1 \end{bmatrix} \quad (2.2d)$$

Thus, the homogeneous transformation matrix between  $\mathcal{A}_{i-1}$  and  $\mathcal{A}_i$  is given by:

$$\begin{aligned} \mathbf{T}_{\mathcal{A}_{i-1},i} &= \begin{bmatrix} \cos(\theta_i) & -\cos(\alpha_i)\sin(\theta_i) & \sin(\alpha_i)\sin(\theta_i) & a_i\cos(\theta_i) \\ \sin(\theta_i) & \cos(\theta_i)\cos(\alpha_i) & -\cos(\theta_i)\sin(\alpha_i) & a_i\sin(\theta_i) \\ 0 & \sin(\alpha_i) & \cos(\alpha_i) & d_i \\ 0 & 0 & 0 & 1 \end{bmatrix} \\ &= \begin{bmatrix} \mathbf{R}_{\mathcal{A}_i} & (\mathbf{r}_{\mathcal{A}_i} - \mathbf{r}_{\mathcal{A}_{i-1}}) \\ \mathbf{0}_{1 \times 3} & 1 \end{bmatrix} \end{aligned} \quad (2.3)$$

where one can distinguish the rotation and translation. The translation is defined by the position,  $\mathbf{r}_{\mathcal{A}_i}$ , of the joint  $\mathcal{A}_i$  in  $\mathcal{R}_{ine}$  and the rotation is given by the DCM<sup>10</sup>,  $\mathbf{R}_{\mathcal{A}_i} \in \mathbb{R}^{3 \times 3}$ , between  $\mathcal{A}_{i-1}$  and  $\mathcal{A}_i$  that gives the direction of the rotation of  $\mathcal{A}_i$  according to the previous joint.

A similar operation can be defined to describe the homogeneous transformation between the links  $\mathcal{S}_{i-1}$  and  $\mathcal{S}_i$ . The frame  $\mathcal{R}_{\mathcal{S}_{i-1}}$  attached to the solid  $\mathcal{S}_{i-1}$  is defined such as its origin  $\mathcal{O}_{\mathcal{S}_{i-1}}$  corresponds to the CoM of  $\mathcal{S}_{i-1}$ ,  $\mathbf{r}_{\mathcal{S}_i}$ , and its axis are collinear to the ones defining the frame  $\mathcal{R}_{\mathcal{A}_i}$ . In particular, the origin of the Cartesian base frame  $\mathcal{R}_{sat}$ <sup>11</sup> is chosen such as  $\mathbf{r}_{\mathcal{S}_i} = \mathbf{r}_{\mathcal{A}_0}$ . Therefore, the homogeneous transformation matrix between the links  $\mathcal{S}_{i-1}$  and  $\mathcal{S}_i$  is given with the DH parameters and (2.3) as:

$$\mathbf{T}_{\mathcal{S}_{i-1},\mathcal{S}_i} = \begin{bmatrix} \mathbf{R}_{\mathcal{S}_i} & (\mathbf{r}_{\mathcal{S}_i} - \mathbf{r}_{\mathcal{S}_{i-1}}) \\ \mathbf{0}_{1 \times 3} & 1 \end{bmatrix} = \begin{bmatrix} \mathbf{R}_{\mathcal{A}_{i+1}} & (\mathbf{r}_{\mathcal{S}_i} - \mathbf{r}_{\mathcal{S}_{i-1}}) \\ \mathbf{0}_{1 \times 3} & 1 \end{bmatrix} \quad (2.4)$$

<sup>10</sup>Direction cosine-matrix

<sup>11</sup>Satellite frame

The rotations of the link  $\mathcal{S}_i$  and the joint  $\mathcal{A}_{i+1}$  are identical, as visualized with Figure 2.1, which leads to the equality  $\mathbf{R}_{\mathcal{S}_i} = \mathbf{R}_{\mathcal{A}_{i+1}}$ .

Finally, a homogeneous transformation matrix from  $\mathcal{S}_i$  to  $\mathcal{A}_{i+1}$ ,  $\mathbf{T}_{\mathcal{S}_i, \mathcal{A}_{i+1}}$ , is given by:

$$\mathbf{T}_{\mathcal{S}_i, \mathcal{A}_{i+1}} = \begin{bmatrix} \mathbf{R}_{\mathcal{A}_{i+1}} & (\mathbf{r}_{\mathcal{A}_{i+1}} - \mathbf{r}_{\mathcal{S}_i}) \\ \mathbf{0}_{1 \times 3} & 1 \end{bmatrix} \quad (2.5)$$

Moreover, to express in the decreasing recursive order the homogeneous transformation from  $\mathcal{A}_i$  to  $\mathcal{A}_{i-1}$ , the following relation is given by:

$$\mathbf{T}_{\mathcal{A}_i, \mathcal{A}_{i-1}} = \mathbf{T}_{\mathcal{A}_{i-1}, \mathcal{A}_i}^{-1} = \begin{bmatrix} \mathbf{R}_{\mathcal{A}_i}^T & -\mathbf{R}_{\mathcal{A}_i}^T (\mathbf{r}_{\mathcal{A}_i} - \mathbf{r}_{\mathcal{A}_{i-1}}) \\ \mathbf{0}_{1 \times 3} & 1 \end{bmatrix} \quad (2.6)$$

For some control purposes, it may be interesting to express the base DCM in function of Euler angles,  $[\phi \ \theta \ \psi]^T$  (roll  $\phi$ , pitch  $\theta$ , yaw  $\psi$ ). With the following rotation sequence  $z - y - x$ , the base DCM is given as:

$$\begin{aligned} \mathbf{R}_{\mathcal{S}_0} = \mathbf{R}_{\mathcal{A}_0} &= \begin{bmatrix} \cos(\psi) & -\sin(\psi) & 0 \\ \sin(\psi) & \cos(\psi) & 0 \\ 0 & 0 & 1 \end{bmatrix} \begin{bmatrix} \cos(\theta) & 0 & \sin(\theta) \\ 0 & 1 & 0 \\ -\sin(\theta) & 0 & \cos(\theta) \end{bmatrix} \begin{bmatrix} 1 & 0 & 0 \\ 0 & \cos(\phi) & -\sin(\phi) \\ 0 & \sin(\phi) & \cos(\phi) \end{bmatrix} \\ &= \begin{bmatrix} \cos(\psi)\cos(\theta) & \cos(\psi)\sin(\theta)\sin(\phi) - \sin(\psi)\cos(\phi) & \sin(\psi)\sin(\theta) + \cos(\psi)\sin(\theta)\cos(\phi) \\ \sin(\psi)\cos(\theta) & \cos(\psi)\sin(\phi) + \sin(\psi)\sin(\theta)\sin(\phi) & -\cos(\psi)\sin(\phi) + \sin(\psi)\sin(\theta)\cos(\phi) \\ -\sin(\theta) & \cos(\theta)\sin(\phi) & \cos(\theta)\cos(\phi) \end{bmatrix} \end{aligned} \quad (2.7)$$

Moreover, the interest of using the DH formalism relies in the recursivity to express a body state. Denoting  $\mathbf{T}_{\mathcal{A}_i, \mathcal{R}_{ine}}$  and  $\mathbf{T}_{\mathcal{S}_i, \mathcal{R}_{ine}}$  respectively the transformation of joint  $\mathcal{A}_i$  and body  $\mathcal{S}_i$  expressed in  $\mathcal{R}_{ine}$ , with the DCM a recursive overall transformation is obtained as:

$$\begin{cases} \mathbf{T}_{\mathcal{A}_0, \mathcal{R}_{ine}} = \mathbf{T}_{\mathcal{S}_0, \mathcal{R}_{ine}} & (2.8a) \end{cases}$$

$$\begin{cases} \mathbf{T}_{\mathcal{A}_1, \mathcal{R}_{ine}} = \mathbf{T}_{\mathcal{S}_0, \mathcal{R}_{ine}} \mathbf{T}_{\mathcal{A}_1, \mathcal{S}_0} = \mathbf{T}_{\mathcal{A}_0, \mathcal{R}_{ine}} \mathbf{T}_{\mathcal{A}_1, \mathcal{A}_0} & (2.8b) \end{cases}$$

$$\begin{cases} \mathbf{T}_{\mathcal{A}_i, \mathcal{R}_{ine}} = \mathbf{T}_{\mathcal{A}_{i-1}, \mathcal{R}_{ine}} \mathbf{T}_{\mathcal{A}_{i-1}, \mathcal{A}_i} = \mathbf{T}_{\mathcal{A}_1, \mathcal{R}_{ine}} \prod_{j=2}^i \mathbf{T}_{\mathcal{A}_{j-1}, \mathcal{A}_j}, \forall i \in [2, n_q] & (2.8c) \end{cases}$$

$$\begin{cases} \mathbf{T}_{\mathcal{S}_i, \mathcal{R}_{ine}} = \mathbf{T}_{\mathcal{A}_i, \mathcal{R}_{ine}} \mathbf{T}_{\mathcal{A}_i, \mathcal{S}_i}, \forall i \in [2, n_q] & (2.8d) \end{cases}$$

One will note that the transformation  $\mathbf{T}_{\mathcal{A}_i, \mathcal{R}_{ine}}$  is composed of the overall DCM of the joint  $\mathcal{A}_i$  expressed in the  $\mathcal{R}_{ine}$ ,  $\mathbf{R}_{\mathcal{A}_i, \mathcal{R}_{ine}}$ , and its position given in  $\mathcal{R}_{ine}$ . This DCM is used to derive the direction of the joint rotation,  $\mathbf{k}_i$ , in the inertial frame as:

$$\mathbf{k}_i = \mathbf{R}_{\mathcal{A}_i, \mathcal{R}_{ine}} \begin{bmatrix} 0 \\ 0 \\ 1 \end{bmatrix} = \mathbf{R}_{\mathcal{A}_0} \prod_{j=1}^i \mathbf{R}_{\mathcal{A}_j} \begin{bmatrix} 0 \\ 0 \\ 1 \end{bmatrix} \quad (2.9)$$

To produce the kinematic model, for each body a mass  $m_i$  ( $i \in [0, n_q]$ ) and an associated inertia  $\mathcal{I}_{\mathcal{S}_i}$  ( $i \in [0, n_q]$ ) expressed in the corresponding body frame are defined. With (2.9), the inertias can be expressed in  $\mathcal{R}_{ine}$ , denoted  $\mathcal{I}_i$  such that:

$$\mathcal{I}_i = \mathbf{R}_{\mathcal{S}_i, \mathcal{R}_{ine}} \mathcal{I}_{\mathcal{S}_i} \mathbf{R}_{\mathcal{S}_i, \mathcal{R}_{ine}}^T \quad (2.10)$$

Denoting  $m_{tot}$  the total mass of the system, the CoM position in  $\mathcal{R}_{ine}$  is expressed in function of each body CoM poses,  $\mathbf{r}_{\mathcal{S}_i}$ , such as:

$$\mathbf{r}_{CoM} = \frac{\sum_{i=0}^{n_q} m_i \mathbf{r}_{\mathcal{S}_i}}{\sum_{i=0}^{n_q} m_i} = \frac{\sum_{i=0}^{n_q} m_i \mathbf{r}_{\mathcal{S}_i}}{m_{tot}} \quad (2.11)$$

Additionally, a recursive expression of the links CoM can be developed as:

$$\mathbf{r}_{\mathcal{S}_i} = \mathbf{r}_{\mathcal{S}_0} + \sum_{j=1}^i (\mathbf{r}_{\mathcal{S}_j} - \mathbf{r}_{\mathcal{S}_{j-1}}), \forall i \in [0, n_q] \quad (2.12)$$

With the DH formalism introduced in this section, expressions of pose and orientation of each element composing a multi-body system with one or more kinematic chain can be obtained with recursivity. The homogeneous transformations between two solids/joints are given in function of the system's DoFs and more generally in function of the nature of the junctions.

## 2.2.2 Velocities and accelerations

In order to describe system velocities, twist vectors are introduced. The twist vector,  $\mathbf{t}_i$ , of the  $i^{th}$  body gathers the angular and linear velocity both expressed in  $\mathcal{R}_{ine}$  and respectively denoted  $\boldsymbol{\omega}_i \in \mathbb{R}^{3 \times 1}$  and  $\dot{\mathbf{r}}_{\mathcal{S}_i} \in \mathbb{R}^{3 \times 1}$ . Therefore,  $\forall i \in [0, n_q]$  the twist of  $\mathcal{S}_i$  is expressed as:

$$\mathbf{t}_i = \begin{bmatrix} \boldsymbol{\omega}_i \\ \dot{\mathbf{r}}_{\mathcal{S}_i} \end{bmatrix}, \forall i \in [0, n_q] \quad (2.13)$$

To develop the kinematic model, the twist expression is given in function of the joint-space velocities. In that matter a generalized joint rate-variables vector,  $\dot{\mathbf{q}} = [\dot{\mathbf{q}}_0^T \ \dots \ \dot{q}_{n_q}]^T \in \mathbb{R}^{(6+n_q) \times 1}$ , is introduced such as  $\dot{\mathbf{q}}_0 \in \mathbb{R}^{6 \times 1}$  is the base linear and angular velocity joint state and  $\forall i \in [1, n_q]$ ,  $\dot{q}_i \in \mathbb{R}$  is the velocity state of the  $i^{th}$  DoF in the kinematic chain(s). In addition, with the DH parameters, one can define  $\forall i \in [1, n_q]$ ,  $\dot{\mathbf{q}}_i$  as:

- $\dot{q}_i = \dot{\theta}_i$  if  $\mathcal{A}_i$  is a rotational joint

- $\dot{q}_i = \dot{d}_i$  if  $\mathcal{A}_i$  is a prismatic joint

The joint-space is defined in function of the nature of the junctions and thus the system's DoFs.

One will note, motivated by control purposes, that the spacecraft angular velocity is preferably expressed in its body frame,  $\mathcal{R}_{sat}$ . Defining  $\dot{\mathbf{q}}_0$  such as  $\dot{\mathbf{q}}_0 = [\boldsymbol{\omega}_0^{satT} \ \dot{\mathbf{r}}_{\mathcal{S}_0}^T]^T$ , with the angular velocity expressed in  $\mathcal{R}_{sat}$  and linear velocity in  $\mathcal{R}_{ine}$ . Its expression allows to obtain the base's twist,  $\mathbf{t}_0$ , expressed in  $\mathcal{R}_{ine}$  operating a base transformation with the matrix  $\mathbf{P}_0$  as:

$$\mathbf{t}_0 = \begin{bmatrix} \boldsymbol{\omega}_0 \\ \dot{\mathbf{r}}_{\mathcal{S}_0} \end{bmatrix} = \begin{bmatrix} \mathbf{R}_{\mathcal{S}_0} & \mathbf{0}_3 \\ \mathbf{0}_3 & \mathbf{I}_3 \end{bmatrix} \begin{bmatrix} \boldsymbol{\omega}_0^{sat} \\ \dot{\mathbf{r}}_{\mathcal{S}_0} \end{bmatrix} = \mathbf{P}_0 \dot{\mathbf{q}}_0 \quad (2.14)$$

One will note that if not specified, all velocities and pose are expressed in  $\mathcal{R}_{ine}$ .

Furthermore, to distinguish a DoF of a kinematic chain from the base's, the joint rate-variables are gathered in another joint-rate-variables vector  $\dot{\mathbf{q}}_m \in \mathbb{R}^{n_q \times 1}$  such as  $\dot{\mathbf{q}}_m = [\dot{q}_1 \ \dot{q}_{n_q}]^T$ .

Defining  $\mathbf{t} = [\mathbf{t}_0^T \ \dots \ \mathbf{t}_{n_q}^T]^T \in \mathbb{R}^{n_q \times 1}$ , the generalized twist vector, a velocity transformation between the task space and the joint space is defined as [AL88]:

$$\mathbf{t} = \begin{bmatrix} \mathbf{I}_6 & \mathbf{0}_6 & \dots & \mathbf{0}_6 \\ \mathbf{B}_{10} & \mathbf{I}_6 & \dots & \mathbf{0}_6 \\ \vdots & \vdots & \ddots & \vdots \\ \mathbf{B}_{n_q 0} & \mathbf{B}_{n_q 1} & \dots & \mathbf{I}_6 \end{bmatrix} \begin{bmatrix} \mathbf{P}_0 & \mathbf{0}_6 & \dots & \mathbf{0}_6 \\ \mathbf{0}_6 & \mathbf{p}_{m_1} & \dots & \mathbf{0}_6 \\ \vdots & \vdots & \ddots & \vdots \\ \mathbf{0}_6 & \mathbf{0}_6 & \dots & \mathbf{p}_{m_{n_q}} \end{bmatrix} \dot{\mathbf{q}} = \mathbf{N}_B \mathbf{N}_p \dot{\mathbf{q}} = \mathbf{N}(\mathbf{q}) \dot{\mathbf{q}} \quad (2.15)$$

with:

- $\mathbf{B}_{kj} = \begin{bmatrix} \mathbf{I}_3 & \mathbf{0}_3 \\ (\mathbf{r}_{\mathcal{S}_k} - \mathbf{r}_{\mathcal{S}_j})^\times & \mathbf{I}_3 \end{bmatrix} \in \mathbb{R}^{6 \times 6}$ , if  $\mathcal{S}_k$  and  $\mathcal{S}_j$  are in the same kinematic chain
- $\mathbf{B}_{kj} = \mathbf{0}_6$ , if  $\mathcal{S}_k$  and  $\mathcal{S}_j$  are in different kinematic chains
- $\mathbf{p}_{m_k} = \begin{bmatrix} \mathbf{k}_k \\ \mathbf{k}_k \times (\mathbf{r}_{\mathcal{S}_k} - \mathbf{r}_{\mathcal{A}_k}) \end{bmatrix} \in \mathbb{R}^{6 \times 1}$ , if  $\mathcal{A}_k$  is a revolute joint
- $\mathbf{p}_{m_k} = \begin{bmatrix} \mathbf{0}_{3 \times 1} \\ \mathbf{k}_k \end{bmatrix} \in \mathbb{R}^{6 \times 1}$ , if  $\mathcal{A}_k$  is a prismatic joint
- $\mathbf{p}_{m_k} = \mathbf{0}_{6 \times 1}$ , if  $\mathcal{A}_k$  is a fixed joint

where  $\mathbf{x}^\times$  refers to the skew-symmetric matrix <sup>12</sup> of vector  $\mathbf{x} \in \mathbb{R}^{3 \times 1}$ ,  $\mathbf{p}_{m_k}$  is the twist

$${}^{12}\mathbf{x}^\times = \begin{bmatrix} x_1 \\ x_2 \\ x_3 \end{bmatrix}^\times = \begin{bmatrix} 0 & -x_3 & x_2 \\ x_3 & 0 & -x_1 \\ -x_2 & x_1 & 0 \end{bmatrix}$$



propagation vector,  $\mathbf{B}_{ij}$  is the twist propagation matrix and  $\mathbf{N}$  is the velocity transformation matrix. Its expression is function of the geometry and configuration of the system.

The matrix  $\mathbf{N}$  can be decoupled into a lower and an upper triangular block matrix [VL+16]. Moreover, one will put the attention on the proposed formalism that allows to consider multiple kinematic chains with a common base thanks to vectors  $\mathbf{p}_{m_k}$  and matrices  $\mathbf{B}_{kj}$ . Furthermore, to benefit from the recursivity offered by the formalism, from (2.15) the twist expression can be expressed as:

$$\begin{cases} \mathbf{t}_0 = \mathbf{P}_0 \dot{\mathbf{q}}_0 & (2.16a) \\ \mathbf{t}_i = \mathbf{B}_{i0} \mathbf{P}_0 \dot{\mathbf{q}}_0 + \sum_{k=1}^{i-1} (\mathbf{B}_{ik} \mathbf{p}_{m_k} \dot{q}_k) + \mathbf{p}_{m_i} \dot{q}_i & (2.16b) \end{cases}$$

In space robotics, and more largely for robots that involve multi-body kinematic chains, the term Jacobian is employed to refer the transformation matrix between a body twist, or the twist of a point in the kinematic chain considered, and the generalized joint rate-variables vector. With the rows of  $\mathbf{N}$ , the twist of the  $i^{th}$  body in the kinematic chain is given in function of the Jacobian matrix,  $\mathbf{J}_i \in \mathbb{R}^{6 \times (6+n_q)}$ , by:

$$\mathbf{t}_i = \begin{bmatrix} \mathbf{B}_{i0} \mathbf{P}_0 & \mathbf{B}_{i1} \mathbf{p}_{m_1} & \dots & \mathbf{B}_{i(i-1)} \mathbf{p}_{m_{i-1}} & \mathbf{p}_{m_i} \end{bmatrix} \dot{\mathbf{q}} = \mathbf{J}_i \dot{\mathbf{q}} \quad (2.17)$$

Likewise,  $\mathbf{J}_i$  can be decomposed into a Jacobian,  $\mathbf{J}_{0_i} \in \mathbb{R}^{6 \times 6}$ , for the base contribution on  $\mathbf{t}_i$  and a second Jacobian,  $\mathbf{J}_{m_i} \in \mathbb{R}^{6 \times n_q}$ , for the kinematic chain(s) DoF contributions. This allows to re-write (2.17),  $\forall i \in [1, n_q - 1]$ :

$$\begin{aligned} \mathbf{t}_i &= \mathbf{B}_{i0} \mathbf{P}_0 \dot{\mathbf{q}}_0 + \begin{bmatrix} \mathbf{B}_{i1} \mathbf{p}_{m_1} & \dots & \mathbf{B}_{i(i-1)} \mathbf{p}_{m_{i-1}} & \mathbf{p}_{m_i} \mathbf{0}_{6 \times (n_q - i)} \end{bmatrix} \begin{bmatrix} \dot{q}_1 \\ \vdots \\ \dot{q}_{n_q} \end{bmatrix} \\ &= \mathbf{J}_{0_i} \dot{\mathbf{q}}_0 + \mathbf{J}_{m_i} \dot{\mathbf{q}}_m \end{aligned} \quad (2.18)$$

and for  $i = n_q$ , the Jacobian  $\mathbf{J}_{m_{n_q}} = \begin{bmatrix} \mathbf{B}_{n_q 1} \mathbf{p}_{m_1} & \dots & \mathbf{B}_{n_q (n_q - 1)} \mathbf{p}_{m_{n_q - 1}} & \mathbf{p}_{m_{n_q}} \end{bmatrix}$ .

For the particular case of a single kinematic chain, the twist  $\mathbf{t}_{EE}$  associated to the end-effector (or the last body of the kinematic chain) can be expressed in function of the base and actuators states adapting (2.18). In case of a single kinematic chain, the twist,  $\mathbf{t}_{EE}$ , of the last body in the chain which is referred as the end-effector, is given as:

$$\begin{aligned} \mathbf{t}_{EE} &= \begin{bmatrix} \boldsymbol{\omega}_{EE} \\ \dot{\mathbf{r}}_{EE} \end{bmatrix} = \mathbf{B}_{n_{EE} 0} \mathbf{P}_0 \dot{\mathbf{q}}_0 + \begin{bmatrix} \mathbf{B}_{n_{EE} 1} \mathbf{p}_{m_1} & \dots & \mathbf{B}_{n_{EE} (n_{EE} - 1)} \mathbf{p}_{m_{n_{EE} - 1}} & \mathbf{p}_{m_{n_{EE}}} \end{bmatrix} \begin{bmatrix} \dot{q}_1 \\ \vdots \\ \dot{q}_{n_{EE}} \end{bmatrix} \\ &= \mathbf{J}_{0_{EE}} \dot{\mathbf{q}}_0 + \mathbf{J}_{m_{EE}} \dot{\mathbf{q}}_m \end{aligned} \quad (2.19)$$

Accelerations of the system are recursively obtained with the time-derivative of the twist

vector (2.18) such that  $\forall i \in [1, n_q]$ :

$$\dot{\mathbf{t}}_i = \dot{\mathbf{J}}_{0_i} \dot{\mathbf{q}}_0 + \mathbf{J}_{0_i} \ddot{\mathbf{q}}_0 + \dot{\mathbf{J}}_{m_i} \dot{\mathbf{q}}_m + \mathbf{J}_{m_i} \ddot{\mathbf{q}}_m \quad (2.20)$$

where:

$$\dot{\mathbf{J}}_{0_i} = \begin{bmatrix} \mathbf{I}_3 & \mathbf{0}_3 \\ (\mathbf{r}_{S_0} - \mathbf{r}_{S_i})^\times & \mathbf{I}_3 \end{bmatrix} \boldsymbol{\Omega}_0 \mathbf{P}_0 + \dot{\mathbf{B}}_{i0} \mathbf{P}_0 \quad (2.21a)$$

$$\boldsymbol{\Omega}_0 = \begin{bmatrix} \boldsymbol{\omega}_0^\times & \mathbf{0}_3 \\ \mathbf{0}_3 & \mathbf{0}_3 \end{bmatrix}$$

$$\dot{\mathbf{B}}_{kj} = \begin{bmatrix} \mathbf{0}_3 & \mathbf{0}_3 \\ (\dot{\mathbf{r}}_{S_k} - \dot{\mathbf{r}}_{S_j})^\times & \mathbf{0}_3 \end{bmatrix} \quad (2.21b)$$

$$\dot{\mathbf{J}}_{m_i} = [\dot{\mathbf{J}}_{m_i,1} \quad \dots \quad \dot{\mathbf{J}}_{m_i,k} \quad \dots \quad \dot{\mathbf{J}}_{m_i,n_q}] \quad (2.21c)$$

$$\dot{\mathbf{J}}_{m_i,k} = \begin{bmatrix} \mathbf{I}_3 & \mathbf{0}_3 \\ (\mathbf{r}_{S_k} - \mathbf{r}_{S_i})^\times & \mathbf{I}_3 \end{bmatrix} \boldsymbol{\Omega}_k \mathbf{P}_{m_k} + \dot{\mathbf{B}}_{ki} \mathbf{P}_{m_k} \quad (2.21d)$$

$$\boldsymbol{\Omega}_k = \begin{bmatrix} \boldsymbol{\omega}_k^\times & \mathbf{0}_3 \\ \mathbf{0}_3 & \boldsymbol{\omega}_k^\times \end{bmatrix} \quad (2.21e)$$

### 2.2.3 Multi-body system dynamics

After expressing the system's velocities and accelerations in the previous section with a recursive formalism developed thanks to the DH parameters, a dynamic model is derived in this section. With a Lagrange approach, the recursivity is taken advantage of associating for each body an energy and then to derive the equations of motions of a rigid multi-body with multi-kinematic chains and a common base evolving on-orbit.

The Lagrangian,  $\mathcal{L}$ , expresses the difference of the system's kinetic energy,  $\mathcal{T}$ , and its potential energy,  $\mathcal{V}$ , as:

$$\mathcal{L} = \mathcal{T} - \mathcal{V} \quad (2.22)$$

In this study and commonly in such context [Wil+18], it is assumed that the effect of Earth (gravity gradient and free-fall environment) on the robotic system are neglected which leads to no potential energy (i.e.  $\mathcal{V} = 0$ ). Thus the evaluation of the Lagrangian (2.22) is reduced to the evaluation of the system's kinetic energy. For each body, the kinetic energy expressed in  $\mathcal{R}_{ine}$  is the sum of a rotational energy and a translation one such as:

$$\begin{aligned} \mathcal{L} = \mathcal{T} &= \frac{1}{2} \sum_{i=0}^{n_q} \left( \boldsymbol{\omega}_i^T \mathcal{I}_i \boldsymbol{\omega}_i + m_i \dot{\mathbf{r}}_{S_i}^T \dot{\mathbf{r}}_{S_i} \right) \\ &= \frac{1}{2} \mathbf{t}_0^T \begin{bmatrix} \mathcal{I}_0 & \mathbf{0}_3 \\ \mathbf{0}_3 & m_0 \mathbf{I}_3 \end{bmatrix} \mathbf{t}_0 + \frac{1}{2} \sum_{i=1}^{n_q} \left( \mathbf{t}_i^T \begin{bmatrix} \mathcal{I}_i & \mathbf{0}_3 \\ \mathbf{0}_3 & m_i \mathbf{I}_3 \end{bmatrix} \mathbf{t}_i \right) \end{aligned} \quad (2.23)$$

With the twist expression (2.18), (2.23) is re-written as:

$$\begin{aligned}
 \mathcal{L} &= \frac{1}{2} \mathbf{t}_0^T \begin{bmatrix} \mathcal{I}_0 & \mathbf{0}_3 \\ \mathbf{0}_3 & m_0 \mathbf{I}_3 \end{bmatrix} \mathbf{t}_0 + \frac{1}{2} \sum_{i=1}^{n_q} \left( \mathbf{t}_i^T \begin{bmatrix} \mathcal{I}_i & \mathbf{0}_3 \\ \mathbf{0}_3 & m_i \mathbf{I}_3 \end{bmatrix} \mathbf{t}_i \right) \\
 &= \frac{1}{2} \mathbf{t}_0^T \left( \begin{bmatrix} \mathcal{I}_0 & \mathbf{0}_3 \\ \mathbf{0}_3 & m_0 \mathbf{I}_3 \end{bmatrix} + \left( \sum_{i=1}^{n_q} \mathbf{B}_{i0}^T \begin{bmatrix} \mathcal{I}_i & \mathbf{0}_3 \\ \mathbf{0}_3 & m_i \mathbf{I}_3 \end{bmatrix} \mathbf{B}_{i0} \right) \right) \mathbf{t}_0 \\
 &+ \frac{1}{2} \left( \mathbf{t}_0^T \left( \sum_{i=1}^{n_q} \mathbf{B}_{i0}^T \begin{bmatrix} \mathcal{I}_i & \mathbf{0}_3 \\ \mathbf{0}_3 & m_i \mathbf{I}_3 \end{bmatrix} \mathbf{J}_{m_i} \right) \dot{\mathbf{q}}_m + \dot{\mathbf{q}}_m^T \left( \sum_{i=1}^{n_q} \mathbf{J}_{m_i}^T \begin{bmatrix} \mathcal{I}_i & \mathbf{0}_3 \\ \mathbf{0}_3 & m_i \mathbf{I}_3 \end{bmatrix} \mathbf{B}_{i0} \right) \mathbf{t}_0 \right) \\
 &+ \frac{1}{2} \dot{\mathbf{q}}_m^T \left( \sum_{i=1}^{n_q} \mathbf{J}_{m_i}^T \begin{bmatrix} \mathcal{I}_i & \mathbf{0}_3 \\ \mathbf{0}_3 & m_i \mathbf{I}_3 \end{bmatrix} \mathbf{J}_{m_i} \right) \dot{\mathbf{q}}_m
 \end{aligned} \tag{2.24}$$

which can be expressed in a compact form as:

$$\mathcal{L} = \frac{1}{2} \begin{bmatrix} \mathbf{t}_0^T & \dot{\mathbf{q}}_m^T \end{bmatrix} \begin{bmatrix} \mathbf{M}_0 & \mathbf{M}_{0m} \\ \mathbf{M}_{0m}^T & \mathbf{M}_m \end{bmatrix} \begin{bmatrix} \mathbf{t}_0 \\ \dot{\mathbf{q}}_m \end{bmatrix} = \frac{1}{2} \begin{bmatrix} \mathbf{t}_0^T & \dot{\mathbf{q}}_m^T \end{bmatrix} \mathbf{M}(\mathbf{x}_0, \mathbf{q}_m) \begin{bmatrix} \mathbf{t}_0 \\ \dot{\mathbf{q}}_m \end{bmatrix} \tag{2.25}$$

with  $\mathbf{x}_0$  the state vector composed of the base rotation DoF,  $\boldsymbol{\theta}_0$ , and position in the inertial frame such that  $\mathbf{x}_0 = [\boldsymbol{\theta}_0 \quad \mathbf{r}_{S_0}^T]^T$ . The detail of matrices composing  $\mathbf{M}$  is given as:

$$\begin{cases} \mathbf{M}_0 = \begin{bmatrix} \mathcal{I}_0 & \mathbf{0}_3 \\ \mathbf{0}_3 & m_0 \mathbf{I}_3 \end{bmatrix} + \sum_{i=1}^{n_q} \mathbf{B}_{i0}^T \begin{bmatrix} \mathcal{I}_i & \mathbf{0}_3 \\ \mathbf{0}_3 & m_i \mathbf{I}_3 \end{bmatrix} \mathbf{B}_{i0} & (2.26a) \\ \mathbf{M}_{0m} = \sum_{i=1}^{n_q} \mathbf{B}_{i0}^T \begin{bmatrix} \mathcal{I}_i & \mathbf{0}_3 \\ \mathbf{0}_3 & m_i \mathbf{I}_3 \end{bmatrix} \mathbf{J}_{m_i} & (2.26b) \\ \mathbf{M}_m = \sum_{i=1}^{n_q} \mathbf{J}_{m_i}^T \begin{bmatrix} \mathcal{I}_i & \mathbf{0}_3 \\ \mathbf{0}_3 & m_i \mathbf{I}_3 \end{bmatrix} \mathbf{J}_{m_i} & (2.26c) \end{cases}$$

The matrix  $\mathbf{M}(\mathbf{x}_0, \mathbf{q}_m)$  corresponds to the system's inertia matrix expressed in  $\mathcal{R}_{ine}$ , which by construction is defined positive and symmetric. Its evaluation depends on the configuration of the system as well as the base orientation and position in  $\mathcal{R}_{ine}$ . It is composed of the base's inertia,  $\mathbf{M}_0 \in \mathbb{R}^{6 \times 6}$ , the links' inertia  $\mathbf{M}_m \in \mathbb{R}^{n_q \times n_q}$  and coupling inertia matrix between the kinematic chain(s) and the base  $\mathbf{M}_{0m} \in \mathbb{R}^{6 \times n_q}$ .

From a general stand point, one can introduce for the 6-DoFs base a control force/torque vector,  $\boldsymbol{\tau}_0 \in \mathbb{R}^{6 \times 1}$ , as well as an external force/torque vector,  $\boldsymbol{\tau}_{ext_0} \in \mathbb{R}^{6 \times 1}$ , that applies on the base. Similarly for the  $n_q$  joints, a control force/torque vector,  $\boldsymbol{\tau}_{q_m} \in \mathbb{R}^{n_q \times 1}$ , and an external force/torque vector,  $\boldsymbol{\tau}_{ext_m} \in \mathbb{R}^{n_q \times 1}$ , can be introduced. The system equation of

motions are obtained by evaluating the Euler-Lagrange equation on each DoF as:

$$\left\{ \begin{array}{l} \frac{d}{dt} \left( \frac{\partial \mathcal{T}}{\partial \dot{\mathbf{t}}_0} \right) - \frac{\partial \mathcal{T}}{\partial \mathbf{x}_0} = \boldsymbol{\tau}_0 + \boldsymbol{\tau}_{ext_0} \end{array} \right. \quad (2.27a)$$

$$\left\{ \begin{array}{l} \frac{d}{dt} \left( \frac{\partial \mathcal{T}}{\partial \dot{\mathbf{q}}_m} \right) - \frac{\partial \mathcal{T}}{\partial \mathbf{q}_m} = \boldsymbol{\tau}_{q_m} + \boldsymbol{\tau}_{ext_m} \end{array} \right. \quad (2.27b)$$

With (2.25) and the symmetric properties of  $\mathbf{M}(\mathbf{x}_0, \mathbf{q}_m)$ , the partial derivative expressions are given as:

$$\left\{ \begin{array}{l} \frac{\partial \mathcal{T}}{\partial \dot{\mathbf{t}}_0} = \frac{1}{2} (\mathbf{M}_0^T + \mathbf{M}_0) \dot{\mathbf{t}}_0 + \mathbf{M}_{0m} \dot{\mathbf{q}}_m = \mathbf{M}_0 \dot{\mathbf{t}}_0 + \mathbf{M}_{0m} \dot{\mathbf{q}}_m \end{array} \right. \quad (2.28a)$$

$$\left\{ \begin{array}{l} \frac{\partial \mathcal{T}}{\partial \dot{\mathbf{q}}_m} = \frac{1}{2} (\mathbf{M}_m^T + \mathbf{M}_m) \dot{\mathbf{q}}_m + \frac{1}{2} (\dot{\mathbf{t}}_0^T \mathbf{M}_{0m})^T + \frac{1}{2} (\mathbf{M}_{0m}^T \dot{\mathbf{t}}_0) = \mathbf{M}_m \dot{\mathbf{q}}_m + \mathbf{M}_{0m}^T \dot{\mathbf{t}}_0 \end{array} \right. \quad (2.28b)$$

Then the time-derivation of (2.28) gives:

$$\left\{ \begin{array}{l} \frac{d}{dt} \left( \frac{\partial \mathcal{T}}{\partial \dot{\mathbf{t}}_0} \right) = \dot{\mathbf{M}}_0 \dot{\mathbf{t}}_0 + \dot{\mathbf{M}}_{0m} \dot{\mathbf{q}}_m + \mathbf{M}_0 \ddot{\mathbf{t}}_0 + \mathbf{M}_{0m} \ddot{\mathbf{q}}_m \end{array} \right. \quad (2.29a)$$

$$\left\{ \begin{array}{l} \frac{d}{dt} \left( \frac{\partial \mathcal{T}}{\partial \dot{\mathbf{q}}_m} \right) = \dot{\mathbf{M}}_m \dot{\mathbf{q}}_m + \dot{\mathbf{M}}_{0m}^T \dot{\mathbf{t}}_0 + \mathbf{M}_m \ddot{\mathbf{q}}_m + \mathbf{M}_{0m}^T \ddot{\mathbf{t}}_0 \end{array} \right. \quad (2.29b)$$

with the expression of the time-derivative inertia matrices detailed with (2.21) as:

$$\left\{ \begin{array}{l} \dot{\mathbf{M}}_0 = \Omega_0 \begin{bmatrix} \mathcal{I}_0 & \mathbf{0}_3 \\ \mathbf{0}_3 & m_0 \mathbf{I}_3 \end{bmatrix} + \sum_{i=1}^{n_q} \dot{\mathbf{B}}_{i0}^T \begin{bmatrix} \mathcal{I}_i & \mathbf{0}_3 \\ \mathbf{0}_3 & m_i \mathbf{I}_3 \end{bmatrix} \mathbf{B}_{i0} + \\ \sum_{i=1}^{n_q} \mathbf{B}_{i0}^T \begin{bmatrix} \dot{\mathcal{I}}_i & \mathbf{0}_3 \\ \mathbf{0}_3 & m_i \mathbf{I}_3 \end{bmatrix} \mathbf{B}_{i0} + \sum_{i=1}^{n_q} \mathbf{B}_{i0}^T \begin{bmatrix} \mathcal{I}_i & \mathbf{0}_3 \\ \mathbf{0}_3 & m_i \mathbf{I}_3 \end{bmatrix} \dot{\mathbf{B}}_{i0} \end{array} \right. \quad (2.30a)$$

$$\left\{ \begin{array}{l} \dot{\mathbf{M}}_{0m} = \sum_{i=1}^{n_q} \dot{\mathbf{B}}_{i0}^T \begin{bmatrix} \mathcal{I}_i & \mathbf{0}_3 \\ \mathbf{0}_3 & m_i \mathbf{I}_3 \end{bmatrix} \mathbf{J}_{m_i} + \sum_{i=1}^{n_q} \mathbf{B}_{i0}^T \begin{bmatrix} \dot{\mathcal{I}}_i & \mathbf{0}_3 \\ \mathbf{0}_3 & m_i \mathbf{I}_3 \end{bmatrix} \mathbf{J}_{m_i} \\ + \sum_{i=1}^{n_q} \mathbf{B}_{i0}^T \begin{bmatrix} \mathcal{I}_i & \mathbf{0}_3 \\ \mathbf{0}_3 & m_i \mathbf{I}_3 \end{bmatrix} \dot{\mathbf{J}}_{m_i} \end{array} \right. \quad (2.30b)$$

$$\left\{ \begin{array}{l} \dot{\mathbf{M}}_m = \sum_{i=1}^{n_q} \dot{\mathbf{J}}_{m_i}^T \begin{bmatrix} \mathcal{I}_i & \mathbf{0}_3 \\ \mathbf{0}_3 & m_i \mathbf{I}_3 \end{bmatrix} \mathbf{J}_{m_i} + \sum_{i=1}^{n_q} \mathbf{J}_{m_i}^T \begin{bmatrix} \dot{\mathcal{I}}_i & \mathbf{0}_3 \\ \mathbf{0}_3 & m_i \mathbf{I}_3 \end{bmatrix} \mathbf{J}_{m_i} \\ + \sum_{i=1}^{n_q} \mathbf{J}_{m_i}^T \begin{bmatrix} \mathcal{I}_i & \mathbf{0}_3 \\ \mathbf{0}_3 & m_i \mathbf{I}_3 \end{bmatrix} \dot{\mathbf{J}}_{m_i} \end{array} \right. \quad (2.30c)$$

Additionally, the time-derivative of the inertia  $\mathcal{I}_i$  (2.10) in the  $\mathcal{R}_{ine}$ , is given by:

$$\dot{\mathcal{I}}_i = \boldsymbol{\omega}_i^\times \mathcal{I}_{\mathcal{S}_i} \mathbf{R}_{\mathcal{S}_i, \mathcal{R}_{ine}}^T + \mathbf{R}_{\mathcal{S}_i, \mathcal{R}_{ine}} \mathcal{I}_{\mathcal{S}_i} \boldsymbol{\omega}_i^{\times T} \quad (2.31)$$

The derivation of the Lagrangian (2.25) in function of  $\mathbf{x}_0$  and  $\mathbf{q}_m$  to evaluate the Euler-

Lagrange equation (2.27) is detailed in appendix A. In that purpose, one introduces  $\mathbf{c}_0 \in \mathbb{R}^{6 \times 6}$ ,  $\mathbf{c}_{m0} \in \mathbb{R}^{n_m \times 6}$ ,  $\mathbf{c}_{0m} \in \mathbb{R}^{6 \times n_m}$  and  $\mathbf{c}_m \in \mathbb{R}^{n_m \times n_m}$  as:

$$\begin{cases} \mathbf{c}_0 = -\frac{1}{2} \frac{\partial}{\partial \mathbf{x}_0} \left( \mathbf{t}_0^T \mathbf{M}_0 + \dot{\mathbf{q}}_m^T \mathbf{M}_{0m}^T \right) & (2.32a) \end{cases}$$

$$\begin{cases} \mathbf{c}_{0m} = -\frac{1}{2} \frac{\partial}{\partial \mathbf{x}_0} \left( \dot{\mathbf{q}}_m^T \mathbf{M}_m + \mathbf{t}_0^T \mathbf{M}_{0m} \right) & (2.32b) \end{cases}$$

$$\begin{cases} \mathbf{c}_{m0} = -\frac{1}{2} \frac{\partial}{\partial \mathbf{q}_m} \left( \mathbf{t}_0^T \mathbf{M}_0 + \dot{\mathbf{q}}_m^T \mathbf{M}_{0m}^T \right) & (2.32c) \end{cases}$$

$$\begin{cases} \mathbf{c}_m = -\frac{1}{2} \frac{\partial}{\partial \mathbf{q}_m} \left( \dot{\mathbf{q}}_m^T \mathbf{M}_m + \mathbf{t}_0^T \mathbf{M}_{0m} \right) & (2.32d) \end{cases}$$

The final evaluation of the Lagrangian (2.25) with (2.27) allows to derive the dynamic model for a rigid multi-body and multi-kinematic chains system as [Wil+18]:

$$\underbrace{\begin{bmatrix} \mathbf{M}_0 & \mathbf{M}_{0m} \\ \mathbf{M}_{0m}^T & \mathbf{M}_m \end{bmatrix}}_{\mathbf{M}(\mathbf{x}_0, \mathbf{q}_m)} \begin{bmatrix} \dot{\mathbf{t}}_0 \\ \dot{\mathbf{q}}_m \end{bmatrix} + \underbrace{\begin{bmatrix} \dot{\mathbf{M}}_0 + \mathbf{c}_0 & \dot{\mathbf{M}}_{0m} + \mathbf{c}_{0m} \\ \dot{\mathbf{M}}_{0m}^T + \mathbf{c}_{m0} & \dot{\mathbf{M}}_m + \mathbf{c}_m \end{bmatrix}}_{\mathbf{D}(\mathbf{x}_0, \mathbf{q}_m, \dot{\mathbf{q}}_0, \dot{\mathbf{q}}_m)} \begin{bmatrix} \mathbf{t}_0 \\ \dot{\mathbf{q}}_m \end{bmatrix} = \begin{bmatrix} \boldsymbol{\tau}_0 \\ \boldsymbol{\tau}_{q_m} \end{bmatrix} + \begin{bmatrix} \boldsymbol{\tau}_{ext_0} \\ \boldsymbol{\tau}_{ext_m} \end{bmatrix} \quad (2.33)$$

The matrix  $\mathbf{M}(\mathbf{x}_0, \mathbf{q}_m)$  is an inertia matrix evaluated from the spacecraft configuration and position in the  $\mathcal{R}_{ine}$  (i.e.  $\mathbf{q}$ ). The matrix  $\mathbf{D}(\mathbf{x}_0, \mathbf{q}_m, \dot{\mathbf{q}}_0, \dot{\mathbf{q}}_m)$  is a convective matrix corresponding to centrifugal and Coriolis terms. Its evaluation depends on the system configuration and velocities such that it traduces the influence of each body's motions on the rest of the system.

As for control purposes, the base rotations are preferably expressed in the body frame  $\mathcal{R}_{sat}$ , the general formulation of the dynamic model (2.33) is modified to express the base angular dynamics in  $\mathcal{R}_{sat}$ . With the transformation (2.14), the equation of motions (2.33) are modified as:

$$\underbrace{\begin{bmatrix} \mathbf{H}_0 & \mathbf{H}_{0m} \\ \mathbf{H}_{0m}^T & \mathbf{H}_m \end{bmatrix}}_{\mathbf{H}(\mathbf{x}_0, \mathbf{q}_m)} \begin{bmatrix} \ddot{\mathbf{q}}_0 \\ \ddot{\mathbf{q}}_m \end{bmatrix} + \underbrace{\begin{bmatrix} \mathbf{P}_0^T (\dot{\mathbf{M}}_0 + \mathbf{c}_0) \mathbf{P}_0 & \mathbf{P}_0^T (\dot{\mathbf{M}}_{0m} + \mathbf{c}_{0m}) \\ (\dot{\mathbf{M}}_{0m}^T + \mathbf{c}_{m0}) \mathbf{P}_0 & \dot{\mathbf{M}}_m + \mathbf{c}_m \end{bmatrix}}_{\mathbf{C}(\mathbf{x}_0, \mathbf{q}_m, \dot{\mathbf{q}}_0, \dot{\mathbf{q}}_m)} \begin{bmatrix} \dot{\mathbf{q}}_0 \\ \dot{\mathbf{q}}_m \end{bmatrix} = \begin{bmatrix} \mathbf{P}_0^T (\boldsymbol{\tau}_0 + \boldsymbol{\tau}_{ext_0}) \\ \boldsymbol{\tau}_{q_m} + \boldsymbol{\tau}_{ext_m} \end{bmatrix} \quad (2.34)$$

One will observe that the base's transformation does not change the properties of the inertia matrix  $\mathbf{H}(\mathbf{x}_0, \mathbf{q}_m)$ , and thus of the convective matrix  $\mathbf{C}(\mathbf{x}_0, \mathbf{q}_m, \dot{\mathbf{q}}_0, \dot{\mathbf{q}}_m)$ .

where:

$$\begin{cases} \mathbf{H}_0 = \mathbf{P}_0^T \mathbf{M}_0 \mathbf{P}_0 & (2.35a) \\ \mathbf{H}_{0m} = \mathbf{P}_0^T \mathbf{M}_{0m} = \sum_{i=1}^{n_q} \begin{bmatrix} \mathbf{R}_{S_0}^T \mathcal{I}_i & -m_i \mathbf{R}_{S_0}^T (\mathbf{r}_{S_0} - \mathbf{r}_{S_i})^\times \\ \mathbf{0}_3 & m_i \mathbf{I}_3 \end{bmatrix} \mathbf{J}_{m_i} \\ \mathbf{H}_m = \mathbf{M}_m & (2.35b) \end{cases}$$

With this modeling effort, based on the DH formalism to develop a kinematic model used to derive a dynamic model with a Lagrangian approach, the equations of motions for an on-orbit robot with multiple-kinematic chains with a common base are given as (2.34). The general formalism can later be modified according to the SMS studied. One will note that this formalism as written with (2.34) corresponds to a flying robot for which external forces/torques (i.e.  $\tau_{ext_0}$  and  $\tau_{ext_m}$ ) are applied. Although, a floating robot will observe a null control torque  $\tau_0$ .

### 2.2.4 Dynamics of a rotation-free-floating SMS

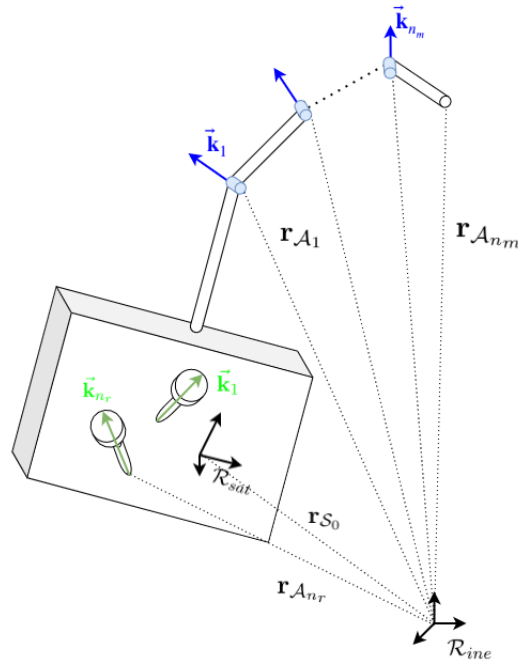


Figure 2.2 – Illustration of a SMS with  $n_r$  reaction-wheels and a  $n_m$ -DoFs manipulator

The present study put the focus on rotation-free-floating manipulators with reaction-wheels to control base orientations. Capitalizing on the general and recursive formalism previously developed to derive the equations of motions of a space robot as (2.34), an adaptation is presented in this section for a free-floating SMS adding reaction-wheels. The multi-kinematic chains formalism is here put to use such that each reaction-wheel,  $\mathcal{A}_{r_i}$ , corresponds to one kinematic chain,  $\mathcal{S}_{r_i}$ , composed of one-DoF joint,  $\mathbf{k}_{r_i}$ , as illustrated with Figure 2.2. This advantageously allows to distinguish the different contributions on the system of each actuators. As one can observe with (2.15), between two kinematic chains there are no direct interactions, the influence of a chain on the other occurs through the base. In that matter of distinguishing reaction-wheels from manipulator's actuators, the subscripts  $m$  and  $r$  are respectively used to indicate manipulator quantities and reaction-wheel ones. Thus, the rotation-free-floating

SMS considered has  $n_r$  reaction-wheels and a  $n_m$  DoFs manipulator.

To emphasize on the reaction-wheels' integration and impact on the system, one will first consider the twist vector by adapting notation from (2.15) such as:

$$\mathbf{t}_{r_i} = \mathbf{J}_{0r_i} \dot{\mathbf{q}}_0 + \mathbf{J}_{r_i} \dot{q}_{r_i}, \forall i \in [1, n_r] \quad (2.36)$$

where the Jacobian matrices are expressed as:

$$\left\{ \begin{array}{l} \mathbf{J}_{r_i} = \mathbf{P}_{m_i} = \begin{bmatrix} \mathbf{k}_i \\ \mathbf{k}_i \times (\mathbf{r}_{S_i} - \mathbf{r}_{A_i}) \end{bmatrix} = \begin{bmatrix} \mathbf{k}_i \\ \mathbf{0}_{3 \times 1} \end{bmatrix} \end{array} \right. \quad (2.37a)$$

$$\left\{ \begin{array}{l} \mathbf{J}_{0r_i} = \begin{bmatrix} \mathbf{I}_3 & \mathbf{0}_3 \\ (\mathbf{r}_{S_0} - \mathbf{r}_{S_i})^\times & \mathbf{I}_3 \end{bmatrix} \begin{bmatrix} \mathbf{R}_{S_0} & \mathbf{0}_3 \\ \mathbf{0}_3 & \mathbf{I}_3 \end{bmatrix} = \mathbf{B}_{i0} \mathbf{P}_0 \end{array} \right. \quad (2.37b)$$

considering these expressions, one can highlight that the reaction-wheels affect the angular velocity of the system in  $\mathcal{R}_{sat}$  and the system's base displacement in  $\mathcal{R}_{ine}$ .

Similarly, adapting (2.15) and (2.16), the twist of a manipulator joint is expressed as:

$$\begin{aligned} \mathbf{t}_{m_i} &= \mathbf{B}_{i0} \mathbf{P}_0 \dot{\mathbf{q}}_0 + \sum_{k=1}^{i-1} (\mathbf{B}_{ik} \mathbf{p}_{m_k} \dot{q}_k) + \mathbf{p}_{m_i} \dot{q}_i \\ &= \mathbf{J}_{0m_i} \dot{\mathbf{q}}_0 + \mathbf{J}_{m_i} \dot{\mathbf{q}}_m, \forall i \in [1, n_m] \end{aligned} \quad (2.38)$$

where the expression of the Jacobian matrices given for a single kinematic chain are obtained with:

$$\left\{ \begin{array}{l} \mathbf{B}_{kj} = \begin{bmatrix} \mathbf{I}_3 & \mathbf{0}_3 \\ (\mathbf{r}_{S_k} - \mathbf{r}_{S_j})^\times & \mathbf{I}_3 \end{bmatrix} \end{array} \right. \quad (2.39a)$$

$$\left\{ \begin{array}{l} \mathbf{p}_{m_k} = \begin{bmatrix} \mathbf{k}_k \\ \mathbf{k}_k \times (\mathbf{r}_{S_k} - \mathbf{r}_{A_k}) \end{bmatrix} \end{array} \right. \quad (2.39b)$$

It allows to highlight that the manipulator's joints also impact the linear dynamic of the overall system in addition to its rotations.

From the twist expressions, a kinematic model can be defined as developed in the previous section. Adding reaction-wheels to the system only modifies the kinetic energy expression without providing any potential energies. Therefore, the Lagrangian expression (2.23) is adapted to distinguish the contribution of base and manipulator actuators in the system energy as:

$$\mathcal{L} = \mathcal{T} = \frac{1}{2} \mathbf{t}_0^T \begin{bmatrix} \mathcal{I}_0 & \mathbf{0}_3 \\ \mathbf{0}_3 & m_0 \mathbf{I}_3 \end{bmatrix} \mathbf{t}_0 + \frac{1}{2} \sum_{i=1}^{n_m} \left( \mathbf{t}_{m_i}^T \begin{bmatrix} \mathcal{I}_i & \mathbf{0}_3 \\ \mathbf{0}_3 & m_i \mathbf{I}_3 \end{bmatrix} \mathbf{t}_{m_i} \right) + \frac{1}{2} \sum_{i=1}^{n_r} \left( \mathbf{t}_{r_i}^T \begin{bmatrix} \mathcal{I}_i & \mathbf{0}_3 \\ \mathbf{0}_3 & m_i \mathbf{I}_3 \end{bmatrix} \mathbf{t}_{r_i} \right) \quad (2.40)$$

Then introducing respectively the reaction-wheels and manipulator joint rate-variables generalized vector  $\dot{\mathbf{q}}_r = [\dot{q}_{r_1}^T \ \dots \ \dot{q}_{r_{n_r}}^T]^T$  and  $\dot{\mathbf{q}}_m = [\dot{q}_{m_1}^T \ \dots \ \dot{q}_{m_{n_m}}^T]^T$ , the kinetic energy (2.40)

can be expressed in a compact form by developing the twist expressions with (2.36) and (2.38) as:

$$\begin{aligned} \mathcal{L} &= \frac{1}{2} \begin{bmatrix} \mathbf{t}_0^T & \dot{\mathbf{q}}_r^T & \dot{\mathbf{q}}_m^T \end{bmatrix} \begin{bmatrix} \mathbf{M}_0 & \mathbf{M}_{0r} & \mathbf{M}_{0m} \\ \mathbf{M}_{0r}^T & \mathbf{M}_r & \mathbf{0}_{n_r \times n_m} \\ \mathbf{M}_{0m}^T & \mathbf{0}_{n_m \times n_r} & \mathbf{M}_m \end{bmatrix} \begin{bmatrix} \mathbf{t}_0 \\ \dot{\mathbf{q}}_r \\ \dot{\mathbf{q}}_m \end{bmatrix} \\ &= \frac{1}{2} \begin{bmatrix} \mathbf{t}_0^T & \dot{\mathbf{q}}_r^T & \dot{\mathbf{q}}_m^T \end{bmatrix} \mathbf{M}(\mathbf{x}_0, \mathbf{q}_m, \mathbf{q}_r) \begin{bmatrix} \mathbf{t}_0 \\ \dot{\mathbf{q}}_m \\ \dot{\mathbf{q}}_r \end{bmatrix} \end{aligned} \quad (2.41)$$

where the inertia matrix  $\mathbf{M}(\mathbf{x}_0, \mathbf{q}_m, \mathbf{q}_r)$  is detailed as:

$$\mathbf{M}_0 = \begin{bmatrix} \mathcal{I}_0 & \mathbf{0}_3 \\ \mathbf{0}_3 & m_0 \mathbf{I}_3 \end{bmatrix} + \sum_{i=1}^{n_q} \mathbf{B}_{i0}^T \begin{bmatrix} \mathcal{I}_i & \mathbf{0}_3 \\ \mathbf{0}_3 & m_i \mathbf{I}_3 \end{bmatrix} \mathbf{B}_{i0} \quad (2.42a)$$

$$\mathbf{M}_{0m} = \sum_{i=1}^{n_m} \mathbf{B}_{i0}^T \begin{bmatrix} \mathcal{I}_i & \mathbf{0}_3 \\ \mathbf{0}_3 & m_i \mathbf{I}_3 \end{bmatrix} \mathbf{J}_{m_i} \quad (2.42b)$$

$$\mathbf{M}_{0r} = \sum_{i=1}^{n_r} \mathbf{B}_{i0}^T \begin{bmatrix} \mathcal{I}_i & \mathbf{0}_3 \\ \mathbf{0}_3 & m_i \mathbf{I}_3 \end{bmatrix} \mathbf{J}_{r_i} \quad (2.42c)$$

$$\mathbf{M}_m = \sum_{i=1}^{n_m} \mathbf{J}_{m_i}^T \begin{bmatrix} \mathcal{I}_i & \mathbf{0}_3 \\ \mathbf{0}_3 & m_i \mathbf{I}_3 \end{bmatrix} \mathbf{J}_{m_i} \quad (2.42d)$$

$$\mathbf{M}_r = \sum_{i=1}^{n_r} \mathbf{J}_{r_i}^T \begin{bmatrix} \mathcal{I}_i & \mathbf{0}_3 \\ \mathbf{0}_3 & m_i \mathbf{I}_3 \end{bmatrix} \mathbf{J}_{r_i} \quad (2.42e)$$

The inertia matrix  $\mathbf{M}(\mathbf{x}_0, \mathbf{q}_m, \mathbf{q}_r)$  remains symmetric and defined strictly positive. One will note that developing the expression of inertia matrix  $\mathbf{M}_r$  allows to highlight that reaction-wheels only affect the angular dynamics of the overall SMS.

In order to alleviate further notations and expressions, reaction wheels and manipulator's actuators state are gathered into the vector  $\mathbf{q} \in \mathbb{R}^{n_q \times 1}$  (with  $n_q = n_r + n_m$ ) as  $\mathbf{q} = [\mathbf{q}_r^T \quad \mathbf{q}_m^T]^T$  and subscript  $q$  denotes the association of reaction-wheels and manipulator quantities, such that  $\mathbf{M}_{0q} = [\mathbf{M}_{0r} \quad \mathbf{M}_{0m}]$  and  $\mathbf{M}_q = \begin{bmatrix} \mathbf{M}_r & \mathbf{0} \\ \mathbf{0} & \mathbf{M}_m \end{bmatrix}$ . Thus, adapting notations of the previous section and observing a similar base transformation (i.e. with 2.14) to express the spacecraft base angular dynamics in  $\mathcal{R}_{sat}$ , the equations of motions of a rigid rotation-free-floating SMS are obtained as [Wil+18]:

$$\underbrace{\begin{bmatrix} \mathbf{H}_0 & \mathbf{H}_{0q} \\ \mathbf{H}_{0q}^T & \mathbf{H}_q \end{bmatrix}}_{\mathbf{H}(\mathbf{x}_0, \mathbf{q})} \begin{bmatrix} \ddot{\mathbf{q}}_0 \\ \ddot{\mathbf{q}} \end{bmatrix} + \underbrace{\begin{bmatrix} \mathbf{P}_0^T (\dot{\mathbf{M}}_0 + \mathbf{c}_0) \mathbf{P}_0 & \mathbf{P}_0^T (\dot{\mathbf{M}}_{0q} + \mathbf{c}_{0q}) \\ (\dot{\mathbf{M}}_{0q}^T + \mathbf{c}_{q0}) \mathbf{P}_0 & \dot{\mathbf{M}}_q + \mathbf{c}_q \end{bmatrix}}_{\mathbf{C}(\mathbf{x}_0, \mathbf{q}, \dot{\mathbf{q}}_0, \dot{\mathbf{q}})} \begin{bmatrix} \dot{\mathbf{q}}_0 \\ \dot{\mathbf{q}} \end{bmatrix} = \begin{bmatrix} \mathbf{P}_0^T (\boldsymbol{\tau}_0 + \boldsymbol{\tau}_{ext_0}) \\ \boldsymbol{\tau}_q + \boldsymbol{\tau}_{ext_q} \end{bmatrix} \quad (2.43)$$

with  $\boldsymbol{\tau}_q = [\boldsymbol{\tau}_r^T \quad \boldsymbol{\tau}_m^T]^T \in \mathbb{R}^{n_q \times 1}$  the actuators control torque composed of the reaction-wheels'



control torques,  $\boldsymbol{\tau}_r$ , and manipulator's control torques,  $\boldsymbol{\tau}_m$ , and  $\boldsymbol{\tau}_{ext_q} \in \mathbb{R}^{n_q \times 1}$  the vector of the external torques/forces applying on the system's actuators equal to zeros with the previous assumptions of not disturbances. One will emphasize on the rotation-free-floating nature of the SMS considered and on the hypothesis of no external perturbations which leads to the torques/forces applying and controlling the base equal to zeros (i.e.  $\boldsymbol{\tau}_0 = \boldsymbol{\tau}_{ext_0} = \mathbf{0}_{6 \times 1}$ ).

## 2.3 Modeling of flexible rotation-free-floating SMS

### 2.3.1 Modeling hypothesis

In this study, a flexible element is attached to the spacecraft's base, or on a body fixed on the base, with a unique rigid junction. The case of flexible element in a kinematic chain is not developed here. The  $i^{th}$  flexible appendage is linked to the rest of the satellite with a fixed joint which pose in  $\mathcal{R}_{ine}$  is denoted  $\mathbf{r}_{P_{f_i}}$  as illustrated with figure 2.3. As proposed in the literature [Lik72], a flexible modeling of appendages is obtained in two steps, first a finite element study is developed to obtain the flexible DoF and then a modal reduction method is employed [Dok72]. The present work does not detail the finite element approach but the DoF reduction is developed with the formalism used in Girard and al. [GR10] and Sanfedino and al. [San+18]. The modal approach consists in a first system studied without excitation sources, corresponding to the finite element approach, to obtain the motion equation and the normal modes, then a second step is the superposition of the flexible modes to reduce their number.

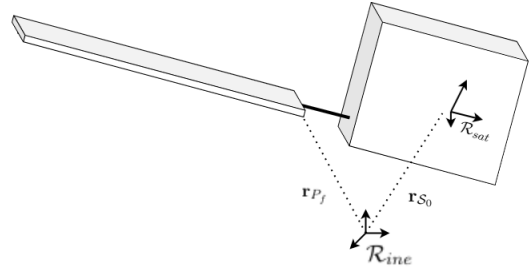


Figure 2.3 – Example of a flexible satellite

From a finite element analysis, each node is associated to a modal linear and angular displacement denoted  $\mathbf{u}$ . The distinction between an internal mode (or DoF) and the ones on the unique junction is made using respectively the subscript  $i$  and  $j$ . Adopting the Lagrangian formalism from the finite element method, the motion equations of the total set of DoFs are a second order involving mass, damping and stiffness matrices as in [San+18]:

$$\underbrace{\begin{bmatrix} \mathbf{M}_{ii} & \mathbf{M}_{ij} \\ \mathbf{M}_{ij}^T & \mathbf{M}_{jj} \end{bmatrix}}_{\mathbf{M}_{flex}} \begin{bmatrix} \ddot{\mathbf{u}}_i \\ \ddot{\mathbf{u}}_j \end{bmatrix} + \underbrace{\begin{bmatrix} \mathbf{C}_{ii} & \mathbf{C}_{ij} \\ \mathbf{C}_{ij}^T & \mathbf{C}_{jj} \end{bmatrix}}_{\mathbf{C}_{flex}} \begin{bmatrix} \dot{\mathbf{u}}_i \\ \dot{\mathbf{u}}_j \end{bmatrix} + \underbrace{\begin{bmatrix} \mathbf{K}_{ii} & \mathbf{K}_{ij} \\ \mathbf{K}_{ij}^T & \mathbf{K}_{jj} \end{bmatrix}}_{\mathbf{K}_{flex}} \begin{bmatrix} \mathbf{u}_i \\ \mathbf{u}_j \end{bmatrix} = \begin{bmatrix} \mathbf{F}_i \\ \mathbf{F}_j \end{bmatrix} \quad (2.44)$$

where  $\mathbf{M}_{flex}$ ,  $\mathbf{C}_{flex}$  and  $\mathbf{K}_{flex}$  are constant symmetric matrices.  $\mathbf{F}_i$  are forces/torques applying on the internal DoFs and  $\mathbf{F}_j$  are reaction forces/torques imposed by the junction on the flexible appendage. This equation traduces that for any external forces/torques, correspond-

ing to an excitation, the internal DoFs will present a linear and/or angular displacement with a given velocity and acceleration and reciprocally for any mode displacement a force/torque is applied on the junction. Moreover, this equation may present an important number of DoFs which some may be neglected considering their physical properties and the application.

In order to reduce the number of flexible DoFs, the normal modes are considered. By definition, it corresponds to the solutions of the equation of motion without any excitation (i.e.  $\mathbf{F}_i = \mathbf{0}_{n_i \times 1}$  and  $\mathbf{u}_j = \mathbf{0}_{n_j \times 1}$ ). Thus, from (2.44) and neglecting the damping terms,  $\mathbf{C}_{flex}$ , the normal modes are the solutions of [San+18]:

$$\mathbf{M}_{ii}\ddot{\mathbf{u}}_i + \mathbf{K}_{ii}\mathbf{u}_i = \mathbf{0}_{n_i \times 1} \quad (2.45)$$

These solutions are the  $n_i$  eigenvalues,  $\lambda_k$  (with  $k \in [1, n_i]$ ), associated to  $k^{th}$  eigenvectors,  $\Phi_{ik}$ , given by [Cra00]:

$$\left(-\lambda_k^2 \mathbf{M}_{ii} + \mathbf{K}_{ii}\right) \Phi_{ik} = \mathbf{0}_{n_i \times 1} \quad (2.46)$$

Then the DoF reduction is obtained by solving (2.44) with a projection of system physical properties in the base composed of the eigenvectors  $\Phi_{ik}$  and the junction mode matrix  $\Psi$ .  $\Psi$  is computed by successively imposing a unit displacement  $\mathbf{u}_j$  while blocking the other junction displacements. In the case of a single junction,  $\Psi$  is defined as [GR10]:

$$\Psi_{jj} = \mathbf{I}_j \quad (2.47)$$

and the terms coupled with internal DoFs are obtained as:

$$\mathbf{K}_{ii}\Psi_{ij} + \mathbf{K}_{ij} = \mathbf{0}_{n_i \times n_j} \Rightarrow \Psi_{ij} = \mathbf{K}_{ii}^{-1}\mathbf{K}_{ij} \quad (2.48)$$

The projection in the normal mode base allows to use the Craig-Bampton transformation [Cra00]:

$$\begin{bmatrix} \mathbf{u}_i \\ \mathbf{u}_j \end{bmatrix} = \begin{bmatrix} \Phi_{ik} & \Psi_{ij} \\ \mathbf{0}_{n_j \times n_k} & \mathbf{I}_j \end{bmatrix} \begin{bmatrix} \boldsymbol{\eta}_k \\ \mathbf{u}_j \end{bmatrix} \quad (2.49)$$

with  $\boldsymbol{\eta}_k \in \mathbb{R}^{n_k \times 1}$  the modal displacement vector. From this transformation, (2.44) is rewritten as [San+18]:

$$\begin{bmatrix} \mathbf{m}_{kk} & \mathbf{L}_{kj} \\ \mathbf{L}_{kj}^T & \bar{\mathbf{M}}_{jj} \end{bmatrix} \begin{bmatrix} \ddot{\boldsymbol{\eta}}_k \\ \ddot{\mathbf{u}}_j \end{bmatrix} + \begin{bmatrix} \mathbf{c}_{kk} & \mathbf{0}_{n_k \times n_j} \\ \mathbf{0}_{n_j \times n_k} & \mathbf{0}_{n_j} \end{bmatrix} \begin{bmatrix} \dot{\boldsymbol{\eta}}_k \\ \dot{\mathbf{u}}_j \end{bmatrix} + \begin{bmatrix} \mathbf{k}_{kk} & \mathbf{0}_{n_k \times n_j} \\ \mathbf{0}_{n_j \times n_k} & \bar{\mathbf{K}}_{jj} \end{bmatrix} \begin{bmatrix} \boldsymbol{\eta}_k \\ \mathbf{u}_j \end{bmatrix} = \begin{bmatrix} \Phi_{ki}\mathbf{F}_i \\ \Psi_{ji}\mathbf{F}_i + \mathbf{F}_j \end{bmatrix} \quad (2.50)$$

where:

- $\boldsymbol{\eta}_k$  is the modal displacement vector
- $\mathbf{u}_j$  is the junction pose and orientation states
- $\mathbf{m}_{kk} = \Phi_{ik}^T \mathbf{M}_{ii} \Phi_{ik}$  is a diagonal equivalent mass matrix which can be expressed in a normalized modal base as  $\mathbf{m}_{kk} = \mathbf{I}_k$

- $\mathbf{c}_{kk} = \Phi_{ik}^T \mathbf{C}_{ii} \Phi_{ik}$  is a damping equivalent matrix. Neglecting the damping terms between two modes, its expression is reduced to a diagonal matrix as  $\mathbf{c}_{kk} = \text{diag}(2\zeta_k \omega_k m_k)$  where  $\zeta_k$ ,  $\omega_k$  and  $m_k$  are respectively the damping, the natural frequency and the generalized mass of the  $k^{\text{th}}$  mode.
- $\mathbf{k}_{kk} = \Phi_{ik}^T \mathbf{K}_{ii} \Phi_{ik} = \text{diag}(m_k \lambda_k^2)$  is the stiffness equivalent matrix
- $\mathbf{L}_{kj} = \Phi_{ik}^T (\mathbf{M}_{ii} \Psi_{ij} + \mathbf{M}_{ij})$  is the matrix of the participation factors
- $\bar{\mathbf{M}}_{jj} = \Psi_{ji} \mathbf{M}_{ii} \Psi_{ij} + \Psi_{ji} \mathbf{M}_{ij} + \mathbf{M}_{ji} \Psi_{ij} + \mathbf{M}_{jj}$  is the condensed mass matrix. With a rigid junction  $\bar{\mathbf{M}}_{jj}$  is equal to the rigid body mass matrix. It includes the information about mass, inertia and CoM of the structure with respect to the junction.
- $\bar{\mathbf{K}}_{jj} = \mathbf{K}_{jj} - \mathbf{K}_{ji} \mathbf{K}_{ii}^{-1} \mathbf{K}_{ij}$  is the condensed stiffness matrix equal to  $\mathbf{0}_{n_j}$  for a rigid junction
- $\mathbf{F}_\eta = \Phi_{ki} \mathbf{F}_i$  is the forces/torques imposed on the internal normal modes
- $\mathbf{F}_P = \Psi_{ji} \mathbf{F}_i + \mathbf{F}_j$  is the forces/torques imposed on the appendage by the junction

An adaptation of the Craig-Bampton transformation with a rigid junction,  $\Psi_{ij} = \mathbf{0}_{n_i \times n_j}$ ,

### 2.3.2 Modeling of a rigid-flexible multi-body system

**Modeling of a rigid hub and  $n_p$  flexible appendages** Similarly to the method formulated in section 2.2.4, a Lagrangian approach is adopted to include the flexible appendage dynamics into the rigid ones of the base. First the twist vector of the  $i^{\text{th}}$  junction is expressed adapting (2.15) with a rigid junction as:

$$\begin{aligned} \mathbf{t}_{P_{f_i}} &= \begin{bmatrix} \boldsymbol{\omega}_{P_{f_i}} \\ \dot{\mathbf{r}}_{P_{f_i}} \end{bmatrix} = \mathbf{B}_{P_{f_i}0} \mathbf{t}_0 = \mathbf{B}_{P_{f_i}0} \mathbf{P}_0 \dot{\mathbf{q}}_0 = \mathbf{J}_{0P_{f_i}} \dot{\mathbf{q}}_0 \\ &= \begin{bmatrix} \mathbf{I}_3 & \mathbf{0}_3 \\ (\mathbf{r}_{S_0} - \mathbf{r}_{P_{f_i}})^\times & \mathbf{I}_3 \end{bmatrix} \mathbf{t}_0 \end{aligned} \quad (2.51)$$

and its time-derivative is given as:

$$\dot{\mathbf{t}}_{P_{f_i}} = \mathbf{J}_{0P_{f_i}} \ddot{\mathbf{q}}_0 + \dot{\mathbf{J}}_{0P_{f_i}} \dot{\mathbf{q}}_0 \quad (2.52)$$

with the expression of the time-derivative of the Jacobian matrix  $\mathbf{J}_{0P_{f_i}}$  developed as:

$$\dot{\mathbf{J}}_{0P_{f_i}} = \begin{bmatrix} \mathbf{I}_3 & \mathbf{0}_3 \\ (\mathbf{r}_{S_0} - \mathbf{r}_{P_{f_i}})^\times & \mathbf{I}_3 \end{bmatrix} \boldsymbol{\Omega}_0 \mathbf{P}_0 + \begin{bmatrix} \mathbf{0}_3 & \mathbf{0}_3 \\ (\dot{\mathbf{r}}_{S_0} - \dot{\mathbf{r}}_{P_{f_i}})^\times & \mathbf{0}_3 \end{bmatrix} \mathbf{P}_0 \quad (2.53)$$

Associating the modal displacement vector  $\boldsymbol{\eta}_i \in \mathbb{R}^{n_{\eta_i} \times 1}$  to the  $i^{th}$  appendage composed of the  $n_{\eta_i}$  flexible DoFs, the motion equations (2.50) is adapted with an appropriate flexible base change and expressed in  $\mathcal{R}_{ine}$  as:

$$\begin{aligned} & \begin{bmatrix} \mathbf{I}_{n_{\eta_i}} & \mathbf{L}_{P_{f_i}} \mathbf{B}_{P_{f_i}0} \\ \mathbf{B}_{P_{f_i}0}^T \mathbf{L}_{P_{f_i}}^T & \mathbf{B}_{P_{f_i}0}^T \begin{bmatrix} \mathcal{I}_i & \mathbf{0}_3 \\ \mathbf{0}_3 & m_i \mathbf{I}_3 \end{bmatrix} \mathbf{B}_{P_{f_i}0} \end{bmatrix} \begin{bmatrix} \dot{\boldsymbol{\eta}}_i \\ \dot{\mathbf{t}}_0 \end{bmatrix} + \begin{bmatrix} \mathbf{c}_{\eta_i} & \mathbf{0}_{n_{\eta_i} \times 6} \\ \mathbf{0}_{6 \times n_{\eta_i}} & \mathbf{0}_6 \end{bmatrix} \begin{bmatrix} \dot{\boldsymbol{\eta}}_i \\ \dot{\mathbf{t}}_0 \end{bmatrix} \\ & + \begin{bmatrix} \mathbf{k}_{n_{\eta_i}} \boldsymbol{\eta}_i \\ \mathbf{0}_{6 \times 1} \end{bmatrix} = \begin{bmatrix} \boldsymbol{\tau}^{ext_{\eta_i}} \\ \boldsymbol{\tau}_0 + \boldsymbol{\tau}^{ext_0} \end{bmatrix}, \forall i \in [1, n_p] \end{aligned} \quad (2.54)$$

with  $\boldsymbol{\tau}^{ext_{\eta_i}} \in \mathbb{R}^{n_{\eta_i} \times 1}$  the external torques/forces applying on the  $i^{th}$  flexible appendage,  $\mathbf{L}_{P_{f_i}}$  expressed in  $\mathcal{R}_{sat}$ ,  $\mathbf{c}_{\eta_i} = \text{diag}(2\zeta_j \omega_j)$  and  $\mathbf{k}_{\eta_i} = \text{diag}(\omega_j^2)$  (with  $j \in [1, n_{\eta_i}]$ ).

A drawback of the dynamics expressed as given in (2.54) is that it neglects existing coupling factors between  $\dot{\boldsymbol{\eta}}_i$  and  $\dot{\mathbf{t}}_0$ . In order to derive those factors,  $\mathbf{c}_{0\eta_i}$  and  $\mathbf{c}_{\eta_i 0}$ , such that no restriction or hypothesis are required on the base velocities, the Lagrangian approach is chosen. From (2.54) the appendages kinetic energy,  $\mathcal{T}_{appendage}$ , the hub composed of the base and payloads kinetic energy,  $\mathcal{T}_{hub}$ , the flexible potential energy,  $\mathcal{V}_{\eta}$ , and dissipative forces,  $\mathbf{F}_{\eta}$ , are expressed for a satellite with only the  $i^{th}$  appendage rigidly attached as:

$$\left\{ \begin{aligned} \mathcal{T}_{appendage} &= \frac{1}{2} \begin{bmatrix} \dot{\boldsymbol{\eta}}_i^T & \dot{\mathbf{t}}_0^T \end{bmatrix} \begin{bmatrix} \mathbf{I}_{n_{\eta_i}} & \mathbf{L}_{P_{f_i}} \mathbf{B}_{P_{f_i}0} \\ \mathbf{B}_{P_{f_i}0}^T \mathbf{L}_{P_{f_i}}^T & \mathbf{B}_{P_{f_i}0}^T \begin{bmatrix} \mathcal{I}_i & \mathbf{0}_3 \\ \mathbf{0}_3 & m_i \mathbf{I}_3 \end{bmatrix} \mathbf{B}_{P_{f_i}0} \end{bmatrix} \begin{bmatrix} \dot{\boldsymbol{\eta}}_i \\ \dot{\mathbf{t}}_0 \end{bmatrix} & (2.55a) \\ \mathcal{T}_{hub} &= \frac{1}{2} \dot{\mathbf{t}}_0^T \begin{bmatrix} \mathcal{I}_0 & \mathbf{0}_3 \\ \mathbf{0}_3 & m_0 \mathbf{I}_3 \end{bmatrix} \dot{\mathbf{t}}_0 & (2.55b) \\ \mathcal{V}_{\eta} &= -\frac{1}{2} \boldsymbol{\eta}_i^T \mathbf{k}_{\eta_i} \boldsymbol{\eta}_i & (2.55c) \\ \mathbf{F}_{\eta} &= -\mathbf{c}_{\eta_i} \dot{\boldsymbol{\eta}}_i & (2.55d) \end{aligned} \right.$$

Then (2.55) is generalized to the  $n_p$  appendages with the introduction of the generalized modal vector  $\boldsymbol{\eta} = [\boldsymbol{\eta}_1^T \ \dots \ \boldsymbol{\eta}_{n_p}^T]^T \in \mathbb{R}^{n_{\eta} \times 1}$  and  $n_{\eta} = \sum_{i=1}^{n_p} n_{\eta_i}$ , the generalized forces/torques applying on appendages  $\boldsymbol{\tau}^{ext_{\eta}} = [\boldsymbol{\tau}^{ext_{\eta_1}} \ \dots \ \boldsymbol{\tau}^{ext_{\eta_{n_p}}}]^T$ , the matrix of participation factor  $\mathbf{L}_{\eta p} = [\mathbf{L}_{P_{f_1}} \mathbf{B}_{P_{f_1}0} \ \dots \ \mathbf{L}_{P_{f_{n_p}}} \mathbf{B}_{P_{f_{n_p}}0}]$  and  $\mathbf{C}_{\eta} = \text{diag}(\mathbf{c}_{\eta_j})$ ,  $\mathbf{K}_{\eta} = \text{diag}(\mathbf{k}_{\eta_j})$  with  $j \in [1, n_p]$ . Thus, the listing of energies and forces present in the system composed of  $n_p$  flexible ap-

pendages rigidly attached to the spacecraft's base is:

$$\left\{ \begin{array}{l} \mathcal{T}_{appendages} = \frac{1}{2} \begin{bmatrix} \dot{\boldsymbol{\eta}}^T & \mathbf{t}_0^T \end{bmatrix} \begin{bmatrix} \mathbf{I}_{n_\eta} & \mathbf{L}_{\eta\mathbf{P}} \\ \mathbf{L}_{\eta\mathbf{P}}^T & \sum_{i=1}^{n_p} \left( \mathbf{B}_{P_{f_i}0}^T \begin{bmatrix} \mathcal{I}_i & \mathbf{0}_3 \\ \mathbf{0}_3 & m_i \mathbf{I}_3 \end{bmatrix} \mathbf{B}_{P_{f_i}0} \right) \end{bmatrix} \begin{bmatrix} \dot{\boldsymbol{\eta}} \\ \mathbf{t}_0 \end{bmatrix} \\ \mathcal{T}_{hub} = \frac{1}{2} \mathbf{t}_0^T \begin{bmatrix} \mathcal{I}_0 & \mathbf{0}_3 \\ \mathbf{0}_3 & m_0 \mathbf{I}_3 \end{bmatrix} \mathbf{t}_0 \\ \mathcal{V}_\eta = -\frac{1}{2} \boldsymbol{\eta}^T \mathbf{K}_\eta \boldsymbol{\eta} \\ \mathbf{F}_\eta = -\mathbf{C}_\eta \dot{\boldsymbol{\eta}} \end{array} \right. \quad \begin{array}{l} (2.56a) \\ (2.56b) \\ (2.56c) \\ (2.56d) \end{array}$$

Flexible appendages induce a variation of the potential energy  $\mathcal{V}_\eta$ , the Lagrangian expression (2.23) then becomes:

$$\mathcal{L}_{flex} = \mathcal{T}_{hub} + \mathcal{T}_{appendages} - \mathcal{V}_\eta \quad (2.57)$$

The dynamics of such systems are derived from the evaluation of (2.57) with the following Euler-Lagrange equations:

$$\left\{ \begin{array}{l} \frac{d}{dt} \left( \frac{\partial \mathcal{L}_{flex}}{\partial \dot{\boldsymbol{\eta}}} \right) - \frac{\partial \mathcal{L}_{flex}}{\partial \boldsymbol{\eta}} = \boldsymbol{\tau}_{ext_\eta} + \mathbf{F}_\eta \\ \frac{d}{dt} \left( \frac{\partial \mathcal{L}_{flex}}{\partial \dot{\mathbf{t}}_0} \right) - \frac{\partial \mathcal{L}_{flex}}{\partial \mathbf{t}_0} = \boldsymbol{\tau}_0 + \boldsymbol{\tau}_{ext_0} \end{array} \right. \quad \begin{array}{l} (2.58a) \\ (2.58b) \end{array}$$

Developing expressions in (2.58) allows to express the system dynamics under a compact form as:

$$\begin{bmatrix} \mathbf{H}_0 & \mathbf{H}_{0\eta} \\ \mathbf{H}_{0\eta}^T & \mathbf{H}_\eta \end{bmatrix} \begin{bmatrix} \ddot{\mathbf{q}}_0 \\ \dot{\boldsymbol{\eta}} \end{bmatrix} + \begin{bmatrix} \mathbf{C}_0 & \mathbf{C}_{0\eta} \\ \mathbf{C}_{\eta 0} & \mathbf{C}_\eta \end{bmatrix} \begin{bmatrix} \dot{\mathbf{q}}_0 \\ \dot{\boldsymbol{\eta}} \end{bmatrix} + \begin{bmatrix} \mathbf{0}_{6 \times n_\eta} \\ \mathbf{K}_\eta \boldsymbol{\eta} \end{bmatrix} = \begin{bmatrix} \mathbf{0}_{6 \times 1} \\ \mathbf{0}_{n_\eta \times 1} \end{bmatrix} \quad (2.59)$$

where inertia matrices are projected in the base such that the angular dynamics of the base are expressed in  $\mathcal{R}_{sat}$  as:

$$\mathbf{H}_\eta = \mathbf{I}_\eta \quad (2.60a)$$

$$\mathbf{H}_{0\eta} = \mathbf{P}_0^T \mathbf{L}_{\eta\mathbf{P}}^T \quad (2.60b)$$

$$\mathbf{M}_0 = \begin{bmatrix} \mathcal{I}_0 & \mathbf{0}_3 \\ \mathbf{0}_3 & m_0 \mathbf{I}_3 \end{bmatrix} + \sum_{i=1}^{n_p} \mathbf{B}_{P_{f_i}0}^T \begin{bmatrix} \mathcal{I}_i & \mathbf{0}_3 \\ \mathbf{0}_3 & m_i \mathbf{I}_3 \end{bmatrix} \mathbf{B}_{P_{f_i}0} \quad (2.60c)$$

$$\mathbf{H}_0 = \mathbf{P}_0^T \mathbf{M}_0 \mathbf{P}_0 \quad (2.60d)$$

convective terms as:

$$\begin{cases} \mathbf{C}_0 = \mathbf{P}_0^T \left( \dot{\mathbf{M}}_0 - \frac{1}{2} \frac{\partial}{\partial \mathbf{x}_0} \left( \dot{\boldsymbol{\eta}}^T \mathbf{L}_{\eta p} + \mathbf{t}_0^T \mathbf{M}_0 \right) \right) \mathbf{P}_0 & (2.61a) \end{cases}$$

$$\begin{cases} \mathbf{C}_{0\eta} = \mathbf{P}_0^T \left( \dot{\mathbf{L}}_{\eta p}^T - \frac{1}{2} \frac{\partial}{\partial \mathbf{x}_0} \left( \mathbf{t}_0^T \mathbf{L}_{\eta p}^T \right) \right) & (2.61b) \end{cases}$$

$$\begin{cases} \mathbf{C}_{\eta 0} = \dot{\mathbf{L}}_{\eta p} \mathbf{P}_0 & (2.61c) \end{cases}$$

where the differentiation of  $\mathbf{L}_{\eta p}$  according to  $\mathbf{x}_0$ , as detailed in appendix A, is the differentiation of matrices  $\mathbf{B}_{P_{f_i}0}$ :

$$\frac{\partial}{\partial \mathbf{x}_0} \left( \dot{\boldsymbol{\eta}}^T \mathbf{L}_{\eta p} \right) = \dot{\boldsymbol{\eta}}^T \left[ \mathbf{L}_{P_{f_1}} \frac{\partial}{\partial \mathbf{x}_0} \mathbf{B}_{P_{f_1}0} \quad \dots \quad \mathbf{L}_{P_{f_{n_p}}} \frac{\partial}{\partial \mathbf{x}_0} \mathbf{B}_{P_{f_{n_p}}0} \right] \quad (2.62)$$

and similarly for the time-derivative:

$$\dot{\mathbf{L}}_{\eta p} = \dot{\boldsymbol{\eta}}^T \left[ \mathbf{L}_{P_{f_1}} \dot{\mathbf{B}}_{P_{f_1}0} \quad \dots \quad \mathbf{L}_{P_{f_{n_p}}} \dot{\mathbf{B}}_{P_{f_{n_p}}0} \right] \quad (2.63)$$

**Integration of flexible appendages onto a rotation-free-floating dynamics** In order to study rotation-free-floating SMS with flexible appendages, illustrated with figure 2.4, the equations of motions are derived from the previous sections capitalizing on the established formalism. It is assumed that flexible bodies are rigidly attached to the base or on the end of a kinematic chain that has no DoF. Then the rigid multi-body dynamics described by (2.43) can be extended onto a coupled flexible-rigid dynamics to include those flexible elements. Based on a Lagrangian formalism, as the actuated rigid kinematic chains only modifies the overall kinetic energy, the Lagrangian expression (2.57) can be extended with the actuators' kinetic energies. As developed in section 2.2.4 for the reaction-wheels integration, with the proposed modeling formalism, separating the kinematic chains allows to naturally decouple the different elements of the system and converge all of each element impacts on the common satellite base.

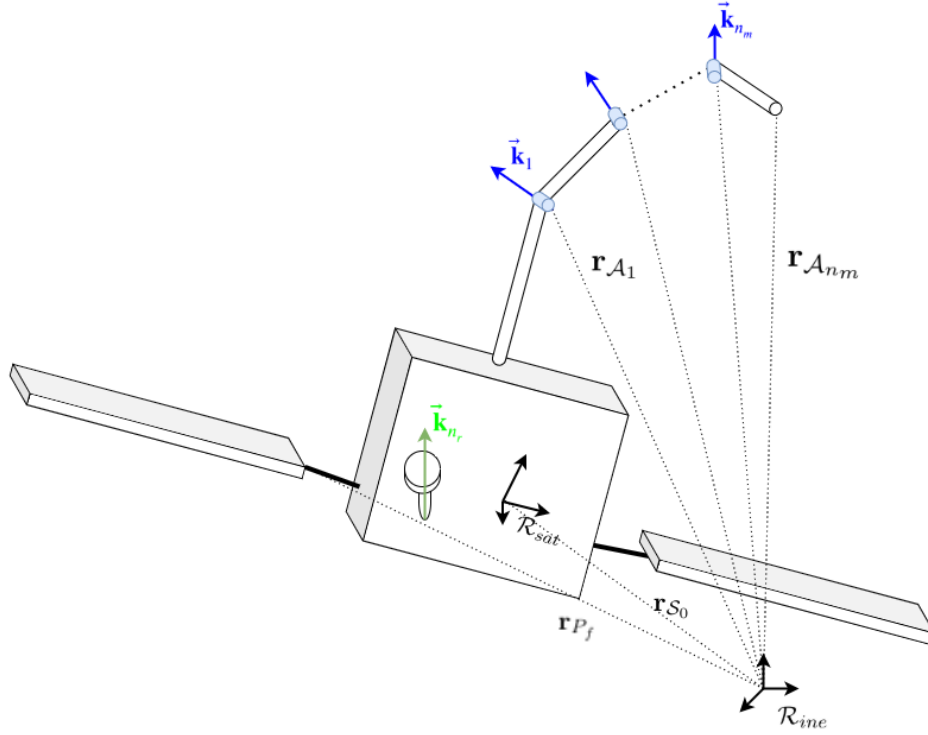


Figure 2.4 – Illustration of a rotation-free-floating SMS equipped with  $n_r$  reaction-wheels, a  $n_m$ -DoFs manipulator and  $n_p$  flexible appendages

Therefore, the Lagrangian expression (2.57) is augmented with the  $n_q$  system's actuators kinetic energy,  $\mathcal{T}_q$ , as:

$$\begin{aligned}\mathcal{L} &= \mathcal{L}_{flex} + \mathcal{T}_q \\ &= \mathcal{L}_{flex} + \frac{1}{2} \sum_{i=1}^{n_q} \left( \mathbf{t}_i^T \begin{bmatrix} \mathcal{I}_i & \mathbf{0}_3 \\ \mathbf{0}_3 & m_i \mathbf{I}_3 \end{bmatrix} \mathbf{t}_i \right)\end{aligned}\quad (2.64)$$

The Euler-Lagrange equations are given in respect to the base and actuator DoFs (i.e.  $\mathbf{q}$  and  $\mathbf{x}_0$ ), introduced in (2.27), and the flexible DoFs (i.e.  $\boldsymbol{\eta}$ ) detailed in (2.58). Remaining as general as possible, the Euler-Lagrange equations are given for a flying SMS with flexible appendages and subject to external forces/torques as:

$$\left\{ \begin{aligned} \frac{d}{dt} \left( \frac{\partial \mathcal{L}}{\partial \dot{\boldsymbol{\eta}}} \right) - \frac{\partial \mathcal{L}}{\partial \boldsymbol{\eta}} &= \boldsymbol{\tau}_{ext\boldsymbol{\eta}} + \mathbf{F}_{\boldsymbol{\eta}} \end{aligned} \right. \quad (2.65a)$$

$$\left\{ \begin{aligned} \frac{d}{dt} \left( \frac{\partial \mathcal{L}}{\partial \dot{\mathbf{t}}_0} \right) - \frac{\partial \mathcal{L}}{\partial \mathbf{x}_0} &= \boldsymbol{\tau}_0 + \boldsymbol{\tau}_{ext0} \end{aligned} \right. \quad (2.65b)$$

$$\left\{ \begin{aligned} \frac{d}{dt} \left( \frac{\partial \mathcal{L}}{\partial \dot{\mathbf{q}}} \right) - \frac{\partial \mathcal{L}}{\partial \mathbf{q}} &= \boldsymbol{\tau}_q + \boldsymbol{\tau}_{ext} \end{aligned} \right. \quad (2.65c)$$

By evaluating the Lagrangian expression (2.64) with these Euler-Lagrange equations, the

equations of motions for a flying SMS with flexible appendages and subject to external forces/-torques are detailed in its most generic form as:

$$\underbrace{\begin{bmatrix} \mathbf{M}_0 & \mathbf{M}_{0q} & \mathbf{M}_{0\eta} \\ \mathbf{M}_{0q}^T & \mathbf{M}_q & \mathbf{0}_{n_q \times n_\eta} \\ \mathbf{M}_{0\eta}^T & \mathbf{0}_{n_\eta \times n_q} & \mathbf{M}_\eta \end{bmatrix}}_{\mathbf{M}(\mathbf{x}_0, \mathbf{q})} \begin{bmatrix} \dot{\mathbf{t}}_0 \\ \ddot{\mathbf{q}} \\ \ddot{\boldsymbol{\eta}} \end{bmatrix} + \underbrace{\begin{bmatrix} \mathbf{D}_0 & \mathbf{D}_{0q} & \mathbf{D}_{0\eta} \\ \mathbf{D}_{q0} & \mathbf{D}_q & \mathbf{0}_{n_q \times n_\eta} \\ \mathbf{D}_{\eta 0} & \mathbf{0}_{n_\eta \times n_q} & \mathbf{D}_\eta \end{bmatrix}}_{\mathbf{D}(\mathbf{q}_0, \mathbf{q}, \dot{\mathbf{q}}_0, \dot{\mathbf{q}})} \begin{bmatrix} \dot{\mathbf{t}}_0 \\ \dot{\mathbf{q}} \\ \dot{\boldsymbol{\eta}} \end{bmatrix} + \begin{bmatrix} \mathbf{0}_{6 \times n_\eta} \\ \mathbf{0}_{n_q \times n_\eta} \\ \mathbf{K}_\eta \boldsymbol{\eta} \end{bmatrix} = \begin{bmatrix} \boldsymbol{\tau}_0 + \boldsymbol{\tau}_{ext_0} \\ \boldsymbol{\tau}_q + \boldsymbol{\tau}_{ext_q} \\ \boldsymbol{\tau}_{ext_\eta} \end{bmatrix} \quad (2.66)$$

with the expressions of the inertia terms detailed as:

$$\mathbf{M}_0 = \begin{bmatrix} \mathcal{I}_0 & \mathbf{0}_3 \\ \mathbf{0}_3 & m_0 \mathbf{I}_3 \end{bmatrix} + \sum_{i=1}^{n_q} \mathbf{B}_{i0}^T \begin{bmatrix} \mathcal{I}_i & \mathbf{0}_3 \\ \mathbf{0}_3 & m_i \mathbf{I}_3 \end{bmatrix} \mathbf{B}_{i0} + \sum_{i=1}^{n_p} \mathbf{B}_{P_{f_i}0}^T \begin{bmatrix} \mathcal{I}_i & \mathbf{0}_3 \\ \mathbf{0}_3 & m_i \mathbf{I}_3 \end{bmatrix} \mathbf{B}_{P_{f_i}0} \quad (2.67a)$$

$$\mathbf{M}_{0q} = \sum_{i=1}^{n_q} \mathbf{B}_{i0}^T \begin{bmatrix} \mathcal{I}_i & \mathbf{0}_3 \\ \mathbf{0}_3 & m_i \mathbf{I}_3 \end{bmatrix} \mathbf{J}_{m_i} \quad (2.67b)$$

$$\mathbf{M}_q = \sum_{i=1}^{n_q} \mathbf{J}_{m_i}^T \begin{bmatrix} \mathcal{I}_i & \mathbf{0}_3 \\ \mathbf{0}_3 & m_i \mathbf{I}_3 \end{bmatrix} \mathbf{J}_{m_i} \quad (2.67c)$$

$$\mathbf{M}_\eta = \mathbf{I}_\eta \quad (2.67d)$$

$$\mathbf{M}_{0\eta} = \mathbf{L}_{\eta p}^T \quad (2.67e)$$

and the convective terms expressions given as:

$$\mathbf{D}_0 = \dot{\mathbf{M}}_0 - \frac{1}{2} \frac{\partial}{\partial \mathbf{x}_0} \left( \mathbf{t}_0^T \mathbf{M}_0 + \dot{\mathbf{q}} \mathbf{M}_{0q}^T + \dot{\boldsymbol{\eta}} \mathbf{M}_{0\eta}^T \right) \quad (2.68a)$$

$$\mathbf{D}_{0q} = \dot{\mathbf{M}}_{0q} - \frac{1}{2} \frac{\partial}{\partial \mathbf{x}_0} \left( \dot{\mathbf{q}}^T \mathbf{M}_q + \mathbf{t}_0^T \mathbf{M}_{0q} \right) \quad (2.68b)$$

$$\mathbf{D}_{q0} = \dot{\mathbf{M}}_{0q}^T - \frac{1}{2} \frac{\partial}{\partial \mathbf{q}} \left( \mathbf{t}_0^T \mathbf{M}_0 + \dot{\mathbf{q}} \mathbf{M}_{0q}^T \right) \quad (2.68c)$$

$$\mathbf{D}_q = \dot{\mathbf{M}}_q - \frac{1}{2} \frac{\partial}{\partial \mathbf{q}} \left( \dot{\mathbf{q}}^T \mathbf{M}_q + \mathbf{t}_0^T \mathbf{M}_{0q} \right) \quad (2.68d)$$

$$\mathbf{D}_{0\eta} = \dot{\mathbf{L}}_{\eta p}^T - \frac{1}{2} \frac{\partial}{\partial \mathbf{x}_0} \left( \mathbf{t}_0^T \mathbf{L}_{\eta p}^T \right) \quad (2.68e)$$

$$\mathbf{D}_{\eta 0} = \dot{\mathbf{L}}_{\eta p} \quad (2.68f)$$

The expressions of the time-derivative matrices are given in (2.30) and differentiations according to  $\mathbf{x}_0$  and  $\mathbf{q}$  are detailed in appendix A.

The addition of the flexible dynamics leads to a second order dynamic model describing the behavior of a flying SMS with flexible appendages. One will note that the actuators have an impact only through the motions of the base and reciprocally the flexible vibrations induce disturbances on the rest of the system by affecting first the base. With such model, no assumption on the angular velocities of the base are made. The only hypothesis is made on the finite element method to obtain the flexible DoFs and the following base reduction to consider a smaller number of DoFs. Moreover, to preserve the expression of matrices of



the participation factors, the junction between a flexible body and the rigid hub should be punctual.

To preferably expressed the dynamic model (2.66) with the base angular dynamics expressed in their body frame (i.e.  $\dot{\mathbf{q}}_0 = [\boldsymbol{\omega}_0^{satT} \quad \dot{\mathbf{r}}_{S_0}^T]^T$ ), the base transformation (2.14) is once again detailed here. The reaction-wheels' velocities,  $\dot{\mathbf{q}}_r$ , and manipulator's joints' ones,  $\dot{\mathbf{q}}_m$ , are expressed in a generalized vector  $\dot{\mathbf{q}} = [\dot{\mathbf{q}}_r^T \quad \dot{\mathbf{q}}_m^T]^T$ . Furthermore, to express the equations of motions for a rotation-free-floating SMS with flexible appendages, only the actuator's control torques are considered and external torques and forces are neglected. Then the overall dynamics are given adapting (2.66) with the appropriate changes as:

$$\underbrace{\begin{bmatrix} \mathbf{H}_0 & \mathbf{H}_{0q} & \mathbf{H}_{0\eta} \\ \mathbf{H}_{0q}^T & \mathbf{H}_q & \mathbf{0}_{n_q \times n_\eta} \\ \mathbf{H}_{0\eta}^T & \mathbf{0}_{n_\eta \times n_q} & \mathbf{H}_\eta \end{bmatrix}}_{\mathbf{H}(\mathbf{x}_0, \mathbf{q})} \begin{bmatrix} \ddot{\mathbf{q}}_0 \\ \ddot{\mathbf{q}} \\ \ddot{\boldsymbol{\eta}} \end{bmatrix} + \underbrace{\begin{bmatrix} \mathbf{C}_0 & \mathbf{C}_{0q} & \mathbf{C}_{0\eta} \\ \mathbf{C}_{q0} & \mathbf{C}_q & \mathbf{0}_{n_q \times n_\eta} \\ \mathbf{C}_{\eta 0} & \mathbf{0}_{n_\eta \times n_q} & \mathbf{C}_\eta \end{bmatrix}}_{\mathbf{C}(\mathbf{q}_0, \mathbf{q}, \dot{\mathbf{q}}_0, \dot{\mathbf{q}})} \begin{bmatrix} \dot{\mathbf{q}}_0 \\ \dot{\mathbf{q}} \\ \dot{\boldsymbol{\eta}} \end{bmatrix} + \begin{bmatrix} \mathbf{0}_{6 \times n_\eta} \\ \mathbf{0}_{n_q \times n_\eta} \\ \mathbf{K}_\eta \boldsymbol{\eta} \end{bmatrix} = \begin{bmatrix} \mathbf{0}_{6 \times 1} \\ \boldsymbol{\tau}_q \\ \mathbf{0}_{n_\eta \times 1} \end{bmatrix} \quad (2.69)$$

with the inertia matrix,  $\mathbf{H}(\mathbf{x}_0, \mathbf{q})$ , expression detailed such that the base angular velocities are expressed in the base body frame,  $\mathcal{R}_{sat}$ , as:

$$\begin{cases} \mathbf{H}_0 = \mathbf{P}_0^T \mathbf{M}_0 \mathbf{P}_0 & (2.70a) \\ \mathbf{H}_{0q} = \mathbf{P}_0^T \mathbf{M}_{0q} & (2.70b) \\ \mathbf{H}_q = \mathbf{M}_q & (2.70c) \\ \mathbf{H}_\eta = \mathbf{M}_\eta & (2.70d) \\ \mathbf{H}_{0\eta} = \mathbf{P}_0^T \mathbf{L}_{\eta p}^T & (2.70e) \end{cases}$$

and the convective matrix,  $\mathbf{C}(\mathbf{q}_0, \mathbf{q}, \dot{\mathbf{q}}_0, \dot{\mathbf{q}})$ , detailed as:

$$\begin{cases} \mathbf{C}_0 = \mathbf{P}_0^T \mathbf{D}_0 \mathbf{P}_0 & (2.71a) \\ \mathbf{C}_{0q} = \mathbf{P}_0^T \mathbf{D}_{0q} & (2.71b) \\ \mathbf{C}_{q0} = \mathbf{D}_{q0} \mathbf{P}_0 & (2.71c) \\ \mathbf{C}_q = \mathbf{D}_q & (2.71d) \\ \mathbf{C}_{0\eta} = \mathbf{P}_0^T \mathbf{D}_{0\eta} & (2.71e) \\ \mathbf{C}_{\eta 0} = \mathbf{D}_{\eta 0} \mathbf{P}_0 & (2.71f) \end{cases}$$

The free-floating mode define the control torques/forces  $\boldsymbol{\tau}_0$  is null and only the controlled reaction-wheels' torque,  $\boldsymbol{\tau}_r$ , and the manipulator's joints control torques apply a torque on the base.

## 2.4 Matlab-Simulink simulation and analysis tools

Deriving the dynamics of a rigid multi-body system with different kinematic-chains and flexible elements rigidly fixed to the system's base has been a first contribution of this work. Capitalizing on this modeling effort that provides recursive computation of the kinematics/-dynamics of such systems, a Matlab-Simulink tool is developed. This section aims at detailing the functionalities and potential uses of the tools.

### 2.4.1 Simulator functionalities

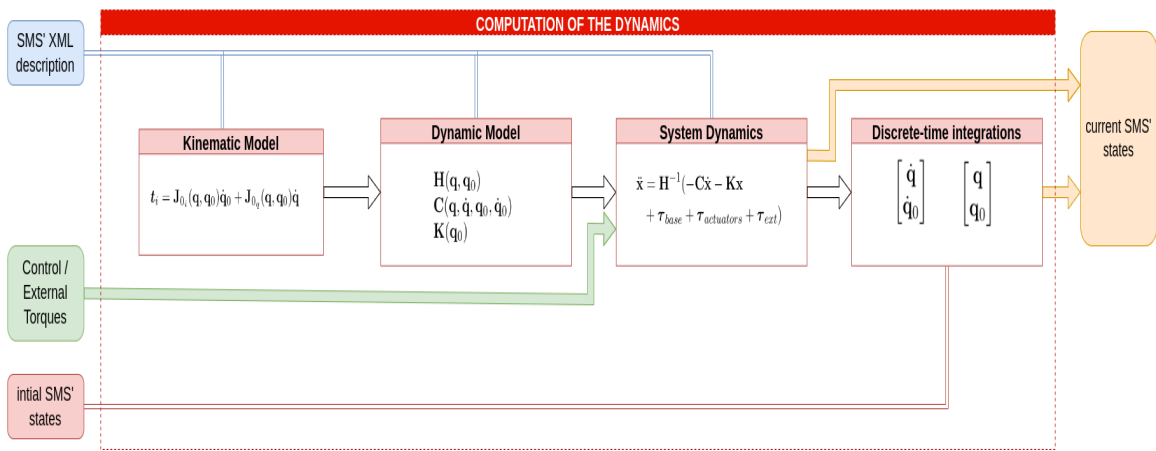


Figure 2.5 – Description of the Simulink model

Developing the kinematics/dynamics of a multi-body and multi-kinematic chains system with a common base from the DH and Lagrangian formalisms advantageously provide a recursive description of the system states. Based on SPART<sup>13</sup> [VL+16], Matlab functions are developed to obtain both direct and inverse kinematic/dynamic models for flying and floating SMS (the difference is in the choice of actuators and control torques). SPART is an open-source software toolkit for modeling kinematic and dynamic of a 6-DoFs actuated spacecraft with different rigid kinematic-chains. Thus, both flying and floating SMS can be modeled and simulated. A robot is described in a standardized XML<sup>14</sup> description which is thus an input of the simulation and analysis tool. Each elements are individually described (dimension, inertia, mass) with the parent and child joints as detailed in appendix B.

From the descriptive functions of SPART that provides a tree mapping of SMS, kinematics/dynamics functions are adapted with our proposed Lagrangian approach developed in sections 2.2 and 2.3 to obtain the dynamics of a rotation-free-floating with flexible appendages

<sup>13</sup>Spacecraft Robotics Toolkit

<sup>14</sup>eXtensible Markup Language

as given by equations (2.66) and (2.69). Moreover, to guarantee computation efficiency, the rigid dynamics as been derived with a Newton-Euler modeling approach [VL+18]. Then as a first input of our elaborated Matlab-Simulink toolbox the studied robot is described in an XML description link by link with the following required informations:

- Physical properties: mass, inertia, size for a rigid body-link and additionally for a flexible appendage the number of flexible modes, their natural frequencies, dampings and the matrix of participation factors
- Position in the kinematic chains: the attached links (one parent-link and for an element other than end-effector a child-link), the initial position according to the referential frame of the parent-link
- Joint nature: either fixed, prismatic or revolute

One will note that actuators' dynamics and effort limits are not considered, however can be easily added in a Simulink model.

Thanks to the overall functions established to compute both direct and inverse kinematics/dynamics time-domain simulations are obtained with Simulink models. For a given spacecraft configuration (joints positions/orientations, base attitude and position in  $\mathcal{R}_{ine}$ ) and joints/links velocities the inverse kinematics/dynamics functions allows to compute inertia and convective matrices. Respectively, the direct kinematics/dynamics functions provide spacecraft configuration and system velocities in function of actuators' torques, base external actuating torques and system's external forces/torques applying on the robot. Thus, from a general standpoint, one can introduce the state vector  $\mathbf{x}$  composed of the 6-DoFs base states, the actuators states and the flexible ones. Then for a flying SMS with flexible appendages its equations of motions are given by a general second order equation (2.72). Such a system can be studied and analyzed with these tools for a given configuration or a manipulator motion.

$$\mathbf{H}\ddot{\mathbf{x}} + \mathbf{C}\dot{\mathbf{x}} + \mathbf{K}\mathbf{x} = \boldsymbol{\tau}_{base} + \boldsymbol{\tau}_{actuators} + \boldsymbol{\tau}_{ext} \quad (2.72)$$

A description of what is latter referred to as the main Simulink function is given in Figure 2.5. In order to obtain the direct dynamics of a system which behaviors is described with (2.72), first an initialization step is established. In this initial step the XML description is converted onto a Matlab structure taking into account the tree topology of the SMS and an initial pose is given. Then for every time step, the overall velocities and Jacobians are computed from the measure of the current state. Therefore equation (2.15) can be evaluated. Then, the inertia, convective and stiffness matrices as developed according to (2.69) are computed with the joints states and the physical properties in the XML description. Finally, for the considered forces/torques (i.e. the base control forces/torques  $\boldsymbol{\tau}_{base}$ , the actuators control forces/torques  $\boldsymbol{\tau}_{actuators}$  or any external forces/torques  $\boldsymbol{\tau}_{ext}$ ) the new state of the SMS is obtained by integration of the system's accelerations.

Furthermore, as one can visualize with Figure 2.6 visualization tools are available. Besides providing a visual of a manipulator motion, it allows to verify in a first step the appropriate

construction of the XML description and likewise visually verify the feasibility of a motion. In Figure 2.6, two SMS examples are provided for which the base is represented as a red cylinder. In both cases, gray cylinders inside the base correspond to the reaction-wheels. Smaller red cylinders correspond to the different junctions/actuators positions. It is likewise illustrated with SMS on the right side of Figure 2.6 that flexible elements can be positioned on a body rigidly fixed to the base. In this case four flexible beams are attached to the first payload.

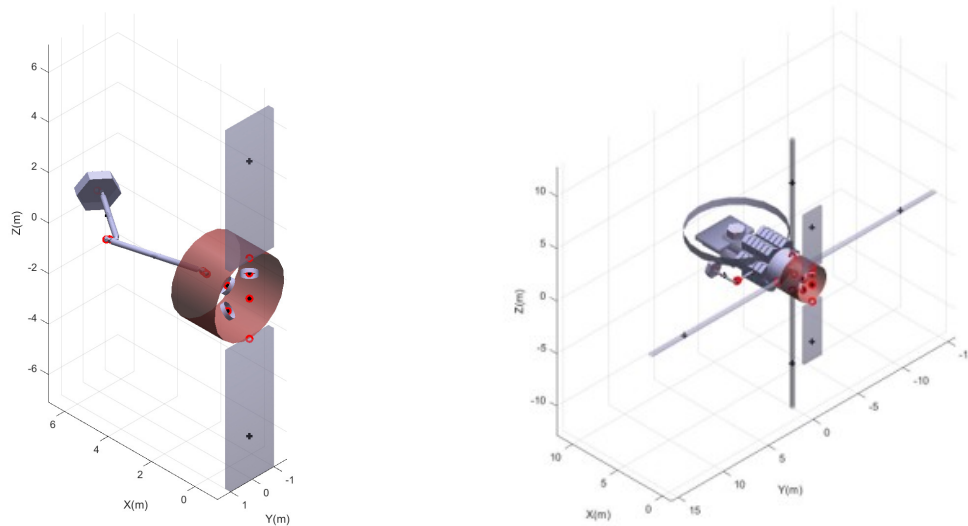


Figure 2.6 – Examples of SMS modeled with the proposed Matlab tools, on the left a SMS composed of a 3-DoFs manipulator, 3 reaction-wheels and 2 flexible solar arrays, on the right a modeled version of the PULSAR telescope use-case <https://www.h2020-pulsar.eu/>

To put it concisely, from a robot description, a pre-analysis can be developed to identify the manipulator’s feasible motions and configurations without reaching conflict with the rest of the system’s elements. Secondly, time-domain simulations can be obtained with Simulink models such that for forces/torques and a given robot structure provided as inputs, an actualized SMS state can be computed at any time.

### 2.4.2 Validation and performances of the developed simulation tools

The modeling formalism has been adapted to first integrate reaction-wheels and secondly an extension of the kinematic/dynamic with flexible behaviors to the pre-existing SPART. Therefore, a validation step is essential to raise the numerous potential coding errors and highlight the limits due to the choice of solver, sampling and other numerical integration induced errors.

We present in this section the validation process divided into two steps. First the correct integration of the base’s actuators is proceeded upon with a system momentum discussion

similarly proposed in [Wil+18] considering a rigid SMS. Secondly, the flexible integration is verified with existing tools that develop kinematic/dynamic models with a Newton-Euler approach [ACT08].

### 2.4.2.1 Simulation of rigid systems

The integration of the base actuators developed in section 2.2.4 to a rigid system is first established. The validation is developed with the SMS described in appendix B and visualized in Figure 2.7 where the flexible modes are not considered. First a numerical criterion is evaluated to observe the numerical limitations constrained by the main Simulink function and the integrations. Then the validation of the correct implementation of functions are discussed with physical properties verified by free-floating SMS.

**Simulator performances** In order to evaluate performances and limitations of the time-domain simulations obtained with the Simulink models, an input/output comparison of the dynamic evaluation bloc is developed. The main function of the Simulink model requires two inputs, the robot's description and the forces/control torques. In the case of the free-floating SMS the input control is denoted  $\boldsymbol{\tau}_{in}$ , such that  $\boldsymbol{\tau}_{in} = \begin{bmatrix} \mathbf{0}_{6 \times 1}^T & \boldsymbol{\tau}_q^T \end{bmatrix}^T$  (with no forces/torques applied on the base) and the system's accelerations (i.e.  $\ddot{\mathbf{x}} = \begin{bmatrix} \ddot{\mathbf{x}}_0^T & \ddot{\mathbf{q}}^T \end{bmatrix}^T$ ) are computed with (2.43). Thus, the simulator's performances are evaluated with the threshold,  $\lambda$ , while considering the error defined from (2.43) as:

$$\|\boldsymbol{\epsilon}_\tau\| = \|\boldsymbol{\tau}_{in} - (\mathbf{H}\ddot{\mathbf{x}} + \mathbf{C}\dot{\mathbf{x}})\| < \lambda \quad (2.73)$$

The value of  $\lambda$  corresponds to the numerical errors or noise which allows to conclude on the consistency of the output data.

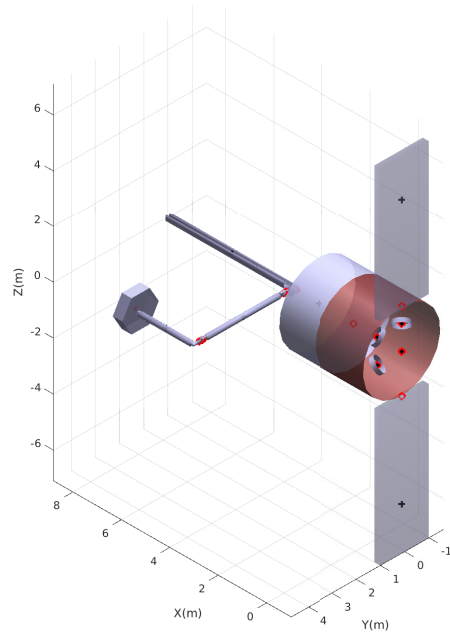


Figure 2.7 – Visual of the illustrative SMS used for tool validations

**Simulator validation** As discussed in [Wil+18], a rigid free-floating SMS that is not subject to external torques/forces will have its CoM and momenta remaining unchanged for a given manipulator maneuver. This property is thus considered in the validation process of a rigid multi-body system. Considering an SMS of which its motions are described by (2.43), for an initially null linear and angular momentum, the momentum expression is given in  $\mathcal{R}_{ine}$  by [Wil+18]:

$$\|\mathbf{M}_0 \mathbf{t}_0 + \mathbf{M}_{0m} \dot{\mathbf{q}}_m + \mathbf{M}_{0r} \dot{\mathbf{q}}_r\| < \lambda \quad (2.74)$$

with the reaction-wheels only affecting the evolution of angular momentum.

In order to consider a stable and feasible SMS maneuver (i.e. without reaching singular configurations) and verify the momentum conservation, a simple control law is established. Based on classical robotic control applications an NDI<sup>15</sup> is introduced to decouple and linearize the system. In addition a simple proportional control of the joints' velocities is used. From (2.43), a control torque that allows to obtain an NDI for a rotation-free-floating SMS is given as:

$$\boldsymbol{\tau}_{q_{in}} = \mathbf{H}_m (\mathbf{K} (\dot{\mathbf{q}}_d - \dot{\mathbf{q}})) + \mathbf{C}_m \dot{\mathbf{q}}_d + \mathbf{H}_{0m}^T \ddot{\mathbf{q}}_0 + \mathbf{C}_{m0} \dot{\mathbf{q}}_0 \quad (2.75)$$

with  $\mathbf{K}$  a diagonal matrix corresponding to a linear proportional control gain and  $\dot{\mathbf{q}}_d$  the desired joint velocities.

**Discussion with Time-domain simulations** To obtain consistent time-domain results, Simulink models are given the following solver parameters:

- Solver: ode45
- Fixed-step: 0.01s

and simulations are run on a standard computer with an Intel i7 CPU.

Firstly, the simulator performances are evaluated to properly comment simulation results. As visualized with the evolution of the torque error signal (2.73) plotted in Figure 2.8, corresponding to the input torques represented in the upper subplot of Figure 2.9, data with values lower than  $\lambda = 10^{-13}$  are considered as under the simulator precision, or in another words corresponds to zero values.

---

<sup>15</sup>Nonlinear Dynamic Inversion

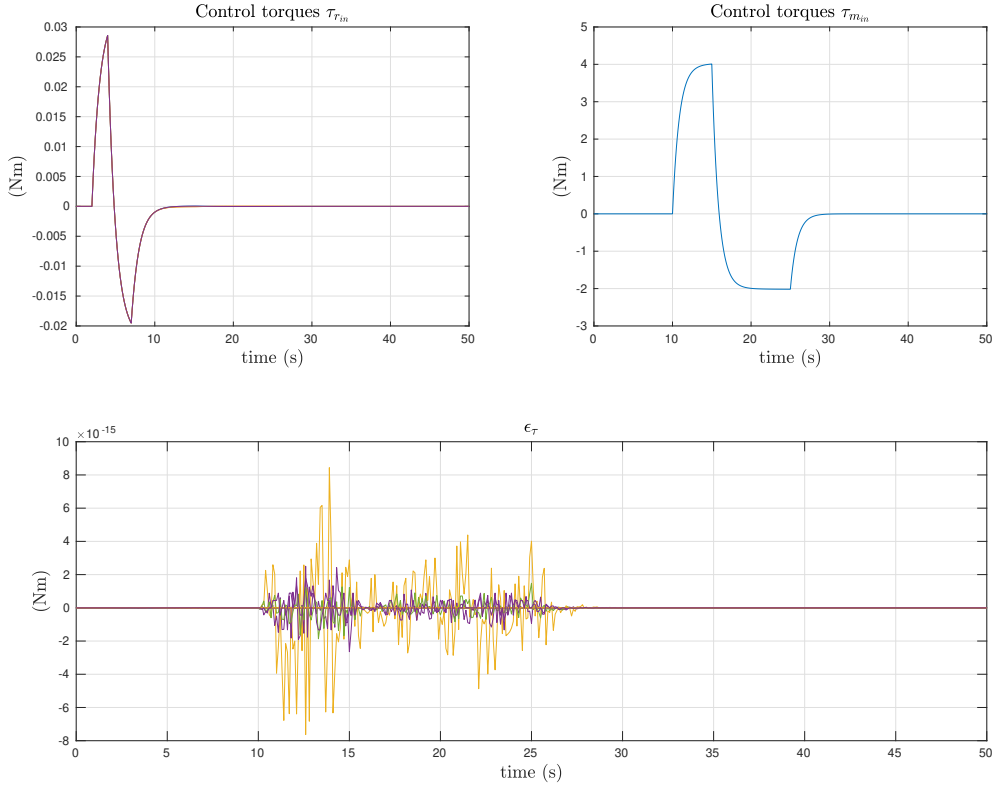


Figure 2.8 – Upper subplots represent the input torques,  $\tau_{rin}$  (left) and  $\tau_{min}$  (right); Lower subplot represents the evolution of the torque error signal  $\epsilon_{\tau}$  (2.73)

Secondly, the developed kinematic/dynamic functions are validated considering the evolution of the system's momentum for a manipulator's/reaction-wheels' motion. With the control torque computation being as in (2.75), first the reaction-wheels are used then the manipulator's joints as one can notice with Figure 2.9. This allows to observe the impact of the SMS's actuators as decomposed in the three first rows of subplot in Figure 2.10. As expected, reaction-wheels only modify angular momentum while the manipulator motions affect both linear and angular. Last row of subplot in Figure 2.10, allows to conclude on the momentum conservation and consequently on the accurate implementation of the modeling functions to study the behavior of a rotation-free-floating SMS. Such conclusion is made considering the values of the angular and linear momentum that remains at the precision  $\lambda$ . Moreover, one will note that the numerical error is due to a coupling transfer between the angular and linear spacecraft's dynamics when the manipulator is moving.

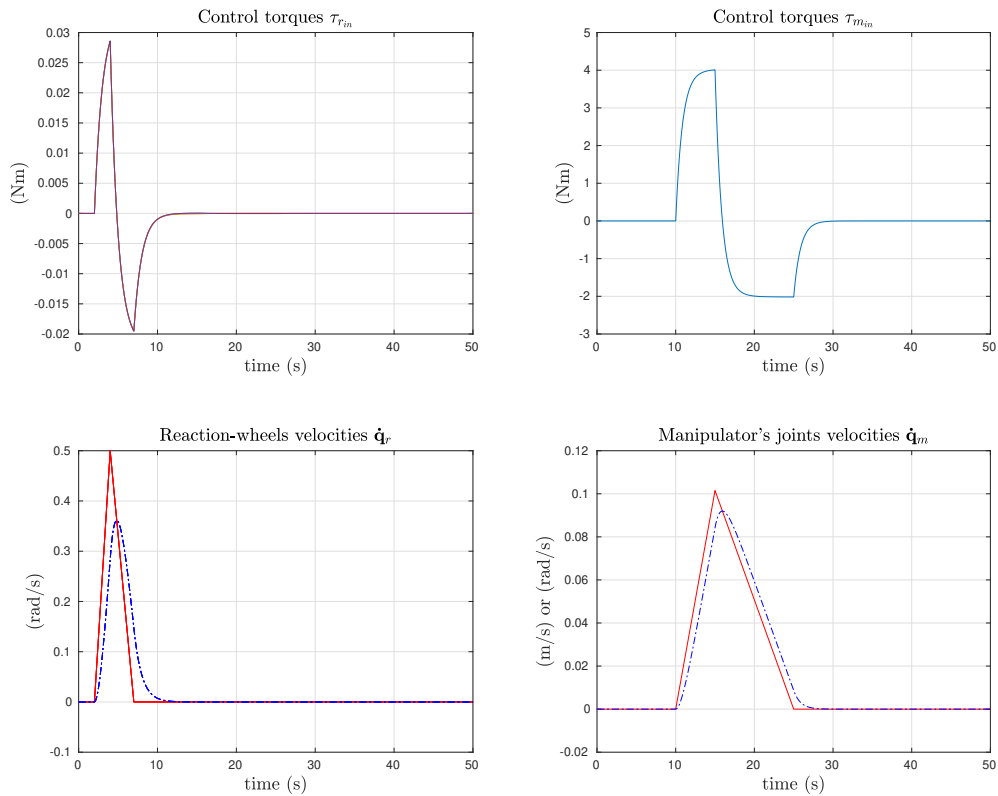


Figure 2.9 – Upper figures represents the input torques  $\tau_{q_{in}}$  ( $\tau_{r_{in}}$  on the left and  $\tau_{m_{in}}$  on the right); Lower figures correspond to the control performances with the desired velocities in the red full-line and the measured velocities in the blue dash-line

Furthermore, interpretations of the momentum distribution can be developed based on its conservation. As visualized with Figure 2.10, for each manipulator's motions a counter-reaction of the base will compensate with a linear motion the accumulated momentum. Similarly, each manipulator's motions inducing angular momentum are compensated with both reaction-wheels and base motions. Similar and reciprocal behaviors occur with the use of reaction-wheels.



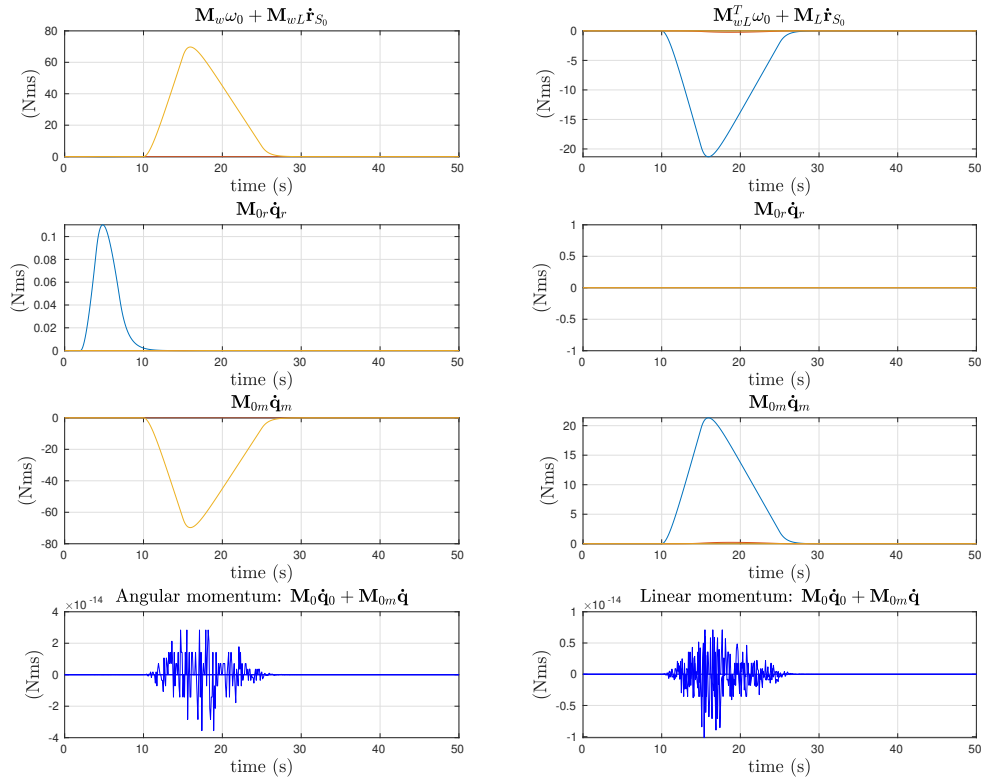


Figure 2.10 – Left subplots represent the system’s angular momentum and right subplots the linear momentum. Sub-figures in first row respectively represent the base momentum, in second row the reaction-wheels momentum, in third row the manipulator momentum and in fourth row the total momentum

### 2.4.2.2 Validation of the flexible dynamics integration

**Tools validation** Flexible dynamics induces dissipative forces and consequently there is no kinetic momentum conservation. For this reason validation cannot be based on a similar conservatism approach as developed in the section 2.4.2.1 and we will therefore use existing and confirmed modeling tools. The toolbox that came by Alazard and al. [ACT08], SDT<sup>16</sup>, allows to develop linear models of multi-body systems for space applications. Based on a Newton-Euler modeling method, for each body a transfer function between the forces/torques and accelerations is associated. In particular, for a spacecraft with flexible appendages attached with a cantilever or revolute joint to the main hub, a hybrid-cantilever model is used to obtain the dynamic model for each appendage. Then, in respect to the topology of the system and through combination of the different transfer function a linearized dynamic model of the overall system is computed. The verification process consists in a comparison of linear

<sup>16</sup>Satellite Dynamic Toolbox

models computed from our tools and the ones obtained with SDT. The following steps are to conclude on the accuracy of functions' implementation integrating the flexible dynamics onto the rigid ones of a flying SMS:

- Comparison between the rigid behaviors obtained with the SDT and our tools by observing the static gains of SDT's direct linear models and the ones linearized from our tools
- Comparison of the singular values of linear inverse dynamic models of the SMS
- Comparison of the eigenvalues of linear inverse dynamic models of the SMS

This validation process is developed on the PULSAR space telescope (<https://www.h2020-pulsar.eu>) in which different flexible appendages are rigidly attached to a fixed element on the base as visualized with the right spacecraft representation in Figure 2.6. A first reduced model of PULSAR, composed by the base, the payload and a sun-shield beam was useful to assess the computation of the generalized inertia matrix, the convective inertia matrix and the generalized stiffness matrix [Cum+21]. The equality of rigid behaviors (the DC gain of the two direct dynamic models of the global spacecraft), the eigenvalues correspondence of the inverse dynamic models of the global satellite system (base + payload + the 4 sun-shield beams + the 2 solar panels), and the superposition of the singular values of their frequency responses are means to assess the developments of the flexible functions (see Figures 2.11 and 2.12 ).

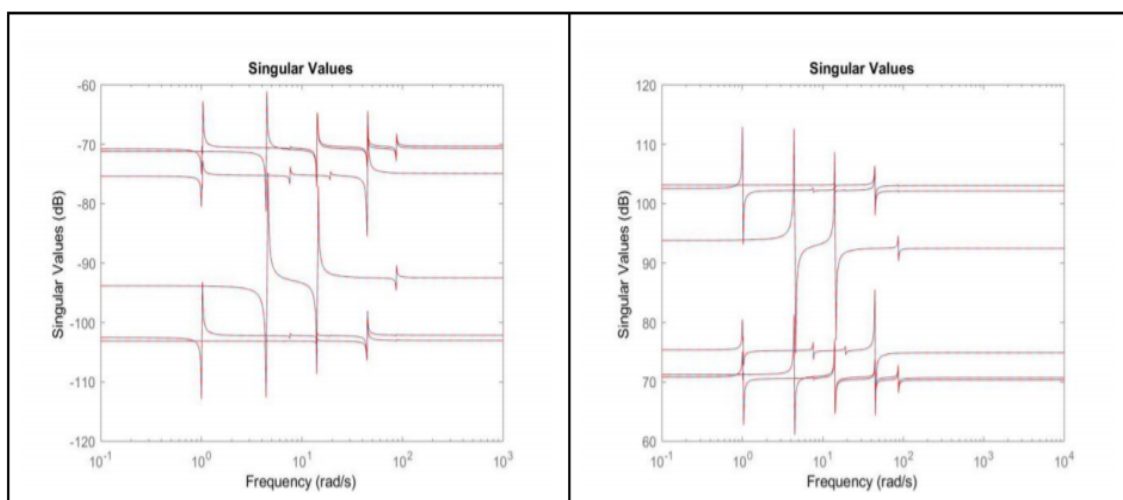


Figure 2.11 – Comparison between singular values of direct linear models: on the left SDT models and on the right models linearized from our tools [Cum+21]

Eigenvalues of the SDT inverse dynamic model			Eigenvalues of the SPART inverse dynamic model		
Pole	Damping	Frequency (rad/s)	Pole	Damping	Frequency (rad/s)
-5.10e-03 +/- 1.01e+00i	5.04e-03	1.01e+00	-5.10e-03 +/- 1.01e+00i	5.04e-03	1.01e+00
-5.30e-03 +/- 1.03e+00i	5.14e-03	1.03e+00	-5.30e-03 +/- 1.03e+00i	5.14e-03	1.03e+00
-2.27e-02 +/- 4.47e+00i	5.08e-03	4.47e+00	-2.27e-02 +/- 4.47e+00i	5.08e-03	4.47e+00
-2.40e-02 +/- 4.60e+00i	5.23e-03	4.60e+00	-2.40e-02 +/- 4.60e+00i	5.23e-03	4.60e+00
-3.39e-02 +/- 6.79e+00i	5.00e-03	6.79e+00	-3.39e-02 +/- 6.79e+00i	5.00e-03	6.79e+00
-3.39e-02 +/- 6.79e+00i	5.00e-03	6.79e+00	-3.39e-02 +/- 6.79e+00i	5.00e-03	6.79e+00
-3.81e-02 +/- 7.61e+00i	5.00e-00	7.61e+00	-3.81e-02 +/- 7.61e+00i	5.00e-00	7.61e+00
-3.81e-02 +/- 7.62e+00i	5.01e-03	7.62e+00	-3.81e-02 +/- 7.62e+00i	5.01e-03	7.62e+00
-7.17e-02 +/- 1.42e+01i	5.05e-03	1.42e+01	-7.17e-02 +/- 1.42e+01i	5.05e-03	1.42e+01
-7.17e-02 +/- 1.42e+01i	5.05e-03	1.42e+01	-7.17e-02 +/- 1.42e+01i	5.05e-03	1.42e+01
-7.50e-02 +/- 1.45e+01i	5.16e-03	1.45e+01	-7.50e-02 +/- 1.45e+01i	5.16e-03	1.45e+01
-9.59e-02 +/- 1.92e+01i	5.00e-03	1.92e+01	-9.59e-02 +/- 1.92e+01i	5.00e-03	1.92e+01
-9.60e-02 +/- 1.92e+01i	5.00e-03	1.92e+01	-9.60e-02 +/- 1.92e+01i	5.00e-03	1.92e+01
-2.26e-01 +/- 4.48e+01i	5.04e-03	4.48e+01	-2.26e-01 +/- 4.48e+01i	5.04e-03	4.48e+01
-2.26e-01 +/- 4.48e+01i	5.05e-03	4.48e+01	-2.26e-01 +/- 4.48e+01i	5.05e-03	4.48e+01
-2.29e-01 +/- 4.51e+01i	5.08e-03	4.51e+01	-2.29e-01 +/- 4.51e+01i	5.08e-03	4.51e+01
-4.37e-01 +/- 8.72e+01i	5.01e-03	8.72e+01	-4.37e-01 +/- 8.72e+01i	5.01e-03	8.72e+01
-4.37e-01 +/- 8.72e+01i	5.01e-03	8.72e+01	-4.37e-01 +/- 8.72e+01i	5.01e-03	8.72e+01
-4.37e-01 +/- 8.72e+01i	5.01e-03	8.72e+01	-4.37e-01 +/- 8.72e+01i	5.01e-03	8.72e+01

Figure 2.12 – Comparison between eigenvalues of direct linear models: on the left SDT models and on the right models linearized from our tools <https://www.h2020-pulsar.eu>

**Simulator limitations** To evaluate any numerical limitations of the Simulink model, a comparison of input/output torques of the main Simulink function is performed. Considering a free-floating SMS with flexible appendages, the input torque, denoted  $\boldsymbol{\tau}_{in} = \begin{bmatrix} \mathbf{0}_{6 \times 1}^T & \boldsymbol{\tau}_q^T & \mathbf{0}_{n_\eta \times 1}^T \end{bmatrix}^T$ , allows to compute the system's accelerations,  $\ddot{\mathbf{x}} = \begin{bmatrix} \ddot{\mathbf{x}}_0^T & \ddot{\mathbf{q}}^T & \ddot{\boldsymbol{\eta}}^T \end{bmatrix}^T$ , with (2.69). Then, the torque error signal, used to consider simulator numerical precision is defined as:

$$\|\boldsymbol{\epsilon}_\tau\| = \left\| \boldsymbol{\tau}_{in} - \left( \mathbf{H}\ddot{\mathbf{x}} + \mathbf{C}\dot{\mathbf{x}} + \begin{bmatrix} \mathbf{0}_{6 \times n_\eta} \\ \mathbf{0}_{n_q \times n_\eta} \\ \mathbf{K}_\eta \boldsymbol{\eta} \end{bmatrix} \right) \right\| < \lambda \quad (2.76)$$

The solver parameters detailed in the previous paragraph are preserved, nevertheless some adjustments may be required with the flexible parameters to accurately compute the flexible dynamics.

Time-domain simulations are run on the SMS detailed in appendix B. Evaluation of  $\boldsymbol{\epsilon}_\tau$  is obtained for a basic SMS motion given with the input torques,  $\boldsymbol{\tau}_q$ , illustrated with the upper subplot in Figure 2.13. The simulator's limitations are quantified with the torque error signal,  $\boldsymbol{\epsilon}_\tau$  (2.76), represented in the lower subplot in Figure 2.13. One can then conclude that data presenting amplitudes lower than  $\lambda = 10^{-13}$  correspond to null values. This consideration may lead to discussions on the physical properties of flexible modes considered.

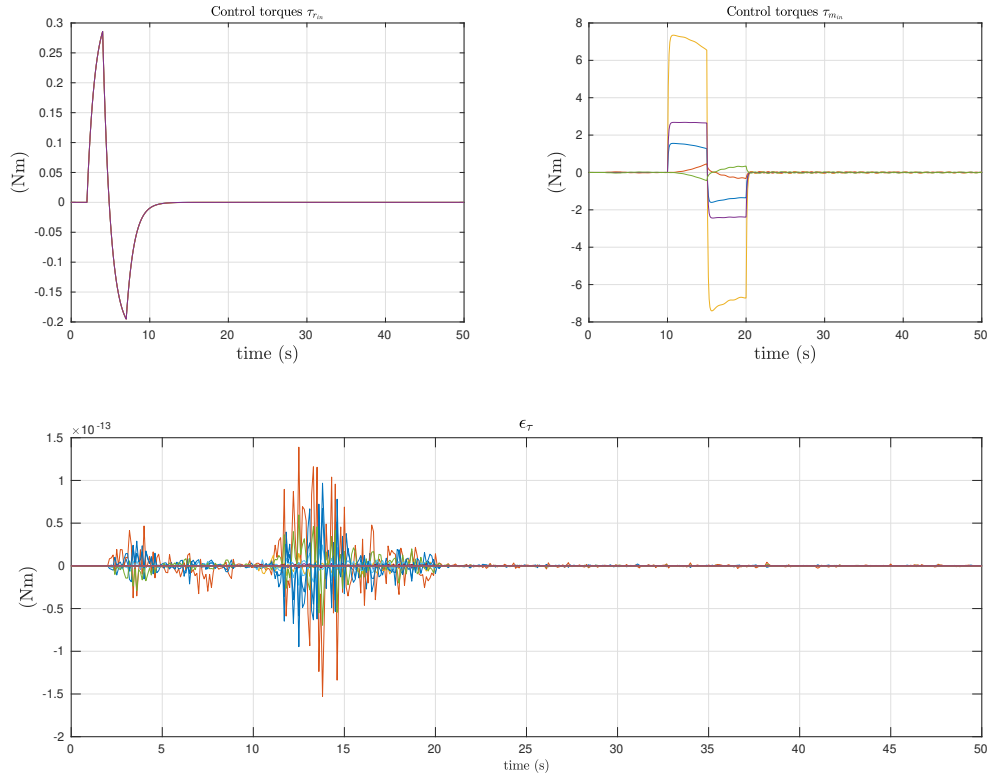


Figure 2.13 – Upper subplot represent the control torques  $\tau_{q_{in}}$ ; Lower subplot illustrates the evolution of the torque error signal  $\epsilon_\tau$  (2.76)

### 2.4.3 Example of possible analysis with modeling tools

SMS couplings studies are primordial prior to developing control strategies. In the literature for rigid systems, the influence between each SMS's body has been based on a momentum conservation hypothesis. However, it is ambitious to develop similar assumptions in presence of flexible appendages. With the modeling effort developed and with the associated tools, an energetic based analysis can be introduced to illustrate and evaluate participations of each elements on the overall system.

In order to analyze flexible dynamics evolution according to manipulator motions, one can consider the comparison between spontaneous powers and works of rigid and flexible elements. To distinguish flexible participations from the rigid ones, (2.69) is rewritten as:

$$\underbrace{\begin{bmatrix} \mathbf{H}_0 & \mathbf{H}_{0q} \\ \mathbf{H}_{0q}^T & \mathbf{H}_q \end{bmatrix} \begin{bmatrix} \ddot{\mathbf{q}}_0 \\ \ddot{\mathbf{q}} \end{bmatrix}}_{\mathcal{F}_{ine}^{rig}} + \underbrace{\begin{bmatrix} \mathbf{C}_0 & \mathbf{C}_{0q} \\ \mathbf{C}_{q0} & \mathbf{C}_q \end{bmatrix} \begin{bmatrix} \dot{\mathbf{q}}_0 \\ \dot{\mathbf{q}} \end{bmatrix}}_{\mathcal{F}_{conv}^{rig}} = \underbrace{\begin{bmatrix} \mathbf{0}_{6 \times 1} \\ \boldsymbol{\tau}_q \end{bmatrix}}_{\mathcal{F}_{ext}^{rig}} - \underbrace{\begin{bmatrix} \mathbf{H}_{0\eta} & \mathbf{C}_{0\eta} \\ \mathbf{0}_{n_q \times n_\eta} & \mathbf{0}_{n_q \times n_\eta} \end{bmatrix} \begin{bmatrix} \ddot{\boldsymbol{\eta}} \\ \dot{\boldsymbol{\eta}} \end{bmatrix}}_{\mathcal{F}_{ext}^{flex \rightarrow rig}} \quad (2.77)$$

with  $\mathcal{F}_{ine}^{rig}$  an inertial force,  $\mathcal{F}_{conv}^{rig}$  a convective force,  $\mathcal{F}_{ext}^{rig}$  an external control torque and  $\mathcal{F}_{ext}^{flex \rightarrow rig}$  an external flexible force affecting the rigid dynamics. Similarly from (2.69), forces/torques can be defined for the flexible dynamics as:

$$\underbrace{\mathbf{H}_\eta \ddot{\boldsymbol{\eta}}}_{\mathcal{F}_{ine}^{flex}} + \underbrace{\mathbf{C}_\eta \dot{\boldsymbol{\eta}}}_{\mathcal{F}_{conv}^{flex}} + \underbrace{\mathbf{K}_\eta \boldsymbol{\eta}}_{\mathcal{F}_{pot}^{flex}} = - \underbrace{\begin{bmatrix} \mathbf{H}_{0\eta}^T & \mathbf{C}_{\eta 0} \end{bmatrix}}_{\mathcal{F}_{ext}^{rig \rightarrow flex}} \begin{bmatrix} \ddot{\mathbf{q}}_0 \\ \dot{\mathbf{q}}_0 \end{bmatrix} \quad (2.78)$$

with respectively  $\mathcal{F}_{ine}^{flex}$ ,  $\mathcal{F}_{conv}^{flex}$  and  $\mathcal{F}_{pot}^{flex}$  an inertial, a convective and a potential flexible force.  $\mathcal{F}_{ext}^{rig \rightarrow flex}$  an external force corresponding to the influence of the rigid elements motions inducing flexible vibrations.

Before introducing the work of each force, the powers are defined with (2.77) and with (2.78) as:

$$\mathcal{P}_{ine}^{rig} = \begin{bmatrix} \dot{\mathbf{q}}_0^T & \dot{\mathbf{q}}^T \end{bmatrix} \mathcal{F}_{ine}^{rig} \quad (2.79a)$$

$$\mathcal{P}_{conv}^{rig} = \begin{bmatrix} \dot{\mathbf{q}}_0^T & \dot{\mathbf{q}}^T \end{bmatrix} \mathcal{F}_{conv}^{rig} \quad (2.79b)$$

$$\mathcal{P}_{ext}^{rig} = \begin{bmatrix} \dot{\mathbf{q}}_0^T & \dot{\mathbf{q}}^T \end{bmatrix} \mathcal{F}_{ext}^{rig} \quad (2.79c)$$

$$\mathcal{P}_{ext}^{flex \rightarrow rig} = \begin{bmatrix} \dot{\mathbf{q}}_0^T & \dot{\mathbf{q}}^T \end{bmatrix} \mathcal{F}_{ext}^{flex \rightarrow rig} \quad (2.79d)$$

$$\mathcal{P}_{ine}^{flex} = \dot{\boldsymbol{\eta}} \mathcal{F}_{ine}^{rig} \quad (2.79e)$$

$$\mathcal{P}_{conv}^{flex} = \dot{\boldsymbol{\eta}} \mathcal{F}_{conv}^{flex} \quad (2.79f)$$

$$\mathcal{P}_{pot}^{flex} = \dot{\boldsymbol{\eta}} \mathcal{F}_{pot}^{flex} \quad (2.79g)$$

$$\mathcal{P}_{ext}^{rig \rightarrow flex} = \dot{\boldsymbol{\eta}} \mathcal{F}_{ext}^{rig \rightarrow flex} \quad (2.79h)$$

and respectively, for each power the work associated is defined as its integral such that:

$$\forall T > 0, \mathcal{W} = \int_0^T \mathcal{P} dt \quad (2.80)$$

If the multi-body system is entirely rigid, one can retrieve the kinetic momentum conservation. Considering either the involved powers of the works, the system conservatism is verified with:

$$\begin{cases} \mathcal{P}_{ine}^{rig} + \mathcal{P}_{conv}^{rig} = \mathcal{P}_{ext}^{rig} & (2.81a) \\ \mathcal{W}_{ine}^{rig} + \mathcal{W}_{conv}^{rig} = \mathcal{W}_{ext}^{rig} & (2.81b) \end{cases}$$

Then extending this observation the coupled rigid-flexible case, a conservatism of powers and works can be verified to analyze the system's elements solicitations and impact on the overall SMS. From both equations (2.77) and (2.78) the flexible-rigid rotation-free-floating SMS verifies:

$$\begin{cases} \mathcal{P}_{ine}^{rig} + \mathcal{P}_{conv}^{rig} = \mathcal{P}_{ext}^{rig} + \mathcal{P}_{ext}^{flex \rightarrow rig} & (2.82a) \\ \mathcal{P}_{ine}^{flex} + \mathcal{P}_{conv}^{flex} + \mathcal{P}_{pot}^{flex} = \mathcal{P}_{ext}^{rig \rightarrow flex} & (2.82b) \\ \mathcal{W}_{ine}^{rig} + \mathcal{W}_{conv}^{rig} = \mathcal{W}_{ext}^{rig} + \mathcal{W}_{ext}^{flex \rightarrow rig} & (2.82c) \\ \mathcal{W}_{ine}^{flex} + \mathcal{W}_{conv}^{flex} + \mathcal{W}_{pot}^{flex} = \mathcal{W}_{ext}^{rig \rightarrow flex} & (2.82d) \end{cases}$$

This allows to quantify the work and power lost when flexible vibrations occur due to system couplings. With (2.82), the respective loss of work and powers are defined as:

$$\begin{cases} \mathcal{W}_l = \mathcal{W}_{ext}^{flex \rightarrow rig} - \mathcal{W}_{ext}^{rig \rightarrow flex} & (2.83a) \\ \mathcal{P}_l = \mathcal{P}_{ext}^{flex \rightarrow rig} - \mathcal{P}_{ext}^{rig \rightarrow flex} & (2.83b) \end{cases}$$

An illustration of the works evolution in the system is developed with Figures 2.14 and 2.15 to analyze the influence of flexible appendages in an SMS. Considering the SMS motions obtained with the input control torques represented in Figure 2.13, a comparison between rigid and flexible elements' works allows to evaluate the actuators' influence on the energetic loss.

- First, the impact of the manipulator is mainly on the variation of the system's inertia as for different configurations the mass distribution changes. This is visualized with the left subplots of Figure 2.14 in which the rigid works are detailed.
- Secondly, reaction-wheels are mostly affecting the evolution of convective terms. Base actuators modify the spacecraft's angular velocities without changing mass distribution in the overall system. Regarding the typically low manipulator's joints velocities in comparison to reaction-wheels, as illustrated with the second row of subplot in Figure 2.14, the base actuators will have a larger impact on the convective terms. This is explained with the convective terms corresponding to cross products of system's DoFs velocities and thus large reaction-wheels velocities lead to large convective terms.

A second observation and analysis can be obtained based on the direct couplings between reaction-wheels, base angular velocities and flexible modes vibrations.

- A first note can be made on the influence of the reaction-wheels use on the flexible appendages vibration. As visualized with the flexible modes' evolutions represented in Figure 2.16, when the base actuators are used. This is easily explained regarding convective terms and system's velocities.
- Considering the works derived from the flexible dynamics, visualized in the right subplots of Figure 2.14, for the given SMS motion, the manipulator poorly affects the base's rotations. Therefore, a flexible dissipative work can be quantified when the reaction-wheels are used with (2.83) as illustrated with Figure 2.15.

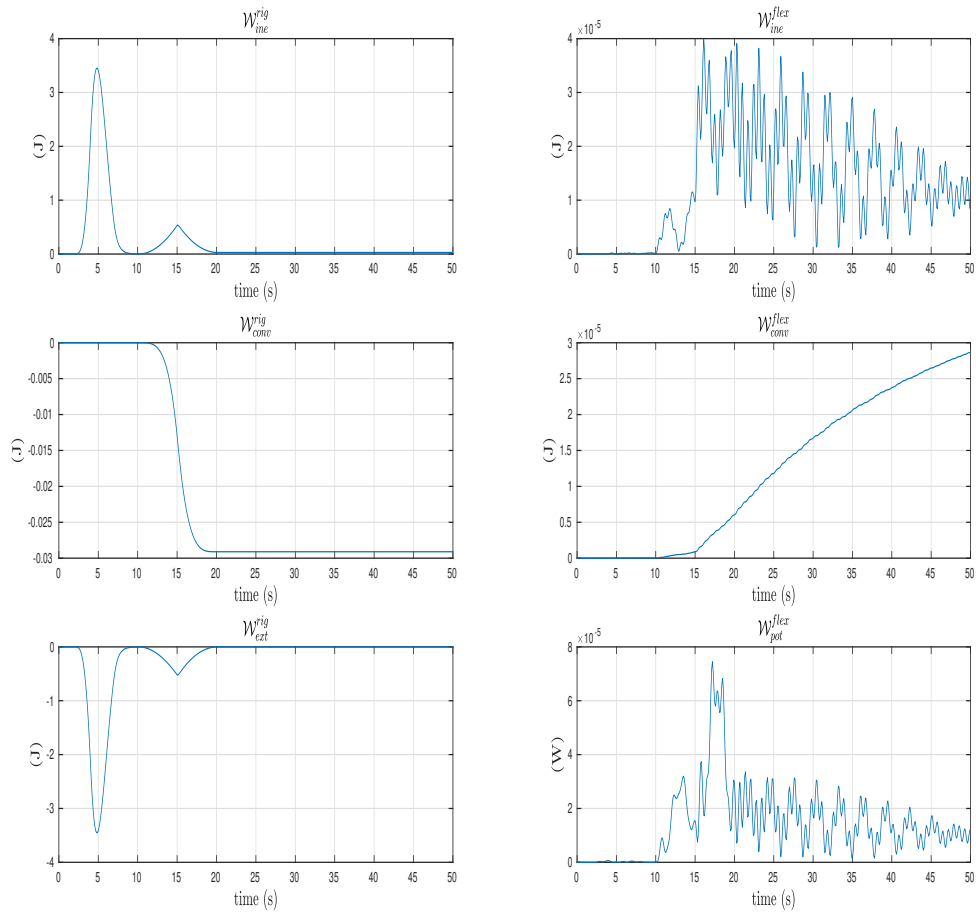


Figure 2.14 – Listing of system’s works evolutions (2.82); Left side subplots represent from top to bottom works derived from: the inertial, convective forces and the external control torques powers; Right side subplots represent from top to bottom works derived from: the inertial, convective and potential forces

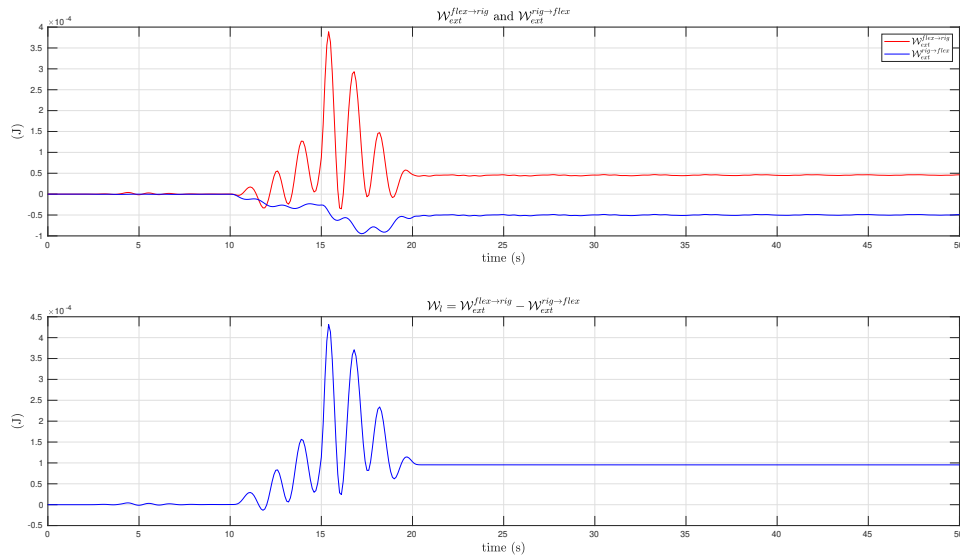


Figure 2.15 – Lost work (2.83) for the SMS motions obtained with input control torques represented in Figure 2.13

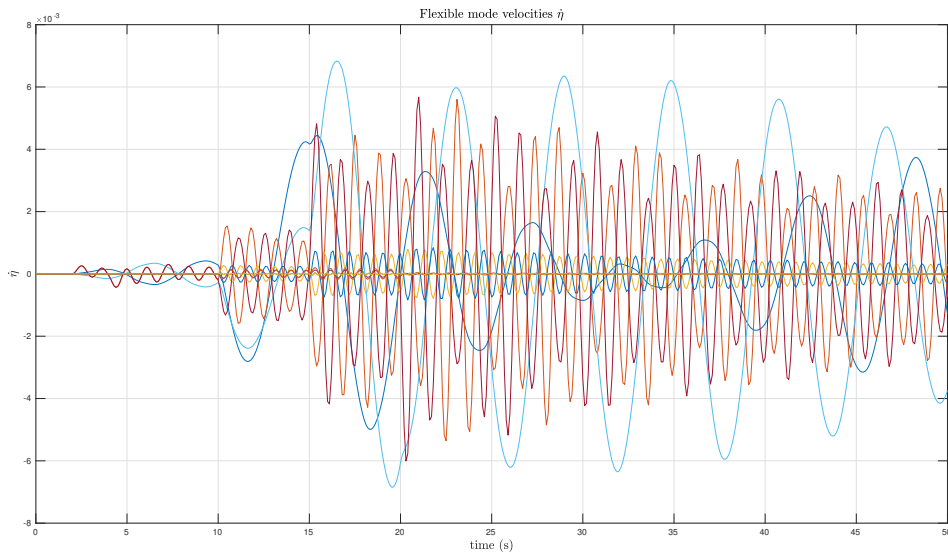


Figure 2.16 – Flexible mode velocities  $\dot{\eta}$  for the input torques represented in Figure 2.13

## 2.5 Chapter conclusions

To summarize the contribution of this chapter, a modeling formalism has been elaborated to establish simulation and analysis tools for a floating SMS with flexible appendages.



It has been identified from the literature review, developed in the previous chapter, that integrating flexible dynamics with those of a floating SMS remained challenging and interesting for the study of current applications. The proposed methods in the literature are either carrying numerous restrictive hypotheses or applying to simple space manipulators. Therefore, after establishing a rigid model of a floating SMS with the DH formalism and a Lagrangian approach, the flexible dynamics is included adapting the Lagrangian approach. The choice of a Lagrangian approach over a Newton-Euler is based on the generality and the simpler for a systematic modeling formalism.

The modeling formalism provides a recursive description of the system kinematics which has allowed to extend existing simulation tools, SPART, with integration of reaction-wheels and flexible dynamics. The new tools allow to produce different analyses of the system, as introduced in this chapter with energetic discussions. Pre-design of the SMS, workspace analyses, path-planning studies, evaluation of coupling influence are few example of the potential use for the analysis tools. With the simulation tools, one can validate control laws or even study stability of a rigid-flexible systems. In the following chapters, they will be use to develop new control strategies.

# Introduction of a steering law for space manipulator system in presence of flexible appendages

---

## Sommaire

---

<b>3.1 Areas of improvements</b> . . . . .	<b>74</b>
3.1.1 Challenges of developing steering law for SMS <sup>1</sup> with flexible appendages .	74
3.1.2 Illustration of a classical control approach limitations . . . . .	76
<b>3.2 Interest of a common base and manipulator control</b> . . . . .	<b>82</b>
3.2.1 SMS workspace . . . . .	82
3.2.2 Distribution of system efforts . . . . .	86
<b>3.3 Joint-space control of an SMS with flexible appendages</b> . . . . .	<b>92</b>
3.3.1 Observer structure . . . . .	93
3.3.2 Control law structure . . . . .	94
3.3.3 Simultaneous synthesis . . . . .	96
<b>3.4 Base and manipulator control of an SMS with flexible appendages</b> .	<b>100</b>
3.4.1 Open-loop dynamics . . . . .	101
3.4.2 Closed-loop dynamics . . . . .	102
<b>3.5 Illustration of the proposed methods</b> . . . . .	<b>103</b>
3.5.1 Joint control results . . . . .	104
3.5.2 Interest of a base-manipulator common control strategy . . . . .	111
<b>3.6 Chapter conclusions</b> . . . . .	<b>115</b>

---

In the previous chapter, a modeling formalism has been introduced such that analysis and simulation tools have been established. At the conclusion of this chapter, the developed tools allow to both study and perform time-domain simulation on flying (and floating) SMS with flexible appendages. In this chapter, steering laws are synthesized and validated with the developed tools. First, from a short literature reviewed, areas of improvement in control strategies for SMS with flexible appendages are listed. After illustrating the limits of a classical control approach of SMS, a control that takes advantage of all the available actuators to

---

<sup>1</sup>Space Manipulator System

improve control performances is proposed and discussed. From the conclusions of a common control of the base and manipulator's joints, a steering law is introduced to deal with flexible appendages vibrations also referred here as system's intern disturbances.

### 3.1 Areas of improvements

#### 3.1.1 Challenges of developing steering law for SMS with flexible appendages

With the large variety of SMS applications comes numerous control challenges [FA+14]; [Li+19b]. Firstly, the space environment in which the manipulator evolves leads to different couplings between each body composing the SMS. It complexifies the control of the system and different solutions have been developed through the years to attenuate the negative effects of these couplings. A second difficulty lies in the presence of flexible appendages. As developed in the previous chapter, for a base motion, either caused by the use of reaction-wheels or from a manipulator's motions, vibrations may destabilize the SMS. Additionally to the couplings between the manipulator's end-effector and the appendages, studied by Meng and al. [Men+17], vibrations of the flexible elements may be caused by unpredictably environmental disturbances as developed by Cao and al. [Cao+20]. For those reasons improving the autonomous control of SMS remains a challenging task.

**System couplings:** In the present study, the focus is made on rotation-free-floating SMS with reaction-wheels as the dedicated base actuators. With such manipulators, the global kinetic momentum remains constant which may induce undesired motions caused by different couplings. The main concern is the influence of the manipulator on the base which should keep a fixed attitude to ensure the quality of the power supply (orientation of solar panels) and communication with the ground (orientation of the antenna). Capitalizing on the momentum conservation, studies have considered path-planning approaches in that matter [PTN05]; [Li+19a] or adapted the motions of the manipulator with kinematic/dynamic constraints based on the GJM<sup>2</sup> expression [HW18]. Moreover, path-planning methods have been established in capture applications such that by reducing the relative motions between the target and the servicer's end-effector, the influences of both impact and manipulator maneuvers are lowered [RSS17]; [Yan+19]; [LY20]. Similarly, impedance control strategies lead to similar results [NY06].

Furthermore, the use of null-space projector, originally introduced by Nenchev and al. [Nen+99], have allowed to develop control strategies in which the manipulator's motions do not affect the base motions [PG15]; [YDH19]. Nevertheless, these methods are mainly based on the momentum properties of the free-floating systems or established for simple manipulators. As discussed in the previous chapter, flexible elements will generate a dissipative force when they will start vibrating. Such force prevents from considering any momentum conservation hypotheses.

---

<sup>2</sup>Generalised Jacobian Matrix

**Active control:** To overcome the difficulty of establishing control laws without a momentum conservation, studies have considered active control. Early strategies were based on simple flexible model and were limited to small satellites. Two main active control methods can be distinguished. First the control of the DoF<sup>3</sup> between the appendage and the spacecraft's base to reject the vibrations effects on the base [Hir+13]; [Hir+14]; [HGY19]; [Guo+20]. Secondly, flexible deformations are rejected with the use of piezoelectric actuators positioned on the appendage [HM05]; [ZMP16]. The placement and number of such actuators have an importance to guarantee a maximal deformation threshold of the appendage while accurately controlling the spacecraft base attitude [Ang+21].

Moreover, the use of control moment gyroscopes between two flexible bodies have been studied by identifying fast and slow sub-systems dynamics [Jia+17]. Control moment gyroscopes have also been considered to be placed on the flexible structure for the active vibration suppression [HZ16]. However, in future space exploitation and exploration missions [Li+19b], the use of dedicated actuators is quite difficult to set up as well as in terms of energetic approach it may be contradictory with the purposes of increasing the lifespan of the missions.

Another difficulty from the active control is that a proper modeling of the flexible dynamics should be established. However, it remains challenging according to the studied space structure. For that concern boundary controllers have been designed to insure asymptotic stability of the satellite attitude control without accurate system modeling [Ata+20].

**Passive control:** Different alternatives to active control have been developed to reject both system internal and external disturbances. With a limited knowledge of perturbation properties, adaptive disturbance rejection filters have been developed to avoid modal excitation of the flexible elements when controlling the manipulator [CC12]. Quantifying the influence of the mutual impacts between a source of an intern disturbance and the manipulator motions have been developed to introduce an SMS control strategy. For instance, Rackl and al. [RGL18] adapted the manipulator control according to the reciprocal influence between the robotic arm and the sloshing of the fuel tank. Moreover, Meng and al. [Men+17] proposed to derive the flexible dynamics of the appendages such that a vibration rejection strategy can be established [Men+18].

Nevertheless, the difficulty of deriving the flexible dynamics motivates the development of robust control strategies. With  $H_\infty$  controllers both modeling uncertainties and external disturbances can be tackled [FTST06]; [Col+20]; [QWY19]. Furthermore, flexible vibrations are usually not measurable and estimation techniques have been developed. Disturbance observer are adopted to decouple the system [ZFJ08], or to improve the perturbation rejections [CCS12]; [QWY19].

**Actual solutions** An important aspect of future space missions is the lifespan. For that purpose, control strategies have focused on a reduced use of base actuators, especially when

---

<sup>3</sup>Degree of Freedom

reaction-jet are involved. Giordano and al. [GCAS18] have first proposed a workspace adjustment strategy to compensate for manipulator motions with an efficient use of thrusters. A later approach developed by Giordano and al. [GOAS19] have been based on the simultaneous control of the SMS global center of mass.

Besides efficient propellant consumption strategies, the use of electrical kinetic moment exchange devices have raised in interest. The common use of reaction-wheels with thrusters has been studied by Giordano and al. [Gio+20] such that only the critical moment of the capture of a non-cooperative target are tackled with the thrusters.

Furthermore, in most applications, manipulator and base control are effectuated separately. This can be illustrated by Wu and al. [Wu+18b] who considered the combination of reaction-wheels and control moment gyroscopes to maintain the satellite platform fixed during manipulator operations. This strategy aimed at dealing with the low reaction-wheels saturation thresholds. Additionally, recent implemented control strategies also illustrate the choice of a separate base and manipulator control [GCAS18]; [Cum+21]; [Col+20]. This presents some benefits to ensure precise control of the robotic arm from one side and the base from the other. However, in this chapter the interest of a common base/manipulator actuators control is proposed.

### 3.1.2 Illustration of a classical control approach limitations

Before developing any further discussion on a common reaction-wheel and manipulator control, a short observation of the limits of a separated control strategy is detailed here on a simple example. A first control law is introduced based on a simplified version of the similar strategies proposed by Cummer and al. [Cum+21]. As illustrated by Figure 3.1, the proposed methods separate the control of the base actuators from the manipulator's joints. Moreover, the control torques are computed from a single system linearization and constant control gains are synthesized with robust control approaches. In order to simply illustrate the potential limits of such methods, a simplification of the control proposed in the literature is considered without developing the  $H_\infty$  synthesis.

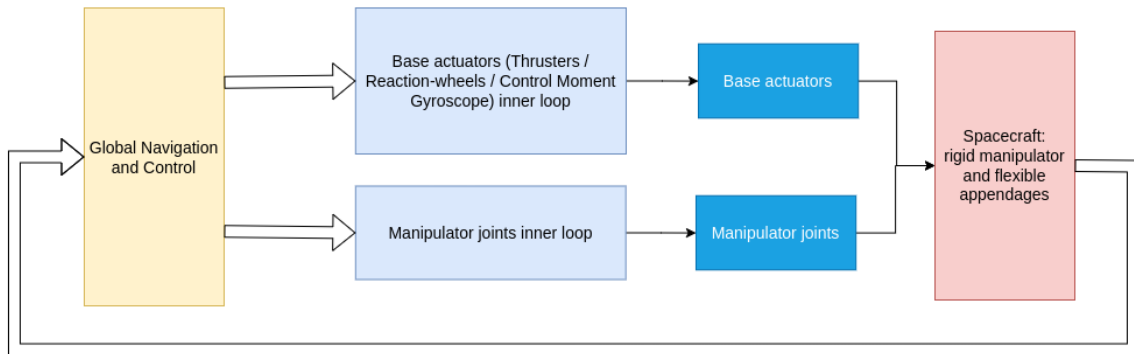


Figure 3.1 – Block diagram of classical control approach in the literature

From the modeling of a rigid system (2.43), developed in the previous chapter, a separate control reaction-wheels and manipulator's joints is introduced inspired from current control methods found in the literature. From one side, the manipulator is considered as a rigid multi-body kinematic chain on a fixed base, thus its equation of motions are adapted from (2.43) by neglecting the base dynamics and coupling such as:

$$\mathbf{H}_m^0 \ddot{\mathbf{q}}_m + \mathbf{C}_m^0 \dot{\mathbf{q}}_m = \boldsymbol{\tau}_m \quad (3.1)$$

where  $\mathbf{H}_m^0$  and  $\mathbf{C}_m^0$  are nominal matrices, obtained from a system linearization. Such expressions of manipulator dynamics consider a fixed spacecraft base.

On the other side, the base rotational dynamic is expressed with only the reaction-wheels as a means of control. Thus, isolating the reaction-wheels and base dynamics by neglecting the coupling with the manipulator from (2.43), one first express the overall base dynamics as:

$$\begin{bmatrix} \mathbf{H}_\omega^0 & \mathbf{H}_{\omega r}^0 \\ \mathbf{H}_{\omega r}^{0T} & \mathbf{H}_r^0 \end{bmatrix} \begin{bmatrix} \dot{\boldsymbol{\omega}}_0^{sat} \\ \dot{\mathbf{q}}_r \end{bmatrix} + \begin{bmatrix} \mathbf{C}_\omega^0 & \mathbf{C}_{\omega r}^0 \\ \mathbf{C}_{r\omega}^0 & \mathbf{C}_r^0 \end{bmatrix} \begin{bmatrix} \boldsymbol{\omega}_0^{sat} \\ \mathbf{q}_r \end{bmatrix} = \begin{bmatrix} \mathbf{0}_{3 \times 1} \\ \boldsymbol{\tau}_r \end{bmatrix} \quad (3.2)$$

with the notation  $^0$  used to indicate nominal values of matrices (or from a linearized model). One will note that  $\mathbf{H}_r^0 = \mathbf{H}_r$  and that for a fixed system's CoM<sup>4</sup> in  $\mathcal{R}_{ine}$ <sup>5</sup>  $\mathbf{H}_{\omega r}^0 = \mathbf{H}_{\omega r}$ . Base rotations (3.2) can be expressed without reaction-wheels' acceleration as they are not necessarily provided for. Combining both lines of (3.2), base dynamics are given by:

$$\left( \mathbf{H}_{\omega r}^{0T} - \mathbf{H}_r \mathbf{H}_{\omega r}^{0+} \mathbf{H}_\omega^0 \right) \dot{\boldsymbol{\omega}}_0^{sat} + \left( \mathbf{C}_{r\omega}^0 - \mathbf{H}_r^0 \mathbf{H}_{\omega r}^{0+} \mathbf{C}_\omega^0 \right) \boldsymbol{\omega}_0^{sat} + \left( \mathbf{C}_r^0 - \mathbf{H}_r^0 \mathbf{H}_{\omega r}^{0+} \mathbf{C}_{\omega r}^0 \right) \dot{\mathbf{q}}_r = \boldsymbol{\tau}_r \quad (3.3)$$

This allows to have a naturally decoupled base/manipulator system. Then introducing the constant linear control gains  $\mathbf{K}_0 \in \mathbb{R}^{3 \times 3}$  and  $\mathbf{K}_m \in \mathbb{R}^{n_m \times n_m}$ , the respective manipulator and reaction-wheels computed torques are given as:

$$\begin{cases} \boldsymbol{\tau}_{m_c} = \mathbf{H}_m^0 \mathbf{K}_m (\dot{\mathbf{q}}_{m_d} - \dot{\mathbf{q}}_{m_d}) + \mathbf{C}_m^0 \dot{\mathbf{q}}_m & (3.4a) \\ \boldsymbol{\tau}_{r_c} = \left( \mathbf{H}_{\omega r}^{0T} - \mathbf{H}_r^0 \mathbf{H}_{\omega r}^{0+} \mathbf{H}_\omega^0 \right) \mathbf{K}_0 \left( \boldsymbol{\omega}_{0_d}^{sat} - \boldsymbol{\omega}_0^{sat} \right) & (3.4b) \\ \quad + \left( \mathbf{C}_{r\omega}^0 - \mathbf{H}_r^0 \mathbf{H}_{\omega r}^{0+} \mathbf{C}_\omega^0 \right) \boldsymbol{\omega}_0^{sat} + \left( \mathbf{C}_r^0 - \mathbf{H}_r^0 \mathbf{H}_{\omega r}^{0+} \mathbf{C}_{\omega r}^0 \right) \dot{\mathbf{q}}_r \end{cases}$$

Thus each actuators are decoupled. Respectively,  $\boldsymbol{\tau}_{m_c}$  allows to decouple the manipulator's joint and  $\boldsymbol{\tau}_{r_c}$  reaction-wheels. Moreover,  $\mathbf{H}_{\omega r}^0$  is a constant matrix depending on the choice of reaction-wheels orientations in the spacecraft base and thus its pseudo-inverse is perfectly defined.

In order to illustrate the performances of this control law, the tools developed in the previous chapter are used. A simple SMS is considered with a 5-DoFs manipulator and four reaction-wheels. Additionally, ten flexible modes are considered, which physical properties, as well as for those of the overall spacecraft, are given in appendix B. The desired SMS

<sup>4</sup>Center of Mass

<sup>5</sup>Inertial frame

motion consists of moving a 150kg mass with the manipulator as illustrated in Figure 3.2 and maintaining the base with a fixed attitude. Control gains are computed with the normalized dynamics (3.1) and (3.3) to guarantee a low closed-loop response time. This can be obtained by imposing the control gains as diagonal matrices with the coefficient corresponding to the inverse of the time response.

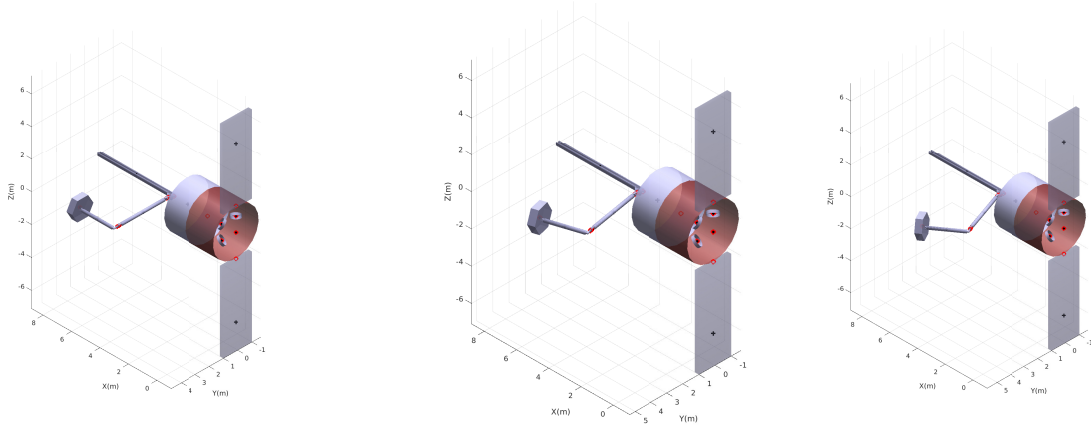


Figure 3.2 – Illustration of the SMS desired motion. Left to right the initial, the mid-configuration and the final configurations

With Figure 3.3, in which the desired manipulator's joints velocities (in dashed-line) and measured ones (in full line) are plotted, one can conclude on the poor performances of the velocity control. One will observe that velocities for joints 2 and 5 from fifty seconds give an increasing tracking error until the end of the manipulator's motion while the three other joints successfully follow the desired velocities. This can be explained by the linearization choice made to develop the computed torques (3.4). With a linearization performed for the nominal SMS configuration, the manipulator is adequately controlled until fifty seconds of motions then the system linearization is too far from the actual state to satisfy appropriate control performances. This is why robust control synthesis and/or adaptive gains are required to perform simple motions as the present one.

"The responsibility" of the linearization is in the poor control performances which are illustrated by the successfully stabilized base with a null angular velocity. Illustrated with Figure 3.4 and the second subplot, the angular rates of the base remains null during the manipulator's motions. Moreover, one will note that imposing fast control dynamics leads to control gains  $\mathbf{K}_0$  sufficiently large to be robust to the influence of floating system's couplings (i.e. between the motions of the manipulator's end-effector and the base). This allows to first conclude that a separated base/manipulator control can achieve good performances at the condition of taking into account the system's variation for the manipulator control.

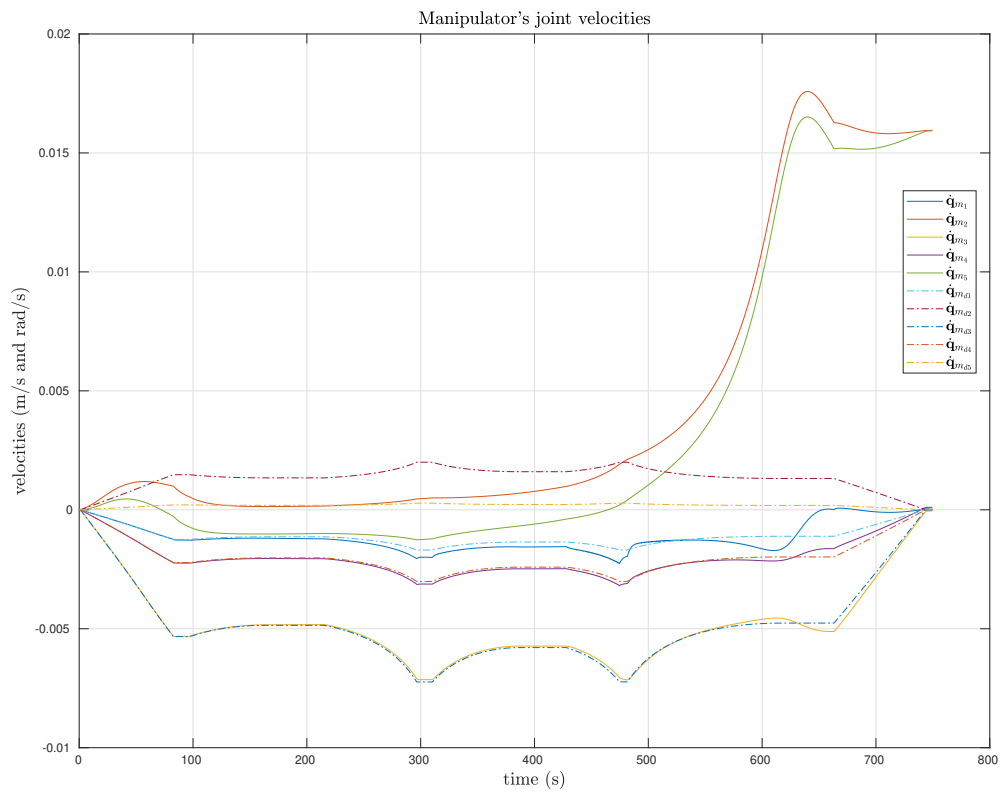


Figure 3.3 – Manipulator's joints control performances, measured velocities (full-line) and desired velocities (dashed-line)



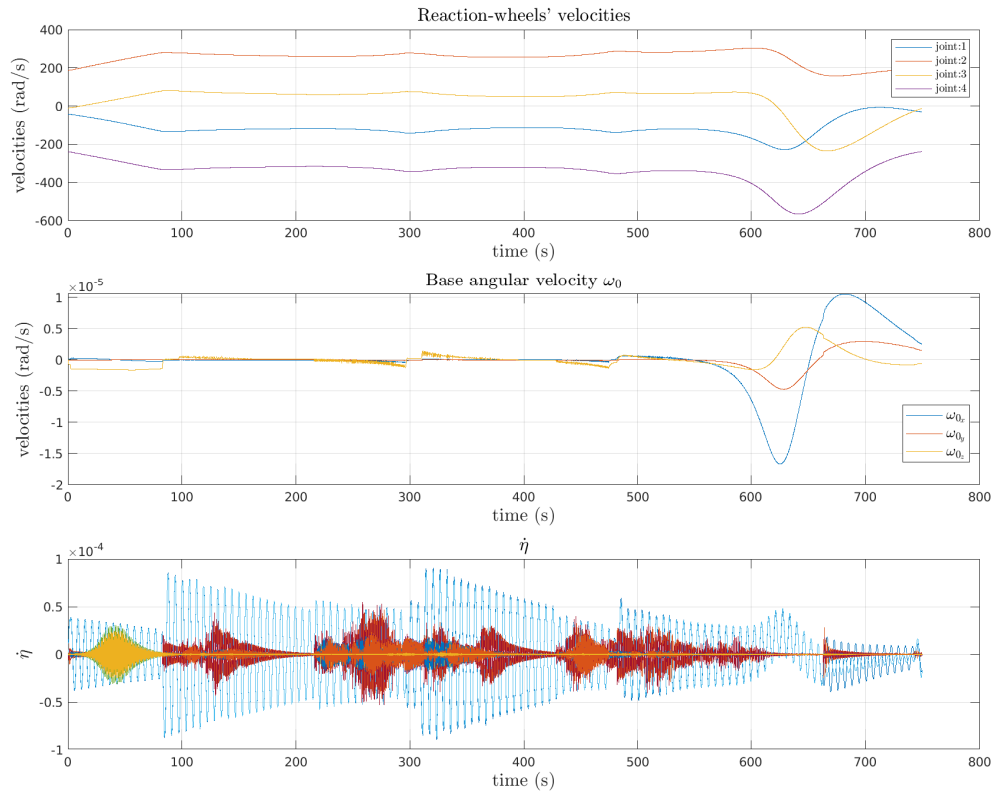


Figure 3.4 – Upper subplot is the measured reaction-wheels' joint velocities second subplot represents the base angular velocity and lower subplot is the flexible modes velocities

Furthermore, successfully maintaining the base with a fixed attitude allows to avoid large flexible vibrations and even reduce them with the available reaction-wheels as illustrated with both first and last subplots of Figure 3.4. The four reaction-wheels provide an over-actuated system that insure base angular velocity to remain at low velocities. As discussed in the previous chapter, considering the convective terms allows to conclude on the minimized dissipative work lost in the flexible modes, as illustrated by Figure 3.5.

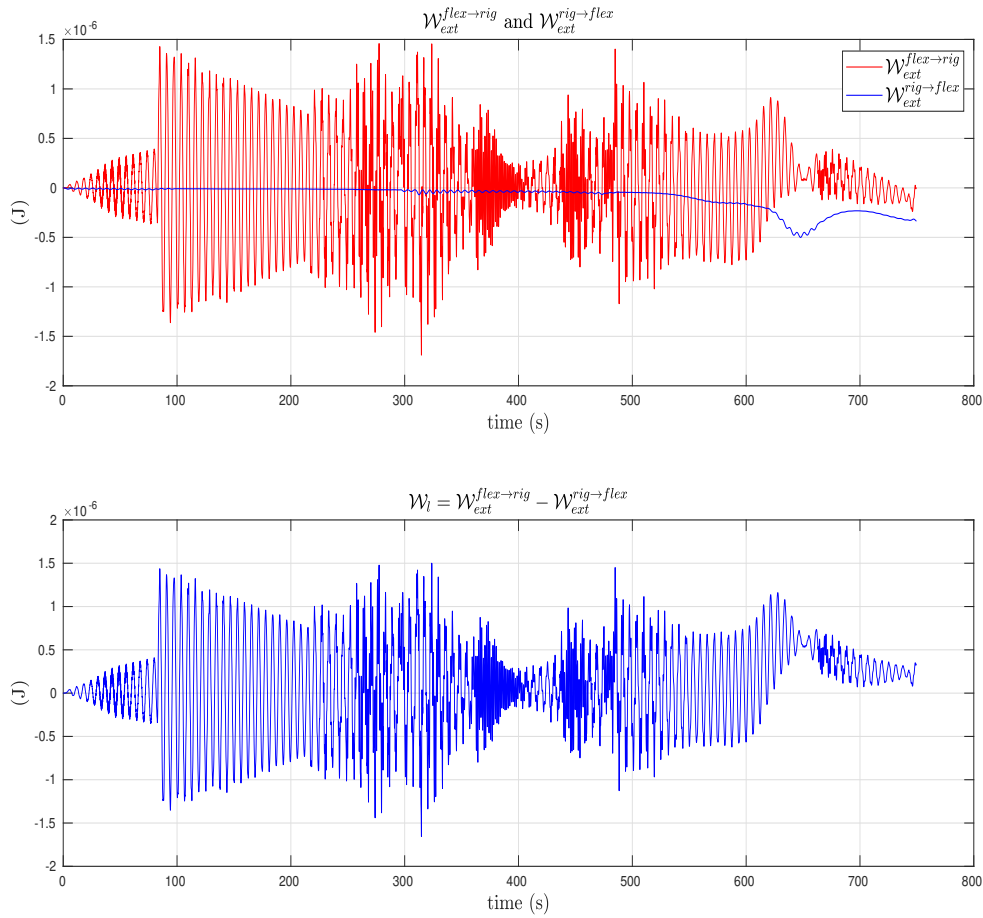


Figure 3.5 – Dissipated work (2.83) during the complete motion with a fixed base attitude

From this short illustrative example of a classical control approach of both base and manipulator, some conclusions can be made and possible improvements.

- Firstly, a separated control provides the possibility of adapting control performances of both base and manipulator. However, regarding the couplings of an SMS, developing a robust control synthesis is a "necessity".
- Secondly, it has allowed to show the limitation in the use of a unique linearization and constant control gains to decouple the system.
- Thirdly, maintaining the base at a constant orientation allows to reduce the potential impact of flexible vibrations on the manipulator and more generally on the rest of the system. In that matter, investigating on a common base and manipulator control approach could lead to a simple control law that provides precise performances.

The chapter is then organized as following: the interest of a common base and manipulator is discussed through a quantitative method, then secondly a control law is developed such that high precision performances are guaranteed despite of the presence of the flexible appendages.

## 3.2 Interest of a common base and manipulator control

In this section, quantitative tools for analysis and control of an SMS are introduced extending our published work in [RKS19]. The presence of kinetic moment exchange actuators in the base of an SMS offers more flexibility in the possible manipulator operations [Rog+19]; [Wil+18]. The objective of the section is to introduce a means to evaluate the interest of using base actuators simultaneously to controlling the manipulator. To do so, a rigid rotation-free-floating SMS is considered as it allows to come up with momentum discussions. Such system behaviors are described by the equations of motions (2.43) detailed in the previous chapter.

First, the definition of usual SMS analysis notions from the literature such as workspace, singularity, redundancy and manipulability are provided. This allows to develop tools to observe the limits and feasible motions of an SMS. Secondly, kinematic indices are introduced to quantify the interest of a common base and manipulator control.

### 3.2.1 SMS workspace

The manipulator workspace defines the set of reachable positions of the end-effector without singular configurations. Its evaluation is obtained studying the GJM which also gives information on singular configurations. The GJM is obtained with the kinetic moment conservation, hence the restriction to the study of a rigid SMS. For an initially null system momentum and without any external sources of disturbances, the system momentum is given in function of the manipulator's joints' velocities,  $\dot{\mathbf{q}}_m$ , and reaction-wheels' velocities,  $\dot{\mathbf{q}}_r$ , as [Wil+18]:

$$\dot{\mathbf{q}}_0 = \begin{bmatrix} \boldsymbol{\omega}_0^{sat} \\ \dot{\mathbf{r}}_0 \end{bmatrix} = -\mathbf{H}_0^{-1} \mathbf{H}_{0m} \dot{\mathbf{q}}_m - \mathbf{H}_0^{-1} \mathbf{H}_{0r} \dot{\mathbf{q}}_r = \mathbf{J}_{m_0}^* \dot{\mathbf{q}}_m + \mathbf{J}_{r_0}^* \dot{\mathbf{q}}_r \quad (3.5)$$

with  $\mathbf{J}_{m_0}^*$  and  $\mathbf{J}_{r_0}^*$  the Jacobian to express respectively the manipulator and reaction-wheels velocities to the base velocity. Then developing the expression of the inertia matrix  $\mathbf{H}_0$  of a rigid floating SMS (2.43), for which the base angular velocity is expressed in the satellite

body frame,  $\mathcal{R}_{sat}$ <sup>6</sup>, allows to isolate the rotational and linear part of it as:

$$\begin{aligned} \mathbf{H}_0 &= \mathbf{P}_0^T \mathbf{M}_0 \mathbf{P}_0 \\ &= \begin{bmatrix} \mathcal{I}_{S_0} + \mathbf{R}_{S_0}^T \left( \sum_{i=1}^{n_q} \mathcal{I}_i - m_i (\mathbf{r}_{S_0} - \mathbf{r}_{S_i})^\times (\mathbf{r}_{S_0} - \mathbf{r}_{S_i})^\times \right) \mathbf{R}_{S_0} & -m_{tot} (\mathbf{r}_{S_0} - \mathbf{r}_{CoM})^\times \\ m_{tot} (\mathbf{r}_{S_0} - \mathbf{r}_{CoM})^\times & m_{tot} \mathbf{I}_3 \end{bmatrix} \\ &= \begin{bmatrix} \mathbf{H}_\omega & -m_{tot} (\mathbf{r}_{S_0} - \mathbf{r}_{CoM})^\times \\ m_{tot} (\mathbf{r}_{S_0} - \mathbf{r}_{CoM})^\times & m_{tot} \mathbf{I}_3 \end{bmatrix} \end{aligned} \quad (3.6)$$

As  $\mathbf{H}_0$  is an inertia matrix, it is defined positive and symmetric. By applying the Banachiewicz inversion [BS02],  $\mathbf{H}_0$  is inverted as:

$$\mathbf{H}_0^{-1} = \begin{bmatrix} \mathcal{S}_U^{-1} & (\mathbf{r}_{S_0} - \mathbf{r}_{CoM})^\times \mathcal{S}_U^{-1} \\ \mathcal{S}_U^{-1} (\mathbf{r}_{S_0} - \mathbf{r}_{CoM})^\times & \frac{1}{m_{tot}} - (\mathbf{r}_{S_0} - \mathbf{r}_{CoM})^\times \mathcal{S}_U^{-1} (\mathbf{r}_{S_0} - \mathbf{r}_{CoM})^\times \end{bmatrix} \quad (3.7)$$

with  $\mathcal{S}_U = \mathbf{H}_\omega + m_{tot} (\mathbf{r}_{S_0} - \mathbf{r}_{CoM})^\times (\mathbf{r}_{S_0} - \mathbf{r}_{CoM})^\times$ .

Thus, the generalized base Jacobian matrices  $\mathbf{J}_{m_0}^*$  and  $\mathbf{J}_{r_0}^*$  can later be developed.

Secondly, the evaluation of the workspace is obtained with the consideration of the end-effector's reachable positions. With a similar approach, generalized Jacobian matrices are introduced for the end-effector such that its twist is evaluated from only actuators' velocities. Injecting the base twist,  $\dot{\mathbf{q}}_0$ , (3.5) in the end-effector's twist (2.19), one can define  $\mathbf{J}_{r_{EE}}^*$  and  $\mathbf{J}_{m_{EE}}^*$ , respectively the generalized Jacobian matrices of the end-effector for reaction-wheels and manipulator's actuators as:

$$\begin{aligned} \mathbf{t}_{EE} &= \mathbf{J}_{0EE} \mathbf{t}_0 + \mathbf{J}_{m_{EE}} \dot{\mathbf{q}}_m = (\mathbf{J}_{0EE} \mathbf{J}_{m_0}^* + \mathbf{J}_{m_{EE}}) \dot{\mathbf{q}}_m + (\mathbf{J}_{0EE} \mathbf{J}_{r_0}^*) \dot{\mathbf{q}}_r \\ &= \mathbf{J}_{m_{EE}}^* \dot{\mathbf{q}}_m + \mathbf{J}_{r_{EE}}^* \dot{\mathbf{q}}_r \end{aligned} \quad (3.8)$$

This relation allows to establish workspace discussions as well as actuators' use rate to perform a given motion. In the literature, the GJM refers only to  $\mathbf{J}_{m_{EE}}^*$  which, if expressed in  $\mathcal{R}_{sat}$ , and only depends on the manipulator configuration.

**Redundancy of SMS:** The non-holonomic constraint of free-floating SMS is due to the non-integrability of the angular momentum equation [NM90]:

$$\mathbf{M}_\omega \boldsymbol{\omega}_0 + \mathbf{M}_{\omega L} \dot{\mathbf{r}}_{S_0} + \mathbf{M}_{\omega r} \dot{\mathbf{q}}_r + \mathbf{M}_{\omega m} \dot{\mathbf{q}}_m = \mathbf{0}_{3 \times 1} \quad (3.9)$$

It traduces that the dynamic couplings between the manipulator and the base leads to an end-effector pose depending on both the manipulator's trajectory and velocities. The redundancy of a manipulator corresponds to the plurality of possible motions (i.e. multiple set of  $\mathbf{q}_m$  and  $\mathbf{q}_r$ ) to reach a base and end-effector rotation. One will note that in the case of a

---

<sup>6</sup>Satellite frame

control of the base position, the end-effector can likewise be controlled in position however the manipulator reaches or not a singularity. The degree of redundancy is the difference between the manipulator's DoFs and the number of end-effector tasks [NUY92]. One can distinguish the main task, following a trajectory by the end-effector controlling its pose and orientation, and secondary tasks, either a trajectory tracking while maintaining a fixed orientation of the base or modifying the base orientation while maintaining the pose and/or orientation of the end-effector. Denoting the number of end-effector tasks,  $n_{t_{EE}}$ ,  $n_{t_b}$  the number of base tasks and  $n_m$  the manipulator DoFs, three redundancy cases can be considered for a free-flying SMS:

- if  $n_m = n_{t_{EE}} + n_{t_b}$ : the redundancy of the manipulator is only sufficient to control both end-effector and base
- if  $n_m > n_{t_{EE}} + n_{t_b}$ : the redundancy of the manipulator is sufficient to perform base and end-effector tasks, additional constraints like actuator saturation, singularity or obstacle avoidance can be considered
- if  $n_m < n_{t_{EE}} + n_{t_b}$ : the redundancy degree is not enough to perform both base and end-effector tasks, a hierarchy of tasks is required. If  $n_m < n_{t_{EE}}$  the end-effector tasks can be chosen to be performed first and if  $n_m < n_{t_b}$  the base control can be privileged.

For rotation-free-floating SMS, the redundancy degree becomes  $n_m + 3$ .

**Singularity and workspace analysis:** A particularity of free-floating SMS is the possibility of reaching a dynamic singularity in addition of kinematic ones. Kinematic singularities correspond to geometrical constraints of the manipulator and joint rotations while a dynamic one occurs when a lack of a means to compensate for the manipulator motions leads to the impossibility of moving the end-effector in any direction [PD93]. These singularities are consequences of the non-holonomic constraints of a free-floating manipulator and also dependent on its physical properties (mass/inertia). The dynamic singularities are studied with the GJM,  $\mathbf{J}_{m_{EE}}^*$ . A dynamic singularity corresponds to a non-redundant manipulator when  $\mathbf{J}_{m_{EE}}^*$  is rank deficient. Thus a dynamically singular configuration is evaluated with the evaluation of the non-inversibility of  $\mathbf{J}_{m_{EE}}^* \mathbf{J}_{m_{EE}}^{*T}$  as:

$$\det \left( \mathbf{J}_{m_{EE}}^* \mathbf{J}_{m_{EE}}^{*T} \right) = 0 \quad (3.10)$$

Moreover, manipulator path-planning benefits from the study of dynamic singularities as the manipulator joint rates become more important near singular configurations. Such path-planning approaches optimize the value of  $\det \left( \mathbf{J}_{m_{EE}}^* \mathbf{J}_{m_{EE}}^{*T} \right)$  to insure configurations far from singular ones. However, the main difficulty of establishing a manipulator path resides in the non-holonomic constraints of a free-floating SMS. Papadopoulos and Dubowsky [PD93] proposed a method decomposing workspaces in path dependent and independent subsets of the complete workspace where respectively dynamic singularities may be encountered or not depending on the path taken. Nanos and Papadopoulos [NP15] developed an analytical

method to find initial base attitude and joint configuration such that the manipulator can move into a workspace without reaching a dynamic singularity. Nevertheless, these approaches only apply for planar manipulator. For spatial cases, Calzolari and al. [CLG20] presented a numerical technique to obtain singularity maps for a 6-DoFs spacecraft in order to develop path-planning method with singularity avoidance.

**Manipulability:** The notion of manipulability for redundant manipulator has been introduced by Yoshikawa [Yos84] to establish and adapt path-planning methods. The manipulability is the quantitative measure of the manipulator ability to perform an end-effector pose and orientation considering the manipulator's kinematics. It can be seen as a means to quantify the proximity with singular configurations. The end-effector manipulability,  $\mu(\mathbf{J}_{mEE}^*)$ , is defined as:

$$\mu(\mathbf{J}_{mEE}^*) = \sqrt{\det(\mathbf{J}_{mEE}^* \mathbf{J}_{mEE}^{*T})} \quad (3.11)$$

Thus, in path-planning approaches the problem of singularity avoidance can be replaced by locally maximizing the manipulability  $\mu$  at each point or satisfying the joint velocity constraints [CLG20].

Furthermore, as accelerations and joint torques do not impact the manipulability evaluation, Yoshikawa [Yos85] proposed a dynamic manipulability to likewise quantify the ability of the manipulator to perform end-effector motions while considering the system's dynamics. Its evaluation is the measure of the volume of the dynamic manipulability ellipsoid formed by the set of all realizable accelerations of the end-effector under joint constraints. For the end-effector it is defined as the set of all end-effector accelerations that joint driving forces can achieve. It is expressed in function of the normalized joint torques,  $\hat{\boldsymbol{\tau}}_m$ , defined with a weight matrix  $\mathbf{W}_\tau$ , such that  $\hat{\boldsymbol{\tau}}_m = \mathbf{W}_\tau \boldsymbol{\tau}_m$ , verifies  $|\hat{\boldsymbol{\tau}}_m^T \hat{\boldsymbol{\tau}}_m| \leq 1$ . Then expressing the joint dynamics as:

$$\mathbf{H}_m^* \ddot{\mathbf{q}}_m + \mathbf{C}_m^* \dot{\mathbf{q}}_m = \boldsymbol{\tau}_m \quad (3.12)$$

and the time-derivative of the end-effector tasks for a fixed base:

$$\dot{\mathbf{t}}_{EE} = \mathbf{J}_{mEE}^* \ddot{\mathbf{q}}_m + \dot{\mathbf{J}}_{mEE}^* \dot{\mathbf{q}}_m \quad (3.13)$$

the dynamic manipulability,  $\mu^*$ , corresponds to the evaluation of the inversibility of the Jacobian matrix  $\mathbf{J}_{mEE}^\diamond = \mathbf{J}_{mEE}^* \mathbf{H}_m^{*-1} \mathbf{W}_\tau$  obtained combining both equations (3.12) and (3.13). Thus it leads to evaluate the determinant of the scaled GJM,  $\mathbf{J}_{mEE}^\diamond$  [KY97]; [XLW20]:

$$\mu^*(\mathbf{J}_{mEE}^\diamond) = \sqrt{\det\left(\left(\mathbf{J}_{mEE}^* \mathbf{H}_m^{*-1} \mathbf{W}_\tau\right)^T \left(\mathbf{J}_{mEE}^* \mathbf{H}_m^{*-1} \mathbf{W}_\tau\right)\right)} \quad (3.14)$$

### 3.2.2 Distribution of system efforts

Besides system singularities, the evaluation of actuators' usage can be interesting in path-planning applications or for pre-sizing an SMS to satisfy mission requirements. In that purpose, kinematic sensitivity indices are first introduced, as another contribution of this work, for rigid rotation-free-floating robots based on the momentum conservation. Then simulation examples to illustrate kinematic indices are shown with physical parameters for a microsatellite from Myriade series equipped with a robotic arm.

#### 3.2.2.1 Kinematic indices

With the expression of the generalized Jacobians (3.5) and (3.8), kinematic indices are introduced to evaluate the participation of actuators in the base and end-effector motions.

**Base kinematic indices:** Base indices are obtained detailing the linear and angular part of Jacobians  $\mathbf{J}_{m_0}^*$  and  $\mathbf{J}_{r_0}^*$  with (3.7) as:

$$\left\{ \begin{array}{l} \mathbf{J}_{m_0}^* = \begin{bmatrix} \mathbf{J}_{m_0}^{\omega_0} \\ \mathbf{J}_{m_0}^{r_0} \end{bmatrix} = -\mathbf{H}_0^{-1} \begin{bmatrix} \mathbf{H}_{\omega m} \\ \mathbf{H}_{Lm} \end{bmatrix} \\ = \begin{bmatrix} -\mathcal{S}_U^{-1} \mathbf{H}_{\omega m} - (\mathbf{r}_{S_0} - \mathbf{r}_{CoM})^\times \mathcal{S}_U^{-1} \mathbf{H}_{Lm} \\ -\mathcal{S}_U^{-1} (\mathbf{r}_{S_0} - \mathbf{r}_{CoM})^\times \mathbf{H}_{\omega m} - \left( \frac{1}{m_{tot}} - (\mathbf{r}_{S_0} - \mathbf{r}_{CoM})^\times \mathcal{S}_U^{-1} (\mathbf{r}_{S_0} - \mathbf{r}_{CoM})^\times \right) \mathbf{H}_{Lm} \end{bmatrix} \\ \mathbf{J}_{r_0}^* = \begin{bmatrix} \mathbf{J}_{r_0}^{\omega_0} \\ \mathbf{J}_{r_0}^{r_0} \end{bmatrix} = -\mathbf{H}_0^{-1} \begin{bmatrix} \mathbf{H}_{\omega r} \\ \mathbf{H}_{Lr} \end{bmatrix} \\ = \begin{bmatrix} -\mathcal{S}_U^{-1} \mathbf{H}_{\omega r} - (\mathbf{r}_{S_0} - \mathbf{r}_{CoM})^\times \mathcal{S}_U^{-1} \mathbf{H}_{Lr} \\ -\mathcal{S}_U^{-1} (\mathbf{r}_{S_0} - \mathbf{r}_{CoM})^\times \mathbf{H}_{\omega r} - \left( \frac{1}{m_{tot}} - (\mathbf{r}_{S_0} - \mathbf{r}_{CoM})^\times \mathcal{S}_U^{-1} (\mathbf{r}_{S_0} - \mathbf{r}_{CoM})^\times \right) \mathbf{H}_{Lr} \end{bmatrix} \end{array} \right.$$

As detailed in the previous chapter, the reaction-wheels do not affect the linear dynamics of the base (i.e.  $\mathbf{H}_{Lr} = \mathbf{0}_{3 \times n_r}$ ) which leads to:

$$\mathbf{J}_{r_0}^* = - \begin{bmatrix} \mathcal{S}_U^{-1} \mathbf{H}_{\omega r} \\ \mathcal{S}_U^{-1} (\mathbf{r}_{S_0} - \mathbf{r}_{CoM})^\times \mathbf{H}_{\omega r} \end{bmatrix} \quad (3.16)$$

As proposed by Xu and al. [Xu+16], this decomposition of the translation and rotation allows to compute joint-to-base coupling factors. In order to deal with the range variation of each actuators, the following scaled Jacobians will be used for analysis:

$$\left\{ \begin{array}{l} \mathbf{J}_{\omega_0}^{scal} = \begin{bmatrix} \mathbf{J}_{m_0}^{\omega_0} \mathbf{Q}_{max} & \mathbf{J}_{r_0}^{\omega_0} \mathbf{\Omega}_{max} \end{bmatrix} \end{array} \right. \quad (3.17a)$$

$$\left\{ \begin{array}{l} \mathbf{J}_{r_0}^{scal} = \begin{bmatrix} \mathbf{J}_{m_0}^{r_0} \mathbf{Q}_{max} & \mathbf{J}_{r_0}^{r_0} \mathbf{\Omega}_{max} \end{bmatrix} \end{array} \right. \quad (3.17b)$$

where  $\mathbf{\Omega}_{max}$  and  $\mathbf{Q}_{max}$  are respectively diagonal matrices of the maximal reaction-wheels and the manipulator's joints' velocities.

By considering the Jacobians  $\mathbf{J}_{m_0}^{\omega_0}$  and  $\mathbf{J}_{r_0}^{\omega_0}$  expressions, one can notice that both are factorized by  $\mathcal{S}_U^{-1}$ . That implies that the relative contributions of the joints and reaction-wheels to the base angular motions do not depend on the base inertia but only on the relative angular momentum capabilities of the manipulator and base actuators. This highlights that the distribution of the angular momentum is a critical point to insure the controllability of the system and dedicated control algorithms are required to deal with a non-null momentum [ONY10]. A dedicated analysis of the components of  $\mathcal{S}_U \mathbf{J}_{\omega_0}^{scal}$  matrix of the system in a design phasis could address this issue. The sum of the reaction-wheels' angular momentum is bounded by  $\|\mathcal{S}_U \mathbf{J}_{r_0}^{\omega_0} \mathbf{\Omega}_{max}\|_{\mathcal{F}}$ . Thus, in the angular momentum space, this sum belongs to the invariant polyedron which faces are normal to the reaction-wheels' axis. For the manipulator, its angular momentum is bounded by  $\|\mathcal{S}_U \mathbf{J}_{m_0}^{\omega_0}\|$ , which is strongly sensitive to the joint configuration (variation of the gravity center position and manipulator inertia). Thus, to separate the joint and reaction-wheel contributions to the base motion according to the joint configuration, we introduce the indices  $\mathcal{K}_{\omega_0}^m$  and  $\mathcal{K}_{\omega_0}^r$  defined as follow:

$$\begin{cases} \mathcal{K}_{\omega_0}^m = \frac{\|\mathcal{S}_U \mathbf{J}_{m_0}^{\omega_0} \mathbf{Q}_{max}\|_{\mathcal{F}}}{\|\mathcal{S}_U \mathbf{J}_{\omega_0}^{scal}\|_{\mathcal{F}}} & (3.18a) \\ \mathcal{K}_{\omega_0}^r = \frac{\|\mathcal{S}_U \mathbf{J}_{r_0}^{\omega_0} \mathbf{\Omega}_{max}\|_{\mathcal{F}}}{\|\mathcal{S}_U \mathbf{J}_{\omega_0}^{scal}\|_{\mathcal{F}}} & (3.18b) \end{cases}$$

where  $\|\mathbf{X}\|_{\mathcal{F}}$  is Frobenius norm of  $\mathbf{X} \in \mathbb{R}^{n \times m}$  defined as:

$$\|\mathbf{X}\|_{\mathcal{F}} = \sqrt{\text{tr}(\mathbf{X}^* \mathbf{X})} = \sqrt{\text{tr}(\mathbf{X} \mathbf{X}^*)} = \sqrt{\sum_{1 \leq i, j \leq n, m} \|\mathbf{X}_{ij}\|^2} \quad (3.19)$$

Separating base and manipulator actuators with the relation  $\|\mathcal{S}_U \mathbf{J}_{\omega_0}^{scal}\|_{\mathcal{F}}^2 = \|\mathcal{S}_U \mathbf{J}_{m_0}^{\omega_0} \mathbf{Q}_{max}\|_{\mathcal{F}}^2 + \|\mathcal{S}_U \mathbf{J}_{r_0}^{\omega_0} \mathbf{\Omega}_{max}\|_{\mathcal{F}}^2$  and by analytically evaluating this norm, the kinematic indicators are interesting to characterize the base controllability on pre-design stages or select preferential joint configuration for control and path-planning purpose. One will note that the separation leads to a complementary between  $\mathcal{K}_{\omega_0}^m$  and  $\mathcal{K}_{\omega_0}^r$ . For instance, in an arbitrary manner, joint configurations whose the index  $\mathcal{K}_{\omega_0}^m$  respects the arbitrary constraint  $\mathcal{K}_{\omega_0}^m < 0.5$  are more suitable to achieve motion without changing the base attitude.

**End-effector indices:** In SMS task prioritization, the highest priority task is the end-effector motions, however with additional tasks for the base motions and with the dynamic couplings of free-floating systems, manipulator capability to perform the end-effector task may significantly be affected. To analyze this problem end-effector kinematic indices are introduced. Similarly than for the base indices, the generalized Jacobians are decomposed as



a translation and rotation sub-Jacobians as:

$$\begin{cases} \mathbf{J}_{mEE}^* = \begin{bmatrix} \mathbf{J}_{mEE}^{\omega EE} \\ \mathbf{J}_{mEE}^{r EE} \end{bmatrix} = -\mathbf{J}_{0EE} \mathbf{H}_0^{-1} \begin{bmatrix} \mathbf{H}_{\omega m} \\ \mathbf{H}_{Lm} \end{bmatrix} + \mathbf{J}_{mEE} \\ \mathbf{J}_{rEE}^* = \begin{bmatrix} \mathbf{J}_{rEE}^{\omega EE} \\ \mathbf{J}_{rEE}^{r EE} \end{bmatrix} = -\mathbf{J}_{0EE} \mathbf{H}_0^{-1} \begin{bmatrix} \mathbf{H}_{\omega r} \\ \mathbf{0} \end{bmatrix} \end{cases}$$

with (2.15), (2.19) and expression of  $\mathbf{J}_{m_0}^*$  and  $\mathbf{J}_{r_0}^*$ , the end-effector generalized Jacobians are detailed as:

$$\mathbf{J}_{mEE}^* = \begin{bmatrix} \mathbf{R}_{S_0} \mathbf{J}_{m_0}^{\omega_0} \\ (\mathbf{r}_{S_0} - \mathbf{r}_{EE})^\times \mathbf{R}_{S_0} \mathbf{J}_{m_0}^{\omega_0} + \mathbf{J}_{m_0}^{r_0} \end{bmatrix} + \mathbf{J}_{mEE} \quad (3.21)$$

and

$$\mathbf{J}_{rEE}^* = \begin{bmatrix} \mathbf{R}_{S_0} \mathcal{S}_U^{-1} \mathbf{H}_{\omega r} \\ (\mathbf{r}_{S_0} - \mathbf{r}_{EE})^\times \mathbf{R}_{S_0} \mathcal{S}_U^{-1} \mathbf{H}_{\omega r} + \mathcal{S}_U^{-1} (\mathbf{r}_{S_0} - \mathbf{r}_{CoM})^\times \mathbf{H}_{\omega r} \end{bmatrix} \quad (3.22)$$

To account for actuator capacity, similarly to (3.17) the following scaled Jacobians are introduced:

$$\begin{cases} \mathbf{J}_{\omega EE}^{scal} = \begin{bmatrix} \mathbf{J}_{mEE}^{\omega EE} \mathbf{Q}_{max} & \mathbf{J}_{rEE}^{\omega EE} \mathbf{\Omega}_{max} \end{bmatrix} \\ \mathbf{J}_{r EE}^{scal} = \begin{bmatrix} \mathbf{J}_{mEE}^{r EE} \mathbf{Q}_{max} & \mathbf{J}_{rEE}^{r EE} \mathbf{\Omega}_{max} \end{bmatrix} \end{cases}$$

As a main control difficulty of free-floating SMS is the coupling between the manipulator and the base, null-motion projector can be used to restrict the redundant manipulator's joints motions to a sub-space which insure zero base attitude disturbance [NYU96]. The proposed control method can be adapted to a rotation-free-floating for a common control of the reaction-wheels and manipulator's joints by introducing the null-motion projector:

$$\mathbf{N}_{\omega_0} = \mathbf{I} - \mathbf{J}_{\omega_0}^+ \mathbf{J}_{\omega_0} \quad (3.24)$$

with  $\mathbf{J}_{\omega_0}^+$  the pseudo-inverse of  $\mathbf{J}_{\omega_0}$ . Thus, with this projector, the manipulability of the end-effector without base motions can be evaluated with the indices:

$$\begin{cases} \mu_{\omega EE}^N = \mu(\mathbf{J}_{\omega EE}^{scal} \mathbf{N}_{\omega_0}) & (3.25a) \\ \mu_{r EE}^N = \mu(\mathbf{J}_{r EE}^{scal} \mathbf{N}_{\omega_0}) & (3.25b) \end{cases}$$

### 3.2.2.2 Simulation example

The interest of the introduced kinematic indices is illustrated with numerical simulations developed on an SMS with a base exhibiting the physical parameters of the first microsatellite in the Myriade series, Demeter [PA06]. Demeter is equipped with three reaction-wheels, which nominally present an inertia of  $4.10^{-4} kg.m^2$  on their main axis and a maximal angular speed of  $2800 rpm$ . The manipulator considered has 3-DoFs with physical parameters given in table 3.1. Moreover, as current space manipulator such as Canadarm2 and JEMRMS do

not exceed joint velocities of  $0.7rpm$  [Lar+02], we assume that for this smaller manipulator maximal joints angular speeds are less than  $0.5rpm$ . The choice of manipulator and base is made such that inertia ratios allow to highlight significant kinetic momentum exchanges between the different SMS parts.

-	Mass ( $kg$ )	Dimension ( $m$ )	Inertia ( $kg.m^2$ )
Base	100	$0.6 \times 0.6 \times 0.6$	$\text{diag}(40, 20, 40)$
link 1	1.97	0.15	$\text{diag}(35, 7, 4)10^{-4}$
link 2	1.58	1	$\text{diag}(28, 917, 268)10^{-4}$
link 3	1.17	0.6	$\text{diag}(7, 924, 273)10^{-4}$

Table 3.1 – Physical parameters of the considered SMS

Focusing on the three linear DoFs, two sets of reaction-wheels are considered to compare with the suggested indices the impact that the manipulator may have on the base. The first configuration is the nominal configuration as described above, the second configuration is modified with an increased capacity of DEMETER ( $\mathbf{H}_r$  replaced by  $2\mathbf{H}_r$ ).

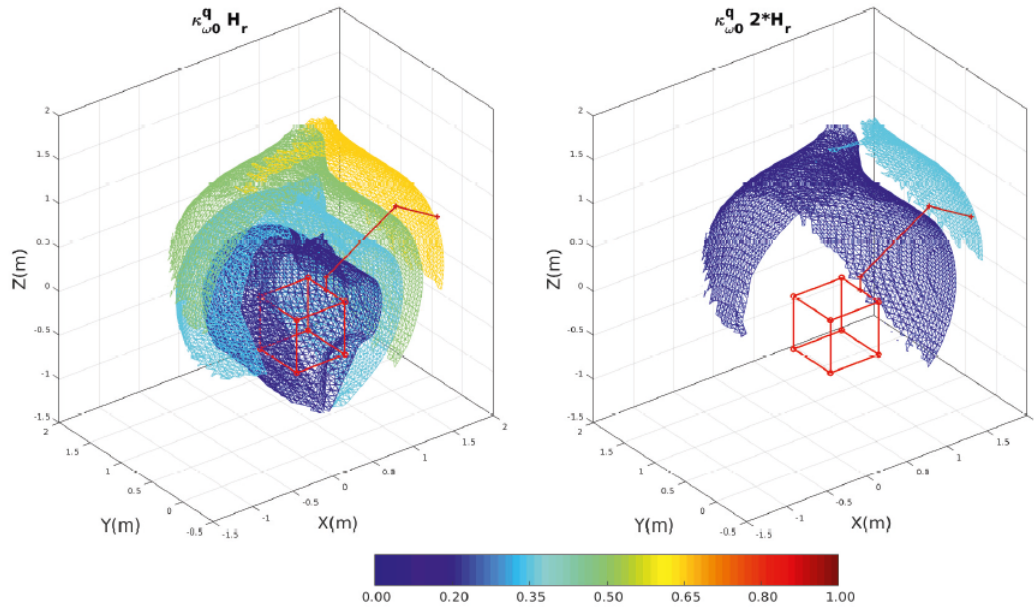


Figure 3.6 – Variation of the joint contribution to the base motion ( $\mathcal{K}_{\omega_0}^m$ ) plotted in  $\mathcal{R}_{sat}$  for the initial reaction-wheels (left) and the second actuators configuration (right)

To achieve this analysis, the indices have been evaluated for the two configurations in 6859 joint-space configurations uniformly distributed in the half-workspace of the manipulator because the system is symmetric about the  $XZ$  plane. In figures 3.6, 3.7 and 3.8 iso-surfaces of these indices are plotted and colors reflect their value for each end-effector pose. In figure 3.7 and 3.8 manipulability indices are normalized by the manipulator's manipulability on a

fixed base. Figure 3.6 points that increasing the reaction-wheels' inertia allows to decrease the contribution of the joints and to raise the one of the reaction-wheels on the base attitude motion, as  $\mathcal{K}_{\omega_0}^m$  and  $\mathcal{K}_{\omega_0}^r$  are complementary. One can also note that, the joint configurations that impact the most the base motions are those where the end-effector is the farthest from the system center of mass. In these critical configurations, doubling the inertia of the reaction wheels allows to reduce the joints' impact on the base from 0.65 to 0.4 and to ensure a stable attitude without using thrusters. However, the manipulability of  $\dot{\mathbf{r}}_{EE}$ , represented in figure 3.7, increases less than 0.1 if the base is able to move during the control of the end-effector. This is due to the small ratio between the maximal spacecraft angular speed and joints angular speed considered in our example. In this case, reducing the joint impact to the base with bigger reaction wheel inertia does not affect the manipulability of  $\dot{\mathbf{r}}_{EE}$ . Nevertheless, when null-motion is used, figure 3.8 highlights an improvement of the manipulability of  $\dot{\mathbf{r}}_{EE}$  with more angular momentum in reaction wheels. As underlined by the figure 3.6, the second configuration presents a better momentum repartition for this type of control.

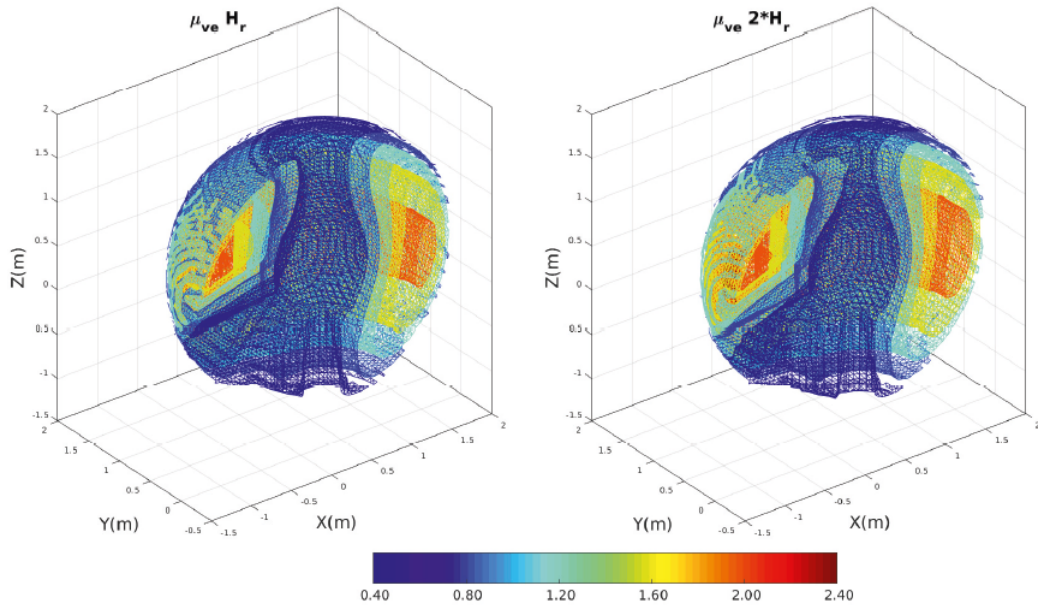


Figure 3.7 – Evolution of the end-effector normalized manipulability indices,  $\mu_{\dot{\mathbf{r}}_{EE}}^N$ , plotted in  $\mathcal{R}_{sat}$  for the initial reaction-wheels (left) and the second actuators configuration (right)

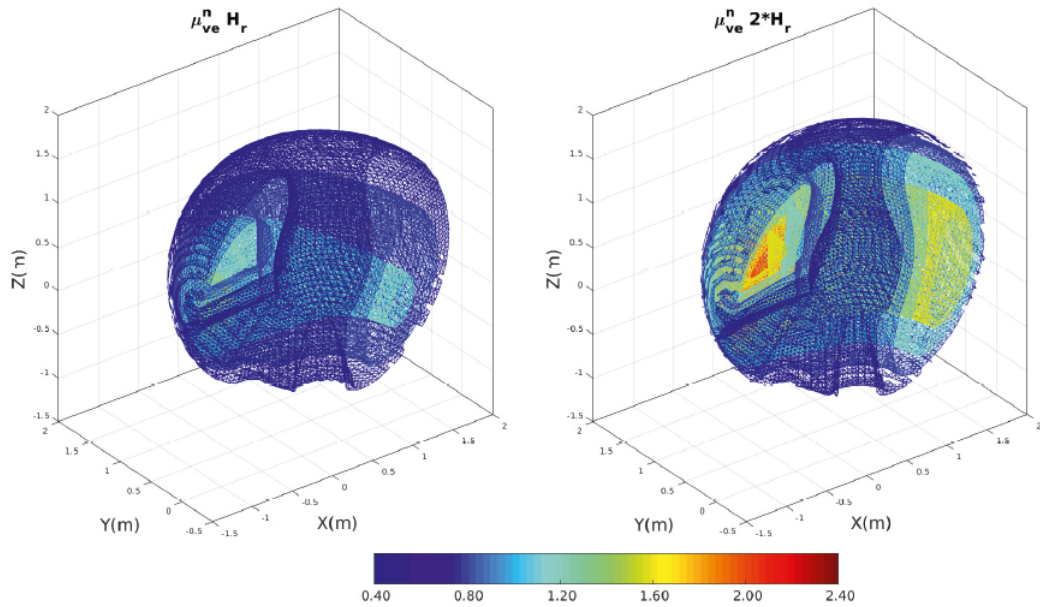


Figure 3.8 – Evolution of the end-effector normalized manipulability indices,  $\mu_{\mathbf{r}_{EE}}^N$ , with a fix base attitude constraint plotted in  $\mathcal{R}_{sat}$  for the initial reaction-wheels (left) and the second actuators configuration (right)

With this example, an illustration of one of the potential use of the kinematic indices is developed. The interest of those indices is not only to pre-size an SMS optimizing the couplings between the manipulator and the base, but likewise to adapt the control strategy. More specifically, when the base is required to maintain a fixed attitude, a suitable set of base actuators allows to balance the impact of the manipulator on the base due to the transfer of kinetic moment in the SMS.

### 3.3 Joint-space control of an SMS with flexible appendages

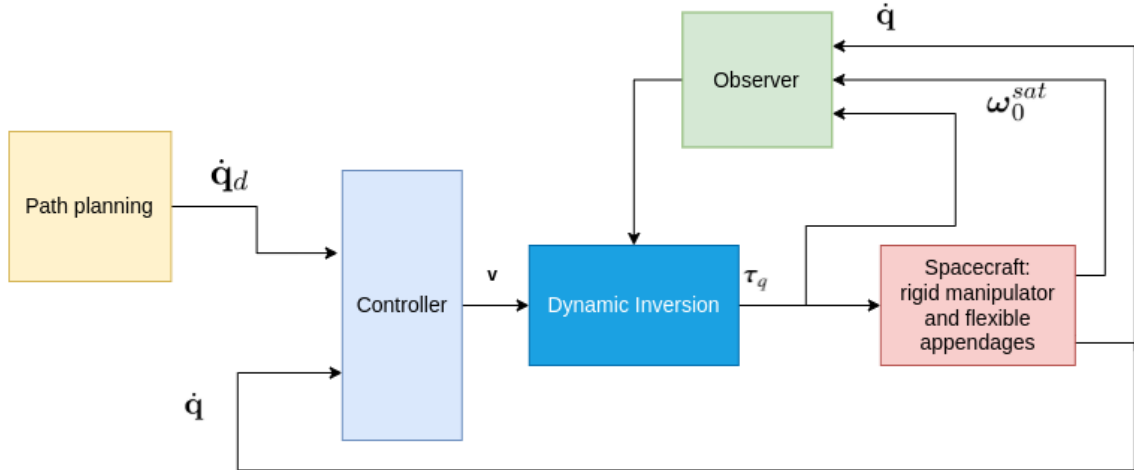


Figure 3.9 – Block diagram of the proposed joint control method

An analysis based on kinetic indices can be used to justify the interest of a simultaneous control of the base and manipulator actuators. An SMS control strategy is developed in this section such that internal perturbations due to flexible appendages will not impact control performances. As illustrated with Figure 3.9, a nonlinear dynamic inversion is performed to both linearize and decouple the system. Thanks to the modeling of a rotation-free-floating SMS with flexible appendages developed in the previous chapter, internal disturbances are included in the system feedback linearization such that actuators decoupling are accurately performed. Moreover, including the disturbances forces/torques in the control torques, it aims at rejecting perturbations with an adapted use of base actuators. With an ESO<sup>7</sup>, the unmeasured states (i.e. the flexible modes displacements/velocities and the base linear velocities) are included in the NDI<sup>8</sup>. This leads to an inter-dependency of observer and control dynamics and performances which motivates a simultaneous synthesis of respective gains based on a Lyapunov stability analysis. Then an LMI<sup>9</sup> resolution allows to obtain linear observer and control gains such that control performances and stability are insured.

First the state observer and control dynamics are developed capitalizing on the modeling effort detailed in the previous chapter. In a second time, the system closed-loop dynamics are detailed highlighting the coupling between observer and control performances, such that a gain synthesis method is proposed to perform a given motion in an SMS workspace. Finally, an illustration of the proposed method efficiency and interest is obtained on a simple SMS example thanks to the developed Matlab simulation tools.

<sup>7</sup>Extended State Observer

<sup>8</sup>Nonlinear Dynamic Inversion

<sup>9</sup>Linear Matrix Inequality

### 3.3.1 Observer structure

As mentioned, an observer is established aiming at including the un-measurable states of the SMS, which behaviors is described by the equations of motions (2.69), in the NDI. It is reminded that the flexible vibrations,  $\boldsymbol{\eta}$  and  $\dot{\boldsymbol{\eta}}$ , as well as the linear dynamics of the spacecraft,  $\dot{\mathbf{r}}_{S_0}$ , are the states requiring an estimation. Likewise, to remain as general as possible, actuators' accelerations measures are supposed to be not available. Therefore, the observer is designed such as:

- the control torque,  $\boldsymbol{\tau}_q$ , and the actuators' velocities,  $\mathbf{q}$ , are used as observer's inputs
- the angular base velocity,  $\boldsymbol{\omega}_0^{sat}$ , is used as observer's input
- the states to be estimated are the flexible displacement and velocities, respectively  $\boldsymbol{\eta}$  and  $\dot{\boldsymbol{\eta}}$ , and the base linear velocity,  $\dot{\mathbf{r}}_{S_0}$ .

Prior to establish the observer dynamics, a re-written effort of the overall system equations of motions (2.69) is necessary to design the observer without actuators' accelerations,  $\ddot{\mathbf{q}}$ . Thus, from (2.69) including the actuators' dynamics:

$$\ddot{\mathbf{q}} = -\mathbf{H}_q^{-1} \left( \mathbf{H}_{0q}^T \ddot{\mathbf{q}}_0 + \mathbf{C}_{q0} \dot{\mathbf{q}}_0 + \mathbf{C}_q \dot{\mathbf{q}} - \boldsymbol{\tau}_q \right) \quad (3.26)$$

onto the base and flexible dynamics:

$$\begin{bmatrix} \mathbf{H}_0 & \mathbf{H}_{0\eta} \\ \mathbf{H}_{0\eta}^T & \mathbf{H}_\eta \end{bmatrix} \begin{bmatrix} \ddot{\mathbf{q}}_0 \\ \ddot{\boldsymbol{\eta}} \end{bmatrix} + \begin{bmatrix} \mathbf{H}_{0q} \\ \mathbf{0} \end{bmatrix} \ddot{\mathbf{q}} + \begin{bmatrix} \mathbf{C}_0 & \mathbf{C}_{0\eta} \\ \mathbf{C}_{\eta 0} & \mathbf{C}_\eta \end{bmatrix} \begin{bmatrix} \dot{\mathbf{q}}_0 \\ \dot{\boldsymbol{\eta}} \end{bmatrix} + \begin{bmatrix} \mathbf{C}_{0q} \\ \mathbf{0} \end{bmatrix} \dot{\mathbf{q}} + \begin{bmatrix} \mathbf{0} \\ \mathbf{K}_\eta \boldsymbol{\eta} \end{bmatrix} = \begin{bmatrix} \mathbf{0}_{6 \times 1} \\ \mathbf{0}_{n_\eta \times 1} \end{bmatrix} \quad (3.27)$$

then the flexible and base dynamics can be expressed without the actuators' accelerations as:

$$\mathbf{M}_{0\eta}^*(\mathbf{x}_0, \mathbf{q}) \begin{bmatrix} \ddot{\mathbf{q}}_0 \\ \ddot{\boldsymbol{\eta}} \end{bmatrix} + \mathbf{D}_{\eta 0\eta}^*(\mathbf{x}_0, \mathbf{q}, \dot{\mathbf{q}}_0, \dot{\boldsymbol{\eta}}) \begin{bmatrix} \dot{\mathbf{q}}_0 \\ \dot{\boldsymbol{\eta}} \end{bmatrix} + \mathbf{D}_q^*(\mathbf{x}_0, \mathbf{q}, \dot{\mathbf{q}}_0, \dot{\boldsymbol{\eta}}) \dot{\mathbf{q}} = \mathbf{J}_q^*(\mathbf{x}_0, \mathbf{q}) \boldsymbol{\tau}_q \quad (3.28)$$

with:

$$\mathbf{M}_{0\eta}^* = \begin{bmatrix} \mathbf{H}_0 & \mathbf{H}_{0\eta} \\ \mathbf{H}_{0\eta}^T & \mathbf{H}_\eta \end{bmatrix} - \begin{bmatrix} \mathbf{H}_{0q} \\ \mathbf{0} \end{bmatrix} \mathbf{H}_q^{-1} \begin{bmatrix} \mathbf{H}_{0q}^T & \mathbf{0} \end{bmatrix} \quad (3.29a)$$

$$\mathbf{D}_{\eta 0\eta}^* = \begin{bmatrix} \mathbf{0} & \mathbf{C}_0 & \mathbf{C}_{0\eta} \\ \mathbf{K}_\eta & \mathbf{C}_{\eta 0} & \mathbf{C}_\eta \end{bmatrix} - \begin{bmatrix} \mathbf{H}_{0q} \\ \mathbf{0} \end{bmatrix} \mathbf{H}_q^{-1} \begin{bmatrix} \mathbf{0} & \mathbf{C}_{q0} & \mathbf{0} \end{bmatrix} \quad (3.29b)$$

$$\mathbf{D}_q^* = \begin{bmatrix} \mathbf{C}_{0q} \\ \mathbf{0} \end{bmatrix} - \begin{bmatrix} \mathbf{H}_{0q} \\ \mathbf{0} \end{bmatrix} \mathbf{H}_q^{-1} \mathbf{C}_q \quad (3.29c)$$

$$\mathbf{J}_q^* = - \begin{bmatrix} \mathbf{H}_{0q} \\ \mathbf{0} \end{bmatrix} \mathbf{H}_q^{-1} \quad (3.29d)$$

The equivalent inertia matrix  $\mathbf{M}_{0\eta}^*(\mathbf{x}_0, \mathbf{q})$  is obtained from the SMS configuration (i.e. actuators' state,  $\mathbf{q}$ , and pose/orientation of the base in  $\mathcal{R}_{ine}$ ,  $\mathbf{x}_0 = [\boldsymbol{\theta}_0^T \ \mathbf{r}_{\mathcal{S}_0}^T]^T$ ). It holds the mathematical properties of inertia matrices, in particular it is defined positive and invertible. The equivalent convective matrices  $\mathbf{D}_{\eta 0\eta}^*(\mathbf{x}_0, \mathbf{q}, \dot{\mathbf{q}}_0, \dot{\mathbf{q}})$  and  $\mathbf{D}_q^*(\mathbf{x}_0, \mathbf{q}, \dot{\mathbf{q}}_0, \dot{\mathbf{q}})$  depend on the SMS configurations but also on the system's velocities.

In order to alleviate further dependency notations, quantities evaluated in the inverse kinematic/dynamic model from the measure of both  $\mathbf{x}_0$  and  $\mathbf{q}$  will be reduced to  $\mathbf{q}$ . This simplification is justified by the fact that  $\mathbf{x}_0$  provides the pose and orientation of  $\mathcal{R}_{sat}$  in  $\mathcal{R}_{ine}$  but does not affect the mass distribution.

Then introducing the state vector to be estimated,  $\mathbf{x} = [\boldsymbol{\eta}^T \ \dot{\mathbf{q}}_0^T \ \ddot{\boldsymbol{\eta}}^T]^T$ , with (3.28) the state space model adapted to estimate  $\mathbf{x}$  is written as:

$$\begin{cases} \dot{\mathbf{x}} = \begin{bmatrix} \dot{\boldsymbol{\eta}} \\ \ddot{\mathbf{q}}_0 \\ \ddot{\boldsymbol{\eta}} \end{bmatrix} = \begin{bmatrix} \mathbf{0}_{n_\eta} & \mathbf{0}_{n_\eta \times n_q} & \mathbf{I}_{n_\eta} \\ & -\mathbf{M}_{0\eta}^{*-1} \mathbf{D}_{\eta 0\eta}^* & \end{bmatrix} \mathbf{x} + \begin{bmatrix} \mathbf{0}_{n_\eta \times n_q} & \mathbf{0}_{n_\eta \times n_q} \\ -\mathbf{M}_{0\eta}^{*-1} \mathbf{D}_q^* & \mathbf{M}_{0\eta}^{*-1} \mathbf{J}_q^* \end{bmatrix} \begin{bmatrix} \dot{\mathbf{q}} \\ \boldsymbol{\tau}_q \end{bmatrix} \\ = \mathbf{A}_e(\mathbf{q}, \dot{\mathbf{q}}, \dot{\mathbf{q}}_0) \mathbf{x} + \mathbf{B}_q(\mathbf{q}, \dot{\mathbf{q}}, \dot{\mathbf{q}}_0) \mathbf{u} \\ \mathbf{y} = \boldsymbol{\omega}_0^{sat} = \begin{bmatrix} \mathbf{0}_{3 \times n_\eta} & [\mathbf{I}_3 & \mathbf{0}_3] & \mathbf{0}_{3 \times n_\eta} \end{bmatrix} \mathbf{x} = \mathbf{C}_e \mathbf{x} \end{cases} \quad (3.30a)$$

$$\quad (3.30b)$$

By introducing the linear estimation gain  $\mathbf{L}$ , the state vector  $\mathbf{x}$  is estimated as  $\mathbf{x}_e$  such that:

$$\dot{\mathbf{x}}_e = \mathbf{A}_e(\mathbf{q}, \dot{\mathbf{q}}, \dot{\mathbf{q}}_0) \mathbf{x}_e + \mathbf{B}_q(\mathbf{q}, \dot{\mathbf{q}}, \dot{\mathbf{q}}_0) \mathbf{u} + \mathbf{L}(\mathbf{y} - \mathbf{C}_e \mathbf{x}_e) \quad (3.31)$$

Then denoting  $\boldsymbol{\epsilon}_e$  the observation error signal, defined as  $\boldsymbol{\epsilon}_e = \mathbf{x} - \mathbf{x}_e$ , with (3.30) and (3.31) the observer error dynamics are expressed as:

$$\dot{\boldsymbol{\epsilon}}_e = (\mathbf{A}_e(\mathbf{q}, \dot{\mathbf{q}}, \dot{\mathbf{q}}_0) - \mathbf{L} \mathbf{C}_e) \boldsymbol{\epsilon}_e \quad (3.32)$$

### 3.3.2 Control law structure

To obtain the control law structure, first a re-written effort of (2.69) is made and secondly the NDI structure is established.

#### 3.3.2.1 Open-loop dynamics

With a similar re-arrangement of (2.69) as operated to design the observer, the actuators' dynamics are re-written from (2.69) without the flexible and base accelerations (i.e.  $[\dot{\mathbf{q}}_0^T \ \ddot{\boldsymbol{\eta}}^T]^T$ ). Therefore, injecting (3.27) in (3.26), actuators' dynamics are re-written as:

$$\mathbf{M}^\diamond(\mathbf{q}) \ddot{\mathbf{q}} + \mathbf{D}^\diamond(\mathbf{q}, \dot{\mathbf{q}}, \dot{\mathbf{q}}_0) \dot{\mathbf{q}} + \mathbf{D}_x^\diamond(\mathbf{q}, \dot{\mathbf{q}}, \dot{\mathbf{q}}_0) \mathbf{x} = \boldsymbol{\tau}_q \quad (3.33)$$

One will notice that the disturbance torque  $\mathbf{D}_x^\diamond(\mathbf{q}, \dot{\mathbf{q}}, \dot{\mathbf{q}}_0)\mathbf{x}$  affects the actuators' dynamics. This torque has the particularity of including, besides the base angular velocity, only states that can be estimated through the proposed observer (3.30). Furthermore, it corresponds to the overall intern perturbations that requires to be rejected for a precise control.

In order to detail the equivalent inertia matrix  $\mathbf{M}^\diamond(\mathbf{q})$  and the equivalent convective matrices  $\mathbf{D}^\diamond(\mathbf{q}, \dot{\mathbf{q}}, \dot{\mathbf{q}}_0)$  and  $\mathbf{D}_x^\diamond(\mathbf{q}, \dot{\mathbf{q}}, \dot{\mathbf{q}}_0)$ , one will first note that  $\begin{bmatrix} \mathbf{H}_0 & \mathbf{H}_{0\eta} \\ \mathbf{H}_{0\eta}^T & \mathbf{H}_\eta \end{bmatrix}$  is an inertia matrix which has an inverse given by:

$$\begin{bmatrix} \mathbf{H}_0 & \mathbf{H}_{0\eta} \\ \mathbf{H}_{0\eta}^T & \mathbf{H}_\eta \end{bmatrix}^{-1} = \begin{bmatrix} (\mathbf{H}_0 - \mathbf{H}_{0\eta}\mathbf{H}_{0\eta}^T)^{-1} & -(\mathbf{H}_0 - \mathbf{H}_{0\eta}\mathbf{H}_{0\eta}^T)^{-1}\mathbf{H}_{0\eta} \\ -\mathbf{H}_{0\eta}^T(\mathbf{H}_0 - \mathbf{H}_{0\eta}\mathbf{H}_{0\eta}^T)^{-1} & \mathbf{I}_{n_\eta} + \mathbf{H}_{0\eta}^T(\mathbf{H}_0 - \mathbf{H}_{0\eta}\mathbf{H}_{0\eta}^T)^{-1}\mathbf{H}_{0\eta} \end{bmatrix} \quad (3.34)$$

with the flexible modeling assumptions detailed in the previous chapter,  $\mathbf{H}_\eta = \mathbf{I}_{n_\eta}$ . The inertial term  $(\mathbf{H}_0 - \mathbf{H}_{0\eta}\mathbf{H}_{0\eta}^T)$  corresponds to a scaled inertia of the base for which the flexible inertia have been subtracted of the spacecraft base.

Then the detail of matrices in (3.33) as:

$$\begin{cases} \mathbf{M}^\diamond = \mathbf{H}_q - \mathbf{H}_{0q}^T(\mathbf{H}_0 - \mathbf{H}_{0\eta}\mathbf{H}_{0\eta}^T)^{-1}\mathbf{H}_{0q} & (3.35a) \end{cases}$$

$$\begin{cases} \mathbf{D}^\diamond = \mathbf{C}_q - \mathbf{H}_{0q}^T(\mathbf{H}_0 - \mathbf{H}_{0\eta}\mathbf{H}_{0\eta}^T)^{-1}\mathbf{C}_{0q} & (3.35b) \end{cases}$$

$$\begin{cases} \mathbf{D}_x^\diamond = \begin{bmatrix} \mathbf{0} & \mathbf{C}_{q0} & \mathbf{0} \\ -\mathbf{H}_{0q}^T [(\mathbf{H}_0 - \mathbf{H}_{0\eta}\mathbf{H}_{0\eta}^T)^{-1} & -(\mathbf{H}_0 - \mathbf{H}_{0\eta}\mathbf{H}_{0\eta}^T)^{-1}\mathbf{H}_{0\eta}] \begin{bmatrix} \mathbf{0} & \mathbf{C}_0 & \mathbf{C}_{0\eta} \\ \mathbf{K}_\eta & \mathbf{C}_{\eta 0} & \mathbf{C}_\eta \end{bmatrix} \end{bmatrix} & (3.35c) \end{cases}$$

Detailing the expression of the matrix  $\mathbf{M}^\diamond(\mathbf{q})$  allows to highlight the effect of the flexible modes' dynamics on the actuators' ones. With the scaled inertia term  $\mathbf{H}_{0q}^T(\mathbf{H}_0 - \mathbf{H}_{0\eta}\mathbf{H}_{0\eta}^T)^{-1}$ , one observes that flexible vibrations will affect the actuators through their impact on the spacecraft base.

### 3.3.2.2 Closed-loop dynamics

In order to decouple and linearize the system, an NDI is developed capitalizing on the observer to likewise include the disturbance torques. By introducing the subscripts  $d$  to designate a desired quantity, the control tracking error,  $\boldsymbol{\epsilon}_c$ , is defined as:

$$\boldsymbol{\epsilon}_c = (\mathbf{q}_d - \mathbf{q}) \quad (3.36)$$

and with a linear control gain,  $\mathbf{K}$ , the desired dynamic,  $\mathbf{v}$ , is imposed as:

$$\mathbf{v} = \ddot{\mathbf{q}}_d + \mathbf{K} \begin{bmatrix} \boldsymbol{\epsilon}_c \\ \dot{\boldsymbol{\epsilon}}_c \end{bmatrix} \quad (3.37)$$



Thus, a control torque,  $\boldsymbol{\tau}_{q_c}$ , that linearizes the system and decouples actuators is given by:

$$\boldsymbol{\tau}_{q_c} = \mathbf{M}^\diamond(\mathbf{q})\mathbf{v} + \mathbf{D}^\diamond(\mathbf{q}, \dot{\mathbf{q}}, \dot{\mathbf{q}}_0)\dot{\mathbf{q}} + \mathbf{D}_x^\diamond(\mathbf{q}, \dot{\mathbf{q}}, \dot{\mathbf{q}}_0)\mathbf{x}_e \quad (3.38)$$

Injecting (3.38) in (3.33) the closed-loop control dynamics is expressed in function of the observer error dynamics (3.32) as:

$$\ddot{\boldsymbol{\epsilon}}_c = -\mathbf{K} \begin{bmatrix} \boldsymbol{\epsilon}_c \\ \dot{\boldsymbol{\epsilon}}_c \end{bmatrix} + \mathbf{M}^{\diamond^{-1}} \mathbf{D}_x^\diamond \boldsymbol{\epsilon}_e \quad (3.39)$$

Introducing the state vector  $\mathbf{z} = [\boldsymbol{\epsilon}_c^T \ \dot{\boldsymbol{\epsilon}}_c^T]^T$ , one can re-write (3.39) as:

$$\begin{cases} \dot{\mathbf{z}} = \left( \begin{bmatrix} 0 & \mathbf{I} \\ 0 & 0 \end{bmatrix} + \begin{bmatrix} 0 \\ -\mathbf{I} \end{bmatrix} \mathbf{K} \right) \mathbf{z} + \begin{bmatrix} \mathbf{0} \\ \mathbf{M}^{\diamond^{-1}} \mathbf{D}_x^\diamond \end{bmatrix} \boldsymbol{\epsilon}_e \\ \boldsymbol{\epsilon}_c = [\mathbf{I} \ \mathbf{0}] \mathbf{z} = \mathbf{C}_z \mathbf{z} \end{cases} \quad (3.40a)$$

$$\boldsymbol{\epsilon}_c = [\mathbf{I} \ \mathbf{0}] \mathbf{z} = \mathbf{C}_z \mathbf{z} \quad (3.40b)$$

With this last expression, one will note that the control performances are dependent on the estimation quality and its convergence. The challenge is then to insure simultaneously the stability of the observer and the controller.

### 3.3.3 Simultaneous synthesis

#### 3.3.3.1 Simple synthesis

To take into account and clearly highlight the dependency between observer and controller performances, the extended state vector  $\mathbf{w} = [\mathbf{z}^T \ \boldsymbol{\epsilon}_e^T]^T$  is introduced such that a compact version of (3.32) and (3.40) is obtained as:

$$\begin{cases} \dot{\mathbf{w}} = \begin{bmatrix} \mathbf{A}_z + \mathbf{B}_z \mathbf{K} & \mathbf{B}_e \\ \mathbf{0} & \mathbf{A}_e - \mathbf{L} \mathbf{C}_e \end{bmatrix} \mathbf{w} \\ \boldsymbol{\epsilon}_c = [\mathbf{C}_z \ \mathbf{0}] \mathbf{w} \end{cases} \quad (3.41a)$$

$$\boldsymbol{\epsilon}_c = [\mathbf{C}_z \ \mathbf{0}] \mathbf{w} \quad (3.41b)$$

With the separation principle, both observer and controller gains could be evaluated separately, however, in this section, a method to synthesize the gains  $\mathbf{K}$  and  $\mathbf{L}$  is proposed such that the system remains stable and a guarantee of similar control performances is insured for a considered servicing operation that induces variations of matrices  $\mathbf{B}_e$  and  $\mathbf{A}_e$ .

Thus, considering a system linearization allowing to evaluate matrices in (3.41) the control and observer gains are synthesized simultaneously with the following proposition based on

a Lyapunov stability analysis. Then, the gains  $\mathbf{K}$  and  $\mathbf{L}$  are finally obtained from an LMI resolution.

**Proposition:** Assuming the initial estimation error verifies  $\boldsymbol{\epsilon}_{e_0}^T \mathbf{E} \boldsymbol{\epsilon}_{e_0} \leq 1$  for a given positive definite matrix  $\mathbf{E}$ , where  $\boldsymbol{\epsilon}_{e_0}$  is the initial condition of the observer error. If there exist symmetric positive definite matrices  $\mathbf{Q}_z$ ,  $\mathbf{P}_\epsilon$  and matrices  $\mathbf{W}_z$ ,  $\mathbf{W}_\epsilon$  such that for a given scalar  $\gamma > 0$ :

$$\left\{ \begin{array}{l} \Omega = \begin{bmatrix} (\mathbf{A}_z \mathbf{Q}_z + \mathbf{B}_z \mathbf{W}_z)^s & \mathbf{B}_\epsilon & \mathbf{Q}_z \mathbf{C}_z^T \\ * & (\mathbf{P}_\epsilon \mathbf{A}_e - \mathbf{W}_\epsilon \mathbf{C}_e)^s & \mathbf{0} \\ * & * & -\gamma^2 \mathbf{I} \end{bmatrix} < 0 \\ \mathbf{P}_\epsilon < \mathbf{E} \end{array} \right. \quad (3.42a)$$

$$(3.42b)$$

where  $\mathbf{X}^s = \mathbf{X} + \mathbf{X}^T$  and  $\Omega$  is a symmetric matrix, then the system (3.41) is stable and the outputs verify:

$$\int_0^\infty \boldsymbol{\epsilon}_c^T \boldsymbol{\epsilon}_c dt < \gamma^2 \quad (3.43)$$

for any conditions  $\mathbf{z}(0) = \mathbf{0}$  and  $\boldsymbol{\epsilon}_{e_0} \in \{\boldsymbol{\epsilon} \mid \boldsymbol{\epsilon}^T \mathbf{E} \boldsymbol{\epsilon} \leq 1\}$ . Moreover, the gains are obtained as:

$$\left\{ \begin{array}{l} \mathbf{K} = \mathbf{W}_z \mathbf{Q}_z^{-1} \\ \mathbf{L} = \mathbf{P}_\epsilon^{-1} \mathbf{W}_\epsilon \end{array} \right. \quad (3.44a)$$

$$(3.44b)$$

**Proof:** Let us introduce the Lyapunov function:

$$\mathbf{V}(\mathbf{w}) = \mathbf{z}^T \mathbf{P}_z \mathbf{z} + \boldsymbol{\epsilon}_e^T \mathbf{P}_\epsilon \boldsymbol{\epsilon}_e \quad (3.45)$$

such that  $\dot{\mathbf{V}} + \gamma^{-2} \boldsymbol{\epsilon}_c^T \boldsymbol{\epsilon}_c < 0$  for a given  $\gamma > 0$ .

By integration:

$$\begin{aligned} \forall T_f > 0, \int_0^{T_f} (\dot{\mathbf{V}} + \boldsymbol{\epsilon}_c^T \boldsymbol{\epsilon}_c) dt < 0 &\Rightarrow \int_0^{T_f} \boldsymbol{\epsilon}_c^T \boldsymbol{\epsilon}_c dt < \gamma^2 (\mathbf{V}(0) - \mathbf{V}(T_f)) \\ &\Rightarrow \int_0^\infty \boldsymbol{\epsilon}_c^T \boldsymbol{\epsilon}_c dt < \gamma^2 \mathbf{V}(0) \end{aligned} \quad (3.46)$$

with  $\mathbf{V}(0) = \mathbf{z}(0)^T \mathbf{P}_z \mathbf{z}(0) + \boldsymbol{\epsilon}_{e_0}^T \mathbf{P}_\epsilon \boldsymbol{\epsilon}_{e_0}$ . For  $\mathbf{z}(0) = \mathbf{0}_{2 \times (3+n_m)}$ ,  $\mathbf{V}(0) = \boldsymbol{\epsilon}_{e_0}^T \mathbf{P}_\epsilon \boldsymbol{\epsilon}_{e_0}$  and if  $\boldsymbol{\epsilon}_{e_0}^T \mathbf{P}_\epsilon \boldsymbol{\epsilon}_{e_0} \leq \boldsymbol{\epsilon}_{e_0}^T \mathbf{E} \boldsymbol{\epsilon}_{e_0} \leq 1$  then (3.43) is verified. This condition is enforced by  $\mathbf{P}_\epsilon \leq \mathbf{E}$ .

The condition  $\dot{\mathbf{V}} + \gamma^{-2} \boldsymbol{\epsilon}_c^T \boldsymbol{\epsilon}_c < 0$  is equivalent to:

$$\left[ \begin{array}{cc} (\mathbf{P}_z (\mathbf{A}_z + \mathbf{B}_z \mathbf{K}))^s + \gamma^{-2} \mathbf{C}_z^T \mathbf{C}_z & \mathbf{P}_z \mathbf{B}_\epsilon \\ * & (\mathbf{P}_\epsilon (\mathbf{A}_e - \mathbf{L} \mathbf{C}_e))^s \end{array} \right] < 0 \quad (3.47)$$

Applying the Schur complement on (3.47) is given by:

$$\begin{bmatrix} (\mathbf{P}_z (\mathbf{A}_z + \mathbf{B}_z \mathbf{K}))^s & \mathbf{P}_z \mathbf{B}_\epsilon & \mathbf{C}_z^T \\ * & (\mathbf{P}_\epsilon (\mathbf{A}_e - \mathbf{L} \mathbf{C}_e))^s & \mathbf{0} \\ * & * & -\gamma^2 \mathbf{I} \end{bmatrix} < 0 \quad (3.48)$$

Pre and post multiplying the above matrix by  $\text{diag}(\mathbf{Q}_z, \mathbf{I}, \mathbf{I}) = \text{diag}(\mathbf{P}_z^{-1}, \mathbf{I}, \mathbf{I})$  and introducing the variable changes  $\mathbf{W}_e = \mathbf{P}_\epsilon \mathbf{L}$  and  $\mathbf{W}_z = \mathbf{K} \mathbf{Q}_z$  one obtains (3.42a) which concludes the proof.

The resolution of the LMI (3.42a), and thus the synthesis of  $\mathbf{K}$  and  $\mathbf{L}$ , is obtained for a given system linearization. Evaluating matrices  $\mathbf{A}_e$  and  $\mathbf{B}_\epsilon$  from that linearization and defining the matrices  $\mathbf{Q}_z$ ,  $\mathbf{P}_\epsilon$ ,  $\mathbf{W}_z$  and  $\mathbf{W}_e$  as LMI variables, it allows to compute the control and observer gains by minimizing the positive LMI variable  $\gamma$ . Additional LMI constraints as (3.42a) can be added for different system linearization with the same LMI variables for each constraint.

### 3.3.3.2 Gains synthesis for a given SMS task

As illustrated with the example of the control law inspired by the literature developed in section 3.1.2, the control gains should be taken into account for system inertia variations to insure similar control performances during a given task operated by the SMS. In that matter, a single system linearization to synthesize the gains as in the proposition 3.3.3.1 may not be sufficient. This will lead to the study of multiple equilibrium points which will correspond to a new LMI constraint as 3.42a for each linearization. In order to avoid such considerations, an approach with introduction of relaxation terms in the LMI 3.42a is developed here.

We consider a typical task consisting in the manipulator moving a given mass from one point to another while the base is maintained with a fixed orientation. Then it can easily be assumed that the manipulator trajectory is restrained in a reduced workspace and that the state vector  $[\boldsymbol{\omega}_0^{satT} \quad \dot{\mathbf{r}}_{S_0}^T \quad \dot{\mathbf{q}}^T \quad \dot{\boldsymbol{\eta}}^T]^T$  is bounded during the manipulator operation. This allows to obtain a bound of the inertia and convective matrices (i.e.  $\mathbf{H}$  and  $\mathbf{C}$  in (2.69)) and consequently matrices in (3.41). Thus from one linearization, let us introduce variations of  $\mathbf{B}_\epsilon$  and  $\mathbf{A}_e$  respectively as  $\Delta \mathbf{B}_\epsilon$  and  $\Delta \mathbf{A}_e$  such that (3.40) and (3.32) are rewritten as:

$$\begin{cases} \dot{\mathbf{z}} = (\mathbf{A}_z + \mathbf{B}_z \mathbf{K}) \mathbf{z} + (\mathbf{B}_\epsilon + \Delta \mathbf{B}_\epsilon) \boldsymbol{\epsilon}_e & (3.49a) \\ \dot{\boldsymbol{\epsilon}}_e = ((\mathbf{A}_e + \Delta \mathbf{A}_e) - \mathbf{L} \mathbf{C}_e) \boldsymbol{\epsilon}_e & (3.49b) \end{cases}$$

The LMI synthesis is modified with the condition (3.42a) that becomes:

$$\Omega = \begin{bmatrix} (\mathbf{A}_z \mathbf{Q}_z + \mathbf{B}_z \mathbf{W}_z)^s & (\mathbf{B}_\epsilon + \Delta \mathbf{B}_\epsilon) & \mathbf{Q}_z \mathbf{C}_z^T \\ * & (\mathbf{P}_\epsilon \mathbf{A}_e + \Delta \mathbf{A}_e - \mathbf{W}_\epsilon \mathbf{C}_e)^s & \mathbf{0} \\ * & * & -\gamma^2 \mathbf{I} \end{bmatrix} < 0 \quad (3.50)$$

Introducing positive relaxation terms  $\rho_1$  and  $\rho_2$  defined as the maximal singular values,  $\bar{\sigma}$ , of respectively matrix  $\mathbf{A}_e$  and  $\mathbf{B}_e$  such that:

$$\begin{cases} 2\bar{\sigma}(\mathbf{A}_e) < \rho_1 \\ \bar{\sigma}(\mathbf{B}_e) < \rho_2 \end{cases} \quad (3.51a)$$

$$\quad (3.51b)$$

then the LMI constraint (3.50) is true if:

$$\begin{aligned} \Omega &= \begin{bmatrix} (\mathbf{A}_z \mathbf{Q}_z + \mathbf{B}_z \mathbf{W}_z)^s & (\mathbf{B}_e + \rho_2 \mathbf{I}) & \mathbf{Q}_z \mathbf{C}_z^T \\ * & (\mathbf{P}_e \mathbf{A}_e - \mathbf{W}_e \mathbf{C}_e)^s + \rho_1 \mathbf{I} & \mathbf{0} \\ * & * & -\gamma^2 \mathbf{I} \end{bmatrix} < 0 \\ \Rightarrow & \begin{bmatrix} (\mathbf{A}_z \mathbf{Q}_z + \mathbf{B}_z \mathbf{W}_z)^s + \rho_2 \mathbf{I} & \mathbf{B}_e & \mathbf{Q}_z \mathbf{C}_z^T \\ * & (\mathbf{P}_e \mathbf{A}_e - \mathbf{W}_e \mathbf{C}_e)^s + (\rho_1 + \rho_2) \mathbf{I} & \mathbf{0} \\ * & * & -\gamma^2 \mathbf{I} \end{bmatrix} < 0 \end{aligned} \quad (3.52)$$

This is verified by observing the following lemma.

**Lemma:**

$$\begin{aligned} \begin{bmatrix} \Psi_1 + \rho \mathbf{I} & \mathbf{B} \\ \mathbf{B}^T & \Psi_2 + \rho \mathbf{I} \end{bmatrix} < 0 &\Rightarrow \begin{bmatrix} \Psi_1 & \mathbf{B} + \Delta \\ \mathbf{B}^T + \Delta^T & \Psi_2 \end{bmatrix} < 0 \\ \forall \Delta \mid \Delta^T \Delta < \rho \mathbf{I} & \end{aligned}$$

**Proof:**

$$\begin{aligned} \begin{bmatrix} \Psi_1 & \mathbf{B} + \Delta \\ \mathbf{B}^T + \Delta^T & \Psi_2 \end{bmatrix} &= \underbrace{\begin{bmatrix} \Psi_1 + \rho \mathbf{I} & \mathbf{B} \\ \mathbf{B}^T & \Psi_2 + \rho \mathbf{I} \end{bmatrix}}_{< 0} + \underbrace{\begin{bmatrix} -\rho \mathbf{I} & \Delta \\ \Delta^T & -\rho \mathbf{I} \end{bmatrix}}_{< 0} < 0 \\ &\Leftrightarrow \rho^2 \mathbf{I} > \Delta^T \Delta \end{aligned}$$

In that respect, the relaxation terms allow to deal with variations and uncertainties of the system during the space-robot motions. For a given manipulator motion (i.e. a trajectory and actuators velocity limit), the variations of matrices  $\mathbf{A}_e$  and  $\mathbf{B}_e$  are considered in the LMI constraint of the proposition 3.3.3.1. Additionally, for relatively small parameter uncertainties present in the system modeling to evaluate the inverse kinematic/dynamic model, the relaxation terms allow to be compensated in the gains synthesis.

To summarize the use of relaxation terms, first a system linearization is performed to evaluate matrices in the LMI constraint (3.42a) then the relaxations terms  $\rho_1$  and  $\rho_2$  are evaluated with a manipulator motion analysis as (3.51). Then defining the LMI variables, the synthesis consists of minimizing  $\gamma$  such that (3.52) holds with the proposition 3.3.3.1.

### 3.4 Base and manipulator control of an SMS with flexible appendages

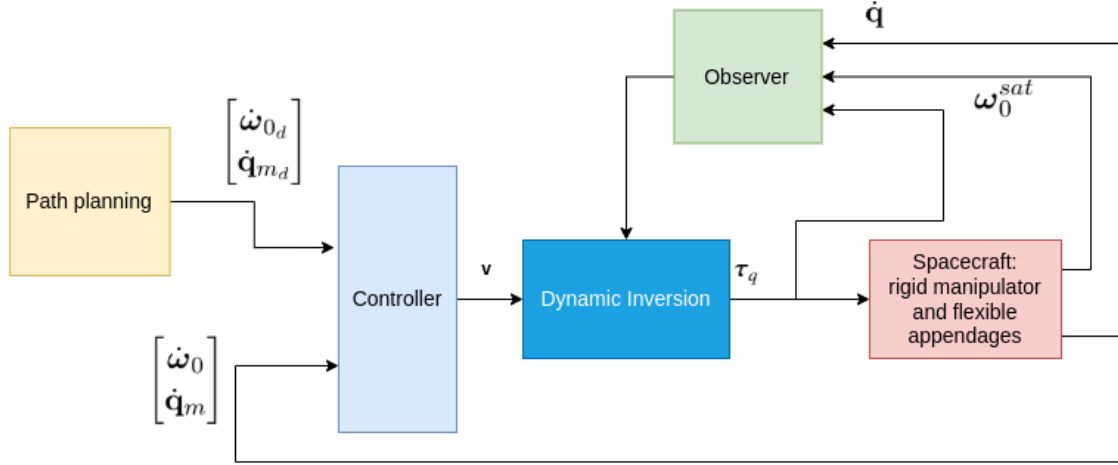


Figure 3.10 – Block diagram of the proposed base-manipulator control method

In order to better illustrate full interest of the proposed control method in section 3.3, the control scheme is adapted for a base and manipulator common control. The NDI with an ESO structure is conserved such that the un-measured states are included in the linearization. In that way, the use of base actuators can be illustrated in the disturbances rejection process.

The hypothesis on the un-measurable states developed in the previous section (i.e. actuators accelerations, flexible modes and base linear dynamics) are conserved here. Moreover, the same observer is used for the estimation of the state vector  $\mathbf{x} = [\boldsymbol{\eta}^T \quad \dot{\mathbf{q}}_0^T \quad \dot{\boldsymbol{\eta}}^T]^T$ . However, in order to distinguished the base rotations from the linear displacements, the subscript  $\omega$  and  $L$  are used to respectively designate a rotational quantity and a linear one. Thus, the overall dynamics of the free-floating SMS considered (2.69) is re-written as:

$$\begin{aligned}
 & \begin{bmatrix} \mathbf{H}_\omega & \mathbf{H}_{\omega L} & \mathbf{H}_{\omega q} & \mathbf{H}_{\omega \eta} \\ \mathbf{H}_{L\omega} & \mathbf{H}_L & \mathbf{H}_{Lq} & \mathbf{H}_{L\eta} \\ \mathbf{H}_{\omega q}^T & \mathbf{H}_{Lq}^T & \mathbf{H}_q & \mathbf{0} \\ \mathbf{H}_{\omega \eta}^T & \mathbf{H}_{L\eta}^T & \mathbf{0} & \mathbf{H}_\eta \end{bmatrix} \begin{bmatrix} \dot{\boldsymbol{\omega}}_0^{sat} \\ \ddot{\mathbf{r}}_{S_0} \\ \ddot{\mathbf{q}} \\ \ddot{\boldsymbol{\eta}} \end{bmatrix} + \begin{bmatrix} \mathbf{C}_\omega & \mathbf{C}_{\omega L} & \mathbf{C}_{\omega q} & \mathbf{C}_{\omega \eta} \\ \mathbf{C}_{L\omega} & \mathbf{C}_L & \mathbf{C}_{Lq} & \mathbf{C}_{L\eta} \\ \mathbf{C}_{q\omega} & \mathbf{C}_{qL} & \mathbf{C}_q & \mathbf{0} \\ \mathbf{C}_{\eta\omega} & \mathbf{C}_{\eta L} & \mathbf{0} & \mathbf{C}_\eta \end{bmatrix} \begin{bmatrix} \boldsymbol{\omega}_0^{sat} \\ \dot{\mathbf{r}}_{S_0} \\ \dot{\mathbf{q}} \\ \dot{\boldsymbol{\eta}} \end{bmatrix} \\
 & + \begin{bmatrix} \mathbf{0}_{3 \times 1} \\ \mathbf{0}_{3 \times 1} \\ \mathbf{0}_{n_q \times 1} \\ \mathbf{K}_\eta \boldsymbol{\eta} \end{bmatrix} = \begin{bmatrix} \mathbf{0}_{3 \times 1} \\ \mathbf{0}_{3 \times 1} \\ \boldsymbol{\tau}_q \\ \mathbf{0}_{n_\eta \times 1} \end{bmatrix}
 \end{aligned} \tag{3.54}$$

Moreover, arranging the actuators such that  $\mathbf{q} = [\mathbf{q}_r^T \quad \mathbf{q}_m^T]^T$ , the convective term,  $\mathbf{C}_q$  is

detailed as:

$$\mathbf{C}_q = \begin{bmatrix} \mathbf{C}_r & \mathbf{C}_{rm} \\ \mathbf{C}_{mr} & \mathbf{C}_m \end{bmatrix} \quad (3.55)$$

and generally for a matrix  $\mathbf{X}_q$ :

$$\mathbf{X}_q = \begin{bmatrix} \mathbf{X}_r & \mathbf{X}_m \end{bmatrix} \quad (3.56)$$

### 3.4.1 Open-loop dynamics

As the actuators' accelerations are assumed to be unavailable, in order to express the open-loop dynamics, a re-writing effort of (3.54) is mandatory to obtain an expression in function of measurable or estimable quantities. Thus, with (3.54), accelerations  $\begin{bmatrix} \ddot{\mathbf{r}}_{S_0}^T & \ddot{\mathbf{q}}_r^T & \ddot{\boldsymbol{\eta}}^T \end{bmatrix}^T$  are given by:

$$\begin{aligned} \begin{bmatrix} \ddot{\mathbf{r}}_{S_0} \\ \ddot{\mathbf{q}}_r \\ \ddot{\boldsymbol{\eta}} \end{bmatrix} &= - \begin{bmatrix} \mathbf{H}_L & \mathbf{H}_{Lr} & \mathbf{H}_{L\eta} \\ \mathbf{H}_{Lr}^T & \mathbf{H}_r & \mathbf{0} \\ \mathbf{H}_{L\eta}^T & \mathbf{0} & \mathbf{H}_\eta \end{bmatrix}^{-1} \left( \begin{bmatrix} \mathbf{H}_{L\omega} & \mathbf{H}_{Lm} \\ \mathbf{H}_{\omega r}^T & \mathbf{0} \\ \mathbf{H}_{\omega\eta}^T & \mathbf{0} \end{bmatrix} \begin{bmatrix} \dot{\boldsymbol{\omega}}_0 \\ \dot{\mathbf{q}}_m \end{bmatrix} + \begin{bmatrix} \mathbf{C}_{L\omega} & \mathbf{C}_{Lm} \\ \mathbf{C}_{r\omega} & \mathbf{C}_{rm} \\ \mathbf{C}_{\eta\omega} & \mathbf{0} \end{bmatrix} \begin{bmatrix} \boldsymbol{\omega}_0 \\ \dot{\mathbf{q}}_m \end{bmatrix} \right. \\ &\quad \left. + \begin{bmatrix} \mathbf{0} & \begin{bmatrix} \mathbf{0} & \mathbf{C}_L \\ \mathbf{0} & \mathbf{C}_{rL} \end{bmatrix} & \mathbf{C}_{L\eta} \\ \mathbf{0} & \begin{bmatrix} \mathbf{0} & \mathbf{C}_{rL} \\ \mathbf{0} & \mathbf{C}_{\eta L} \end{bmatrix} & \mathbf{0} \end{bmatrix} \mathbf{x} + \begin{bmatrix} \mathbf{C}_{Lr} \\ \mathbf{C}_r \\ \mathbf{0} \end{bmatrix} \dot{\mathbf{q}}_r - \begin{bmatrix} \mathbf{0} \\ \boldsymbol{\tau}_r \\ \mathbf{0} \end{bmatrix} \right) \end{aligned} \quad (3.57)$$

and similarly, from (3.54), the accelerations  $\begin{bmatrix} \dot{\boldsymbol{\omega}}_0^T & \dot{\mathbf{q}}_m^T \end{bmatrix}^T$  expression is given as:

$$\begin{aligned} \begin{bmatrix} \dot{\boldsymbol{\omega}}_0 \\ \dot{\mathbf{q}}_m \end{bmatrix} &= - \begin{bmatrix} \mathbf{H}_\omega & \mathbf{H}_{\omega m} \\ \mathbf{H}_{\omega m}^T & \mathbf{H}_m \end{bmatrix}^{-1} \left( \begin{bmatrix} \mathbf{C}_\omega & \mathbf{C}_{\omega m} \\ \mathbf{C}_{\omega m}^T & \mathbf{C}_m \end{bmatrix} \begin{bmatrix} \boldsymbol{\omega}_0 \\ \dot{\mathbf{q}}_m \end{bmatrix} + \begin{bmatrix} \mathbf{H}_{\omega L} & \mathbf{H}_{\omega r} & \mathbf{H}_{\omega\eta} \\ \mathbf{H}_{Lm}^T & \mathbf{0} & \mathbf{0} \end{bmatrix} \begin{bmatrix} \ddot{\mathbf{r}}_{S_0} \\ \ddot{\mathbf{q}}_r \\ \ddot{\boldsymbol{\eta}} \end{bmatrix} \right. \\ &\quad \left. + \begin{bmatrix} \mathbf{0} & \begin{bmatrix} \mathbf{0} & \mathbf{C}_{\omega L} \\ \mathbf{0} & \mathbf{C}_{\omega m}^T \end{bmatrix} & \mathbf{C}_{\omega\eta} \\ \mathbf{0} & \begin{bmatrix} \mathbf{0} & \mathbf{C}_{\omega m}^T \\ \mathbf{0} & \mathbf{0} \end{bmatrix} & \mathbf{0} \end{bmatrix} \mathbf{x} + \begin{bmatrix} \mathbf{C}_{\omega r} \\ \mathbf{C}_{mr} \end{bmatrix} \dot{\mathbf{q}}_r - \begin{bmatrix} \mathbf{0} \\ \boldsymbol{\tau}_m \end{bmatrix} \right) \end{aligned} \quad (3.58)$$

Combining (3.57) and (3.58), the open-loop dynamics are obtained as:

$$\mathbf{M}_{\omega m}^\diamond(\mathbf{q}) \begin{bmatrix} \dot{\boldsymbol{\omega}}_0 \\ \dot{\mathbf{q}}_m \end{bmatrix} + \mathbf{D}_{\omega m}^\diamond(\mathbf{q}, \dot{\mathbf{q}}, \dot{\mathbf{q}}_0) \begin{bmatrix} \boldsymbol{\omega}_0 \\ \dot{\mathbf{q}}_m \end{bmatrix} + \mathbf{D}_x^\diamond(\mathbf{q}, \dot{\mathbf{q}}, \dot{\mathbf{q}}_0) \mathbf{x} + \mathbf{D}_r^\diamond(\mathbf{q}, \dot{\mathbf{q}}, \dot{\mathbf{q}}_0) \dot{\mathbf{q}}_r = \mathbf{J}_r^\diamond(\mathbf{q}) \boldsymbol{\tau}_q \quad (3.59)$$

with:

$$\mathbf{H}_{Lr\eta}^\diamond = \begin{bmatrix} \mathbf{H}_{\omega L} & \mathbf{H}_{\omega r} & \mathbf{H}_{\omega\eta} \\ \mathbf{H}_{Lm}^T & \mathbf{0} & \mathbf{0} \end{bmatrix} \begin{bmatrix} \mathbf{H}_L & \mathbf{H}_{Lr} & \mathbf{H}_{L\eta} \\ \mathbf{H}_{Lr}^T & \mathbf{H}_r & \mathbf{0} \\ \mathbf{H}_{L\eta}^T & \mathbf{0} & \mathbf{H}_\eta \end{bmatrix}^{-1} = \begin{bmatrix} \mathbf{H}_L^\diamond & \mathbf{H}_r^\diamond & \mathbf{H}_\eta^\diamond \end{bmatrix} \quad (3.60a)$$

$$\mathbf{M}_{\omega m}^\diamond = \begin{bmatrix} \mathbf{H}_\omega & \mathbf{H}_{\omega m} \\ \mathbf{H}_{\omega m}^T & \mathbf{H}_m \end{bmatrix} - \mathbf{H}_{Lr\eta}^\diamond \begin{bmatrix} \mathbf{H}_{L\omega} & \mathbf{H}_{Lm} \\ \mathbf{H}_{\omega r}^T & \mathbf{0} \\ \mathbf{H}_{\omega\eta}^T & \mathbf{0} \end{bmatrix} \quad (3.60b)$$

$$\mathbf{D}_{\omega m}^\diamond = \begin{bmatrix} \mathbf{C}_\omega & \mathbf{C}_{\omega m} \\ \mathbf{C}_{m\omega} & \mathbf{C}_m \end{bmatrix} - \mathbf{H}_{Lr\eta}^\diamond \begin{bmatrix} \mathbf{C}_{L\omega} & \mathbf{C}_{Lm} \\ \mathbf{C}_{r\omega} & \mathbf{C}_{rm} \\ \mathbf{C}_{\omega\eta}^T & \mathbf{0} \end{bmatrix} \quad (3.60c)$$

$$\mathbf{D}_r^\diamond = \begin{bmatrix} \mathbf{C}_{\omega r} \\ \mathbf{C}_{mr} \end{bmatrix} - \mathbf{H}_{Lr\eta}^\diamond \begin{bmatrix} \mathbf{C}_{Lr} \\ \mathbf{C}_r \\ \mathbf{0} \end{bmatrix} \quad (3.60d)$$

$$\mathbf{D}_x^\diamond = \begin{bmatrix} \mathbf{0} & \begin{bmatrix} \mathbf{0} & \mathbf{C}_{\omega L} \\ \mathbf{0} & \mathbf{C}_{m\omega} \end{bmatrix} \\ \mathbf{0} & \begin{bmatrix} \mathbf{0} & \mathbf{C}_{\omega\eta} \\ \mathbf{0} & \mathbf{0} \end{bmatrix} \end{bmatrix} - \mathbf{H}_{Lr\eta}^\diamond \begin{bmatrix} \mathbf{0} & \begin{bmatrix} \mathbf{0} & \mathbf{C}_L \\ \mathbf{0} & \mathbf{C}_{rL} \end{bmatrix} \\ \mathbf{0} & \begin{bmatrix} \mathbf{0} & \mathbf{C}_{L\eta} \\ \mathbf{0} & \mathbf{C}_\eta \end{bmatrix} \end{bmatrix} \quad (3.60e)$$

$$\mathbf{J}_r^\diamond \boldsymbol{\tau}_q = \begin{bmatrix} \mathbf{0} \\ \boldsymbol{\tau}_m \end{bmatrix} - \mathbf{H}_{Lr\eta}^\diamond \begin{bmatrix} \mathbf{0} \\ \boldsymbol{\tau}_r \\ \mathbf{0} \end{bmatrix} = \begin{bmatrix} -\mathbf{H}_r^\diamond \\ \mathbf{I} \end{bmatrix} \boldsymbol{\tau}_q \quad (3.60f)$$

with  $\mathbf{H}_L^\diamond \in \mathbb{R}^{(3+n_r+n_\eta) \times 3}$ ,  $\mathbf{H}_r^\diamond \in \mathbb{R}^{(3+n_r+n_\eta) \times n_r}$  and  $\mathbf{H}_\eta^\diamond \in \mathbb{R}^{(3+n_r+n_\eta) \times n_\eta}$ . Moreover, one will note that  $\mathbf{D}_r^\diamond$  is the combination of an equivalent stiffness and convective matrix. The term  $\mathbf{D}_x^\diamond \mathbf{x}$  in (3.59) represents an internal disturbance torque which impacts manipulator and base dynamics while  $\mathbf{D}_r^\diamond \dot{\mathbf{q}}_r$  corresponds to the impact of reaction-wheels on the rest of the system.

### 3.4.2 Closed-loop dynamics

Similarly to the computation of the closed-loop for the joint-space control, developed in section 3.3.2.2, the system is first linearized and the closed-loop is express in an equivalent formulation.

In order to decouple and linearize the system, an NDI is developed including those disturbance torques. The control tracking error,  $\boldsymbol{\epsilon}_c$ , is now defined as:

$$\boldsymbol{\epsilon}_c = \left( \begin{bmatrix} \boldsymbol{\theta}_0 \\ \mathbf{q}_m \end{bmatrix}_d - \begin{bmatrix} \boldsymbol{\theta}_0 \\ \mathbf{q}_m \end{bmatrix} \right) \quad (3.61)$$

and with a linear control gain,  $\mathbf{K}$ , the desired dynamic,  $\mathbf{v}$ , is defined as:

$$\mathbf{v} = \begin{bmatrix} \dot{\boldsymbol{\omega}}_0 \\ \ddot{\mathbf{q}}_m \end{bmatrix}_d + \mathbf{K} \begin{bmatrix} \boldsymbol{\epsilon}_c \\ \dot{\boldsymbol{\epsilon}}_c \end{bmatrix} \quad (3.62)$$

Thus, a control torque,  $\boldsymbol{\tau}_{q_c}$ , that linearizes the system and decouples actuators is given by:

$$\boldsymbol{\tau}_{q_c} = \mathbf{J}_\tau^{\diamond+} \left( \mathbf{M}_{\omega m}^\diamond(\mathbf{q})\mathbf{v} + \mathbf{D}_{\omega m}^\diamond(\mathbf{q}, \dot{\mathbf{q}}, \dot{\mathbf{q}}_0) \begin{bmatrix} \boldsymbol{\omega}_0 \\ \dot{\mathbf{q}}_m \end{bmatrix} + \mathbf{D}_x^\diamond(\mathbf{q}, \dot{\mathbf{q}}, \dot{\mathbf{q}}_0)\mathbf{x}_e + \mathbf{D}_r^\diamond(\mathbf{q}, \dot{\mathbf{q}}, \dot{\mathbf{q}}_0)\dot{\mathbf{q}}_r \right) \quad (3.63)$$

with  $\mathbf{J}_\tau^{\diamond+}$  the pseudo-inverse of  $\mathbf{J}_\tau^\diamond$ . One will note that  $\mathbf{J}_\tau^{\diamond+}$  is always well-conditioned as the reaction-wheels' inertia matrix remains constant (i.e.  $\mathbf{H}_r$ ).

Injecting (3.63) in (3.59) the closed-loop control dynamics is expressed in function of the observer error dynamics (3.32) as:

$$\ddot{\boldsymbol{\epsilon}}_c = -\mathbf{K} \begin{bmatrix} \boldsymbol{\epsilon}_c \\ \dot{\boldsymbol{\epsilon}}_c \end{bmatrix} + \mathbf{M}_{\omega m}^{\diamond-1} \mathbf{D}_x^\diamond \boldsymbol{\epsilon}_e \quad (3.64)$$

Introducing the state vector  $\mathbf{z} = [\boldsymbol{\epsilon}_c^T \quad \dot{\boldsymbol{\epsilon}}_c^T]^T$ , one can re-write (3.64) as:

$$\begin{cases} \dot{\mathbf{z}} = \left( \begin{bmatrix} 0 & \mathbf{I} \\ 0 & 0 \end{bmatrix} + \begin{bmatrix} 0 \\ -\mathbf{I} \end{bmatrix} \mathbf{K} \right) \mathbf{z} + \begin{bmatrix} \mathbf{0} \\ \mathbf{M}_{\omega m}^{\diamond-1} \mathbf{D}_x^\diamond \end{bmatrix} \boldsymbol{\epsilon}_e \\ \boldsymbol{\epsilon}_c = [\mathbf{I} \quad \mathbf{0}] \mathbf{z} = \mathbf{C}_z \mathbf{z} \end{cases} \quad (3.65a)$$

$$\begin{cases} \dot{\mathbf{z}} = (\mathbf{A}_z + \mathbf{B}_z \mathbf{K}) \mathbf{z} + \mathbf{B}_\epsilon(\mathbf{q}, \dot{\mathbf{q}}, \dot{\mathbf{q}}_0) \boldsymbol{\epsilon}_e \\ \boldsymbol{\epsilon}_c = [\mathbf{I} \quad \mathbf{0}] \mathbf{z} = \mathbf{C}_z \mathbf{z} \end{cases} \quad (3.65b)$$

Therefore, the closed-loop of the base/manipulator controlled system is expressed as the joint-space closed-loop system (3.40). Advantageously, the formalism to obtain the closed-loop system allows to re-use the similar gains synthesis established in 3.3.3 where only the matrix  $\mathbf{B}_\epsilon(\mathbf{q}, \dot{\mathbf{q}}, \dot{\mathbf{q}}_0)$  differs.

### 3.5 Illustration of the proposed methods

In order to illustrate the interest of the proposed method and its utilization, a simple SMS is used in this section. To consider a realistic illustrative example, a reduced version of the manipulator used in the PULSAR telescope deployment (<https://www.h2020-pulsar.eu>) is used. It consists of a 5-DoFs manipulator with a first prismatic joint and four revolute joints. The base is actuated by four reaction-wheels with similar capacities. Two identical solar arrays are disposed on both sides such that 10 total flexible modes are responsible of vibrations. Inertia, sizes and other physical parameters are detailed in appendix B and the significant parameters are gathered in the following table 3.2.



-	Mass (kg)	Inertia ( $kg.m^2$ )	CoM (m)
Base	1960	diag(3345,2202,2202)	[0.9 0 0]
Payload	1440	diag(2458,1499,1499)	[0.55 0 0]
Solar array $\times 2$	61	-	[0.001 0.001 3.845]
Reaction-wheel $\times 4$	4	diag(0.065,0.065,0.1322)	[0 0 0]
link 1	235	diag(0.065,0.065,0.1322)	[0 0 0]
link 2	7	diag(0.021,0.021,0.01)	[0 0 0.09]
link 3	27	diag(51,0.15,51)	[0 0 0.09]
link 4	7	diag(0.021,0.01,0.021)	[0 0 0]
link 5	18	diag(0.14,15.7,15.7)	[0 0 0]
End-effector	150	diag(6,6,6)	[0 0 0]

Table 3.2 – Detail of the SMS' physical properties

and for the two identical flexible arrays the same 5 modes are considered and detailed in table 3.3.

-	pulse (rad/s)	damping	$\mathbf{L}_{P_{f_i}}$
mode 1	$0,16*2*\pi$	0.005	[-6.4 0 0 0 -35 0]
mode 2	$0,70*2*\pi$	0.005	[0 -6.7 0 35.4 0 0]
mode 3	$1.08*2*\pi$	0.005	[-0.1 -0.1 0 0.3 0 3.8]
mode 4	$1.21*2*\pi$	0.005	[-3.2 0 0 0 -3 -0.01]
mode 5	$3.05*2*\pi$	0.005	[2.3 0 -0.3 0 1.3 0]

Table 3.3 – Flexible modes' physical properties

This section is then divided in two parts. A first analysis and method of the gains synthesis and the interest of the control structure in which an ESO is included in the NDI are realized for the joint control approach (i.e. section 3.3). Secondly, the benefits of such structure and its adaptability to a "task" space control introduced in section 3.4 are discussed with time-domain simulations.

### 3.5.1 Joint control results

#### 3.5.1.1 Gains synthesis

The gains synthesis is developed such that the closed-loop system remains stable during a complete task. While the manipulator operates, an evolution of the inertia and convective terms may be significant to impose multiple constraints as (3.42a) in the LMI resolution (3.3.3.1). In order to avoid discussion on the choice of equilibrium points for additional LMI constraints, relaxation terms have been employed such that (3.51). After establishing a manipulator maneuver with path-planning methods and singularity-free approaches that

are not developed in this work, the relaxation terms can be evaluated. Their evaluation requires joint position and velocities to develop the direct dynamics of the SMS. To tackle the variations during the maneuver, a sequencing in  $n_{seq}$  sub-motions of the complete task is made. Thus, according to the manipulator's configuration and velocities the gains ensure the dealing with the largest variations. The detail of the design procedure is given by the following algorithm:

---

**Algorithm 1** Design procedure for an on-orbit servicing task
 

---

Define the LMI variables,  $\mathbf{Q}_z$ ,  $\mathbf{P}_\epsilon$ ,  $\mathbf{W}_z$  and  $\mathbf{W}_\epsilon$ , as in the proposition in section 3.3.3.1  
 Define an equilibrium point to evaluate matrices,  $\mathbf{A}_\epsilon$  and  $\mathbf{B}_\epsilon$ , in the LMI constraint (3.42a) from system's equation of motions (3.35)

**for**  $i \leq n_{seq}$  **do**

    For  $\mathbf{q}_i$  and  $\dot{\mathbf{q}}_i$  evaluate matrices in (3.28) and (3.35)

    Evaluate singular values  $\sigma_{\mathbf{A}_\epsilon}^i = \bar{\sigma}(\mathbf{A}_\epsilon)$  and  $\sigma_{\mathbf{B}_\epsilon}^i = \bar{\sigma}(\mathbf{B}_\epsilon)$

**end for**

Evaluate relaxation terms  $\rho_1 = 2\max([\sigma_{\mathbf{A}_\epsilon}^1 \ \dots \ \sigma_{\mathbf{A}_\epsilon}^{n_{seq}}])$  and  $\rho_2 = \max([\sigma_{\mathbf{B}_\epsilon}^1 \ \dots \ \sigma_{\mathbf{B}_\epsilon}^{n_{seq}}])$  such as (3.51)

Establish the LMI constraint  $\Omega$  as in (3.52)

Minimize the LMI variable  $\gamma > 0$  such that  $\Omega < 0$

**Return**  $\mathbf{K}$ ,  $\mathbf{L}$

---

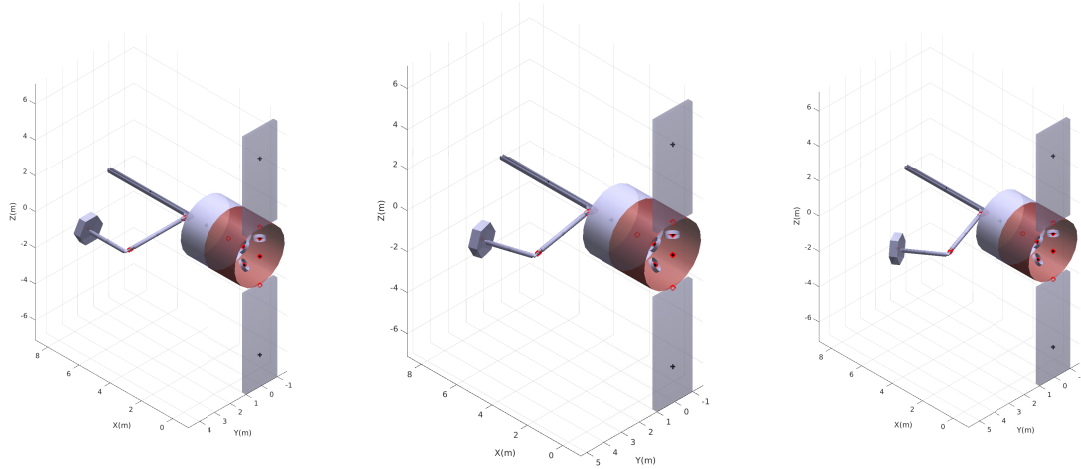


Figure 3.11 – Illustration of the SMS task: the initial configuration (left), the mid-task configuration (middle) and the final configuration (right)

Considering the task illustrated with Figure 3.11, in the pre-analysis process one can visualize the variation during the system's motions with Figure 3.12. As the relaxation term  $\rho_1$  reaches significant values, one can first highlight the interest of considering relaxation terms to avoid multiple LMI constraints. Furthermore,  $\rho_2$  corresponds to the level of control degradation from the observer error. With the lower subplot of Figure 3.12, one will note

that regarding the system's evolution, the impact of low observer error should not affect the control performances.

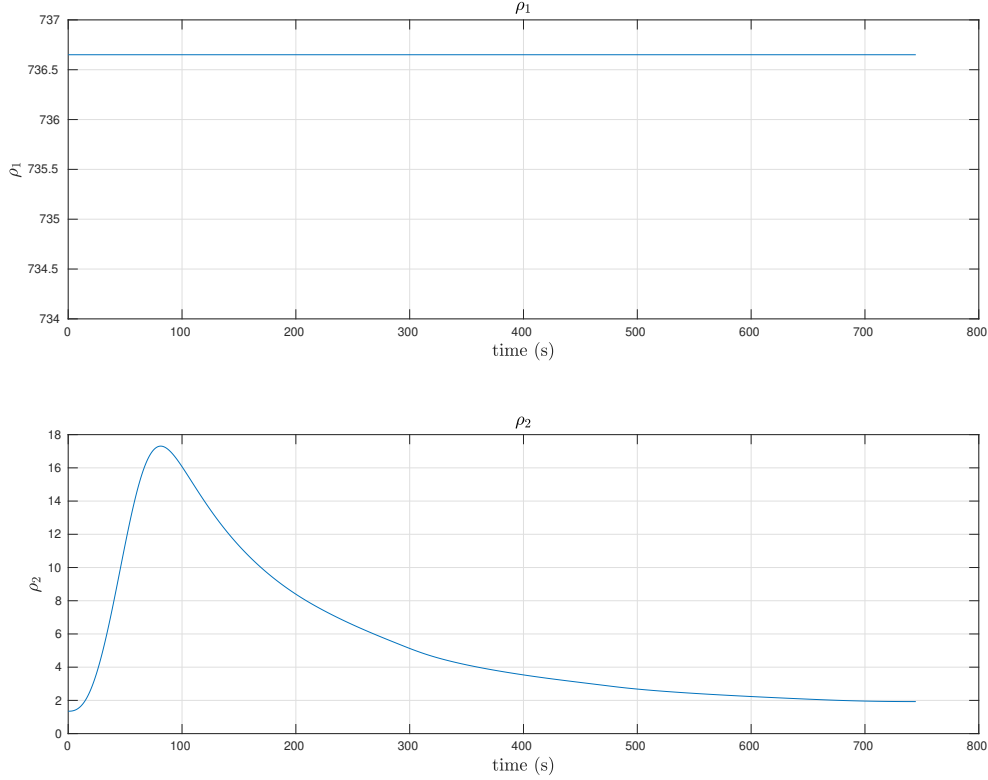


Figure 3.12 – Evolution of system variation for a given task, upper subplot represents the evolution of the relaxation term  $\rho_1$  and the lower subplot represents  $\rho_2$ 's evolution

In order to solve the proposition in 3.3.3.1 and the LMI constraints, the YALMIP toolbox [Lof04] is used with the MOSEK solver. This allows to reduce the computation time when multiple large LMI dimension constraints are considered. In the present case, LMI variables  $\mathbf{Q}_z$  is a  $18 \times 18$  square matrix and  $\mathbf{P}_\epsilon$  a  $26 \times 26$  square matrix. Moreover, with actuators decoupling, the control gains can be decomposed as  $\mathbf{K} = \begin{bmatrix} \mathbf{K}_p & \mathbf{K}_v \end{bmatrix}$  with  $\mathbf{K}_p$  and  $\mathbf{K}_v$  two diagonal matrices.

Moreover, a discussion on the different actuators' dynamics can be developed. Reaction-wheels present slower dynamics than manipulator's joints. The proposed gains synthesis as detailed in algorithm 1 does not consider these difference of dynamics or saturation thresholds. In order to introduce such considerations, after a pre-analysis of matrices  $\mathbf{A}_e$  and  $\mathbf{B}_e$ , additional constraints on the control gains  $\mathbf{K}_p$  and  $\mathbf{K}_v$  can be defined. Such constraints are developed on the LMI variable  $\mathbf{Q}_z$  which can be imposed as a diagonal matrix thanks to the decoupled system. Furthermore, distinguishing reaction-wheels to manipulator's joints in  $\mathbf{Q}_z$ , an upper-bound limit can be defined to avoid actuator's saturation thresholds. Such addi-

tional constraints are proper to the studied SMS and are tuned with trial and error approach, it remains difficult to develop a general formalism.

### 3.5.1.2 Simulation results

From path-planning methods, manipulator motions (i.e. joint angular pose and velocities) are provided with the PULSAR application (<https://www.h2020-pulsar.eu>) to perform a given task. As it is usual to maintain the spacecraft base with a fixed attitude, reaction-wheels velocities are deduced from the manipulator's with a momentum conservation approach. One will note that this hypothesis is not verified with flexible elements but allows to define the desired velocities as:

$$\dot{\mathbf{q}}_{r_d} = -\mathbf{H}_{0r}^+ (\mathbf{H}_{0m} \dot{\mathbf{q}}_{m_d} + \mathbf{H}_0 \dot{\mathbf{q}}_0) = -\mathbf{H}_{0r}^+ \mathbf{H}_{0m} \dot{\mathbf{q}}_{m_d} \quad (3.66)$$

with initially non-null reaction-wheels' velocities such that no base rotation occurs during manipulator motions.

Figures 3.13 and 3.14 illustrate control performances. With upper subplots in both figure, the measured velocities are represented. In order to visualize and quantify the control performances, for each actuators a relative tracking error signal is plotted in the respective lower subplot of manipulator and reaction-wheels figures. This signal is defined as:

$$\dot{\epsilon}_{tc}(\dot{q}_i) = \frac{(\dot{q}_{d_i} - \dot{q}_i)}{\max(\dot{q}_i)} \quad (3.67)$$

One can conclude on the efficiency of the proposed method considering this relative error signal remains under  $10^{-3}$ .

Considering the detail of the computed torque (3.38) given in Figure 3.15, the interest of the control method can be illustrated. The control torques can be decomposed into three signals. The first one is the feedback control torque ( $\mathbf{M}^\diamond \mathbf{v}$ ), visualized in the upper subplot in Figure 3.15. The second, ( $\mathbf{D}^\diamond \dot{\mathbf{q}}$ ), defined as the feedback linearizing torque, visualized in the second subplot of Figure 3.15. The last one, ( $\mathbf{D}_x^\diamond \mathbf{x}_e$ ), is the intern disturbance torque that appears in the lower plot in Figure 3.15. The intern disturbance torque is composed of unmeasured states and included in the system linearization thanks to the observer developed in section 3.3.1. With an amplitude comparison of the three signals composing the computed torque, one can conclude on their interests in the NDI. Regarding the low velocities involved in this illustrative example and with reaction-wheels used to maintain the base fixed, a comparison of the feedback linearizing torques and intern disturbances one is relevant to conclude on the control strategy. As these two signals present similar amplitudes, including an estimation of unmeasured states (i.e. flexible dynamics and linear base velocities) in the computed torque it allows to improve the decoupling quality. However, as physical properties of the flexible modes may be significantly different from one appendage to another, the vibrations could be difficult to properly be estimated. More precisely, the LMI resolution

does not easily provide the possibility of frequency analysis. This leads to not focusing on the observation quality in this control approach. However, the synthesis ensures stability for a bounded observer error which is also guaranteed by the gains synthesis for a given motion. Thus, estimating amplitudes of the fastest unmeasured states is sufficient to adequately linearize and decouple the considered system.

A second interest of the proposed method is illustrated with Figure 3.16 in which the base angular velocities are visualized in the upper subplot and the flexible mode velocities are represented in the lower plot. As the reaction-wheels are employed to maintain a null base angular velocity, the flexible modes are only excited with the indirect couplings between the manipulator motions and the flexible dynamics through the base motions. As one can notice with the lower subplot in Figure 3.16, when the manipulator presents constant velocities, the flexible modes vibrations are dumped. Using the reaction-wheels to maintain a fixed base, and including the intern disturbance in the computed torque allows to adapt reaction-wheels usage to reject these un-controllable and un-measurable states.

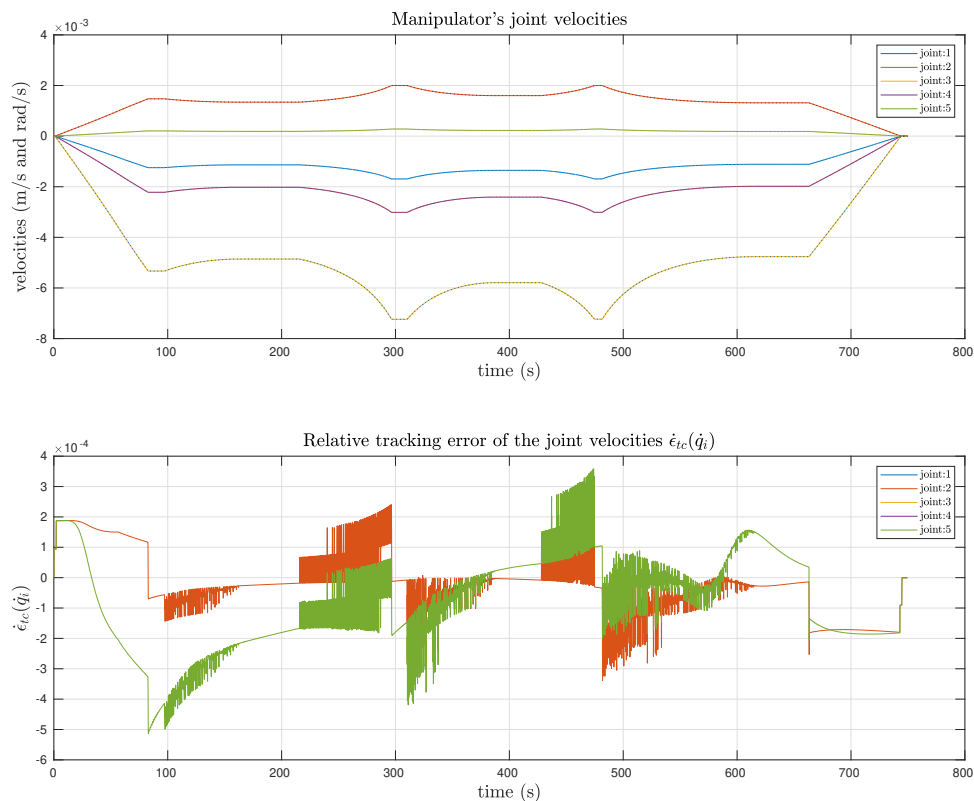


Figure 3.13 – Manipulator's joints measured velocities and control performances; upper subplot is the measured manipulator's joint velocities and lower subplot is the relative tracking error

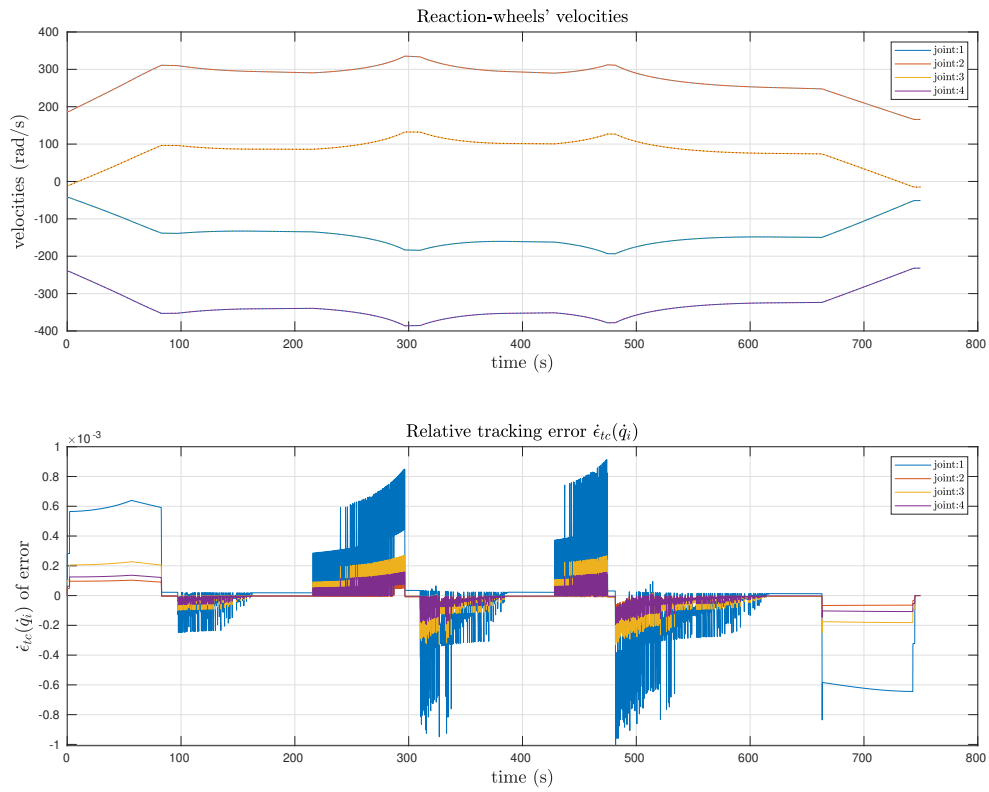


Figure 3.14 – Reaction-wheels measured velocities and control performances; upper subplot is the reaction-wheels' joint velocities and lower subplot is the relative tracking error

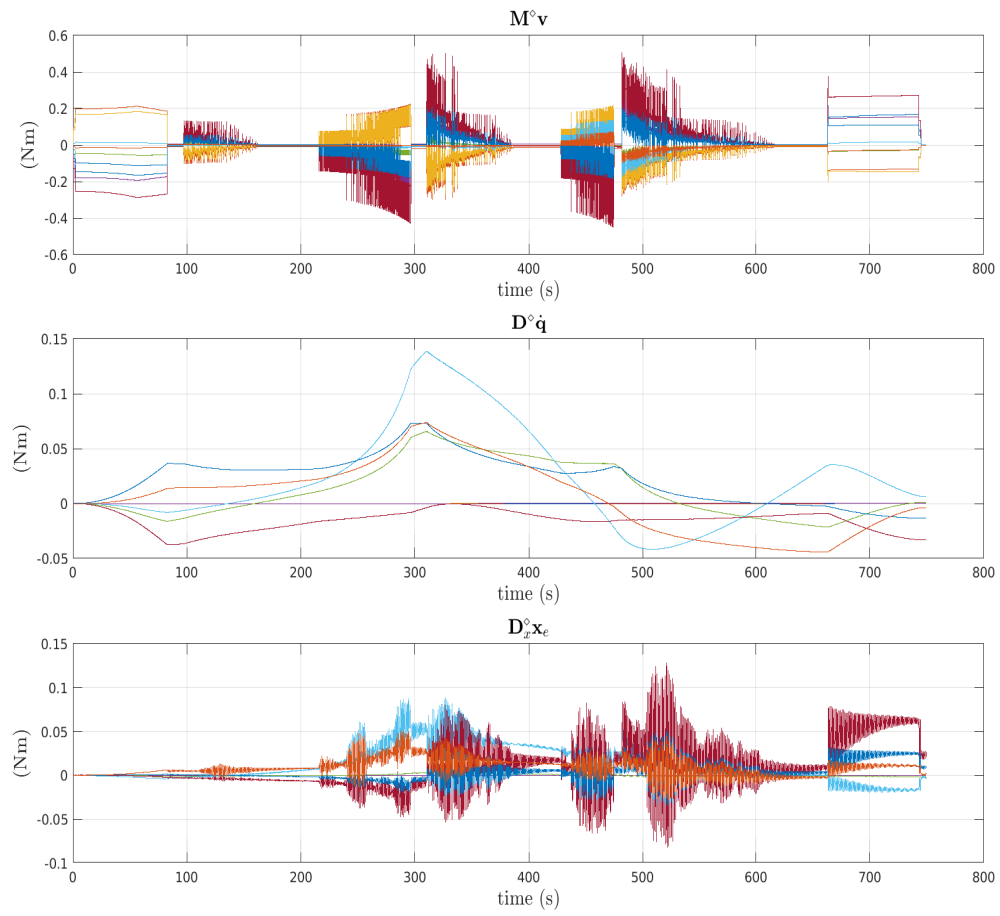


Figure 3.15 – Detail of the computed torque (3.38) highlighting interests of including un-measured states in the NDI

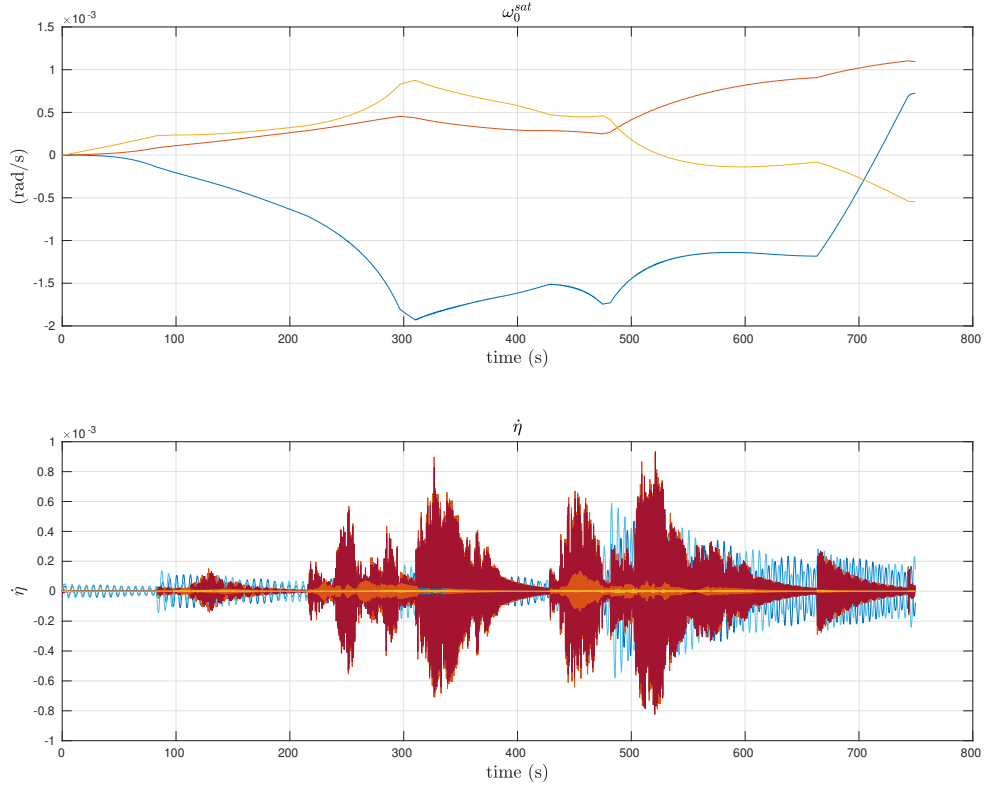


Figure 3.16 – Upper subplot represents base angular velocities; Lower subplot represents the flexible vibration  $\dot{\eta}$

### 3.5.2 Interest of a base-manipulator common control strategy

With a base-manipulator control, besides providing a larger manipulability, the rejection of disturbances can be better illustrated with the NDI/ESO control structure. Considering the same manipulator motion to illustrate the joint-space control, a comparison of the results obtained with similar control objectives are considered in this section.

With a first comparison of manipulator's control performances visualized in Figures 3.13 and 3.17, one can note similar results. This allows to focus on the base and flexible dynamics to better illustrate disturbance rejections obtained with the computed torque (3.63). With the second subplot in Figure 3.18, one easily verifies that the base is successfully maintained at a fixed attitude during the manipulator maneuver. This corresponds to relatively similar reaction-wheels' velocities that the desired ones in the previous joint-space control. As the base is less rotating, the flexible appendages are less affected by the manipulator as illustrated by the lower subplot in Figure 3.18 but are still excited when joints' velocities are changing. Capitalizing on the reaction-wheels' constant inertia matrices ( $\mathbf{H}_{0r}$  and  $\mathbf{H}_r$ ), detailing the computed torque (3.18) controlling the four reaction-wheels allows to obtain information



on the linearization/decoupling of the system. One defines the four following signals: the feedback control torque ( $\mathbf{J}_\tau^{\diamond+} \mathbf{M}_{\omega m}^\diamond \mathbf{v}$ ), the feedback linearizing torque ( $\mathbf{J}_\tau^{\diamond+} \mathbf{D}_{\omega m}^\diamond \begin{bmatrix} \boldsymbol{\omega}_0 \\ \dot{\mathbf{q}}_m \end{bmatrix}$ ), the measured reaction-wheels linearizing torque ( $\mathbf{J}_\tau^{\diamond+} \mathbf{D}_r^\diamond \dot{\mathbf{q}}_r$ ) and the intern disturbance torque ( $\mathbf{J}_\tau^{\diamond+} \mathbf{D}_x^\diamond \mathbf{x}_e$ ). With Figure 3.19, each signals are detailed to highlight their role in the reaction-wheels control maintaining the base with a null angular velocity. Regarding amplitudes of each signals, one can note that the intern disturbance torques, visualized in the third subplot of Figure 3.19, have nearly similar importance than the feedback linearizing torques, visualized in the second subplot of Figure 3.19. Thus, including an estimation of the unmeasured states in (2.69) allows to properly decouple the system and linearize it as well as using the reaction-wheels as mean of rejection to base disturbances.

Additionally, maintaining the base fixed allows to limit the dissipation in the overall system due to flexible appendages. As illustrated with Figure 3.20 and comparing with Figure 3.5 allows to highlight this observation.

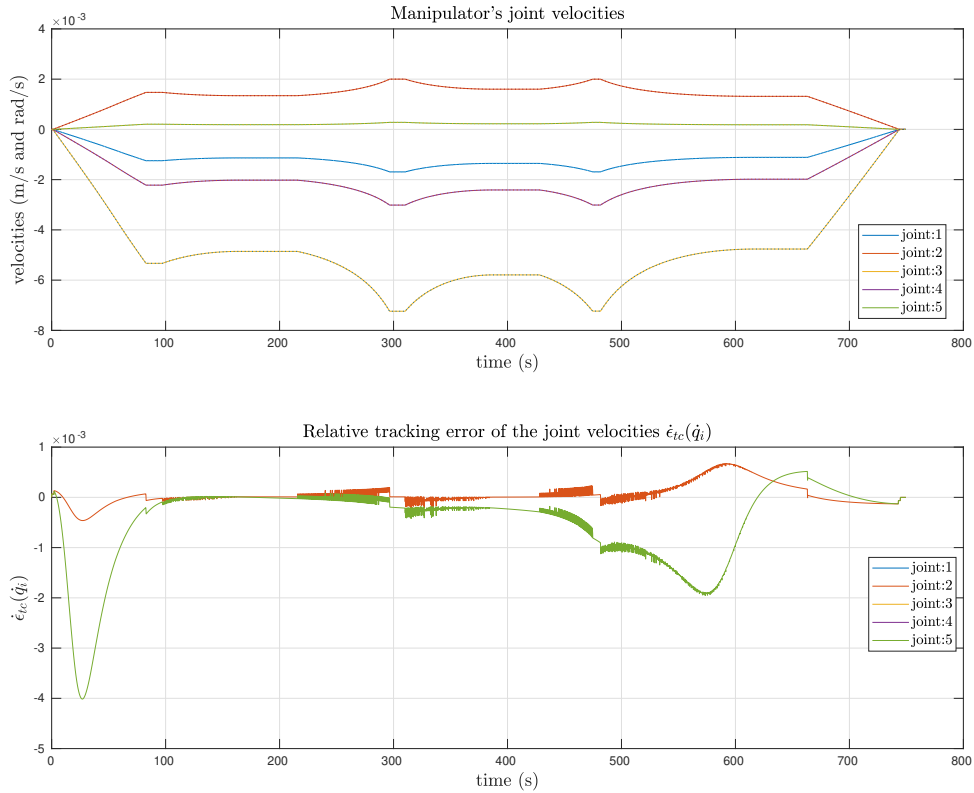


Figure 3.17 – Manipulator's joints measured velocities and control performances; upper subplot is the measured manipulator's joint velocities and lower subplot is the relative tracking error

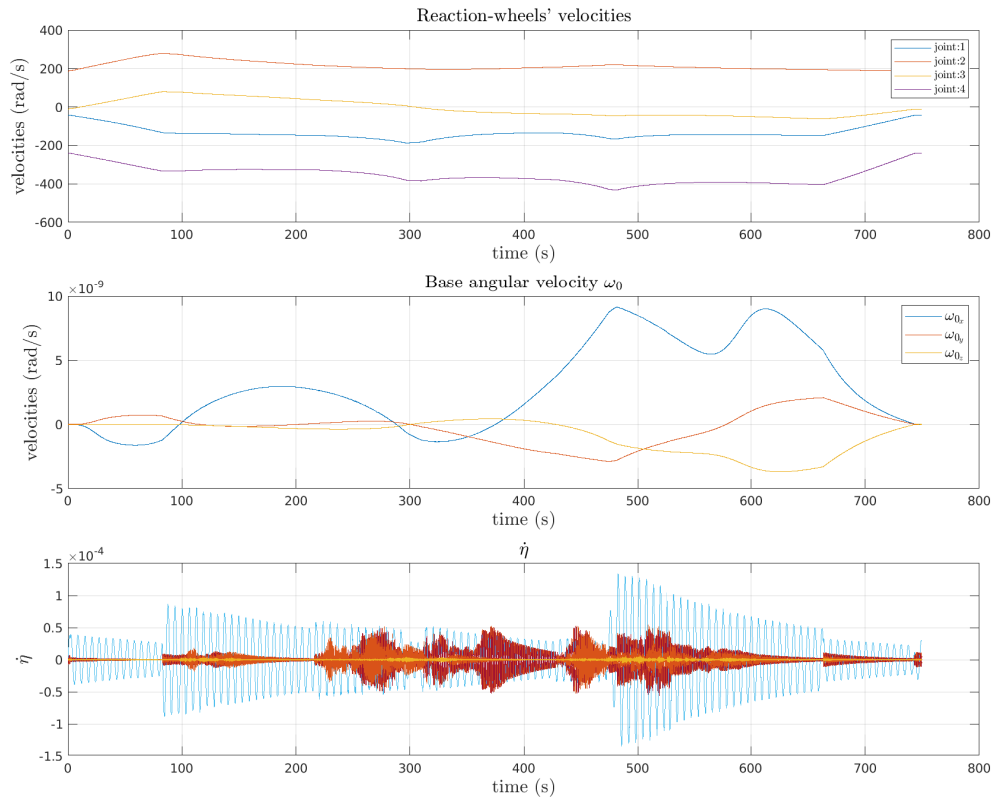


Figure 3.18 – Upper subplot is the measured reaction-wheels' joint velocities second subplot represents the base angular velocity and lower subplot is the flexible modes velocities

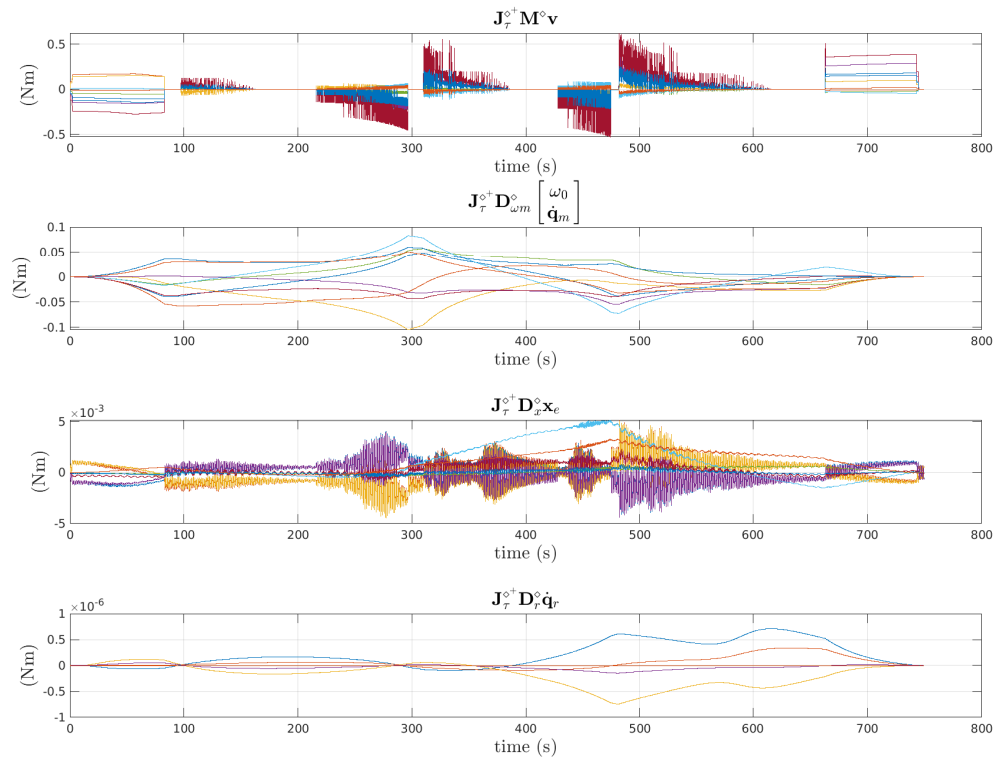


Figure 3.19 – Detail of the computed torques (3.63) for the four reaction-wheels

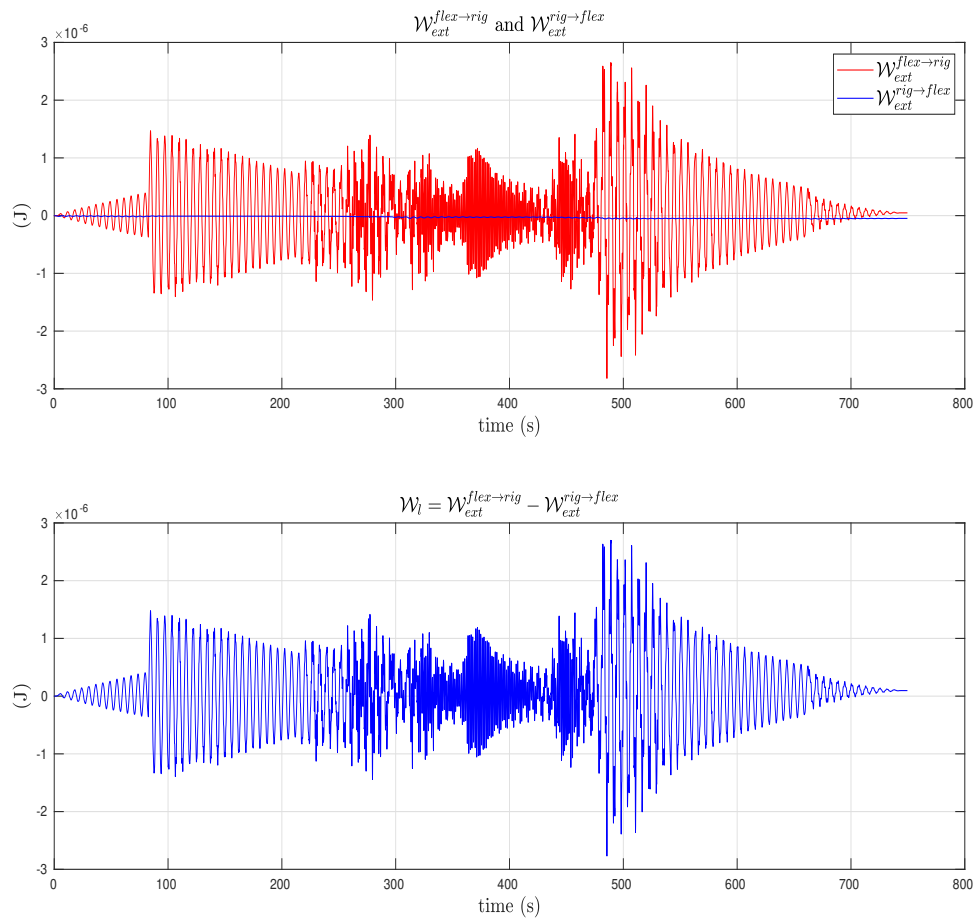


Figure 3.20 – Dissipated work (2.83) during the complete motion

### 3.6 Chapter conclusions

In this chapter, the modeling developed in chapter 2 and the analysis/simulation tools have been used to introduce novel control strategies. After a first review of the literature to identify possible improvement areas to control SMS, a main concern was raised with the presence of flexible appendages.

Considering rotation-free-floating SMS, discussions on the benefits of simultaneously controlling the base actuators and the manipulator have been developed. With the introduction of new kinetic indices, a quantitative analysis can be developed to both justify the common control and developed adapted motions. In addition, these indices are suitable for designing an SMS and justifying the placement and number of actuators.

Motivated by the conclusions resulting of the kinetic indices use, a common base and

manipulator joint control law has been introduced to perform precise SMS control in presence of internal disturbance mainly due to the flexible vibrations and the spacecraft's drift. This control strategy is based on an NDI that capitalizes on the modeling effort developed in the previous chapter. Thanks to the modeling of the flexible dynamics, an ESO is established to improve the NDI quality and thus the decoupling of actuators. Both joint-space and base-manipulator control have been developed under a similar formalism to illustrate the advantages of such control scheme.

Another contribution lies in the gains synthesis that is simultaneously performed through an LMI resolution problem. It is based on a Lyapunov stability analysis, the resolution ensure control performances for a given task. It precisely requires a manipulator path with joints velocities to evaluate relaxation terms introduced to reduce the number of LMI constraints.

With time-domain simulations effectuated on a simple SMS, the interest of such control scheme has been attested. Therefore, this chapter introduces a formalism to establish a control of an SMS in presence of flexible appendages. However, improvements are required to be implemented on actual systems. For that purpose, in the next chapter the focus is made on presenting a robust control strategy based on the one presented in this chapter. Modeling uncertainties, measurement errors, notable system variations are considered to perform various tasks precisely and safely.

The control schemes and the gains synthesis presented in this chapter have been extended from published works in [Kra+21a] and [Kra+21b]. One will find in [Kra+21a] the base-manipulator control scheme with a similar ESO and control gains synthesis. Then in [Kra+21b] one will find an extension of the control framework for a joint-space control of the SMS. Moreover, additional robust criteria are introduced in the simultaneous gains synthesis. This last work allows to introduce the control remaining difficulties and a first approach to consider significant system variations.

# Robust joint-space control for a space manipulator system in presence of flexible appendages

---

## Sommaire

---

<b>4.1 Robust control challenges</b>	<b>118</b>
4.1.1 Area of improvement	118
4.1.2 Limits of the control introduced in chapter 3	119
<b>4.2 Control strategy</b>	<b>120</b>
4.2.1 Joint open-loop behavior	121
4.2.2 State Observer model	123
4.2.3 Nonlinear Disturbance Observer model	124
4.2.4 Closed-loop dynamics	125
4.2.5 Simultaneous gains synthesis	127
<b>4.3 Illustration of the proposed method</b>	<b>133</b>
4.3.1 Study case	133
4.3.2 Simulations results	140
<b>4.4 Chapter conclusions</b>	<b>164</b>

---

In the previous chapter, the motivations to perform common base and manipulator control of rotation-free-floating SMS<sup>1</sup> with flexible appendages have been introduced and its benefits have been widely discussed. However, to face actual control difficulties robust criteria must be added in the control scheme. With the modeling derivation detailed in chapter 2, uncertainties on physical parameters may be taken into account in the gains synthesis. Thus, for modeling and measurement errors an NDO<sup>2</sup> is introduced and included in the system linearization. A similar gains synthesis as the one proposed in chapter 3 is developed based on a stability analysis and performed through an LMI<sup>3</sup> resolution. Moreover, one advantage offered by an SMS is the possibility of performing different OOS<sup>4</sup> missions. Then, an additional objective in the gains synthesis focus on the system variations corresponding to different OOS tasks.

---

<sup>1</sup>Space Manipulator System

<sup>2</sup>Nonlinear Disturbance Observer

<sup>3</sup>Linear Matrix Inequality

<sup>4</sup>On-Orbit Servicing

To summarize this chapter, the control strategy introduced in the previous one is extended to answer current OOS problems with an additional observer and a new gains synthesis. Then the approach is validated in a realistic environment with extensive tests on an on-orbit space telescope assembly use-case performed on the simulation tools detailed in chapter 2.

## 4.1 Robust control challenges

### 4.1.1 Area of improvement

As the first difficulty of controlling an SMS resides in the couplings between each bodies, robust control strategies have been focusing on rejecting the coupling effects. Such approaches have mainly been developed for capturing targets as they may present large and unknown disturbance on the manipulator's end-effector and thus an important momentum variation. Besides developing an impedance control strategy [Yos+04]; [NY06] or focusing on a path-planning method [HW18]; [Zha+20] to reduce the capture impact, robust control schemes have been proposed to deal with the impact and the post-capture of a target. Dong and al. [DC14] established a robust adaptive compound control algorithm to suppress the motions that destabilize the robotic system after the capture. However, their method based on a momentum conservation requires strong assumptions to verify the modeling of the system composed of the free-floating SMS and the target that they proposed.

Capture scenarios also highlight the problems due to an incorrect or a poor modeling. Adaptive control methods have been providing interesting features to deal with the capture of an unknown target. Nguyen and al. [NHS11] proposed an adaptive control to stabilize a captured target with a reaction-less motion of the chaser's base. Furthermore, the estimation of the system physical properties (i.e. mass, dimensions, CoM<sup>5</sup>) remains challenging. Model uncertainties have been one motivation of introducing robust strategies for SMS control. Luo and al. [Luo+18] proposed a robust inertia-free attitude to detumble a spacecraft without inertial property and subject to external disturbance. Similarly in the detumbling procedure, Gangapersaud and al. [GLR19] considered a force control to avoid identifying the target's inertia parameters. Aghili and al. [Agh20] have developed an optimal detumbling control strategy to cancel the momentum dissipation of the grasped non-cooperative target with forces/torques limitations. Dubanchet and al. [Dub+15] established a fixed-structure  $H_\infty$  synthesis to separately control the manipulator and base to extend the work of Aghili and al. [Agh09b] and optimally capture a tumbling satellite.

The presence of external disturbances is another source of motivation for robust controls. The different external perturbations are affecting either directly the manipulator and/or the spacecraft's base or will excite flexible vibrations of the appendages [Cao+20].  $H_\infty$  controllers have been established to deal with external and internal perturbations [FTST06]; [SS19]; [QWY19]. These methods allow to answer different problems or difficulties in SMS control. First the modeling uncertainties of the system [Zha+15] and likewise it avoids the difficult

---

<sup>5</sup>Center of Mass

modeling of a rigid and flexible multi-body system [Col+18].

Furthermore, in the previous chapter the established control law highlights some benefits by controlling both the manipulator and the base simultaneously. The promising results obtained motivate to pursue the effort of improving such design to answer the requirements of current and future OOS operations. Likewise, with the possible complete modeling of rigid-flexible systems, one capitalizes on this to obtain adapted control solutions and efficient use of actuators such that the mission lifespan can be optimized.

#### 4.1.2 Limits of the control introduced in chapter 3

The proposed control scheme established in the previous chapter aimed at introducing the interest of a common base and manipulator control in presence of perturbations inside the system. Nevertheless, one can identify the following necessary improvements to answer actual OOS requirements:

- A primary interest of using SMS to proceed to OOS missions is the possibility of performing a multi-task mission [FA+14]. In that purpose the proposed gains synthesis requires adjustments to consider different mass distribution and end-effector motions.
- With a similar objective, the actual synthesis is based on a well-known manipulator task. Such synthesis is restrictive to a particular task, requiring a precise path and motions' velocities. Therefore, extending the synthesis to a given workspace could be a significant improvement of the method.
- A second weakness of the proposed method is on the modeling assumptions to perform the system linearization and designing of the observer. Developing accurate kinematic/-dynamic models remains challenging especially when integrating the flexible behaviors onto the overall system equations of motions. Thus, in order to deal with modeling uncertainties the control scheme requires other adaptations.
- Additionally to model errors, the quality of measured states should also be discussed. Typically, besides the actuators velocities, the base orientations' measures incorporate some measurement noises.



## 4.2 Control strategy

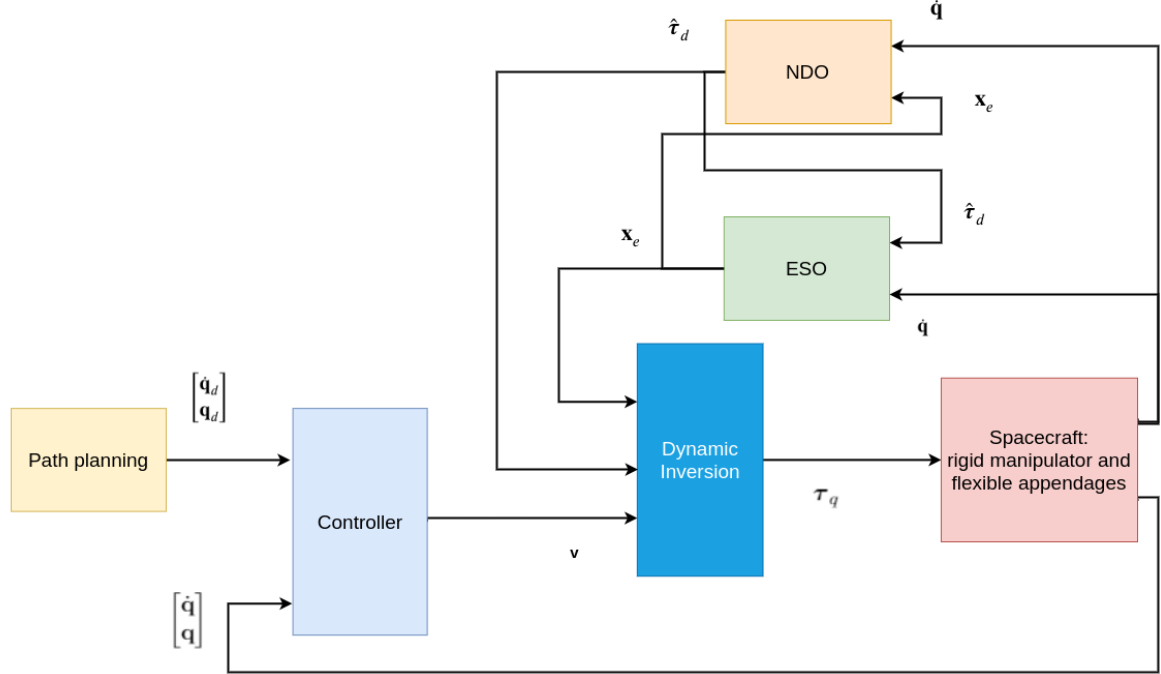


Figure 4.1 – Block diagram of the proposed joint space control method

In this section, a novel control scheme is introduced to bring the different improvements previously enumerated. As illustrated with Figure 4.1, the control law is based on a system dynamic inversion (with an NDI<sup>6</sup>) in which the unmeasured states (i.e. the flexible and linear spacecraft dynamics) are included with an ESO<sup>7</sup> as well as an estimation of a disturbance torque induced by the modeling error with an NDO.

The contribution of this strategy is the introduction of a disturbance torque,  $\tau_d$ , due to both modeling uncertainties and measurement errors. As concluded with the previous control scheme detailed in chapter 3, including un-measured states in the system decoupling allows to both improve its quality and adapt the use of actuators. With the same ambition, an NDO is developed to estimate an additional perturbation torque introduced with the evaluation of the inverse uncertain kinematic/dynamic model. Both observers are designed thanks to the modeling effort developed in chapter 2.

Moreover, the same assumptions as in chapter 3 on the available measurements are made to establish the new control scheme. The actuators' accelerations,  $\ddot{\mathbf{q}}$ , the flexible dynamics,  $\boldsymbol{\eta}$ ,  $\dot{\boldsymbol{\eta}}$  and  $\ddot{\boldsymbol{\eta}}$ , and the SMS base's linear dynamics,  $\dot{\mathbf{r}}_{S_0}$  and  $\ddot{\mathbf{r}}_{S_0}$  are presumed not measured. Therefore, the ESO is designed by slightly adapting the observer proposed in section 3.3.1 to

<sup>6</sup>Nonlinear Dynamic Inversion

<sup>7</sup>Extended State Observer

include the modeling/measurement errors. The NDO is similarly developed with the use of actuators' velocities.

Before developing the open-loop dynamics, notations are introduced in order to consider errors in evaluation of inverse kinematics/dynamics due to modeling uncertainties and measurement errors. A quantity  $\mathbf{X}$  obtained or evaluated from measurement is indicated as  $\hat{\mathbf{X}}$  such that  $\hat{\mathbf{X}} = \mathbf{X} + \Delta\mathbf{X}$  with  $\Delta\mathbf{X}$  representing the difference between the actual value and the measured one. Thus, the system's dynamics (2.69) obtained from the modeled spacecraft can be expressed as:

$$\hat{\mathbf{H}}(\hat{\mathbf{q}}) \begin{bmatrix} \ddot{\mathbf{q}}_0 \\ \ddot{\mathbf{q}} \\ \ddot{\boldsymbol{\eta}} \end{bmatrix} + \hat{\mathbf{C}}(\hat{\mathbf{q}}, \dot{\hat{\mathbf{q}}}, \dot{\hat{\mathbf{q}}}_0) \begin{bmatrix} \dot{\mathbf{q}}_0 \\ \dot{\mathbf{q}} \\ \dot{\boldsymbol{\eta}} \end{bmatrix} + \hat{\mathbf{K}} \begin{bmatrix} \mathbf{q}_0 \\ \mathbf{q} \\ \boldsymbol{\eta} \end{bmatrix} = \begin{bmatrix} \mathbf{0}_{6 \times 1} \\ \boldsymbol{\tau}_q \\ \mathbf{0}_{n_\eta \times 1} \end{bmatrix} - \begin{bmatrix} \boldsymbol{\tau}_{\Delta_1}(\hat{\mathbf{q}}, \dot{\hat{\mathbf{q}}}, \dot{\hat{\mathbf{q}}}_0) \\ \boldsymbol{\tau}_{\Delta_2}(\hat{\mathbf{q}}, \dot{\hat{\mathbf{q}}}, \dot{\hat{\mathbf{q}}}_0) \\ \boldsymbol{\tau}_{\Delta_3}(\hat{\mathbf{q}}, \dot{\hat{\mathbf{q}}}, \dot{\hat{\mathbf{q}}}_0) \end{bmatrix} \quad (4.1)$$

with the following hypothesis:

- the terms  $\Delta\mathbf{x}\Delta\mathbf{y}$  are neglected,
- the base linear velocity is estimated by the state observer detailed in section 4.2.2 such that  $\dot{\hat{\mathbf{q}}}_0 = \begin{bmatrix} \hat{\boldsymbol{\omega}}_0^{satT} & \hat{\mathbf{r}}_{0e}^T \end{bmatrix}^T$ ,
- measurements of actuators position and velocities are considered good enough to assume  $\hat{\mathbf{q}} = \mathbf{q}$  and  $\dot{\hat{\mathbf{q}}} = \dot{\mathbf{q}}$

Modeling and measurement errors are then gathered in a disturbance torque defined as:

$$\boldsymbol{\tau}_\Delta(\hat{\mathbf{q}}, \dot{\hat{\mathbf{q}}}, \dot{\hat{\mathbf{q}}}_0) = \begin{bmatrix} \boldsymbol{\tau}_{\Delta_1}(\hat{\mathbf{q}}, \dot{\hat{\mathbf{q}}}, \dot{\hat{\mathbf{q}}}_0) \\ \boldsymbol{\tau}_{\Delta_2}(\hat{\mathbf{q}}, \dot{\hat{\mathbf{q}}}, \dot{\hat{\mathbf{q}}}_0) \\ \boldsymbol{\tau}_{\Delta_3}(\hat{\mathbf{q}}, \dot{\hat{\mathbf{q}}}, \dot{\hat{\mathbf{q}}}_0) \end{bmatrix} = \Delta\mathbf{H} \begin{bmatrix} \ddot{\mathbf{q}}_0 \\ \ddot{\mathbf{q}} \\ \ddot{\boldsymbol{\eta}} \end{bmatrix} + \Delta\mathbf{C} \begin{bmatrix} \dot{\mathbf{q}}_0 \\ \dot{\mathbf{q}} \\ \dot{\boldsymbol{\eta}} \end{bmatrix} + \Delta\mathbf{K} \begin{bmatrix} \mathbf{q}_0 \\ \mathbf{q} \\ \boldsymbol{\eta} \end{bmatrix} \quad (4.2)$$

$$- \hat{\mathbf{H}}(\mathbf{q})\Delta \begin{bmatrix} \ddot{\mathbf{q}}_0 \\ \ddot{\mathbf{q}} \\ \ddot{\boldsymbol{\eta}} \end{bmatrix} - \hat{\mathbf{C}}(\hat{\mathbf{q}}, \dot{\hat{\mathbf{q}}}, \dot{\hat{\mathbf{q}}}_0)\Delta \begin{bmatrix} \dot{\mathbf{q}}_0 \\ \dot{\mathbf{q}} \\ \dot{\boldsymbol{\eta}} \end{bmatrix} - \hat{\mathbf{K}}\Delta \begin{bmatrix} \mathbf{q}_0 \\ \mathbf{q} \\ \boldsymbol{\eta} \end{bmatrix}$$

#### 4.2.1 Joint open-loop behavior

In order to establish a joint-space control, a rewriting effort of the full system dynamic followed by the modeled manipulator (4.1) is required. This effort aims at expressing the joints' dynamics in function of either measurable states or quantities that can be estimated with the observers detailed in sections 4.2.2 and 4.2.3. First, with (4.1) actuators' dynamics are expressed as:

$$\hat{\mathbf{H}}_q \ddot{\mathbf{q}} + \hat{\mathbf{C}}_q \dot{\mathbf{q}} = - \begin{bmatrix} \hat{\mathbf{H}}_{0q}^T & \mathbf{0} \end{bmatrix} \begin{bmatrix} \ddot{\mathbf{q}}_0 \\ \ddot{\boldsymbol{\eta}} \end{bmatrix} - \begin{bmatrix} \mathbf{0} & \hat{\mathbf{C}}_{q0} & \mathbf{0} \end{bmatrix} \begin{bmatrix} \dot{\boldsymbol{\eta}} \\ \dot{\mathbf{q}}_0 \\ \dot{\mathbf{q}} \end{bmatrix} + \boldsymbol{\tau}_{\Delta_2} + \boldsymbol{\tau}_q \quad (4.3)$$

Secondly, from (4.1), the unmeasured states are isolated as:

$$\begin{bmatrix} \hat{\mathbf{H}}_0 & \hat{\mathbf{H}}_{0\eta} \\ \hat{\mathbf{H}}_{0\eta}^T & \hat{\mathbf{H}}_\eta \end{bmatrix} \begin{bmatrix} \ddot{\mathbf{q}}_0 \\ \ddot{\boldsymbol{\eta}} \end{bmatrix} + \begin{bmatrix} \hat{\mathbf{H}}_{0q} \\ \mathbf{0} \end{bmatrix} \ddot{\mathbf{q}} + \begin{bmatrix} \mathbf{0} & \hat{\mathbf{C}}_0 & \hat{\mathbf{C}}_{0\eta} \\ \hat{\mathbf{K}}_\eta & \hat{\mathbf{C}}_{\eta 0} & \hat{\mathbf{C}}_\eta \end{bmatrix} \begin{bmatrix} \eta \\ \dot{\mathbf{q}}_0 \\ \dot{\boldsymbol{\eta}} \end{bmatrix} + \begin{bmatrix} \hat{\mathbf{C}}_{0q} \\ \mathbf{0} \end{bmatrix} \dot{\mathbf{q}} = \begin{bmatrix} \boldsymbol{\tau}_{\Delta_1} \\ \boldsymbol{\tau}_{\Delta_3} \end{bmatrix} \quad (4.4)$$

One can note that the matrix  $\begin{bmatrix} \hat{\mathbf{H}}_0 & \hat{\mathbf{H}}_{0\eta} \\ \hat{\mathbf{H}}_{0\eta}^T & \hat{\mathbf{H}}_\eta \end{bmatrix}$  is an inertia matrix which by definition has an inverse given by:

$$\begin{bmatrix} \hat{\mathbf{H}}_0 & \hat{\mathbf{H}}_{0\eta} \\ \hat{\mathbf{H}}_{0\eta}^T & \hat{\mathbf{H}}_\eta \end{bmatrix}^{-1} = \begin{bmatrix} (\hat{\mathbf{H}}_0 - \hat{\mathbf{H}}_{0\eta} \hat{\mathbf{H}}_{0\eta}^T)^{-1} & -(\hat{\mathbf{H}}_0 - \hat{\mathbf{H}}_{0\eta} \hat{\mathbf{H}}_{0\eta}^T)^{-1} \hat{\mathbf{H}}_{0\eta} \\ -\hat{\mathbf{H}}_{0\eta}^T (\hat{\mathbf{H}}_0 - \hat{\mathbf{H}}_{0\eta} \hat{\mathbf{H}}_{0\eta}^T)^{-1} & \mathbf{I}_{n_\eta} + \hat{\mathbf{H}}_{0\eta}^T (\hat{\mathbf{H}}_0 - \hat{\mathbf{H}}_{0\eta} \hat{\mathbf{H}}_{0\eta}^T)^{-1} \hat{\mathbf{H}}_{0\eta} \end{bmatrix} \quad (4.5)$$

with  $\hat{\mathbf{H}}_\eta = \mathbf{I}_{n_\eta}$ . The inertial term  $(\hat{\mathbf{H}}_0 - \hat{\mathbf{H}}_{0\eta} \hat{\mathbf{H}}_{0\eta}^T)$  corresponds to a scaled inertia of the base for which the flexible inertia have been subtracted of the spacecraft base. Then by injecting (4.4) in (4.3) and by introducing the state vector  $\mathbf{x} = [\boldsymbol{\eta}^T \ \dot{\mathbf{q}}_0^T \ \dot{\boldsymbol{\eta}}^T]^T$ , actuators' dynamics are obtained as:

$$\mathbf{M}^\diamond(\mathbf{q})\ddot{\mathbf{q}} + \mathbf{D}^\diamond(\mathbf{q}, \dot{\mathbf{q}}, \dot{\mathbf{q}}_0)\dot{\mathbf{q}} + \mathbf{D}_x^\diamond(\mathbf{q}, \dot{\mathbf{q}}, \dot{\mathbf{q}}_0)\mathbf{x} = \boldsymbol{\tau}_q + \mathbf{J}_\Delta^\diamond(\mathbf{q})\boldsymbol{\tau}_\Delta \quad (4.6)$$

with:

$$\mathbf{M}^\diamond = \hat{\mathbf{H}}_q - \hat{\mathbf{H}}_{0q}^T (\hat{\mathbf{H}}_0 - \hat{\mathbf{H}}_{0\eta} \hat{\mathbf{H}}_{0\eta}^T)^{-1} \hat{\mathbf{H}}_{0q} \quad (4.7a)$$

$$\mathbf{D}^\diamond = \hat{\mathbf{C}}_q - \hat{\mathbf{H}}_{0q}^T (\hat{\mathbf{H}}_0 - \hat{\mathbf{H}}_{0\eta} \hat{\mathbf{H}}_{0\eta}^T)^{-1} \hat{\mathbf{C}}_{0q} \quad (4.7b)$$

$$\mathbf{D}_x^\diamond = \begin{bmatrix} \mathbf{0} & \hat{\mathbf{C}}_{q0} & \mathbf{0} \end{bmatrix} \quad (4.7c)$$

$$- \hat{\mathbf{H}}_{0q}^T \begin{bmatrix} (\hat{\mathbf{H}}_0 - \hat{\mathbf{H}}_{0\eta} \hat{\mathbf{H}}_{0\eta}^T)^{-1} & -(\hat{\mathbf{H}}_0 - \hat{\mathbf{H}}_{0\eta} \hat{\mathbf{H}}_{0\eta}^T)^{-1} \hat{\mathbf{H}}_{0\eta} \end{bmatrix} \begin{bmatrix} \mathbf{0} & \hat{\mathbf{C}}_\eta & \hat{\mathbf{C}}_{0\eta} \\ \hat{\mathbf{K}}_\eta & \hat{\mathbf{C}}_{\eta 0} & \hat{\mathbf{C}}_\eta \end{bmatrix} \quad (4.7d)$$

Thus, the joints' dynamics depends on an un-measurable state vector  $\mathbf{x}$  and a disturbance torque  $\boldsymbol{\tau}_d = \mathbf{J}_\Delta^\diamond(\mathbf{q})\boldsymbol{\tau}_\Delta$ . The state vector  $\mathbf{x}$  includes spacecraft linear drift and flexible dynamics while the disturbance torque gathers modeling and measurement errors. Splitting the sources of disturbances applying on actuators presents the advantage of clearly identifying the perturbations with different dynamics properties such that a rejection strategy can be developed.

Moreover, one can note that matrix  $\mathbf{D}_x^\diamond$  gathers an equivalent stiffness and a convective term multiplied by a scaled inertia. This scaling corresponds to the impact of flexible dynamics onto the actuators' ones.

In order to linearize the system a state observer and a nonlinear disturbance observer are detailed in the following sections.

## 4.2.2 State Observer model

An extended state observer is developed such that the flexible and the spacecraft's linear dynamics can be included in the system linearization detailed in section 4.2.4. The ESO is established using the control torque and the measure of actuators' velocities as input and the spacecraft's angular velocities as output measurements.

As the actuators' accelerations are not available, by injecting (4.3) in (4.4), the dynamic of the un-measured state can be written as:

$$\mathbf{H}_{0\eta}^* \begin{bmatrix} \ddot{\mathbf{q}}_0 \\ \ddot{\boldsymbol{\eta}} \end{bmatrix} + \mathbf{C}_{\eta 0\eta}^* \begin{bmatrix} \dot{\mathbf{q}}_0 \\ \dot{\boldsymbol{\eta}} \end{bmatrix} + \mathbf{C}_q^* \dot{\mathbf{q}} = \mathbf{J}_\Delta^* \boldsymbol{\tau}_\Delta + \mathbf{J}_q^* \boldsymbol{\tau}_q \quad (4.8)$$

with:

$$\mathbf{H}_{0\eta}^* = \begin{bmatrix} \hat{\mathbf{H}}_0 & \hat{\mathbf{H}}_{0\eta} \\ \hat{\mathbf{H}}_{0\eta}^T & \hat{\mathbf{H}}_\eta \end{bmatrix} - \begin{bmatrix} \hat{\mathbf{H}}_{0q} \\ \mathbf{0} \end{bmatrix} \hat{\mathbf{H}}_q^{-1} \begin{bmatrix} \hat{\mathbf{H}}_{0q}^T & \mathbf{0} \end{bmatrix} \quad (4.9a)$$

$$\mathbf{C}_{\eta 0\eta}^* = \begin{bmatrix} \mathbf{0} & \hat{\mathbf{C}}_0 & \hat{\mathbf{C}}_{0\eta} \\ \hat{\mathbf{K}}_\eta & \hat{\mathbf{C}}_{\eta 0} & \hat{\mathbf{C}}_\eta \end{bmatrix} - \begin{bmatrix} \hat{\mathbf{H}}_{0q} \\ \mathbf{0} \end{bmatrix} \hat{\mathbf{H}}_q^{-1} \begin{bmatrix} \mathbf{0} & \hat{\mathbf{C}}_{q0} & \mathbf{0} \end{bmatrix} \quad (4.9b)$$

$$\mathbf{C}_q^* = \begin{bmatrix} \hat{\mathbf{C}}_{0q} \\ \mathbf{0} \end{bmatrix} - \begin{bmatrix} \hat{\mathbf{H}}_{0q} \\ \mathbf{0} \end{bmatrix} \hat{\mathbf{H}}_q^{-1} \hat{\mathbf{C}}_q \quad (4.9c)$$

$$\mathbf{J}_\Delta^* = \begin{bmatrix} \mathbf{I} & -\hat{\mathbf{H}}_{0q} \hat{\mathbf{H}}_q^{-1} & \mathbf{0} \\ \mathbf{0} & \mathbf{0} & \mathbf{I} \end{bmatrix} \quad (4.9d)$$

$$\mathbf{J}_q^* = - \begin{bmatrix} \hat{\mathbf{H}}_{0q} \\ \mathbf{0} \end{bmatrix} \hat{\mathbf{H}}_q^{-1} \quad (4.9e)$$

Introducing the state vector to be estimated,  $\mathbf{x} = [\boldsymbol{\eta}^T \quad \dot{\mathbf{q}}_0^T \quad \dot{\boldsymbol{\eta}}^T]^T$ , one can re-write (4.8) as:

$$\begin{cases} \dot{\mathbf{x}} = \begin{bmatrix} \dot{\boldsymbol{\eta}} \\ \ddot{\mathbf{q}}_0 \\ \ddot{\boldsymbol{\eta}} \end{bmatrix} = \begin{bmatrix} \mathbf{0}_{n_\eta} & \mathbf{0}_{n_\eta \times n_q} & \mathbf{I}_{n_\eta} \\ & -\mathbf{H}_{0\eta}^{*-1} \mathbf{C}_{\eta 0\eta}^* & \end{bmatrix} \mathbf{x} + \begin{bmatrix} \mathbf{0}_{n_\eta \times n_q} & \mathbf{0}_{n_\eta \times n_q} \\ -\mathbf{H}_{0\eta}^{*-1} \mathbf{C}_q^* & \mathbf{H}_{0\eta}^{*-1} \mathbf{J}_q^* \end{bmatrix} \begin{bmatrix} \dot{\mathbf{q}} \\ \boldsymbol{\tau}_q \end{bmatrix} \end{cases} \quad (4.10a)$$

$$\begin{cases} + \begin{bmatrix} \mathbf{0}_{n_\eta \times (6+n_q+n_\eta)} \\ \mathbf{H}_{0\eta}^{*-1} \mathbf{J}_\Delta^* \end{bmatrix} \boldsymbol{\tau}_\Delta \\ = \mathbf{A}_e(\mathbf{q}, \dot{\mathbf{q}}, \dot{\mathbf{q}}_0) \mathbf{x} + \mathbf{B}_q(\mathbf{q}, \dot{\mathbf{q}}, \dot{\mathbf{q}}_0) \mathbf{u} + \mathbf{B}_\Delta(\mathbf{q}, \dot{\mathbf{q}}, \dot{\mathbf{q}}_0) \boldsymbol{\tau}_\Delta \\ \mathbf{y} = \boldsymbol{\omega}_0^{sat} = \begin{bmatrix} \mathbf{0} & \mathbf{I} & \mathbf{0} & \mathbf{0} \end{bmatrix} \mathbf{x} = \mathbf{C}_e \mathbf{x} \end{cases} \quad (4.10b)$$

The ESO dynamics includes the disturbance torque which requires to be estimated in order to linearize the system as well as insuring an accurate state estimation. By introducing the linear estimation gain  $\mathbf{L}_x$  and  $\hat{\boldsymbol{\tau}}_d$  the estimation of  $\boldsymbol{\tau}_d$ , the state vector  $\mathbf{x}$  is estimated as

$\mathbf{x}_e$  such that:

$$\dot{\mathbf{x}}_e = \mathbf{A}_e(\mathbf{q}, \dot{\mathbf{q}}, \dot{\hat{\mathbf{q}}}_0)\mathbf{x}_e + \mathbf{B}_q(\mathbf{q}, \dot{\mathbf{q}}, \dot{\hat{\mathbf{q}}}_0)\mathbf{u} + \mathbf{B}_\Delta(\mathbf{q}, \dot{\mathbf{q}}, \dot{\hat{\mathbf{q}}}_0)\mathbf{J}_\Delta^{\diamond+}(\mathbf{q})\hat{\boldsymbol{\tau}}_d + \mathbf{L}_x(\mathbf{y} - \mathbf{C}_e\mathbf{x}_e) \quad (4.11)$$

### 4.2.3 Nonlinear Disturbance Observer model

Similarly to the state observer, an estimation of the disturbance torques in the system linearization aims at improving the control performances. In particular, the present disturbance torque includes both modeling error and measurement errors which allows to compensate different uncertainties of the manipulator model and maintain high control performances.

The disturbance observer is developed capitalizing on the structure of the joint's dynamics (4.6) by introducing a gain  $\mathbf{L}_d$ , the disturbance observer is given by [Moh+13]:

$$\dot{\hat{\boldsymbol{\tau}}}_d = -\mathbf{L}_d\hat{\boldsymbol{\tau}}_d + \mathbf{L}_d(\mathbf{M}^\diamond\ddot{\mathbf{q}} + \mathbf{D}^\diamond\dot{\mathbf{q}} + \mathbf{D}_x^\diamond\mathbf{x}_e - \boldsymbol{\tau}_q) \quad (4.12)$$

However, actuators' accelerations are usually not available. To overcome this drawback, a new variable  $\mathbf{w}$  is introduced, such that [Che+00]:

$$\mathbf{w} = \hat{\boldsymbol{\tau}}_d - \mathbf{p}(\mathbf{q}, \dot{\mathbf{q}}) \quad (4.13)$$

where the vector  $\mathbf{p}(\mathbf{q}, \dot{\mathbf{q}})$  can be computed from the nonlinear gain  $\mathbf{L}_d(\mathbf{q}, \dot{\mathbf{q}})$  as [Moh+13]:

$$\frac{d}{dt}\mathbf{p}(\mathbf{q}, \dot{\mathbf{q}}) = \mathbf{L}_d(\mathbf{q}, \dot{\mathbf{q}})\mathbf{M}^\diamond(\mathbf{q})\ddot{\mathbf{q}} \quad (4.14)$$

With (4.6), (4.12) and (4.14), one can describe the nonlinear disturbance observer with the time-derivative of (4.13):

$$\begin{aligned} \dot{\mathbf{w}} &= \dot{\hat{\boldsymbol{\tau}}}_d - \frac{d}{dt}\mathbf{p}(\mathbf{q}, \dot{\mathbf{q}}) \\ &= -\mathbf{L}_d(\mathbf{q}, \dot{\mathbf{q}}) + \mathbf{L}_d(\mathbf{M}^\diamond(\mathbf{q})\ddot{\mathbf{q}} + \mathbf{D}^\diamond(\mathbf{q}, \dot{\mathbf{q}}, \dot{\hat{\mathbf{q}}}_0)\dot{\mathbf{q}} + \mathbf{D}_x^\diamond(\mathbf{q}, \dot{\mathbf{q}}, \dot{\hat{\mathbf{q}}}_0)\mathbf{x}_e - \boldsymbol{\tau}_q) \\ &= -\mathbf{L}_d(\mathbf{q}, \dot{\mathbf{q}})\hat{\boldsymbol{\tau}}_d + \mathbf{L}_d(\mathbf{q}, \dot{\mathbf{q}}) \left( \mathbf{D}^\diamond(\mathbf{q}, \dot{\mathbf{q}}, \dot{\hat{\mathbf{q}}}_0)\dot{\mathbf{q}} + \mathbf{D}_x^\diamond(\mathbf{q}, \dot{\mathbf{q}}, \dot{\hat{\mathbf{q}}}_0)\mathbf{x} - \boldsymbol{\tau}_q \right) \\ &\quad + \mathbf{L}_d(\mathbf{q}, \dot{\mathbf{q}})\mathbf{D}_x^\diamond(\mathbf{q}, \dot{\mathbf{q}}, \dot{\hat{\mathbf{q}}}_0)(\mathbf{x}_e - \mathbf{x}) \\ &= -\mathbf{L}_d(\mathbf{q}, \dot{\mathbf{q}})\mathbf{w} + \mathbf{L}_d(\mathbf{q}, \dot{\mathbf{q}}) \left( \mathbf{D}^\diamond(\mathbf{q}, \dot{\mathbf{q}}, \dot{\hat{\mathbf{q}}}_0)\dot{\mathbf{q}} + \mathbf{D}_x^\diamond(\mathbf{q}, \dot{\mathbf{q}}, \dot{\hat{\mathbf{q}}}_0)\mathbf{x} - \boldsymbol{\tau}_q - \mathbf{p}(\mathbf{q}, \dot{\mathbf{q}}) \right) \\ &\quad + \mathbf{L}_d(\mathbf{q}, \dot{\mathbf{q}})\mathbf{D}_x^\diamond(\mathbf{q}, \dot{\mathbf{q}}, \dot{\hat{\mathbf{q}}}_0)(\mathbf{x}_e - \mathbf{x}) \end{aligned} \quad (4.15)$$

Hence the nonlinear disturbance with only measurable or estimated states is defined as:

$$\begin{cases} \dot{\mathbf{w}} = -\mathbf{L}_d(\mathbf{q}, \dot{\mathbf{q}})\mathbf{w} + \mathbf{L}_d(\mathbf{q}, \dot{\mathbf{q}}) \left( \mathbf{D}^\diamond(\mathbf{q}, \dot{\mathbf{q}}, \dot{\mathbf{q}}_0)\dot{\mathbf{q}} + \mathbf{D}_x^\diamond(\mathbf{q}, \dot{\mathbf{q}}, \dot{\mathbf{q}}_0)\mathbf{x}_e - \boldsymbol{\tau}_q - \mathbf{p}(\mathbf{q}, \dot{\mathbf{q}}) \right) & (4.16a) \\ \hat{\boldsymbol{\tau}}_d = \mathbf{w} + \mathbf{p}(\mathbf{q}, \dot{\mathbf{q}}) & (4.16b) \\ \frac{d}{dt}\mathbf{p}(\mathbf{q}, \dot{\mathbf{q}}) = \mathbf{L}_d(\mathbf{q}, \dot{\mathbf{q}})\mathbf{M}^\diamond(\mathbf{q})\ddot{\mathbf{q}} & (4.16c) \end{cases}$$

#### 4.2.4 Closed-loop dynamics

After establishing the different observer models and the open-loop control behavior, one can note the different inter-dependencies between each dynamics. In order to insure stability of the closed-loop system, the tracking control error signal and the observers' error signals are considered in this section to highlight the notable dependencies between the dynamics. The tracking error control signal is defined as  $\boldsymbol{\epsilon}_c = (\mathbf{q}_d - \mathbf{q})$ , with  $\mathbf{q}_d$  the desired joint space trajectory, the state observer error signal  $\boldsymbol{\epsilon}_e = (\mathbf{x} - \mathbf{x}_e)$  and the nonlinear disturbance error signal  $\boldsymbol{\epsilon}_d = (\boldsymbol{\tau}_d - \hat{\boldsymbol{\tau}}_d)$ .

The state observer error signal dynamics can be obtained with (4.10) and (4.11) such that:

$$\begin{aligned} \dot{\boldsymbol{\epsilon}}_e &= \dot{\mathbf{x}} - \dot{\mathbf{x}}_e \\ &= \left( \mathbf{A}_e\mathbf{x} + \mathbf{B}_q\mathbf{u} + \mathbf{B}_\Delta\mathbf{J}_\Delta^{\diamond+}\boldsymbol{\tau}_d \right) - \left( \mathbf{A}_e\mathbf{x} + \mathbf{B}_q\mathbf{u} + \mathbf{B}_\Delta\mathbf{J}_\Delta^{\diamond+}\hat{\boldsymbol{\tau}}_d + \mathbf{L}_x(\mathbf{y} - \mathbf{C}_e\mathbf{x}_e) \right) \\ &= (\mathbf{A}_e - \mathbf{L}_x\mathbf{C}_e)\boldsymbol{\epsilon}_e + \mathbf{B}_\Delta\mathbf{J}_\Delta^{\diamond+}\boldsymbol{\epsilon}_d \end{aligned} \quad (4.17)$$

In order to obtain the nonlinear disturbance observer error dynamics, one can make a first assumption on the relative convergence rate of the error signals compared with the evolution of the torque disturbance. By construction, the disturbance torque  $\boldsymbol{\tau}_d$  present slow dynamics as the  $\Delta$  matrices have relatively low amplitudes. One can then assume that  $\dot{\boldsymbol{\tau}}_d \approx 0$  [Che+00] and in the case of fast disturbance dynamics, one can adapt the gain synthesis detailed in section 4.2.5 such that the convergence rate of  $\boldsymbol{\epsilon}_d$  is exponential when  $\dot{\boldsymbol{\tau}}_d$  is bounded [Moh+13]. Thus, the respective error dynamics is approximated by:

$$\dot{\boldsymbol{\epsilon}}_d = \dot{\boldsymbol{\tau}}_d - \dot{\hat{\boldsymbol{\tau}}}_d \approx -\dot{\hat{\boldsymbol{\tau}}}_d = -\dot{\mathbf{w}} - \frac{d}{dt}\mathbf{p} \quad (4.18)$$

Then with (4.16) and (4.18), the error signal of the NDO in function of the state observer error signal can be detailed as:

$$\begin{aligned} \dot{\boldsymbol{\epsilon}}_d &= \mathbf{L}_d\mathbf{w} - \mathbf{L}_d(\mathbf{D}^\diamond\dot{\mathbf{q}} + \mathbf{D}_x^\diamond\mathbf{x} - \boldsymbol{\tau}_q - \mathbf{p}) + \mathbf{L}_d\mathbf{D}_x^\diamond\boldsymbol{\epsilon}_e - \frac{d}{dt}\mathbf{p} \\ &= \mathbf{L}_d(\mathbf{w} + \mathbf{p}) - \mathbf{L}_d(\mathbf{M}^\diamond\ddot{\mathbf{q}} + \mathbf{D}^\diamond\dot{\mathbf{q}} + \mathbf{D}_x^\diamond\mathbf{x} - \boldsymbol{\tau}_q) + \mathbf{L}_d\mathbf{D}_x^\diamond\boldsymbol{\epsilon}_e \\ &= -\mathbf{L}_d\boldsymbol{\epsilon}_d + \mathbf{L}_d\mathbf{D}_x^\diamond\boldsymbol{\epsilon}_e \end{aligned} \quad (4.19)$$

Before establishing the tracking control error dynamics, a control torque that allows to

linearize and decouple the system is introduced. For a desired actuator dynamics,  $\mathbf{v}$ , such that:

$$\mathbf{v} = \mathbf{K} \begin{bmatrix} \mathbf{q}_d - \mathbf{q} \\ \dot{\mathbf{q}}_d - \dot{\mathbf{q}} \end{bmatrix} = \mathbf{K} \begin{bmatrix} \boldsymbol{\epsilon}_c \\ \dot{\boldsymbol{\epsilon}}_c \end{bmatrix} \quad (4.20)$$

where  $\mathbf{K}$  is a linear control gain, a control torque that realizes this objectives is given by:

$$\boldsymbol{\tau}_{q_c} = \mathbf{M}^\diamond \mathbf{K} \begin{bmatrix} \boldsymbol{\epsilon}_c \\ \dot{\boldsymbol{\epsilon}}_c \end{bmatrix} + \mathbf{D}^\diamond \dot{\mathbf{q}} + \mathbf{D}_x^\diamond \mathbf{x}_e - \hat{\boldsymbol{\tau}}_d \quad (4.21)$$

By injecting (4.21) in (4.6), the actuators closed-loop dynamics is given as:

$$\mathbf{M}^\diamond \ddot{\mathbf{q}} + \mathbf{D}^\diamond \dot{\mathbf{q}} + \mathbf{D}_x^\diamond \mathbf{x} - \boldsymbol{\tau}_d = \mathbf{M}^\diamond \mathbf{K} \begin{bmatrix} \boldsymbol{\epsilon}_c \\ \dot{\boldsymbol{\epsilon}}_c \end{bmatrix} + \mathbf{D}^\diamond \dot{\mathbf{q}} + \mathbf{D}_x^\diamond \mathbf{x}_e - \hat{\boldsymbol{\tau}}_d \quad (4.22)$$

matrix  $\mathbf{M}^\diamond$  is defined positive and symmetric as it an inertia matrix, thus by rewriting the close-loop dynamics, the tracking control error dynamics is obtained as:

$$\dot{\boldsymbol{\epsilon}}_c = -\mathbf{K} \begin{bmatrix} \boldsymbol{\epsilon}_c \\ \dot{\boldsymbol{\epsilon}}_c \end{bmatrix} + \mathbf{M}^{\diamond-1} \mathbf{D}_x^\diamond \boldsymbol{\epsilon}_e - \mathbf{M}^{\diamond-1} \boldsymbol{\epsilon}_d \quad (4.23)$$

Let's introduce the state vector  $\mathbf{z} = [\boldsymbol{\epsilon}_c^T \ \dot{\boldsymbol{\epsilon}}_c^T]^T$ , then (4.23) can be re-written as a state representation:

$$\begin{cases} \dot{\mathbf{z}} = \left( \begin{bmatrix} \mathbf{0} & \mathbf{I} \\ \mathbf{0} & \mathbf{0} \end{bmatrix} + \begin{bmatrix} \mathbf{0} \\ -\mathbf{I} \end{bmatrix} \mathbf{K} \right) \mathbf{z} + \begin{bmatrix} \mathbf{0} \\ \mathbf{M}^{\diamond-1} \mathbf{D}_x^\diamond \end{bmatrix} \boldsymbol{\epsilon}_e + \begin{bmatrix} \mathbf{0} \\ -\mathbf{M}^{\diamond-1} \end{bmatrix} \boldsymbol{\epsilon}_d \\ = (\mathbf{A}_z + \mathbf{B}_z \mathbf{K}) \mathbf{z} + \mathbf{B}_{z_e} \boldsymbol{\epsilon}_e + \mathbf{B}_{z_d} \boldsymbol{\epsilon}_d \\ \boldsymbol{\epsilon}_c = [\mathbf{I} \ \mathbf{0}] \mathbf{z} = \mathbf{C}_z \mathbf{z} \end{cases} \quad \begin{matrix} (4.24a) \\ (4.24b) \end{matrix}$$

Thus, by considering (4.17), (4.19) and (4.24) one can note that the system's stability depends on the convergence of coupled observers dynamics. A new hypothesis on the convergence rates can be made to reduce the coupling of the observers dynamics and enforce the hypothesis of  $\dot{\boldsymbol{\tau}}_d \approx 0$ . The disturbance observer error present lower amplitudes than  $\mathbf{x}$  as it mainly corresponds to residual modeling errors. In consequence, the emphasis on an accurate estimation of  $\mathbf{x}_e$  should be made over  $\hat{\boldsymbol{\tau}}_d$  estimation. Imposing a faster convergence time on the state estimation than on the disturbances allows to simplify the coupling dependency in (4.17) such that:

$$\dot{\boldsymbol{\epsilon}}_e = (\mathbf{A}_e - \mathbf{L}_x \mathbf{C}_e) \boldsymbol{\epsilon}_e \quad (4.25)$$

With this last hypothesis, (4.19) and (4.24), a compact version of the closed-loop dynamics

is obtained by introducing  $\mathbf{X} = [\mathbf{z}^T \quad \boldsymbol{\epsilon}_e^T \quad \boldsymbol{\epsilon}_d^T]^T$ :

$$\dot{\mathbf{X}} = \begin{bmatrix} (\mathbf{A}_z + \mathbf{B}_z \mathbf{K}) & \mathbf{B}_{z_e} & \mathbf{B}_{z_d} \\ \mathbf{0} & (\mathbf{A}_e - \mathbf{L}_x \mathbf{C}_e) & \mathbf{0} \\ \mathbf{0} & \mathbf{L}_d \mathbf{D}_x^\diamond & -\mathbf{L}_d \end{bmatrix} \mathbf{X} = \mathbf{A}(\mathbf{q}, \dot{\mathbf{q}}, \ddot{\mathbf{q}}_0) \mathbf{X} \quad (4.26)$$

### 4.2.5 Simultaneous gains synthesis

With the closed-loop expression as expressed in (4.26), the separation principle could allow to obtain the different controller and observer gains imposing negative eigen values of  $(\mathbf{A}_z + \mathbf{B}_z \mathbf{K})$ ,  $(\mathbf{A}_e - \mathbf{L}_x \mathbf{C}_e)$  and  $-\mathbf{L}_d$  to insure stability of the system. However, a simultaneous synthesis is proposed to insure disturbances rejections with observers with slower dynamics than the controller one. The synthesis is firstly developed for a linearized system and then extended to deal with workspace considerations. Secondly, the synthesis method is adapted to deal with large system evolutions mainly due to the mass distribution variations.

#### 4.2.5.1 Robustness to modeling and measurement errors

With the following proposition, the gains synthesis allows to insure control performances in presence of modeling uncertainties and measurement errors for a given linearized system.

**Proposition:** If there exist symmetric definite matrices  $\mathbf{Q}_z$ ,  $\mathbf{Q}_d$  and  $\mathbf{P}_e$  and matrices  $\mathbf{W}_z$  and  $\mathbf{W}_e$  of appropriate dimensions such that for a given scalar  $\gamma > 0$  the following LMI constraint holds:

$$\Theta = \begin{bmatrix} (\mathbf{A}_z \mathbf{Q}_z + \mathbf{B}_z \mathbf{W}_z)^s & \mathbf{B}_{z_e} & \mathbf{B}_{z_d} \mathbf{Q}_d & \mathbf{Q}_z \mathbf{C}_z^T \\ * & (\mathbf{P}_e \mathbf{A}_e - \mathbf{W}_e \mathbf{C}_e)^s & \mathbf{D}_x^{\diamond T} & \mathbf{0} \\ * & * & (-\mathbf{Q}_d + \mathbf{D}^\diamond)^s & \mathbf{0} \\ * & * & * & -\gamma^2 \mathbf{I} \end{bmatrix} < 0 \quad (4.27)$$

with  $\mathbf{X}^s = \mathbf{X} + \mathbf{X}^T$ , Then system is quadratically stabilized with  $\mathbf{K} = \mathbf{W}_z \mathbf{Q}_z^{-1}$ ,  $\mathbf{L}_x = \mathbf{P}_e^{-1} \mathbf{W}_e$  and  $\mathbf{L}_d = \mathbf{P}_d^{-1} \mathbf{M}^{\diamond^{-1}}$ . Moreover, the outputs  $\boldsymbol{\epsilon}_c$  verify:

$$\int_0^\infty \boldsymbol{\epsilon}_c(t)^T \boldsymbol{\epsilon}_c(t) dt < \gamma^2 \quad (4.28)$$

for any conditions  $\mathbf{z}(0) = \mathbf{0}$  and  $\boldsymbol{\epsilon}_{e_0}, \boldsymbol{\epsilon}_{d_0} \in \{\boldsymbol{\epsilon} \mid \boldsymbol{\epsilon}^T \mathbf{E} \boldsymbol{\epsilon} \leq 1\}$ .



**Proof:** As the matrix  $\mathbf{M}^\diamond$  is positive definite, one can choose the following Lyapunov function:

$$\begin{aligned} \mathbf{V}(\mathbf{X}) &= \mathbf{z}^T \mathbf{P}_z \mathbf{z} + \boldsymbol{\epsilon}_e^T \mathbf{P}_e \boldsymbol{\epsilon}_e + \boldsymbol{\epsilon}_d^T \mathbf{P}_d^T \mathbf{M}^\diamond \mathbf{P}_d \boldsymbol{\epsilon}_d \geq 0 \\ &= \mathbf{X}^T \begin{bmatrix} \mathbf{P}_z & \mathbf{0} & \mathbf{0} \\ \mathbf{0} & \mathbf{P}_e & \mathbf{0} \\ \mathbf{0} & \mathbf{0} & (\mathbf{P}_d^T \mathbf{M}^\diamond \mathbf{P}_d) \end{bmatrix} \mathbf{X} = \mathbf{X}^T \mathbf{P} \mathbf{X} \end{aligned} \quad (4.29)$$

such that  $\dot{\mathbf{V}} + \gamma^{-2} \boldsymbol{\epsilon}_c^T \boldsymbol{\epsilon}_c \leq 0$  for a given  $\gamma > 0$ .

Then by integration of this constraint:

$$\begin{aligned} \forall \mathbf{T} > 0, \int_0^{\mathbf{T}} \dot{\mathbf{V}} + \gamma^{-2} \boldsymbol{\epsilon}_c^T \boldsymbol{\epsilon}_c dt &< 0 \\ \Rightarrow \gamma^2 \int_0^{\mathbf{T}} \boldsymbol{\epsilon}_c^T \boldsymbol{\epsilon}_c dt &< \gamma^2 (\mathbf{V}_0 - \mathbf{V}_T) \\ \Rightarrow \gamma^2 \int_0^{\mathbf{T}} \boldsymbol{\epsilon}_c^T \boldsymbol{\epsilon}_c dt &< \gamma^2 \mathbf{V}_0 = \gamma^2 \begin{bmatrix} \boldsymbol{\epsilon}_{e_0}^T & \boldsymbol{\epsilon}_{d_0}^T \end{bmatrix} \begin{bmatrix} \mathbf{P}_e & \mathbf{0} \\ \mathbf{0} & \mathbf{P}_d^T \mathbf{M}^\diamond \mathbf{P}_d \end{bmatrix} \begin{bmatrix} \boldsymbol{\epsilon}_{e_0} \\ \boldsymbol{\epsilon}_{d_0} \end{bmatrix} \\ &< \begin{bmatrix} \boldsymbol{\epsilon}_{e_0}^T & \boldsymbol{\epsilon}_{d_0}^T \end{bmatrix} \mathbf{E} \begin{bmatrix} \boldsymbol{\epsilon}_{e_0} \\ \boldsymbol{\epsilon}_{d_0} \end{bmatrix} < \gamma^2 \end{aligned} \quad (4.30)$$

this condition is enforced by  $\begin{bmatrix} \mathbf{P}_e & \mathbf{0} \\ \mathbf{0} & \mathbf{P}_d^T \mathbf{M}^\diamond \mathbf{P}_d \end{bmatrix} \leq \mathbf{E}$ .

The time derivative of the proposed Lyapunov function is then given by:

$$\begin{aligned} \dot{\mathbf{V}}(\mathbf{X}) &= \mathbf{X}^T \left( \mathbf{A}^T \mathbf{P} + \mathbf{P} \mathbf{A} + \begin{bmatrix} \mathbf{0} & \mathbf{0} & \mathbf{0} \\ \mathbf{0} & \mathbf{0} & \mathbf{0} \\ \mathbf{0} & \mathbf{0} & \mathbf{P}_d^T \dot{\mathbf{M}}^\diamond \mathbf{P}_d \end{bmatrix} \right) \mathbf{X} \\ &= \mathbf{X}^T \begin{bmatrix} (\mathbf{P}_z \mathbf{A}_z + \mathbf{P}_z \mathbf{B}_z \mathbf{K})^s & \mathbf{P}_z \mathbf{B}_{z_e} & \mathbf{P}_z \mathbf{B}_{z_d} \\ * & (\mathbf{P}_e (\mathbf{A}_e - \mathbf{L}_x \mathbf{C}_e))^s & (\mathbf{L}_d \mathbf{D}_x^{\diamond T})^T (\mathbf{P}_d^T \mathbf{M}^\diamond \mathbf{P}_d)^T \\ * & * & (-\mathbf{P}_d^T \mathbf{M}^\diamond \mathbf{P}_d)^s + \mathbf{P}_d^T \dot{\mathbf{M}}^\diamond \mathbf{P}_d \end{bmatrix} \mathbf{X} \end{aligned} \quad (4.31)$$

where the time derivative of the equivalent inertia matrix can be defined as a function of the convective matrix as [Moh+13]:

$$\dot{\mathbf{M}}^\diamond = \mathbf{D}^\diamond + \mathbf{D}^{\diamond T} \quad (4.32)$$

As proposed by Mohammadi and al. [Moh+13], a candidate nonlinear gain observer can be chosen as:

$$\mathbf{L}_d = \mathbf{P}_d^{-1} \mathbf{M}^{\diamond^{-1}} \quad (4.33)$$

which leads with (4.16) to the auxiliary variable:

$$\frac{d}{dt} \mathbf{p} = \mathbf{P}_d^{-1} \ddot{\mathbf{q}} \quad (4.34)$$

Thus, simplification can be made to obtain the expression of the time-derivative of the Lyapunov function:

$$\dot{\mathbf{V}}(\mathbf{X}) = \mathbf{X}^T \begin{bmatrix} (\mathbf{P}_z(\mathbf{A}_z + \mathbf{B}_z\mathbf{K}))^s & \mathbf{P}_z\mathbf{B}_{z_e} & \mathbf{P}_z\mathbf{B}_{z_d} \\ * & (\mathbf{P}_e(\mathbf{A}_e - \mathbf{L}_x\mathbf{C}_e))^s & \mathbf{D}_x^{\diamond T}\mathbf{P}_d \\ * & * & (-\mathbf{P}_d^T)^s + (\mathbf{P}_d^T\mathbf{M}^{\diamond}\mathbf{P}_d) \end{bmatrix} \mathbf{X} \quad (4.35)$$

Then the constraint  $\dot{\mathbf{V}} + \gamma^{-2}\boldsymbol{\epsilon}_c^T\boldsymbol{\epsilon}_c \leq 0$  is equivalent to:

$$\begin{bmatrix} (\mathbf{P}_z(\mathbf{A}_z + \mathbf{B}_z\mathbf{K}))^s + \gamma^{-2}\mathbf{C}_z^T\mathbf{C}_z & \mathbf{P}_z\mathbf{B}_{z_e} & \mathbf{P}_z\mathbf{B}_{z_d} \\ * & (\mathbf{P}_e(\mathbf{A}_e - \mathbf{L}_x\mathbf{C}_e))^s & \mathbf{D}_x^{\diamond T}\mathbf{P}_d \\ * & * & (-\mathbf{P}_d^T)^s + (\mathbf{P}_d^T\mathbf{M}^{\diamond}\mathbf{P}_d) \end{bmatrix} < 0 \quad (4.36)$$

By applying the Schur complement, the condition becomes:

$$\begin{bmatrix} (\mathbf{P}_z(\mathbf{A}_z + \mathbf{B}_z\mathbf{K}))^s & \mathbf{P}_z\mathbf{B}_{z_e} & \mathbf{P}_z\mathbf{B}_{z_d} & \mathbf{C}_z^T \\ * & (\mathbf{P}_e(\mathbf{A}_e - \mathbf{L}_x\mathbf{C}_e))^s & \mathbf{D}_x^{\diamond T}\mathbf{P}_d & \mathbf{0} \\ * & * & (-\mathbf{P}_d^T)^s + (\mathbf{P}_d^T\mathbf{M}^{\diamond}\mathbf{P}_d) & \mathbf{0} \\ * & * & * & \gamma^2 \end{bmatrix} < 0 \quad (4.37)$$

By introducing the variable changes  $\mathbf{W}_z = \mathbf{K}\mathbf{Q}_z$  and  $\mathbf{W}_e = \mathbf{P}_e^{-1}\mathbf{L}_x$ , and pre and post multiplying the above matrix by  $\text{diag}(\mathbf{Q}_z, \mathbf{I}, \mathbf{Q}_d, \mathbf{I}) = \text{diag}(\mathbf{P}_z^{-1}, \mathbf{I}, \mathbf{P}_d^{-1}, \mathbf{I})$  one obtains the LMI constraint (4.27).

This concludes the proof.

As such, for a linearized system the matrices  $\mathbf{A}_e$ ,  $\mathbf{D}_x^{\diamond}$ ,  $\mathbf{D}^{\diamond}$ ,  $\mathbf{B}_{z_d}$  and  $\mathbf{B}_{z_e}$  are evaluated. Then defining the LMI variables  $\mathbf{Q}_z$ ,  $\mathbf{Q}_d$ ,  $\mathbf{P}_e$ ,  $\mathbf{W}_z$  and  $\mathbf{W}_e$  the LMI (4.27) is resolved by minimizing the parameter  $\gamma$ . This allows to obtain the control and observers gains suitable to insure stability for a given motions for which the linearization is sufficient. For large variations the LMI (4.27) is evaluated for different system linearizations.

#### 4.2.5.2 Robustness to system variations

During an on-orbit servicing operation, the distribution of mass is led to face significant changes through the different manipulations. Thus the resolution of the LMI (4.27), which is verified around a system's equilibrium state, needs to be slightly changed in order to consider those system variations without considering multiple equilibrium points which would prohibitively increase the number of LMI constraints in the design process. In this section, under mild assumptions, it is highlighted that system velocities can be neglected in a variations preliminary analysis to focus on a workspace analysis. In other words, in the inequality (4.27), convective terms have much less influence than inertial terms.

A first modification of the gains synthesis can be observed by considering a previous assumption on the convergence rate of the disturbance torque estimation. Compared to both

control and state observer error signals, the dynamics of the disturbance torque estimator are slow enough to be neglected. Consequently, the tracking error dynamics (4.24) can be approximated as:

$$\dot{\mathbf{z}} = (\mathbf{A}_z + \mathbf{B}_z \mathbf{K}) \mathbf{z} + \mathbf{B}_{z_e} \boldsymbol{\epsilon}_e \quad (4.38)$$

With these considerations, the LMI (4.27) including system variations during OOS operations is modified as follows (with the Deltas blocs and simplification of the coupling dynamics):

$$\Theta = \begin{bmatrix} (\mathbf{A}_z \mathbf{Q}_z + \mathbf{B}_z \mathbf{K})^s & \mathbf{B}_{z_e} + \Delta \mathbf{B}_{z_e} & \mathbf{0} & \mathbf{Q}_z \mathbf{C}_z^T \\ * & (\mathbf{P}_e \mathbf{A}_e - \mathbf{W}_e \mathbf{C}_e)^s & \mathbf{D}_x^{\diamond T} + \Delta \mathbf{D}_x^{\diamond T} & \mathbf{0} \\ * & * & (-\mathbf{Q}_d + \mathbf{D}^{\diamond})^s + \Delta \mathbf{D}^{\diamond} + \Delta \mathbf{D}^{\diamond T} & \mathbf{0} \\ * & * & * & -\gamma^2 \mathbf{I} \end{bmatrix} < 0 \quad (4.39)$$

Let us now introduce bounds  $\rho_1$ ,  $\rho_2$  and  $\rho_3$  on the maximum singular values of the interest variations:

$$\begin{cases} \bar{\sigma}(\Delta \mathbf{B}_{z_e}) < \rho_1 & (4.40a) \\ \bar{\sigma}(\Delta \mathbf{D}_x^{\diamond}) < \rho_2 & (4.40b) \\ \bar{\sigma}(\Delta \mathbf{D}^{\diamond} + \Delta \mathbf{D}^{\diamond T}) < \rho_3 & (4.40c) \end{cases}$$

Using a Schur-complement based argument, it is readily checked that the inequalities (4.39) are enforced by:

$$\Theta = \begin{bmatrix} (\mathbf{A}_z \mathbf{Q}_z + \mathbf{B}_z \mathbf{K})^s + \rho_1 \mathbf{I} & \mathbf{B}_{z_e} \\ * & (\mathbf{P}_e \mathbf{A}_e - \mathbf{W}_e \mathbf{C}_e)^s + (\rho_1 + \rho_2) \mathbf{I} \\ * & * \\ * & * \end{bmatrix} \begin{bmatrix} \mathbf{0} & \mathbf{Q}_z \mathbf{C}_z^T \\ \mathbf{D}_x^{\diamond T} & \mathbf{0} \\ (-\mathbf{Q}_d + \mathbf{D}^{\diamond})^s + (\rho_2 + \rho_3) \mathbf{I} & \mathbf{0} \\ * & -\gamma^2 \mathbf{I} \end{bmatrix} < 0 \quad (4.41)$$

Let us now evaluate the bounds introduced in (4.40). From equations (4.7) and (4.24), one can identify the matrix terms that are dependent on the workspace and those that also require system velocities to be evaluated. Decomposing  $\mathbf{D}_x^{\diamond}$  with a stiffness and a convective equivalent term such that  $\mathbf{D}_x^{\diamond}(\mathbf{q}, \dot{\mathbf{q}}) = [\mathbf{K}_\eta^{\diamond}(\mathbf{q}) \quad \mathbf{D}_{t,\eta}^{\diamond}(\mathbf{q}, \dot{\mathbf{q}})]$  defined as:

$$\begin{cases} \mathbf{K}_\eta^{\diamond} = \hat{\mathbf{H}}_{0q}^T (\hat{\mathbf{H}}_0 - \hat{\mathbf{H}}_{0\eta} \hat{\mathbf{H}}_{0\eta}^T)^{-1} \hat{\mathbf{H}}_{0\eta} \hat{\mathbf{K}}_\eta & (4.42a) \end{cases}$$

$$\begin{cases} \mathbf{D}_{t,\eta}^{\diamond} = \left[ \hat{\mathbf{C}}_{q0} - \hat{\mathbf{H}}_{0q}^T (\hat{\mathbf{H}}_0 - \hat{\mathbf{H}}_{0\eta} \hat{\mathbf{H}}_{0\eta}^T)^{-1} \hat{\mathbf{C}}_\eta + \hat{\mathbf{H}}_{0q}^T (\hat{\mathbf{H}}_0 - \hat{\mathbf{H}}_{0\eta} \hat{\mathbf{H}}_{0\eta}^T)^{-1} \hat{\mathbf{H}}_{0\eta} \hat{\mathbf{C}}_{\eta 0} \right. \\ \quad \left. - \hat{\mathbf{H}}_{0q}^T (\hat{\mathbf{H}}_0 - \hat{\mathbf{H}}_{0\eta} \hat{\mathbf{H}}_{0\eta}^T)^{-1} \hat{\mathbf{C}}_{0\eta} + \hat{\mathbf{H}}_{0q}^T (\hat{\mathbf{H}}_0 - \hat{\mathbf{H}}_{0\eta} \hat{\mathbf{H}}_{0\eta}^T)^{-1} \hat{\mathbf{H}}_{0\eta} \hat{\mathbf{C}}_\eta \right] & (4.42b) \end{cases}$$

one can consider matrices  $\mathbf{M}^\diamond(\mathbf{q})$  and  $\mathbf{K}_\eta^\diamond(\mathbf{q})$  on one side and velocity dependent term matrices  $\mathbf{D}^\diamond$  and  $\mathbf{D}_{t,\eta}^\diamond$  on an other side. Firstly, the common factor term  $\hat{\mathbf{H}}_{0q}^T (\hat{\mathbf{H}}_0 - \hat{\mathbf{H}}_{0\eta} \hat{\mathbf{H}}_{0\eta}^T)^{-1}$ , which corresponds to a scaled inertia can be constrained as:

$$\bar{\sigma} \left( \hat{\mathbf{H}}_{0q}^T (\hat{\mathbf{H}}_0 - \hat{\mathbf{H}}_{0\eta} \hat{\mathbf{H}}_{0\eta}^T)^{-1} \right) \leq \frac{\bar{\sigma} (\hat{\mathbf{H}}_{0q}^T)}{\underline{\sigma} (\mathbf{H}_0 - \mathbf{H}_{0\eta} \mathbf{H}_{0\eta}^T)} = \beta \quad (4.43)$$

where  $\underline{\sigma}(\mathbf{A})$  denotes the minimum singular value of matrix  $\mathbf{A}$ . Thus, matrices  $\mathbf{M}^\diamond(\mathbf{q})$  and  $\mathbf{K}_\eta^\diamond(\mathbf{q})$  can be bounded as:

$$\left\{ \begin{array}{l} \underline{\sigma}(\mathbf{M}^\diamond) \mathbf{I} \leq \mathbf{M}^\diamond \leq \bar{\sigma}(\mathbf{M}^\diamond) \mathbf{I} \\ \bar{\sigma}(\mathbf{K}_\eta^\diamond) \leq \beta \bar{\sigma}(\hat{\mathbf{H}}_{0\eta} \hat{\mathbf{K}}_\eta) \end{array} \right. \quad (4.44a)$$

$$(4.44b)$$

Then, the velocity dependent terms can be simplified thanks to specific assumptions in space robotic applications. In order to maintain system stability, actuators velocities remain low enough to develop slow manipulator motions such that flexible modes excitation are limited. Moreover, system variations correspond to the different mass distributions which are not affected by the reaction-wheels velocities. The study of matrices  $\mathbf{D}_{t,\eta}^\diamond$  and  $\mathbf{D}^\diamond$  results in identifying the impact of the manipulator motions in the considered workspace.

The rewriting effort made to obtain the joint-space dynamics (4.6) has allowed to define  $\mathbf{D}_x$  as an equivalent Coriolis matrix. This convective term can be bounded as a function of the SMS configuration and the actuators' capacity such that [MM07]:

$$\sigma(\mathbf{D}^\diamond(\mathbf{q}, \dot{\mathbf{q}})) \leq \bar{\sigma}(\mathbf{D}^\diamond(\mathbf{q}, \dot{\mathbf{q}})) \leq \lambda \|\dot{\mathbf{q}}\|_{max}^2 \quad (4.45)$$

where the parameter  $\lambda$  is defined as a function of the studied workspace [MM07]:

$$\lambda = \frac{3}{2} \sup \left( \sum_{i=1}^{n_q} \left\| \frac{\partial \mathbf{M}^\diamond(\mathbf{q})}{\partial \mathbf{q}_i} \right\| \right) \quad (4.46)$$

Furthermore, with the assumption of slow manipulator motions, the evaluation of  $\mathbf{D}_x^\diamond$  can be reduced to the variations of  $\mathbf{K}_\eta^\diamond$ . By definition, convective matrices correspond to the cross product terms between  $\dot{\mathbf{q}}$ ,  $\dot{\boldsymbol{\eta}}$  and  $\boldsymbol{\omega}_0$ . For slow manipulator and base motions, flexible modes vibration amplitudes are limited. These general assumptions allow to neglect convective term variations compared with inertia/mass ones. Bounding  $\mathbf{D}_x^\diamond$  as follows

$$\bar{\sigma}(\mathbf{D}_x^\diamond) \leq \bar{\sigma}(\mathbf{K}_\eta^\diamond) + \bar{\sigma}(\mathbf{D}_{t,\eta}^\diamond) \quad (4.47)$$

and  $\mathbf{D}_{t,\eta}^\diamond$  with only convective terms such that:

$$\bar{\sigma}(\mathbf{D}_{t,\eta}^\diamond) \leq \bar{\sigma}(\hat{\mathbf{C}}_{q0}) + \beta \bar{\sigma}(\hat{\mathbf{H}}_{0q}^T) \left( \bar{\sigma}(\hat{\mathbf{C}}_\eta) + \bar{\sigma}(\hat{\mathbf{H}}_{0\eta} \hat{\mathbf{C}}_{\eta 0}) + \bar{\sigma}(\hat{\mathbf{C}}_{0\eta}) + \bar{\sigma}(\hat{\mathbf{H}}_{0\eta} \hat{\mathbf{C}}_\eta) \right) \quad (4.48)$$

one finally obtains:

$$\bar{\sigma}(\mathbf{D}_x^\diamond) \leq \bar{\sigma}(\mathbf{K}_\eta^\diamond) \quad (4.49)$$

Thus, with (4.44), (4.45) and (4.49) the required bounds can be evaluated as:

$$\left\{ \begin{array}{l} \rho_1 = \frac{\bar{\sigma}(\mathbf{K}_\eta^\diamond)}{\underline{\sigma}(\mathbf{M}^\diamond)} \end{array} \right. \quad (4.50a)$$

$$\left\{ \begin{array}{l} \rho_2 = \bar{\sigma}(\mathbf{K}_\eta^\diamond) \end{array} \right. \quad (4.50b)$$

$$\left\{ \begin{array}{l} \rho_3 = 2\lambda \|\dot{\mathbf{q}}\|_{max}^2 \end{array} \right. \quad (4.50c)$$

with  $\bar{\sigma}(\mathbf{K}_\eta^\diamond)$  corresponding to the greatest singular value of matrix  $(\mathbf{K}_\eta^\diamond)$  and  $\underline{\sigma}(\mathbf{M}^\diamond)$  lowest singular value of matrix  $(\mathbf{M}^\diamond)$ .

#### 4.2.5.3 Proposed design methodology

The design procedure is now generalized to a multi-task on-orbit servicing scenario in which from one task to another the mass distribution may significantly differ as well as the size of the workspace. To optimally consider the system changes through the different tasks and obtain optimal constant control and observer gains, let us define  $n$  tasks, denoted  $t_{1 \leq i \leq n} \in \mathcal{T}$ , where  $\mathcal{T}$  denotes the entire set of tasks corresponding to the total servicing scenario. The details of the design procedure are given by the following algorithm:

---

**Algorithm 2** Design procedure for a multi-task on-orbit servicing scenario

---

Define the set of tasks  $\mathcal{T}$  and for each task  $t_{1 \leq i \leq n}$  with an associated workspace  $w_{1 \leq i \leq n}$   
 Define the different LMI variables,  $\mathbf{Q}_z$ ,  $\mathbf{Q}_d$ ,  $\mathbf{P}_e$ ,  $\mathbf{W}_z$  and  $\mathbf{W}_e$ , as in the proposition in section 4.2.5.1

**for**  $i \leq n$  **do**

Define an equilibrium point to evaluate matrices,  $\mathbf{A}_e$ ,  $\mathbf{D}_x^\diamond$ ,  $\mathbf{D}^\diamond$ ,  $\mathbf{B}_{z_d}$  and  $\mathbf{B}_{z_e}$ , in the LMI constraint (4.27) from (4.1) Minimize the LMI variable  $\gamma > 0$  such that  $\Theta_{1 \leq i \leq n} < 0$

Evaluate the relaxation terms  $\rho_1$ ,  $\rho_2$  and  $\rho_3$  as in (4.50)

Define a  $\Theta_i$  as in (4.41)

**end for**

**Return**  $\mathbf{K}$ ,  $\mathbf{L}_x$ ,  $\mathbf{P}_d = \mathbf{Q}_d^{-1}$

---

Thereby, algorithm 2 provides controller and observer gains suitable for a space manipulator system to perform different tasks while preserving similar control performances for each task.

## 4.3 Illustration of the proposed method

### 4.3.1 Study case

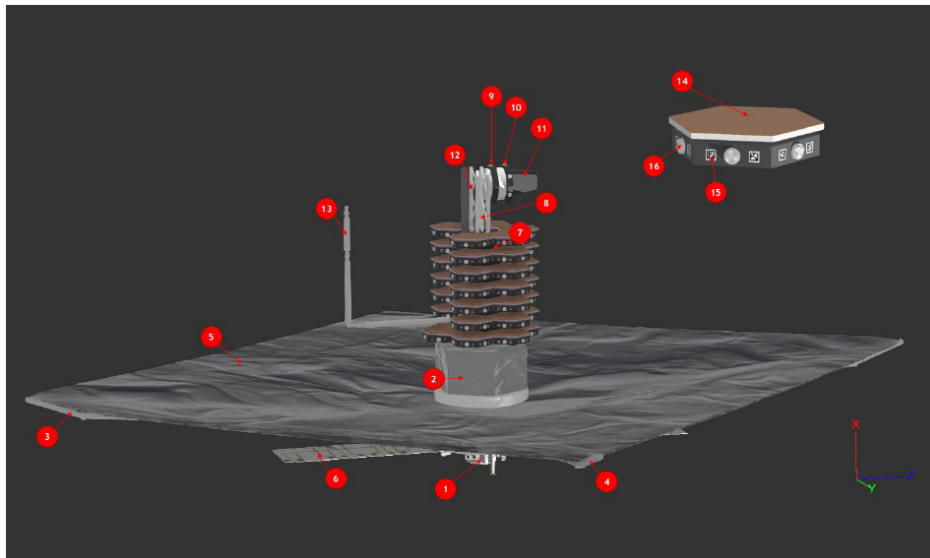


Figure 4.2 – Spacecraft component overview (elements are detailed in tables 4.1 and 4.2), <https://www.h2020-pulsar.eu>

In order to illustrate our proposed method, the on-orbit deployment of the PULSAR telescope presented in Rognant and al. [Rog+19] is used. Figure 4.2 shows the elements composing the PULSAR telescope. In order to relieve the load on the simulator physics, the geometries are simplified compared to the real components. The current properties have been estimated from the James Webb Space Telescope.

Tables 4.1 and 4.2 present the sub-components of the spacecraft represented in Figure 4.2. Their main physical properties (dimension, mass, CoM) have been specified, inertias are given in the XML description detailed in appendix B.

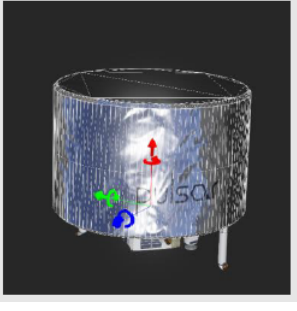
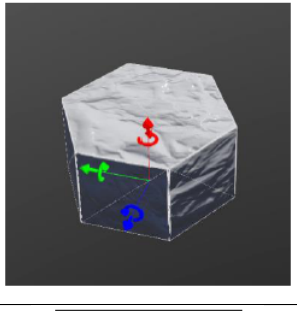
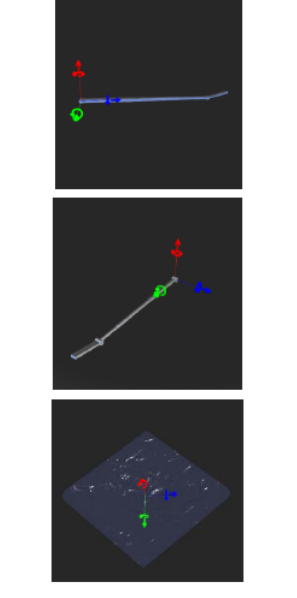
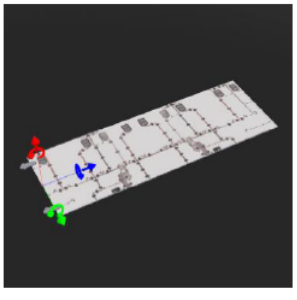
	<p>The spacecraft's base (1). It is the main structure including power supply, on-board computer, attitude control actuators and sensors, etc.</p> <p>Dimensions XYZ (m): <math>2 \times 3,2 \times 2,7817</math> (diameter 3,2)  Mass (Kg): 1960  CoM XYZ (m): <math>[0,9 \ 0 \ 0]</math></p>
	<p>The payload module (2). In a real mission, this part would contain all the electronics and data handling needed to support the instruments.</p> <p>Dimensions XYZ (m): <math>1,5 \times 3,2 \times 2,7817</math> (diameter 3,2)  Mass (Kg): 1440  CoM XYZ (m): <math>[0,55 \ 0 \ 0]</math></p>
	<p>The sun shield which is used to protect the telescope from light interference. Its large size can introduce perturbations in the AOCS<sup>8</sup>. It is composed of:</p> <p>Two long beams (3)  Dimensions XYZ (m): <math>3,3871 \times 0,3 \times 13,788</math>  Mass (Kg): 84  CoM XYZ (m): <math>[0 \ 0 \ 7,1]</math></p> <p>Two medium beams (4)  Dimensions XYZ (m): <math>2,6442 \times 10,986 \times 0,3</math>  Mass (Kg): 66  CoM XYZ (m): <math>[0 \ 5,65 \ 0]</math></p> <p>And the shield itself (5).</p>
	<p>Two solar arrays (6).  Dimensions XYZ (m): <math>0,02 \times 2 \times 5,5</math>  Mass (Kg): 61  CoM XYZ (m): <math>[0,001 \ 0,001 \ 3,845]</math></p>

Table 4.1 – Spacecraft sub-components, <https://www.h2020-pulsar.eu>

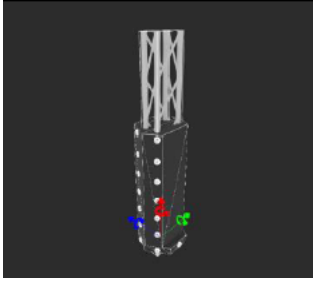
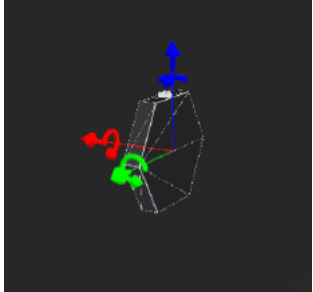
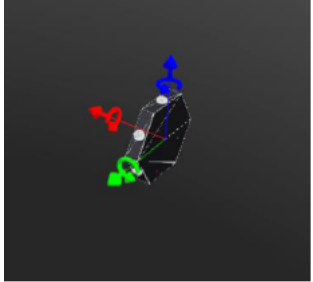
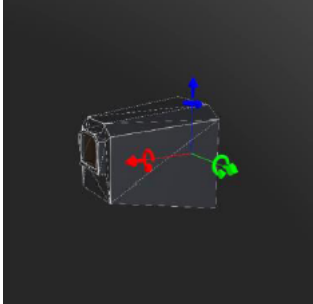
	<p>The SMT<sup>9</sup> container (7) with the main mast (8):  Dimensions XYZ (m): <math>6 \times 1,42541 \times 1,2344</math>  Mass (Kg): 1132  CoM XYZ (m): [1,5 0 0]</p> <p>Its function is to store the 36 segmented mirror tiles at the beginning of assembly scenario. Its configuration consists in a first row of 6 tiles at the bottom, and 6 consequential rows of 5 tiles. This allows for the rail of the robotic assembly system to pass between the tiles, enabling access of all the tiles to the robotic arm.</p>
	<p>The pre-assembly site (9) with its unique standard interface which will be used for attaching SMTs to form a preassembly.  Dimensions XYZ (m): <math>0,2 \times 1,42541 \times 1,2344</math> (diameter 1.42541)  Mass (Kg): 22  CoM XYZ (m): [0 0 0]</p>
	<p>The assembly site (10) around which will be assembled the primary mirror.  Dimensions XYZ (m): <math>0,2 \times 1,42541 \times 1,2344</math> (diameter 1.42541)  Mass (Kg): 28  CoM XYZ (m): [0 0 0]</p>
	<p>The optics system (11) which only simulates the physics (mass and collisions), not the optical part:  Dimensions XYZ (m): <math>0.994646 \times 0.781024 \times 0.835381</math>  Mass (Kg): 425  CoM XYZ (m): [0 0 0]</p>

Table 4.2 – Spacecraft sub-components, <https://www.h2020-pulsar.eu>

The manipulator has been adapted from the Compliant Assistance and Exploration Space Robot (CAESAR)<sup>1</sup>. The CAESAR robotic arm is a 7-DoF<sup>10</sup>, modular manipulator designed for space applications. Its original total length is  $\sim 3m$ . To increase the original workspace, its length was increased by  $\sim 1m$  (50cm between joints 2-3 and 50cm between joints 4-5) to allow for the complete assembly process. Figure 4.3 illustrates the latest CAESAR

<sup>10</sup>Degree of Freedom



configuration as integrated on the PULSAR telescope with an additional prismatic DoF at its origin corresponding to the rail. In addition, 6 reaction-wheels, positioned inside the spacecraft's base ((1) in Figure 4.2), allow to actively control the 3 rotational DoFs of the space telescope. Moreover, with the two solar arrays and the sun-shield, represented by four flexible beams, 22 flexible modes are integrated to the equations of motions as detailed in section 2.3. The total spacecraft mass is 6892kg. The base weighs 1960 kg while the robotic arm is limited to 60 kg.

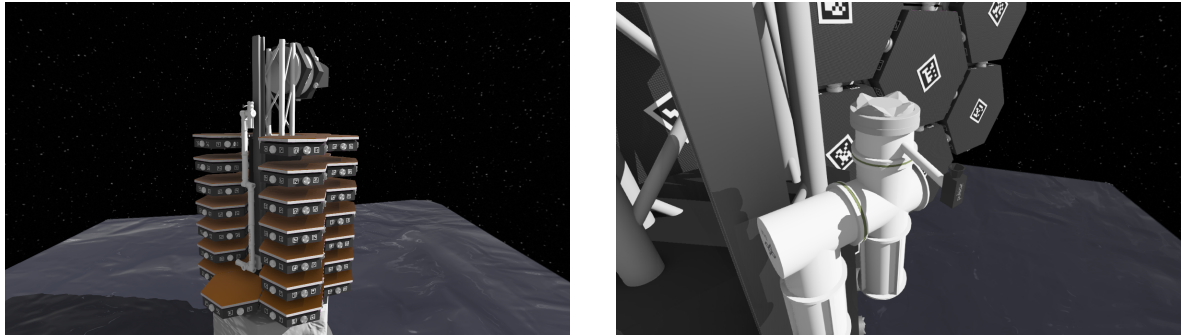


Figure 4.3 – Stowed view (left) and end-effector closeup (right) of CAESAR arm, <https://www.h2020-pulsar.eu>

The scenario of a complete assembly can be divided into 372 sub-tasks,  $t_{1 \leq i \leq 372}$ . The sequencing allows to break down complex actions into more simple ones among which inspections tasks and tile displacements. Limited by the manipulator workspace, the mirror assembly is decomposed into a first pre-assembly of bundles of five tiles during which the manipulator unstacks tiles from the container and free the space in the bottom part of the assembly site. Therefore, the manipulator is moving between one to four tiles before establishing a pre-assembly bundle. An illustration of the scenario is developed with the following snapshots.

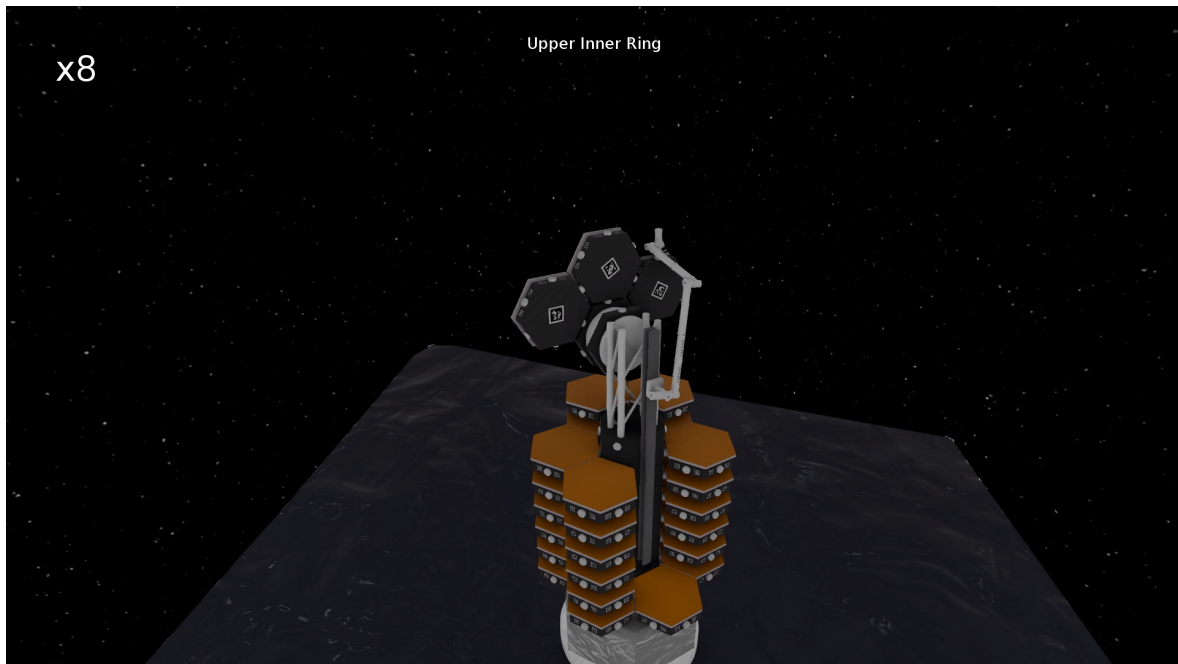


Figure 4.4 – Snapshot after the assembly of the upper inner ring, <https://www.h2020-pulsar.eu>

The first three tiles can be directly assembled to form the upper part of the inner ring assembly, as illustrated in Figure 4.4.

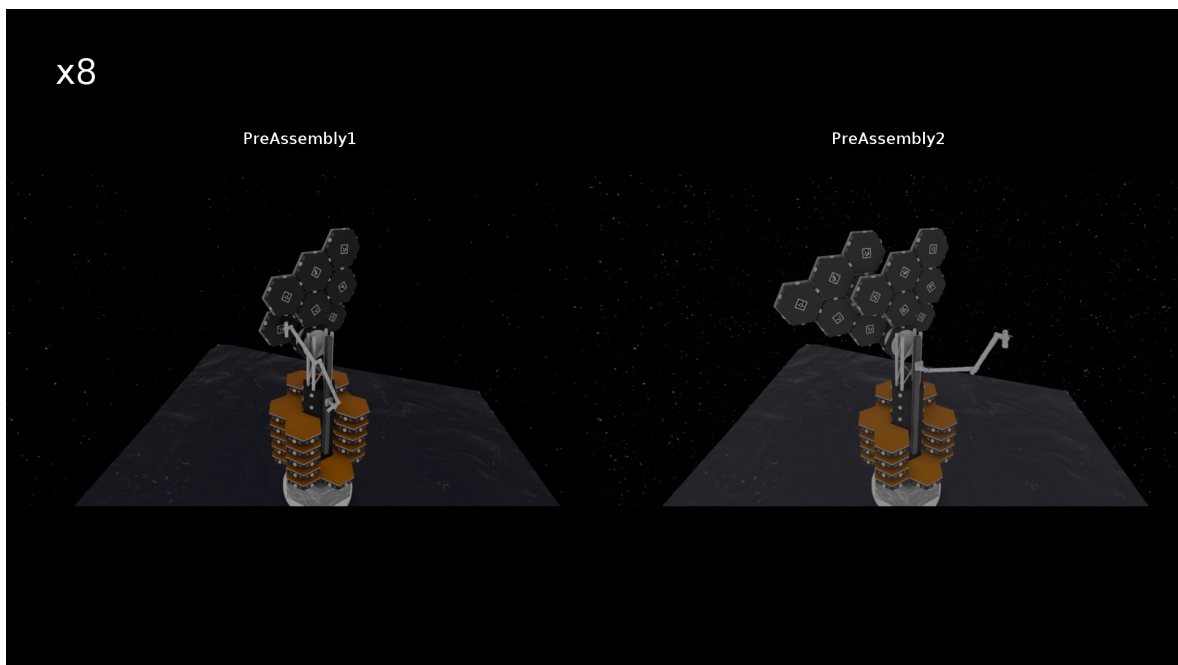


Figure 4.5 – Snapshots after the two first pre-assembly operations, <https://www.h2020-pulsar.eu>

Next operation consists in building first pre-assembly and placing it on the assembly site. Same set of operations are done to build the second pre-assembly, and placing it at the correct location on the assembly site (as visualized in Figure 4.5).

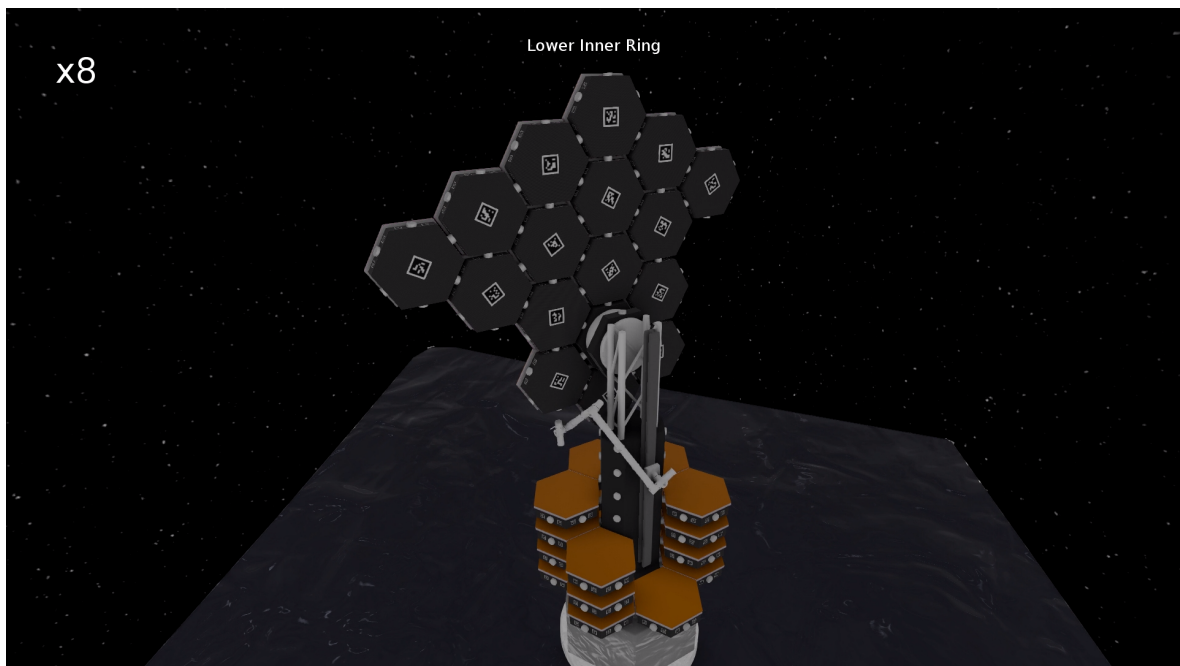


Figure 4.6 – Snapshot after the lower inner ring assembly, <https://www.h2020-pulsar.eu>

Assembly of the lower inner ring follows the completion of assembly of the second pre-assembly (Figure 4.6). Tiles are directly assembled, without the need to use the pre-assembly site.

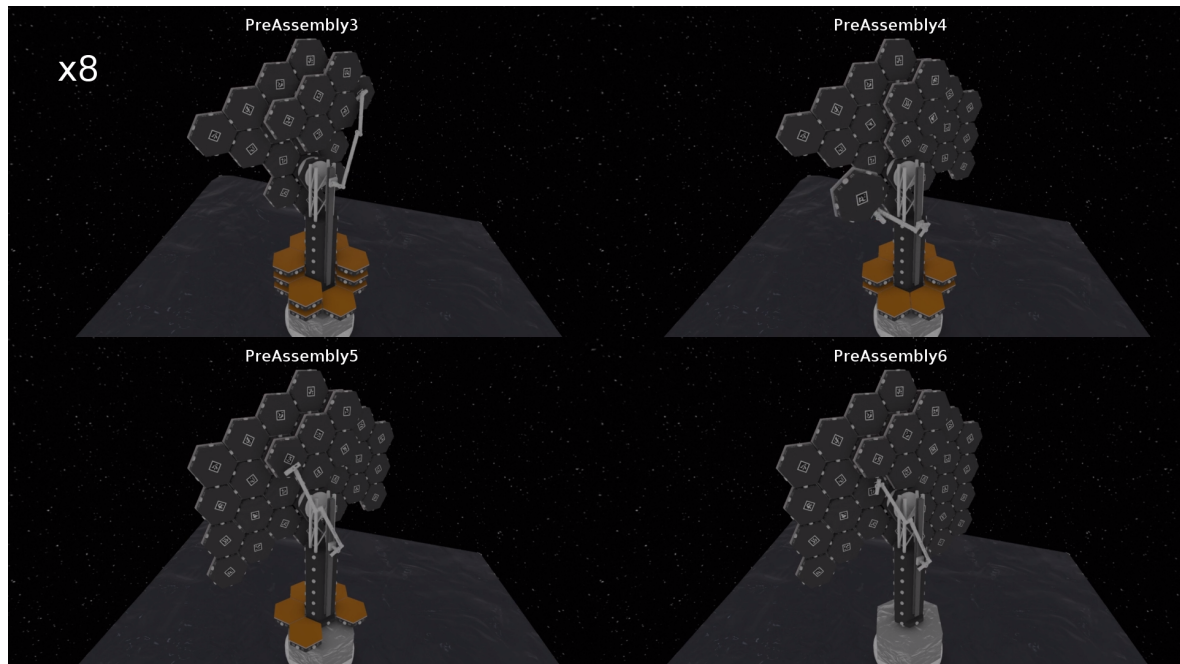


Figure 4.7 – Snapshots of the four consecutive pre-assembly operations, <https://www.h2020-pulsar.eu>

Finally, the last four pre-assembly/assembly operations are executed consecutively, five tiles are first assembled on the pre-assembly site, and then the pre-assembly is positioned at the correct location on the final assembly system.

Figure 4.8 shows the final view of the space telescope after completion of all the different robotic tasks.

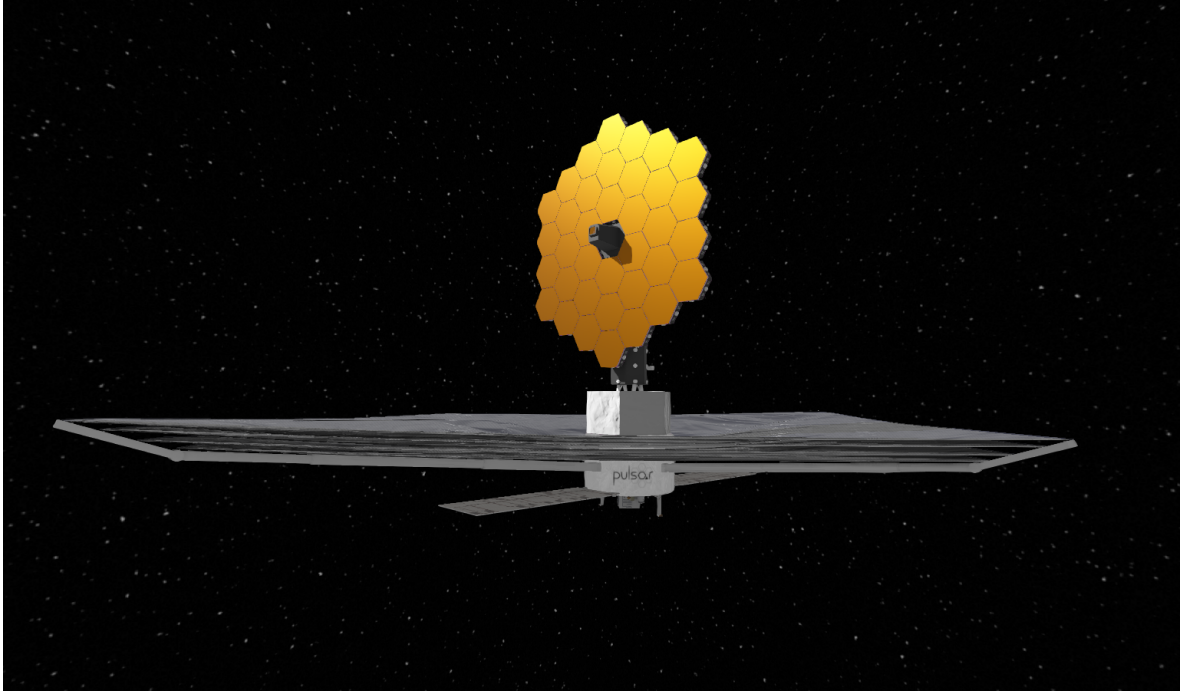


Figure 4.8 – Final view of PULSAR, <https://www.h2020-pulsar.eu>

## 4.3.2 Simulations results

### 4.3.2.1 Gains synthesis solver

The LMI resolution involves high-dimensional matrices and a large set of constraints (according to the considered scenario) which may lead to significant computational times. In the present application, each constraint (4.27) corresponds to a  $106 \times 106$  matrix inequality where the decision variables  $\mathbf{Q}_z$ ,  $\mathbf{Q}_d$  and  $\mathbf{P}_e$  are respectively  $28 \times 28$ ,  $14 \times 14$  and  $50 \times 50$  symmetric matrices. In order to better control the resolution time, the YALMIP toolbox [Lof04] is interfaced here with the MOSEK solver. To assess the computation cost, table 4.3 gathers, for different sizes of the set of tasks  $\mathcal{T}$ , the resolution times which have been obtained on a standard computer equipped with an Intel i7 Processor.

As expected, the CPU time considerably increases with the size of  $\mathcal{T}$ . However, the number of needed iterations is not much affected. It should also be emphasized that, without major degradation, the controllers gains can be restricted to diagonal matrices thus slightly reducing the number of decision variables.

size of $\mathcal{T}$	10	20	30	40	50	80	100	154
LMI resolution time (s)	35	130	122	186	245	426	550	833
Iterations	27	53	33	38	39	38	39	43

Table 4.3 – LMI resolution times according to the size of  $\mathcal{T}$

If the time resolution becomes an issue, as it directly depends on the number of decision variables and LMI constraints, the use of further relaxations can be considered at the cost of possibly increased conservatism.

#### 4.3.2.2 Analysis of system variations

During the on-orbit assembly of the PULSAR telescope, important system variations occur due to mass distribution changes. A preliminary analysis of the impact of such variations – through the evaluation of the bounds detailed in (4.40) for each sub-task of the deployment scenario – is useful to reduce the size of  $\mathcal{T}$  in the design process. Sub-tasks presenting lowest variations correspond to verification maneuvers or small adjustment of end-effector rotations. Consequently such tasks share similar physical properties with the following longer manipulation task justifying the reduction of tasks considered in the gains synthesis.

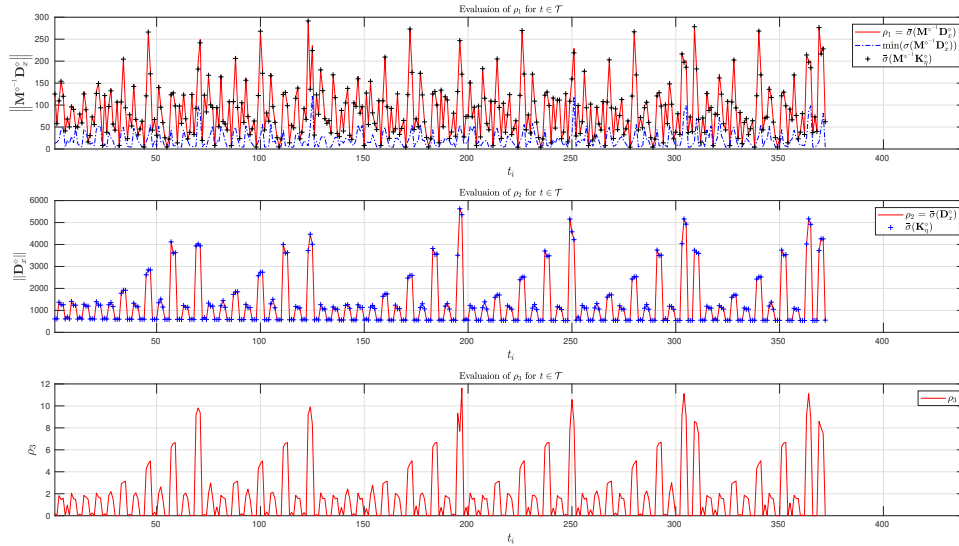


Figure 4.9 – Evolution of relaxation terms for each tasks of the PULSAR scenario

Figure 4.9 illustrates variations of the three bounds for each task  $t \in \mathcal{T}$  for unused reaction-wheels (i.e.  $\dot{\mathbf{q}}_r = 0$ ) as they do not affect the mass distribution in the workspace. For each task, the norms are evaluated for the maximal joint velocities and uniformly distributed manipulator joint configurations in the corresponding workspace  $w_i$ . As a first observation, it can be noted that a workspace approach is a suitable method to evaluate the bounds  $\rho_i$ . Observing from the upper subplot of Figure 4.9, the similar evolutions of  $\bar{\sigma}(\mathbf{M}^{\diamond-1} \mathbf{D}_x^\diamond)$  and  $\bar{\sigma}(\mathbf{M}^{\diamond-1} \mathbf{K}_\eta^\diamond)$  and then comparing  $\bar{\sigma}(\mathbf{D}_x^\diamond)$  with  $\bar{\sigma}(\mathbf{K}_\eta^\diamond)$  on the central subplot, we can validate the approximations of section 4.2.5.2 from which the bounds (4.50) are derived. Regarding the actuators' velocities and the variations of  $\rho_3$  from the lower subplot of Figure 4.9 in comparison to the evolutions of  $\rho_1$  and  $\rho_2$  the study of system variations with a workspace

analysis can be justified.

A second observation can be made on the large system variations for each task by considering the evolution  $\bar{\sigma}(\mathbf{M}^{\diamond^{-1}}\mathbf{K}_{\eta}^{\diamond})$ , whose maximum (red full line) and minimum (blue dashed line) values are visualized on the upper subplot of figure 4.9. These variations motivate the use of bounds to be incorporated as a single constraint instead of considering multiple equilibrium points for each task which would generate numerous constraints and would lead to an unsolvable optimization problem.

Moreover, according to the considered scenario, some successive tasks may exhibit similar workspaces and mass distributions. Then, a reduced set of tasks can be used in the design procedure. In our context, further simplifications could be achieved by eliminating short tasks or those whose impact on the system variations remains small enough.

#### 4.3.2.3 System performances in simulation

In this section, the interest of the control method is illustrated with time-domain simulations. In order to validate the efficiency of the design procedure, simulation are performed on multiple similar tasks through the deployment scenario. Three sets of tasks are considered for the validation process:  $\mathcal{T}_{2T} = \{34, 88, 160, 214, 268, 328\}$ ,  $\mathcal{T}_{3T} = \{46, 100, 172, 226, 280, 340\}$  and  $\mathcal{T}_{4T} = \{58, 112, 184\}$ . The first set,  $\mathcal{T}_{2T}$ , gathers six tasks through which the manipulator moves a bundle of 2 tiles with a similar motion (i.e. same velocities and amplitude). Similarly, the second set,  $\mathcal{T}_{3T}$ , gathers six tasks for which similar motions allow to move 3 tiles and the last set,  $\mathcal{T}_{4T}$ , gathers three tasks where 4 tiles are moved. Choosing similar tasks through the scenario aims at evaluating the robustness to system variations with comparison of control tracking performances. Indeed, first by comparing the moving of a same mass at the end-effector but with different overall mass distribution and secondly comparing performances for a significantly different mass at the end-effector and a different overall mass distribution, one will be able to conclude on the robustness of the control. The system mass or inertia variations can be evaluated with the relaxation term  $\rho_1$  from (4.50) which its evolution for each tasks in the scenario is plotted in the upper subplot of Figure 4.9 and likewise the values for the considered simulated tasks are given in the Table 4.4. Furthermore, one will note that the chosen tasks present significant variations considering the complete deployment.

$t_i$	34	46	58	88	100	112	160	172	184	214	226	268	280	328	340
$\rho_1$	204	266	128	206	268	129	209	273	131	206	205	270	203	203	269

Table 4.4 – Values of  $\rho_1(t_i)$

Regarding modeling errors, which impact the evaluation of the inverse kinematics/dynamics, a degraded space manipulator model is considered. From the nominal model of the PULSAR telescope, the following levels of uncertainties are considered:  $\pm 3\%$  on the inertia  $\mathcal{I}_{S_i}$ ,  $+10\%$  on the flexible parameters and  $\pm 10\%$  on the position of the CoM. Likewise, a noise bias is included on the measure of  $\omega_0$  corresponding to a  $\pm 10\%$  of error such that state

observer efficiency can be tested.

In the studied application, manipulator trajectories and velocities are provided with singularity free path-planning strategies also taking into account the actuators capacities (<https://www.h2020-pulsar.eu>). Reaction-wheels desired velocities are deduced from those of the manipulator joints assuming a kinetic momentum conservation and by imposing a fixed based such that:

$$\dot{\mathbf{q}}_{r_d} = -\mathbf{H}_{0r}^+ (\mathbf{H}_{0m} \dot{\mathbf{q}}_{m_d} + \mathbf{H}_0 \mathbf{t}_0) = -\mathbf{H}_{0r}^+ \mathbf{H}_{0m} \dot{\mathbf{q}}_{m_d} \quad (4.51)$$

with an initial moment considered null. The choice of imposing a fixed spacecraft attitude is justified by the reduction of the impact of the indirect coupling effects between the manipulator and the flexible appendages as developed in the previous chapter.

The validation process is divided into two main discussions. First the control performances are evaluated considering for each set,  $\mathcal{T}_{2T}$ ,  $\mathcal{T}_{3T}$  and  $\mathcal{T}_{4T}$ , the tracking error of both the manipulator's joints and the reaction-wheels' velocities. This aims at concluding on the robustness to system variations, modeling and measurement errors. Secondly, with a decomposition of the computed torque (4.21), the contribution of including the estimations of the un-measured states and compensating for the modeling uncertainties is discussed.

**Control robustness:** For each set  $\mathcal{T}_{2T}$ ,  $\mathcal{T}_{3T}$  and  $\mathcal{T}_{4T}$  similar motions are executed by the manipulator moving respectively 2, 3 and 4 tiles. To first illustrate the precision of the manipulator's joints velocity control, Figures 4.10, 4.11 and 4.12 respectively represent the measured joints' velocities for  $\mathcal{T}_{2T}$ ,  $\mathcal{T}_{3T}$  and  $\mathcal{T}_{4T}$ . The dotted-line corresponds to the desired joint' velocity,  $q_{m_d}$ , and in full-lines represents the velocities measures. Individually considering each three Figures 4.10, 4.11 and 4.12, one will first note that for each  $t_i$  in the respective sets present similar control performances (as full-lines are overlapping). First, by obtaining for a given set the same closed-loop response allows to conclude on the robustness of system variations. As tasks are sorted in different set, for each set a same number of tiles and a similar motions are considered. In one given set, for each tasks the SMS exhibits different inertia properties due to the overall mass distribution.



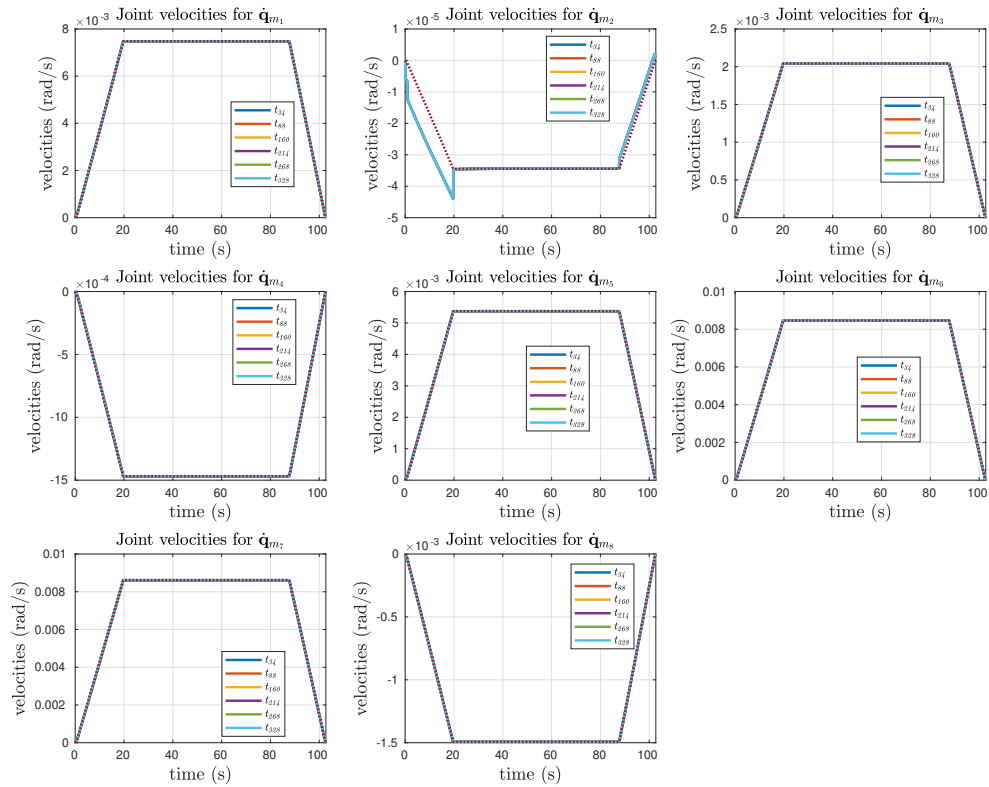


Figure 4.10 – Evolutions of all the manipulator's joints for each  $t_i \in \mathcal{T}_{2T}$ ; the dotted-line represents the desired velocity  $\dot{\mathbf{q}}_{m_d}$  and the full-lines correspond to each  $\dot{\mathbf{q}}_m$  for each task

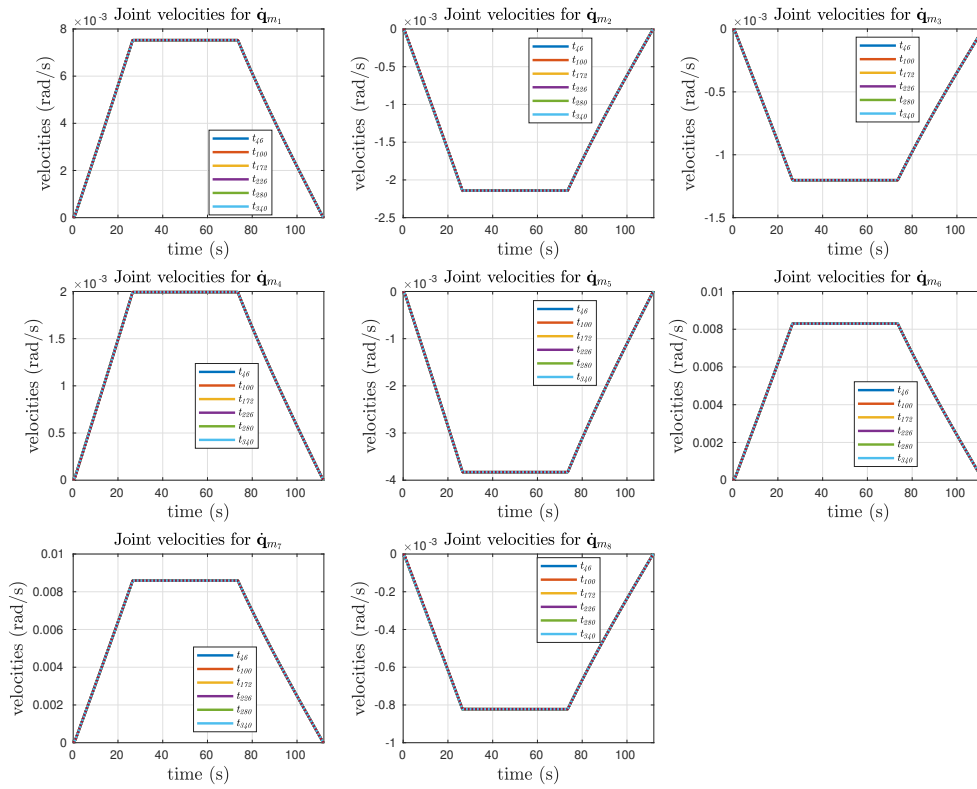


Figure 4.11 – Evolutions of all the manipulator's joints for each  $t_i \in \mathcal{T}_{3T}$ ; the dotted-line represents the desired velocity  $\dot{q}_{m_d}$  and the full-lines correspond to each  $\dot{q}_m$  for each task

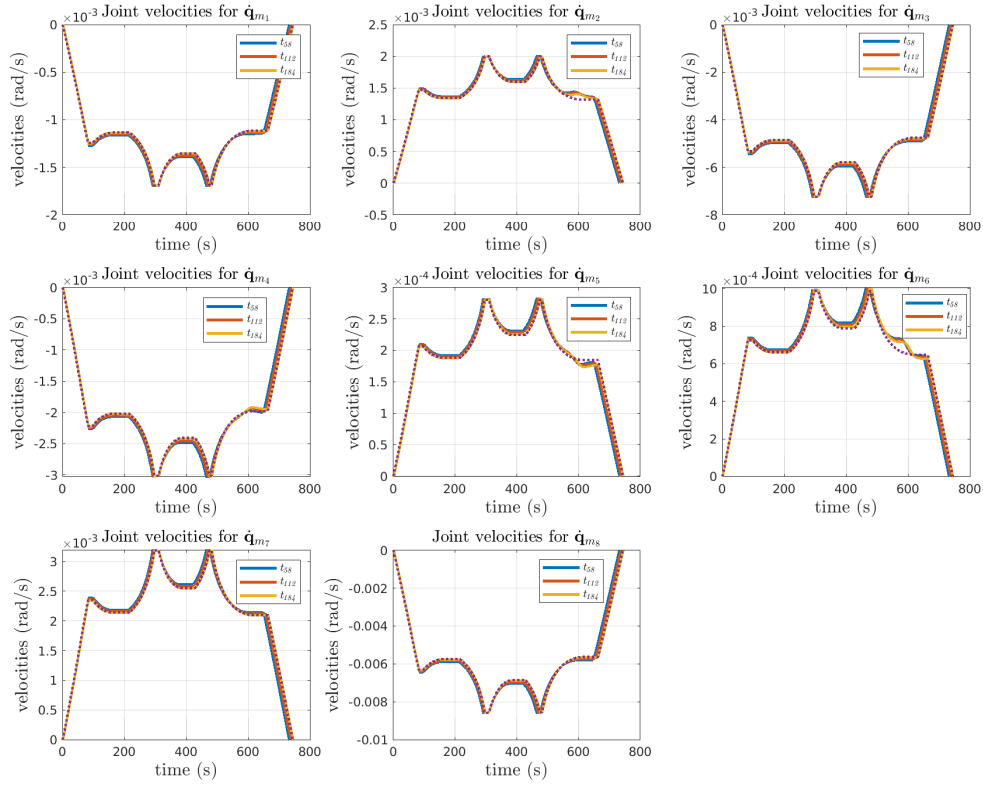


Figure 4.12 – Evolutions of all the manipulator's joints for each  $t_i \in \mathcal{T}_{4T}$ ; the dotted-line represents the desired velocity  $\dot{q}_{m_d}$  and the full-lines correspond to each  $\dot{q}_m$  for each task

To emphasize on the system variations, one can analyze the difference between reaction-wheels' velocities insuring a fixed attitude of the base for each tasks in a given set. In that purpose, Figures 4.13, 4.14 and 4.15 respectively represent the six reaction-wheels' velocities in function of each tasks respectively in  $\mathcal{T}_{2T}$ ,  $\mathcal{T}_{3T}$  and  $\mathcal{T}_{4T}$ . Considering for instance Figure 4.13, one will note that for each  $q_{r_i}$  different desired velocities (in dotted-lines) are required for each tasks  $t_i \in \mathcal{T}_{2T}$ . This traduces that the mass, initially near the base, is moved to the mirror position through the scenario which corresponds to modifications of the system's inertia matrix. As the reaction-wheels' inertia remains constant, the velocity varies to satisfy (4.51). Then similar observations can be made for Figures 4.14 and 4.13.

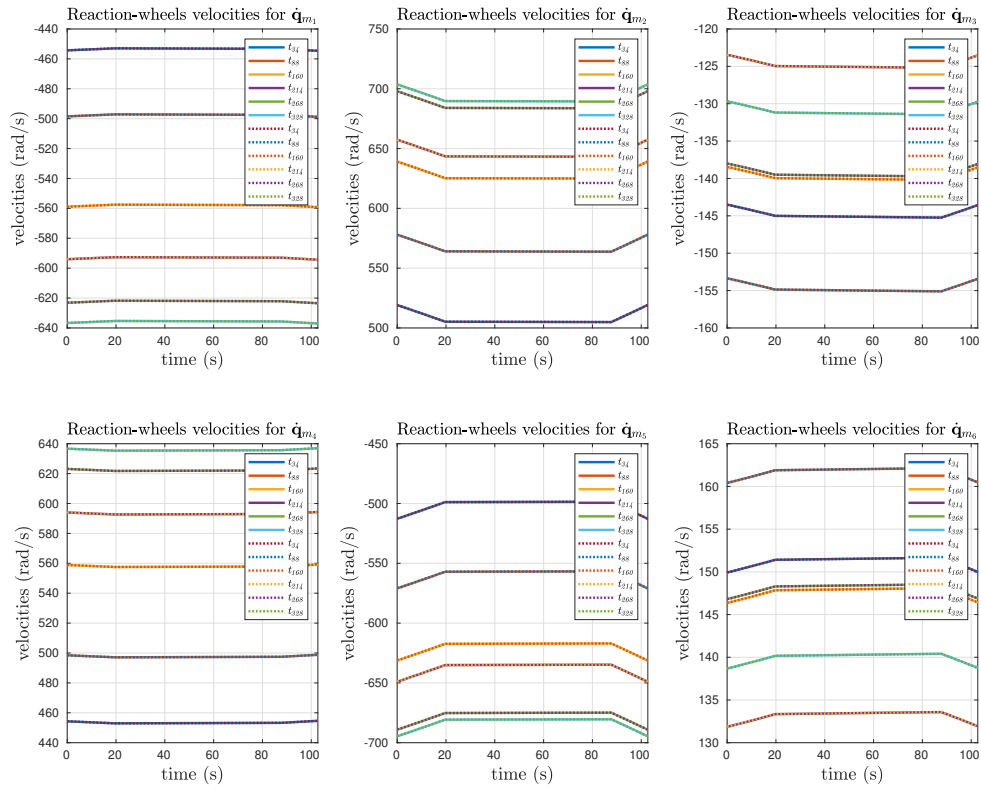


Figure 4.13 – Evolutions of all the reaction-wheels' joints for each  $t_i \in \mathcal{T}_{2T}$ ; the dotted-lines represent the desired velocities  $\dot{q}_{r,d}$  and the full-lines correspond to each  $\dot{q}_r$  for each task

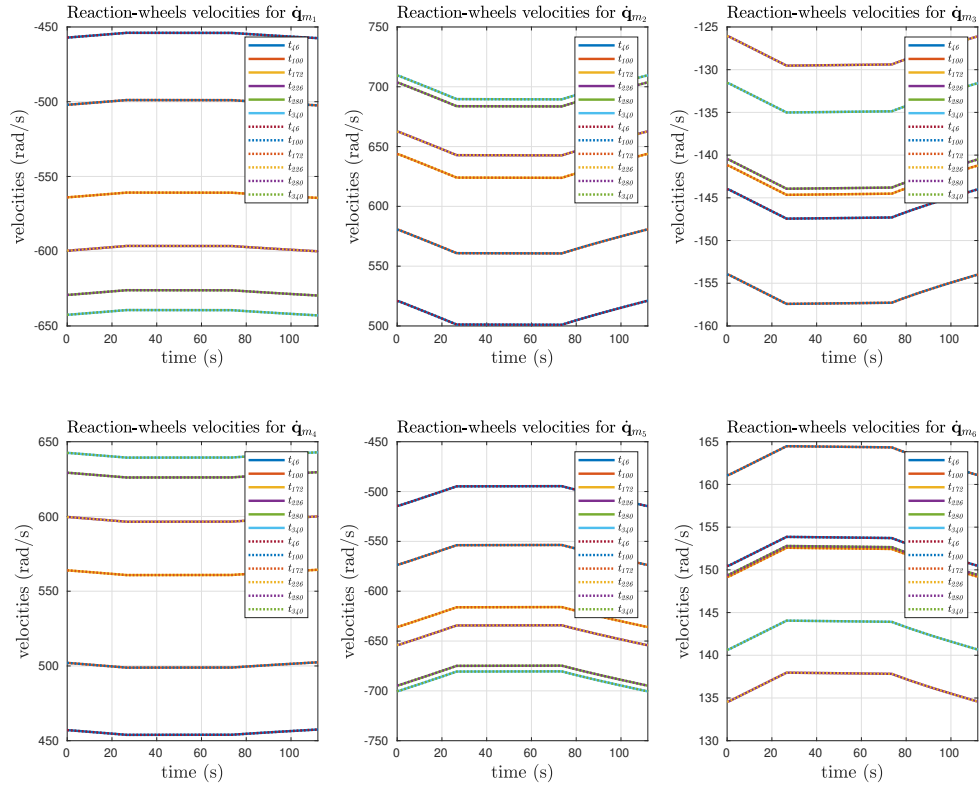


Figure 4.14 – Evolutions of all the reaction-wheels' joints for each  $t_i \in \mathcal{T}_{3T}$ ; the dotted-lines represent the desired velocities  $\dot{q}_{r,d}$  and the full-lines correspond to each  $\dot{q}_r$  for each task

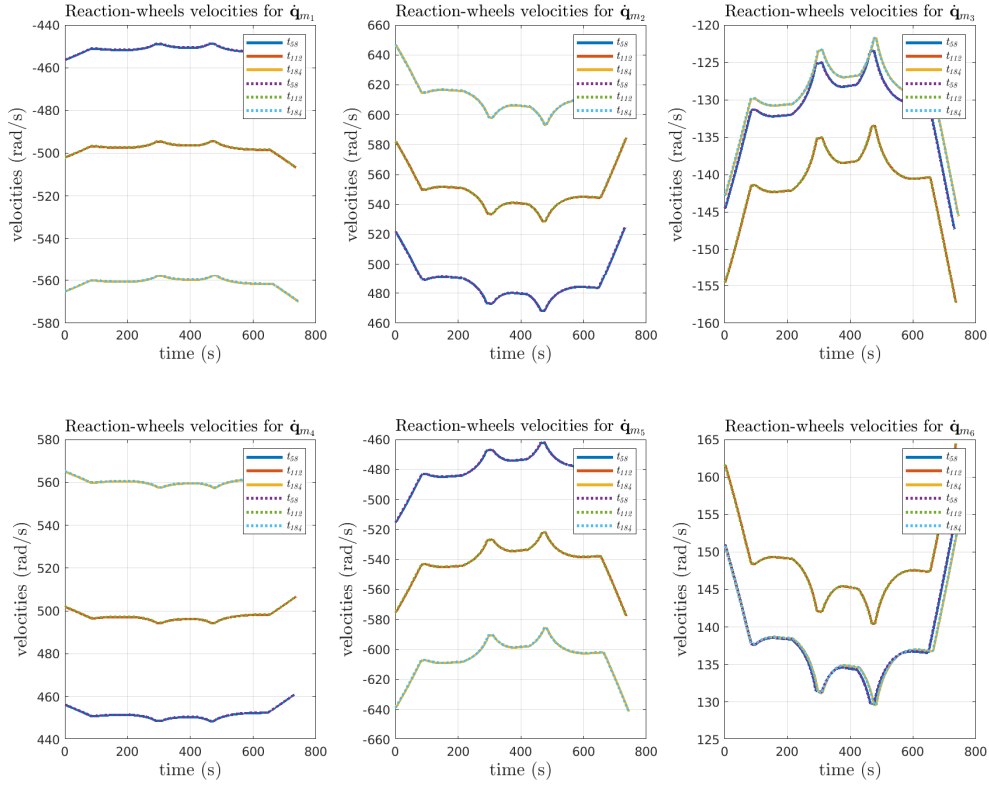


Figure 4.15 – Evolutions of all the reaction-wheels' joints for each  $t_i \in \mathcal{T}_{4T}$ ; the dotted-lines represent the desired velocities  $\dot{q}_{r,d}$  and the full-lines correspond to each  $\dot{q}_r$  for each task

Then, to guarantee that the system provides satisfying performances one will consider the relative tracking errors defined for each joints as in (3.67) (i.e.  $\epsilon_{tc}(\dot{q}_i) = (\dot{q}_{d_i} - \dot{q}_i) / \max(\dot{q}_i)$ ). As similar measured velocities of the manipulator's joints, the relative error for all joints are plotted in Figure 4.16 for each tasks  $t_i \in \mathcal{T}_{2T}$  on the left, for  $t_i \in \mathcal{T}_{3T}$  on the middle and for  $t_i \in \mathcal{T}_{4T}$  on the right. One will note that in the transient state, this signal reaches the largest amplitudes. However, the overall relative error's amplitudes are similar to those obtained in the previous chapter (see Figure 3.13).

Considering the reaction-wheels, a similar relative tracking error is plotted for each set  $\mathcal{T}_{2T}$ , visualized in the left subplot of Figure 4.17,  $\mathcal{T}_{3T}$  in the middle subplot of Figure 4.17 and  $\mathcal{T}_{4T}$  in the right subplot of Figure 4.17. Similarly to the manipulator, during the transient state, the relative error reaches its maximal values and are equivalent to those obtained in the previous chapter (see Figure 3.14).

These observations allow to first highlight that the global control performances are satisfying regarding the large system variations and ratio of mass moved with the manipulator. Secondly, it shows a first limit of the proposed gains synthesis. As it is difficult to impose a closed-loop dynamic for each actuators but only insure convergence of the system, the tran-

sient states are providing the worst performances. Moreover, no consideration on the control torques' limitations are considered in the synthesis which allows to consider large control gains responsible of the transient states obtained.

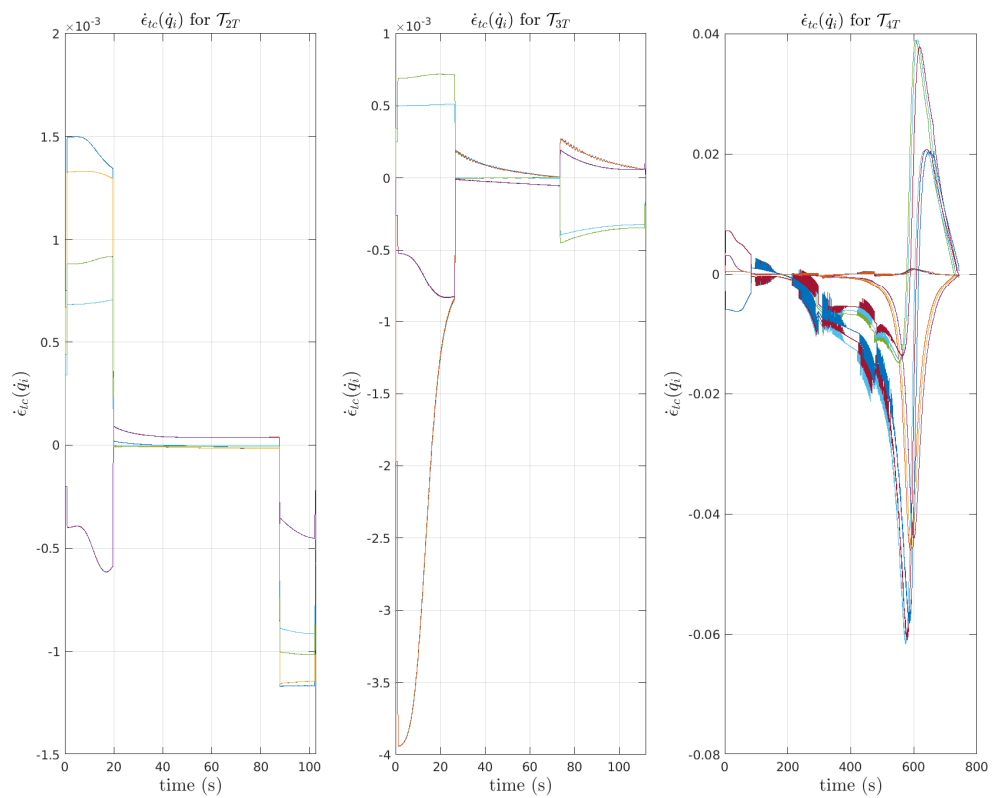


Figure 4.16 – Illustration of the manipulator control performances; For each manipulator joints the relative tracking error  $\dot{\epsilon}_{tc}(\dot{q}_i)$  of each  $t_i \in \mathcal{T}_{2T}$  on the left, for each  $t_i \in \mathcal{T}_{3T}$  on the middle, for each  $t_i \in \mathcal{T}_{4T}$  on the right

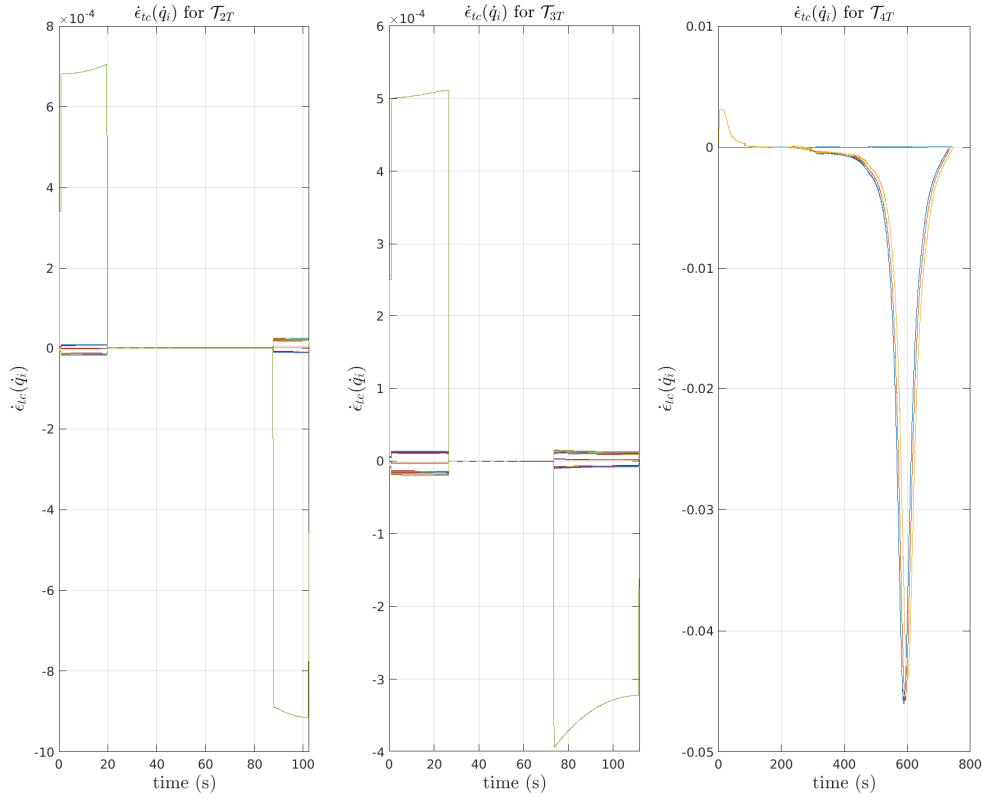


Figure 4.17 – Illustration of the reaction-wheels control performances; For each reaction-wheels the relative tracking error  $\dot{\epsilon}_{tc}(\dot{q}_i)$  of each  $t_i \in \mathcal{T}_{2T}$  on the left, for each  $t_i \in \mathcal{T}_{3T}$  on the middle, for each  $t_i \in \mathcal{T}_{4T}$  on the right

Thus, from these observations one can conclude on the robustness to system's variations and in particular emphasize on the possibility of performing different tasks with significant mass to move. Moreover, it highlights the gains synthesis efficiency as it was made for motions of end-effector's loads between nothing and  $220kg$  (corresponding to 4 tiles).

**Interest of the control scheme:** In order to illustrate the usefulness of disturbance and state observers to properly linearize and decouple the system, the detailed components of the control torques (4.21) are visualized for tasks in  $\mathcal{T}_{2T}$  in Figures 4.18, 4.19 and 4.20, for tasks in  $\mathcal{T}_{3T}$  in Figures 4.21, 4.22 and 4.23 and for tasks in  $\mathcal{T}_{4T}$  in Figures 4.24, 4.25 and 4.26.

The control torques (4.21) can be decomposed into three signals. The first one ( $\mathbf{M}^\circ \mathbf{v}$ ), visualized in Figures 4.18, 4.21 and 4.24 corresponds to the feedback control torque. The second one ( $\mathbf{D}_x^\circ \dot{\mathbf{q}}$ ) is a linearizing torque and is visualized in Figures 4.19, 4.22 and 4.25. The last one ( $\mathbf{D}_x^\circ \mathbf{x}_e + \hat{\boldsymbol{\tau}}_d$ ) can be interpreted as a generalized disturbance torque. It appears in Figures 4.20, 4.23 and 4.26. Since the joints velocities and mass to move are significantly



different during each of the considered tasks, it can be noted that disturbances differently impact the control performances. Thus an amplitude comparison between each signals allows to evaluate their influence on the system linearization quality.

First, considering each set of tasks  $\mathcal{T}_{2T}$ ,  $\mathcal{T}_{3T}$  and  $\mathcal{T}_{4T}$  individually and the different torques composing (4.21), one can note that similar control torques are developed for each task. More precisely, considering Figure 4.18 one will note similar amplitude of torques for each tasks in  $\mathcal{T}_{2T}$ . The same observations can be made for the linearization torques with Figure 4.19 and disturbance torques represented in Figure 4.20. Similarly for  $\mathcal{T}_{3T}$  and  $\mathcal{T}_{4T}$  the torques correspond for each tasks.

Concerning the feedback torques visualized in Figures 4.18, 4.21 and 4.24, this is explained by similar desired velocities and a common linear control gain,  $\mathbf{K}$ . Moreover, for the same motions the linearization torques, represented in Figures 4.19, 4.22 and 4.25, will provide comparable amplitudes. Additionally, the generalized disturbance torques plotted in Figures 4.20, 4.23 and 4.26, the similitude for each tasks can be interpreted by an identical estimation quality that persists through the scenario progression.

Then to evaluate the influence of each torque on the decoupling quality, one will simultaneously consider all the tasks simulated. This allows to compare different behaviors in function of system variations. Thus, the following discussions can be developed from the overall comparisons.

- Regarding the linearized torques and the feedback ones, a first observation on similar amplitudes can be made. For both set  $\mathcal{T}_{2T}$  and  $\mathcal{T}_{3T}$ , the linearized torques reach 10% of the feedback torques amplitudes, as illustrated comparing Figures 4.18 with 4.19 and Figures 4.21 with 4.22. For  $\mathcal{T}_{4T}$  the amplitudes are equivalent (i.e. 0.2Nm for the feedback torques and 0.1Nm for the linearized ones) as visualized with Figures 4.24 with 4.25. This first note simply highlight the interest of developing an NDI control scheme.
- Considering the linearized torques and generalized disturbances ones will allow to conclude on the interest to develop observers in the purpose of improving the system linearization and decoupling. Therefore, respectively comparing Figures 4.19 with 4.20, Figures 4.22 with 4.23 and Figures 4.25 with 4.26 one will note that the disturbance torques approximately reach 10% of the linearization torques. From this observation, two remarks can be developed. Firstly, such equivalent amplitudes indicate that the estimations provide useful information on the system linearization and decoupling. Secondly, as developed in the previous chapter, maintaining the base with a fixed attitude allows to reduce the impact of the internal disturbances and thus the amplitudes of the disturbance torques are minimized.
- A last observation can be made on the influence of the measurement errors on the base angular velocities. As a null base angular velocity is imposed with the use of reaction-wheels, one will note that for the considered sensors the noise has low effects on the disturbance torques as their amplitudes remain lower than those of the linearization

torques.

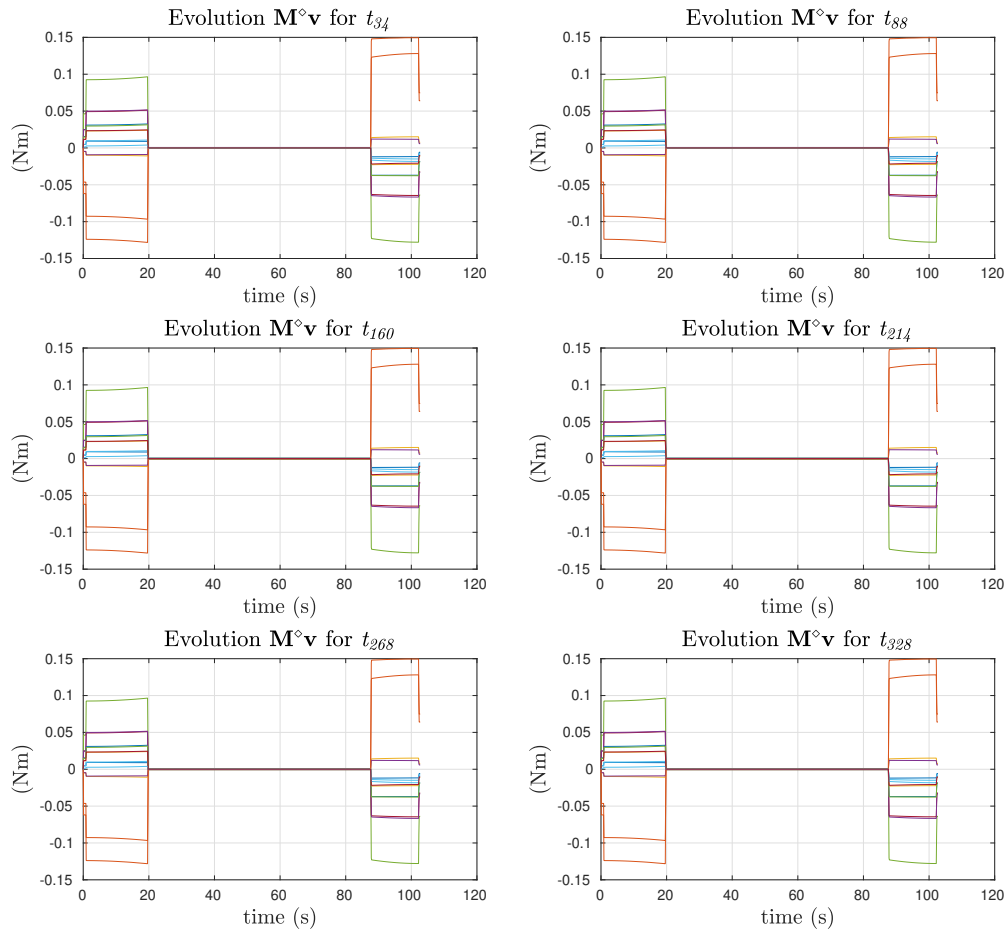


Figure 4.18 – Represent the feedback control torques  $(\mathbf{M}^\circ \mathbf{v})$  evolution for lower sub-figures illustrate the linearizing torques evolution for  $i \in \mathcal{T}_{2T}$

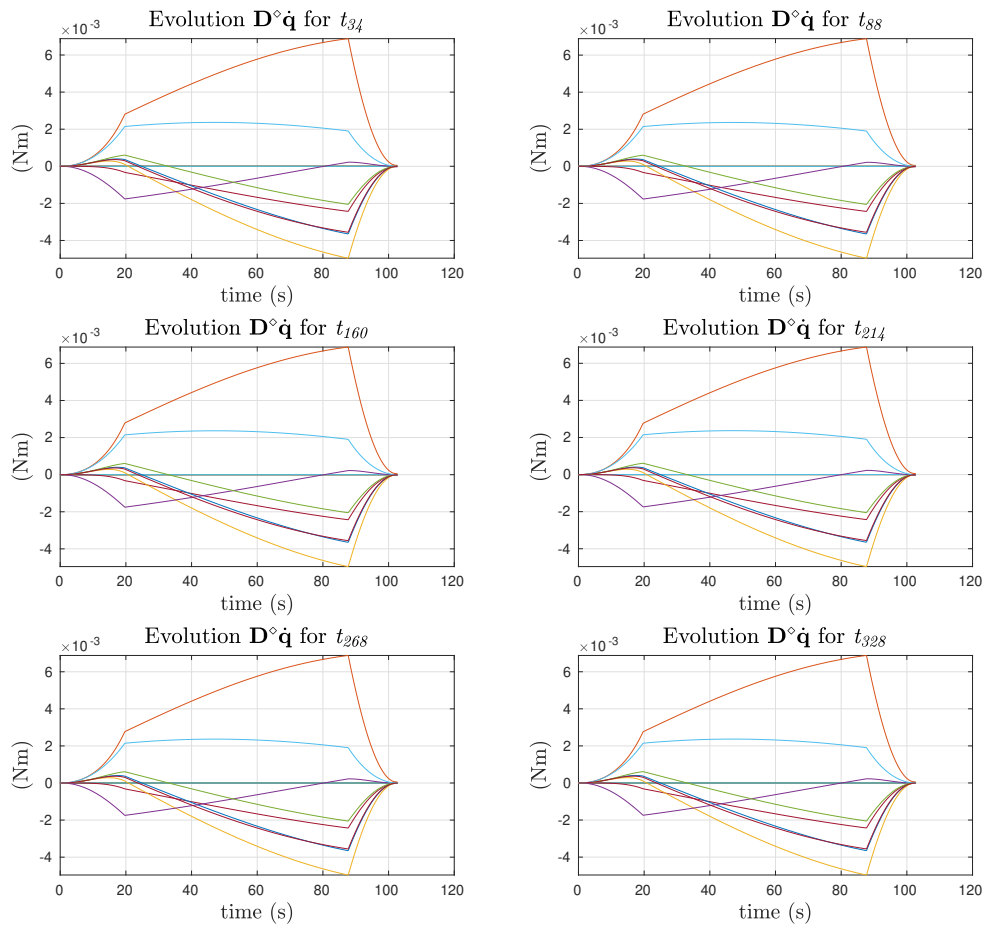


Figure 4.19 – Illustrate the linearizing torques  $(\mathbf{D}^\circ \dot{\mathbf{q}})$  evolution for  $t_i \in \mathcal{T}_{2T}$

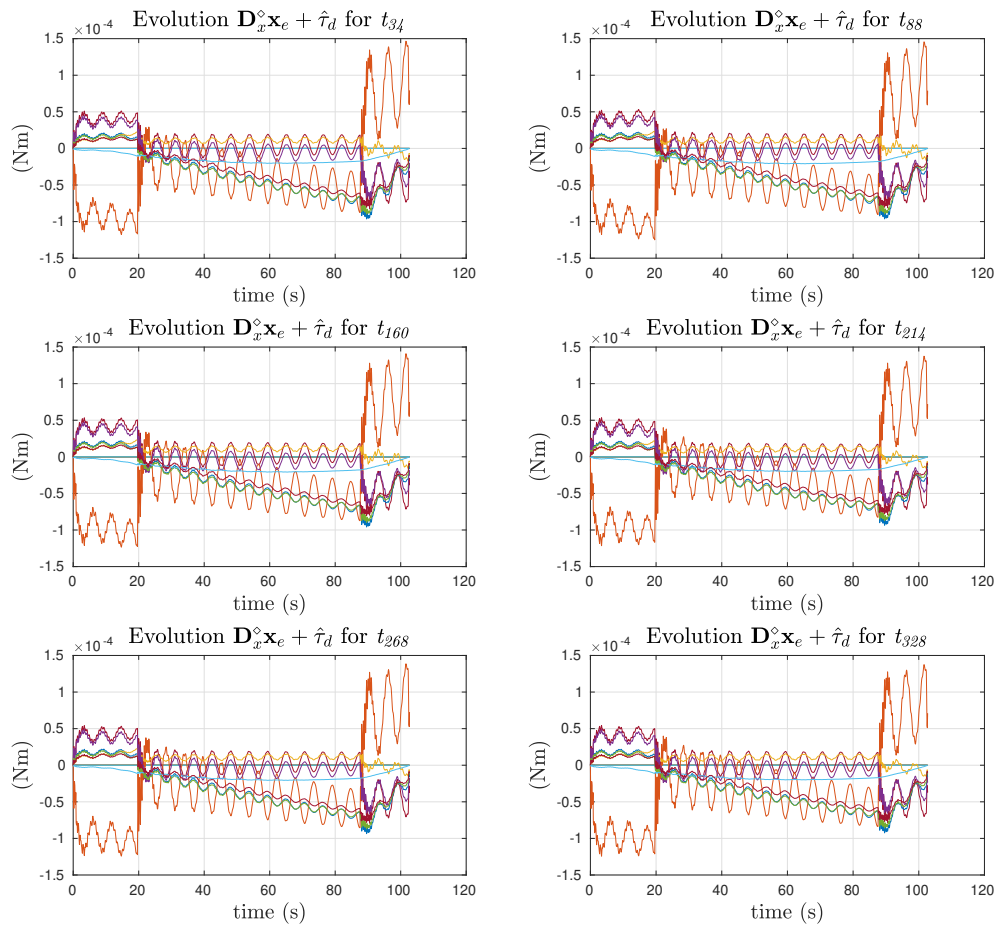


Figure 4.20 – Illustrate the evolution of the estimated disturbance torques ( $\mathbf{D}_x^\diamond \mathbf{x}_e + \hat{\tau}_d$ ) for  $\mathcal{T}_{2T}$

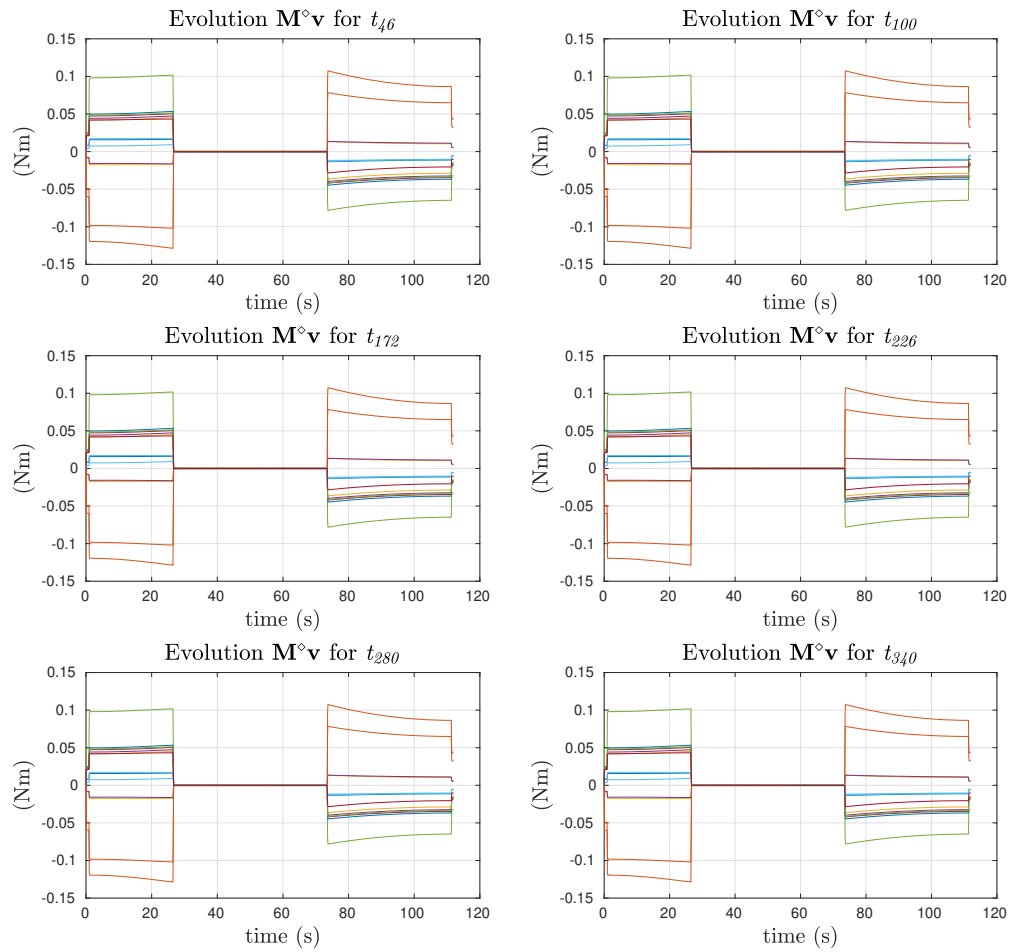


Figure 4.21 – Represent the feedback control torques ( $\mathbf{M}^\diamond \mathbf{v}$ ) evolution for  $i \in \mathcal{T}_{3T}$

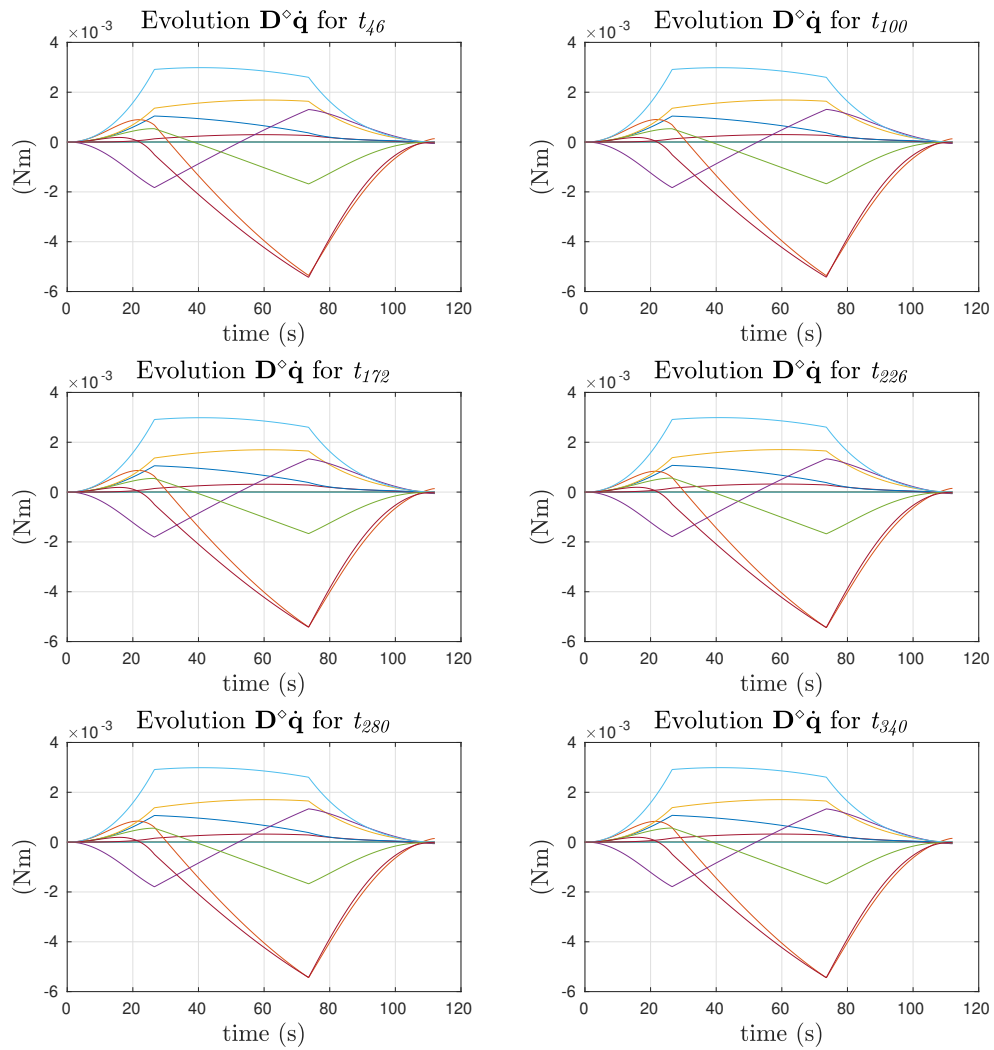


Figure 4.22 – Illustrate the linearizing torques  $(\mathbf{D}^\diamond \dot{\mathbf{q}})$  evolution for  $t_i \in \mathcal{T}_{3T}$

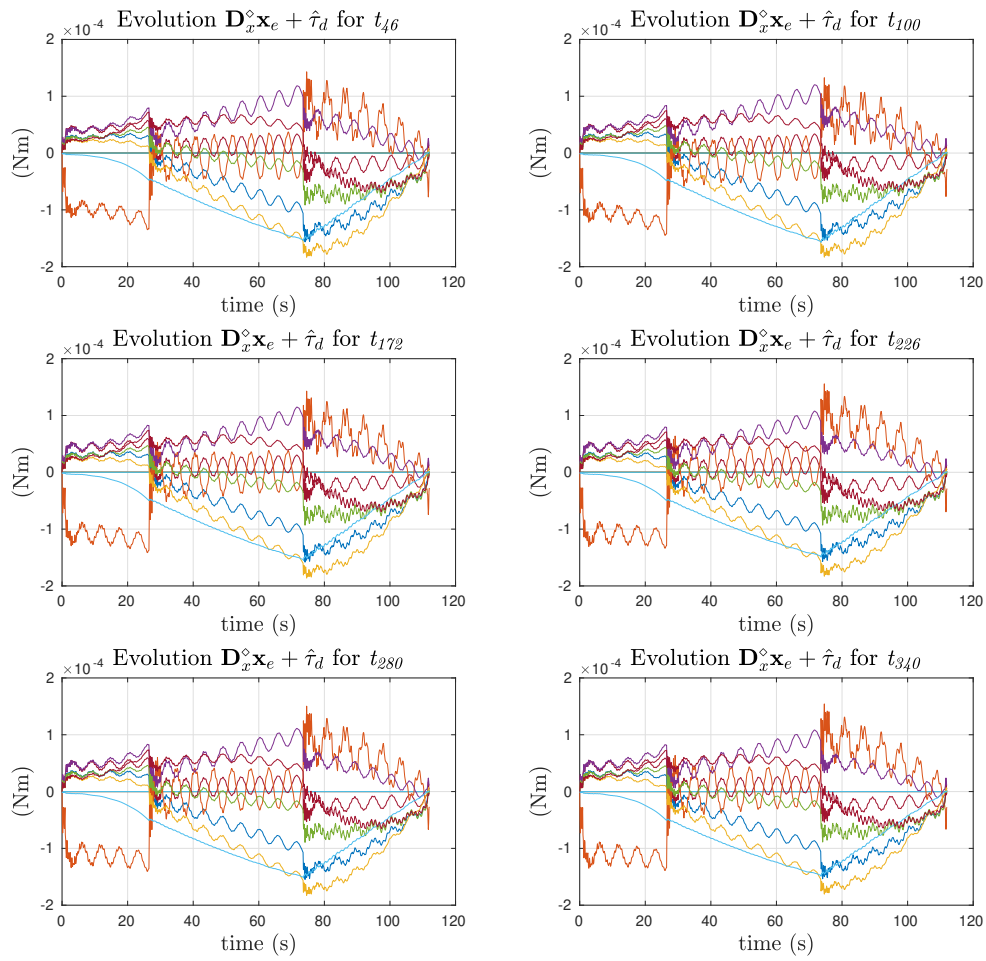


Figure 4.23 – Illustrate the evolution of the estimated disturbance torques  $(\mathbf{D}_x^\circ \mathbf{x}_e + \hat{\tau}_d)$  for  $\mathcal{T}_{3T}$

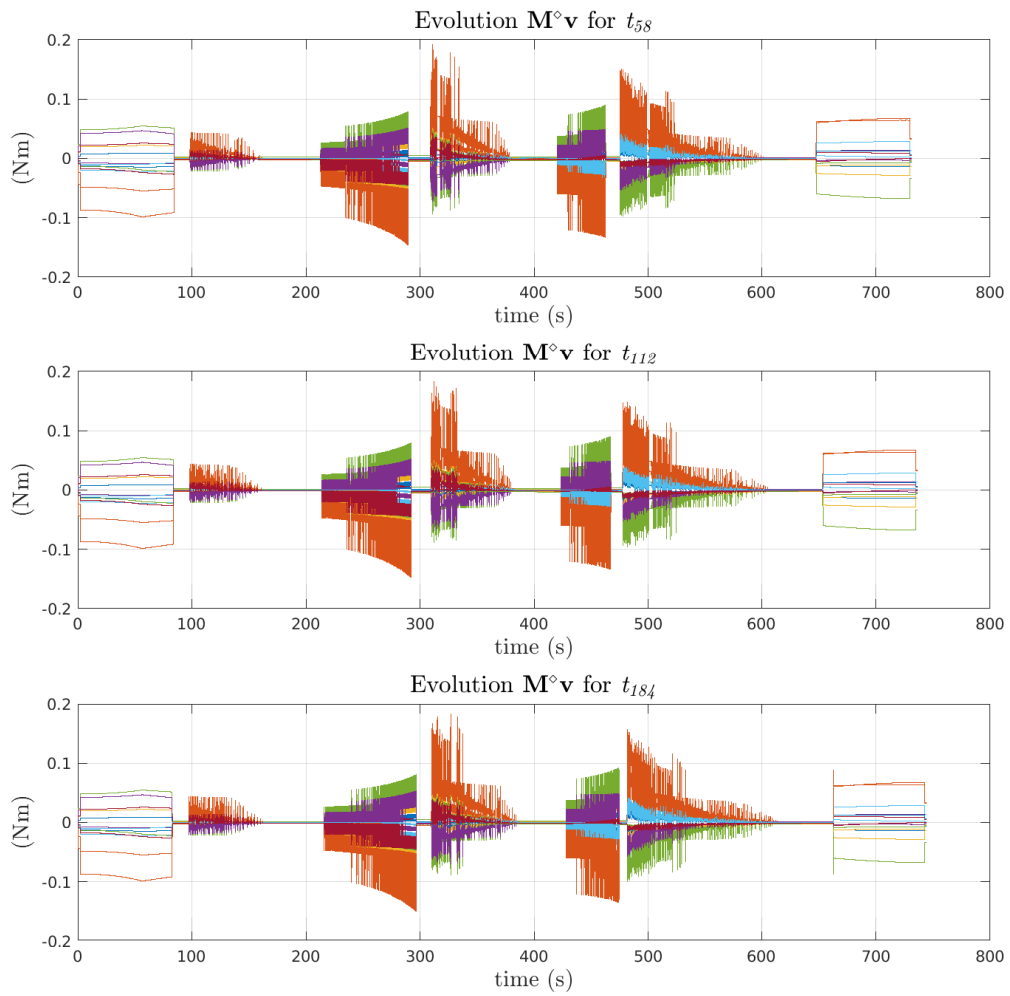


Figure 4.24 – Represent the feedback control torques  $(\mathbf{M}^\diamond \mathbf{v})$  evolution for  $i \in \mathcal{T}_{4T}$



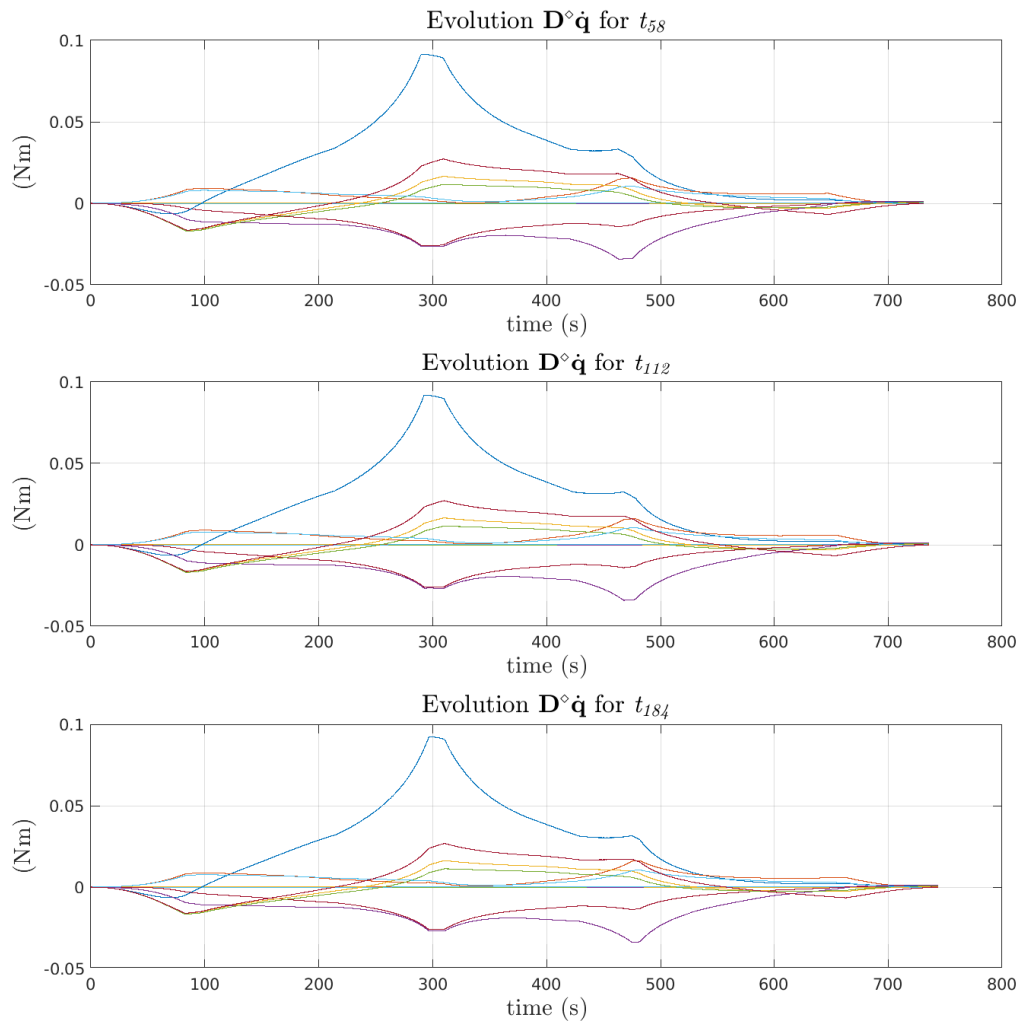


Figure 4.25 – Illustrate the linearizing torques  $(\mathbf{D}^\diamond \dot{\mathbf{q}})$  evolution for  $t_i \in \mathcal{T}_{4T}$

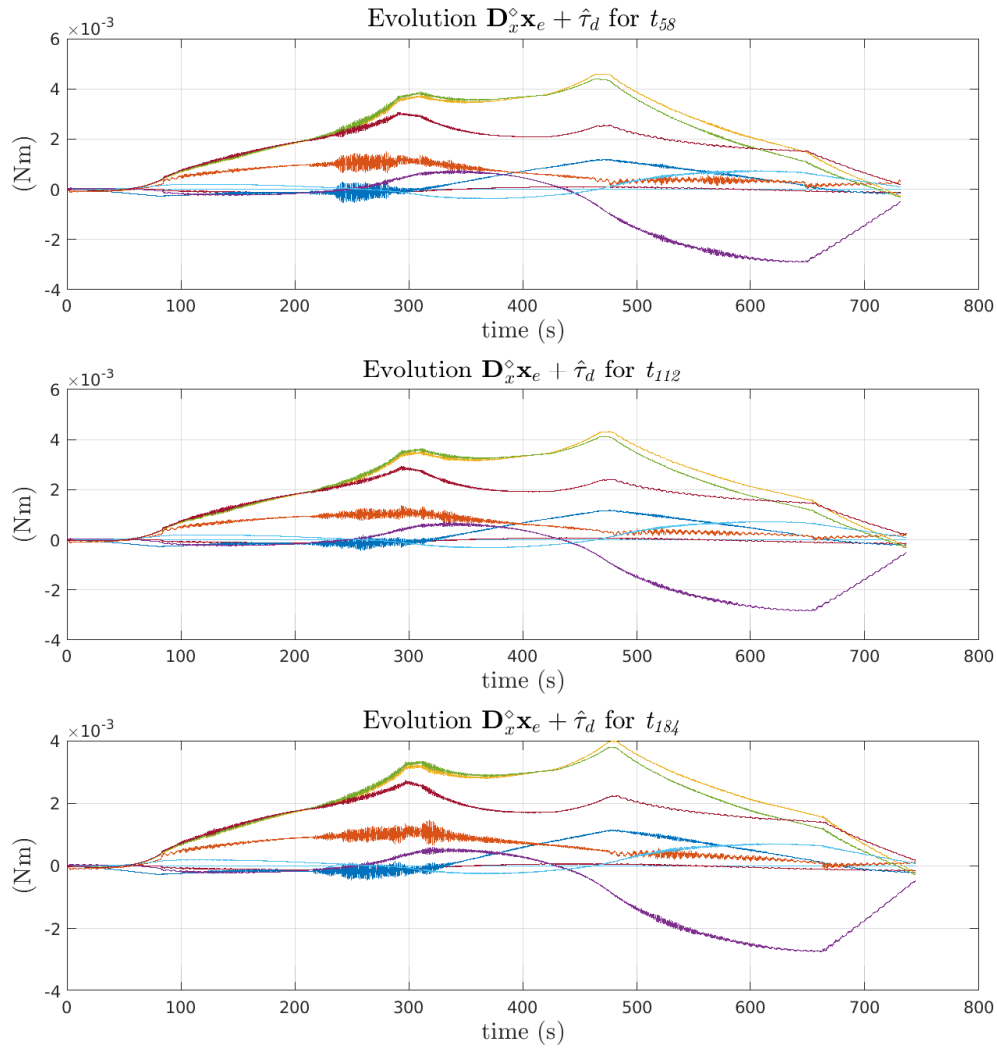


Figure 4.26 – Illustrate the evolution of the estimated disturbance torques ( $\mathbf{D}_x^\diamond \mathbf{x}_e + \hat{\tau}_d$ ) for  $\mathcal{T}_{4T}$

To emphasize on the generalized disturbance torques amplitudes, one can consider the evolution of the system internal disturbances from one side and then discuss on the quality of the estimation. First considering the evolution of the flexible mode velocities  $\dot{\boldsymbol{\eta}}$  visualized in Figures 4.27, 4.28 and 4.29 respectively for tasks in  $\mathcal{T}_{2T}$ ,  $\mathcal{T}_{3T}$  and  $\mathcal{T}_{4T}$ , one can observe small and reducing vibration amplitudes. This can be justified by the reaction-wheels control that successfully maintain the base at a null angular velocity.

Moreover, similarly to the gains synthesis developed in section 3.3.3, the one proposed in section 4.2.5 the NDI does not require a perfect estimation to adequately control the actuators. In addition to the difficulty of estimating the fastest flexible modes, the NDO also

present difficulties to properly estimate the disturbance torques as modeling errors are not quantifiable. For this reason, the synthesis offers flexibility on the tolerable amplitudes of observer errors' signals,  $\epsilon_e$  (4.17) and  $\epsilon_d$  (4.19). It is sufficient for these signals to be bounded to insure the stability and convergence of the closed-loop system.

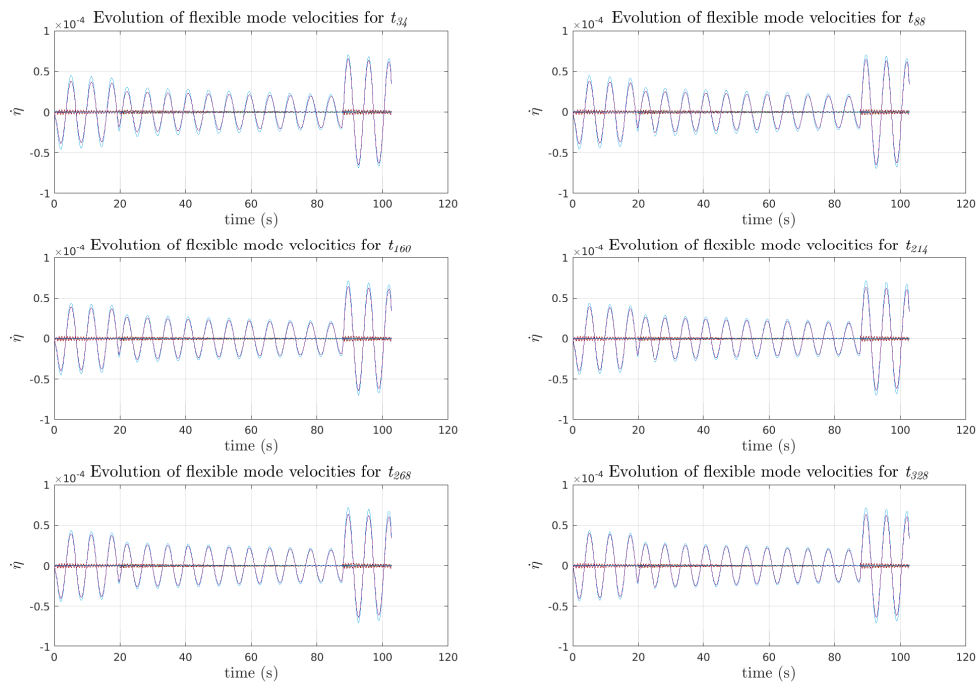


Figure 4.27 – Represent the evolution of the flexible mode velocities,  $\dot{\eta}$ , for  $\mathcal{T}_{2T}$

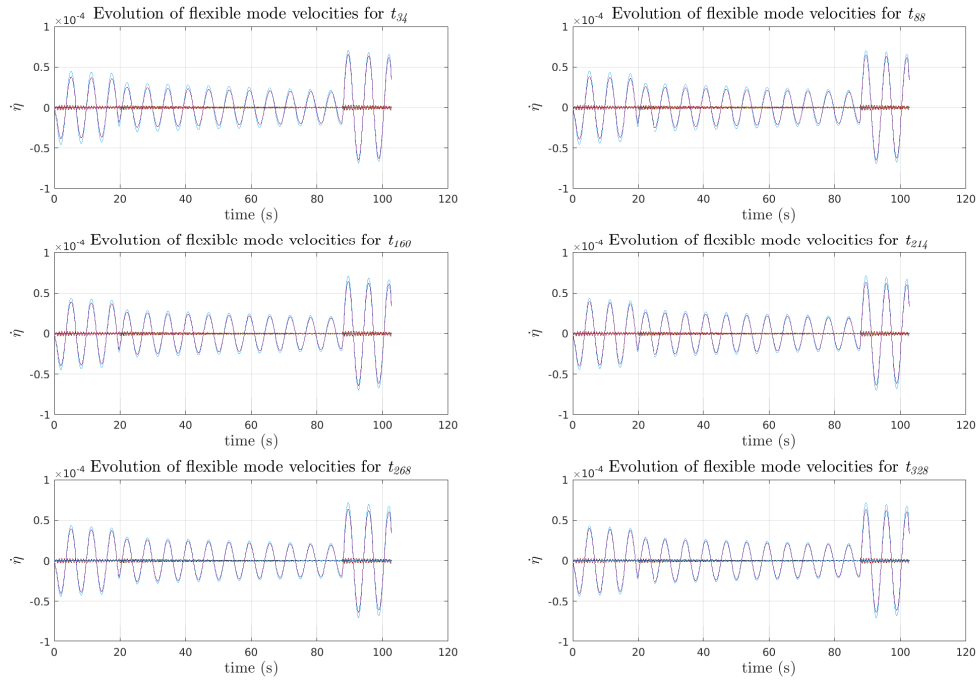


Figure 4.28 – Represent the evolution of the flexible mode velocities,  $\dot{\eta}$ , for  $\mathcal{T}_{3T}$

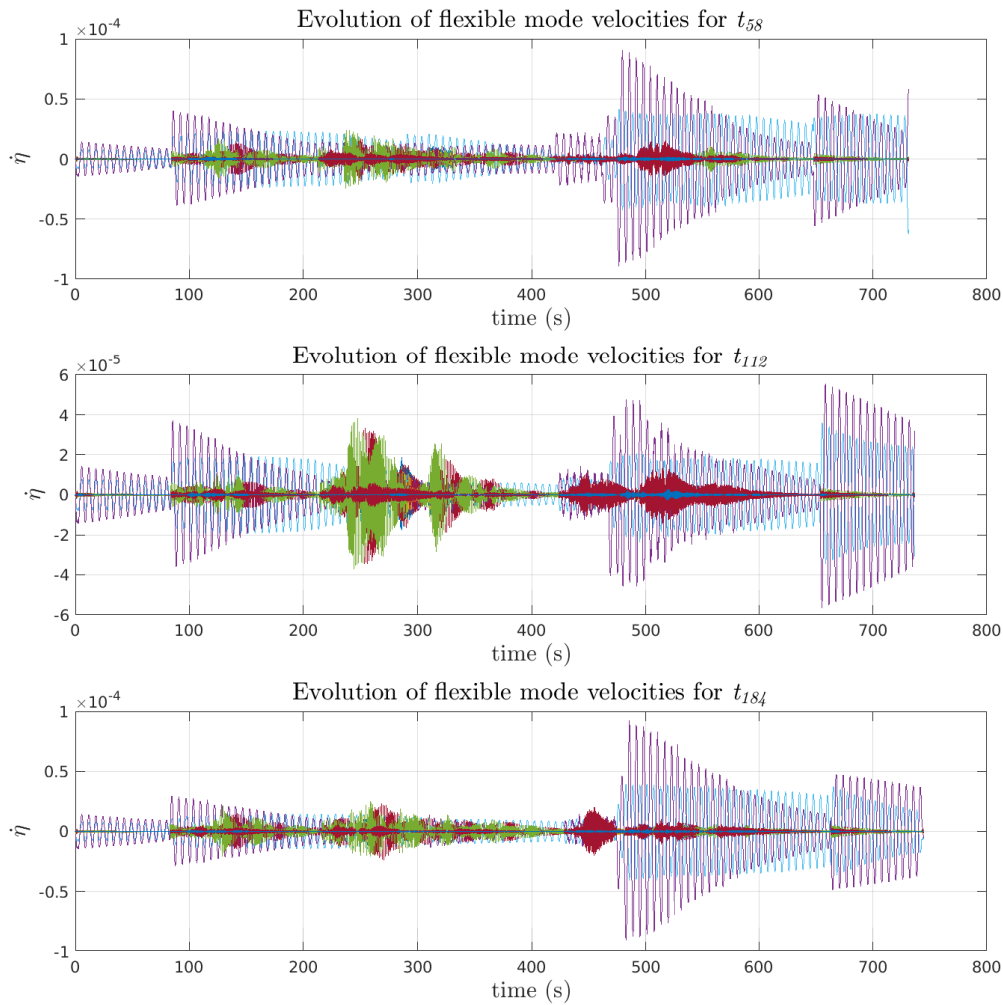


Figure 4.29 – Represent the evolution of the flexible mode velocities,  $\dot{\eta}$ , for  $\mathcal{T}_{4T}$

#### 4.4 Chapter conclusions

In this chapter, a novel robust joint-space control scheme has been introduced. Inspired by the control method developed in chapter 3, robust criteria have been considered to improve the joint-space control scheme. The focus has been made on modeling uncertainties, measurement errors, system variations and proceeding to various tasks. The NDI structure has been conserved with the inclusion of un-measured states thanks to an ESO. Additionally, the modeling and measurements errors have been tackled by expressing the equations of motions of a rotation-free-floating SMS with an external disturbance torque. With similar objectives than those developed for using an ESO, an NDO is designed to include an estimation of the

disturbance torques induced by modeling and measurement errors. Once again, the modeling work detailed in chapter 2 has been advantageously used in the design of the observers and the NDI.

After developing the overall design, a second contribution of this chapter is the common synthesis of the control and the two observers gains to satisfy precise control and disturbance rejections. The synthesis is based on a Lyapunov stability analysis and performed through an LMI resolution. An advantage of the synthesis is that it is developed for different workspaces without consideration of restrictive velocities as observed in the chapter 3. Furthermore, it is suitable to perform a wide range of tasks with an SMS in the way that significant variations of mass are considered on the base and at the end-effector.

Validation of the proposed method has been developed on an actual on-orbit deployment scenario that offers consequent system variations to validate the robustness and the interest of the control method. Therefore, the chapter provides a joint-space control scheme with a gains synthesis that allows to answer actual problematics of OOS. Extensive simulations have provided conclusive results. The significant modeling uncertainties have been successfully tackled thanks to the NDO. Some limits have been observed with the difficulty of imposing closed-loop dynamics with the LMI resolution. However, the general control performances show the effectiveness of the method and benefits of the common base and manipulator control in OOS operations.



# Conclusion and perspectives

**Contribution of the thesis:** Robotic systems have a key role to play in space exploitation and exploration. A SMS<sup>11</sup> presents multiple benefits in OOS<sup>12</sup> applications, such as the versatility in performing various tasks. Space manipulators provide the safest and more reliable solutions to deal with increasing debris number, structure too large to be self-deployed or satellite's life extension missions. As it can be illustrated with the Canadarms and their use to develop the MIR space station and the ISS<sup>13</sup>, their assistance to astronauts during extra-vehicular for the different Hubble Space Telescope's servicing missions or the recent use to inspect parts of the ISS. The complexity of operations lead to the necessity of improving the autonomous control of such a system to consider their use in the future space missions. In that purpose this thesis aims at providing autonomous control methods for OOS applications. Through the last thirty years, notable interests and advancements have been made to improve space robotics technologies but some challenges remains to tackle the new requirements that robotics are facing.

From the literature review, developed in chapter 1, the recent requirements for SMS are addressed. The main improvements identified are first the need to tackle system couplings to perform precise manipulator control. Then, for most of spacecrafts the presence of flexible appendages, such as solar arrays, sun-shields or even antennas, has led to new challenges in the improvement of control technologies. A requirement for establishing high accuracy modeling and simulation tools of a rigid-flexible SMS is made to design and validate new control strategies. Moreover, dealing with system physical properties variations has raised interest not only for ADR<sup>14</sup>, in which the manipulator is required to deal with external and additional forces/torques, but also to perform multi-tasks such as for an in-space assembly or deployment. In addition, the use of kinetic moment exchange devices to actively control the SMS' base has raised interest to increase the field of possible motions of the SMS.

In this thesis we aimed at developing modeling tools and control algorithm suitable to increase the autonomy of SMS.

In order to deal with the high control precision required to perform on-orbit manipulator's operations, a generic approach to derive accurate non-linear model of a free-floating SMS motions with flexible appendages have been developed. This contribution is detailed in chapter 2, which details its implementation as a Matlab toolbox. The modeling method, based on an adapted DH<sup>15</sup> formalism and with a Lagrangian approach, allows to recursively derive kinematic and dynamic models for a multi-body system with multiple kinematic chains and flexible elements attached to the common system's base. The relevance of this approach and the precision of the tools have been illustrated through extensive studies with (and without)

---

<sup>11</sup>Space Manipulator System

<sup>12</sup>On-Orbit Servicing

<sup>13</sup>International Space Station

<sup>14</sup>Active Debris Removal

<sup>15</sup>Denavit-Hartenberg



flexible appendages.

As mentioned in the literature review, few studies consider potential contribution of kinetic momentum exchange actuator available on the satellite base. Thus in chapter 3 to assess the interest to control such base's actuators when the manipulator performs some tasks, kinetic indices have been first introduced. They allow to develop quantitative analysis of the couplings existing between the manipulator's end-effector and the base's motions. As the couplings in SMS is the principal difficulty to develop autonomous control strategies, pre-designing an SMS with the help of these indices could benefit in future control applications. Moreover, the system analysis detailed in chapter 3, based on this indices and perform with the tools developed in chapter 2, led to the conclusion that a common base and manipulator control would be more efficient to achieve the expected tasks.

As the SMS' motions could lead to flexible appendage vibrations, the development of suitable control scheme to ensure system stability was another challenge of this thesis. This point was handle in the second part of the chapter 3 with the design of steering laws and joint controller of the base and the manipulator. The proposed control framework is based on an NDI<sup>16</sup> where an ESO<sup>17</sup> is introduced to perform an accurate system linearization. Its design is possible thanks to the non-trivial modeling developed in chapter 2. Additionally to the control scheme, the second contribution is the synthesis of both control and observer gains based on a Lyapunov stability proof and obtained from an LMI<sup>18</sup> resolution. The simulations of the controllers thus obtained highlight the interest of reaction-wheels to efficiently reject undesired flexible vibrations when the manipulator operates.

However, in order to be able to apply the solutions proposed above to real systems, it is necessary to first consider the robustness of the designed controller in a realistic scenario. Especially as NDI controller efficiency relies on the accuracy of its design model. Therefore, the control framework proposed has been extended in chapter 4 to deal with modeling uncertainties. It has been proposed to be tackled with a disturbance torque added to the overall SMS dynamic model. With the ambition to improve the system's decoupling quality and reject the modeling and measurement errors, an NDO<sup>19</sup> has been design to include a disturbance torque estimation in the NDI in addition to the flexibility estimation perform by the ESO.

Finally, the relevance of SMS resides in their ability to perform different complex tasks in a same mission. Thus, in chapter 4, the gains synthesis process has been also adapted to ensure the closed-loop system for a set of tasks. This synthesis is likewise based on a Lyapunov stability constraint leading to an LMI resolution. It includes robustness to system variations such that the SMS can perform different tasks from which its physical properties varies. Therefore, the contribution of chapter 4 is the overall control framework and design method to autonomously control an SMS that requires to deal with the current and future challenges of space exploitation and exploration. Extensive tests were developed in a realistic environment to perform a on-orbit space telescope assembly use-case highlighting the efficiency of the

---

<sup>16</sup>Nonlinear Dynamic Inversion

<sup>17</sup>Extended State Observer

<sup>18</sup>Linear Matrix Inequality

<sup>19</sup>Nonlinear Disturbance Observer

proposed method.

### Perspectives:

- After developing a rigid-flexible model of an SMS with a rigid manipulator, one could consider a flexible manipulator and extend the Lagrangian approach developed in chapter 2 such that junctions between a flexible element and another one (rigid or not) could have one DoF<sup>20</sup>. Flexible manipulators provides a means to absorb the contact in a capture of a target and thus brings new solutions in ADR [SGS18].
- Capitalizing on the robust joint-space control established in chapter 4, one could initiate task-space control strategies. With the rejection of intern disturbances, controlling the manipulator end-effector and the base developing assumptions on the behaviors of the joint-space inner loop control. Such method would benefits in capture scenarios as well as improving the precision of manipulator's operations [Gio+21]; [Pap+21].
- Some applications consider multi-manipulator robotic systems to benefit on the possibility of stabilizing the system with the unused manipulators while one manipulator operates [SGM20]. Further analysis on the contributions the manipulators' joints with the presence of reaction-wheels could be developed. Likewise, the consideration of closed-kinematic chains could provide interesting information preliminary to establish detumbling strategies.
- Concerning robust criteria, a drawback of the LMI resolution is the difficulty to consider actuators dynamics and adapt the closed-loop performances for a tight requirement list. With implementation purposes, further improvements of the approach could be investigated or compared with other synthesis methods, such as developing an  $\mathbf{H}_\infty$  synthesis. Moreover, another interesting robustness criterion to consider would be to deal with external forces/torques applying on the end-effector in order to initiate the control for capture applications.

---

<sup>20</sup>Degree of Freedom

**Publications:**

- Mathieu Rognant, Sofiane Kraïem, and Jurek Sasiadek. “Kinematic Indices of rotation-floating space robots for on-orbit servicing”. In: *IFTToMM World Congress on Mechanism and Machine Science*. Springer. 2019, pp. 3107–3116 (cit. on p. 82).
- Sofiane Kraïem, Mathieu Rognant, Jean-Marc Biannic, Yves Brière. “Control of rotation-floating space robots with flexible appendages for on-orbit servicing”. In: *2021 European Control Conference (ECC)*. IEEE. 2021, pp. 249–254 (cit. on p. 116).
- Sofiane Kraïem, Mathieu Rognant, Jean-Marc Biannic, Yves Brière. “Robust control of rotation-floating space robots with flexible appendages for on-orbit servicing”. In: *IFAC-PapersOnLine* 54.20 (2021), pp. 134–140 (cit. on p. 116).
- Sofiane Kraïem, Mathieu Rognant, Jean-Marc Biannic, Yves Brière. "Dynamics and Robust control of a rotation-free-floating space manipulator with flexible appendages for On-Orbit Servicing", submitted to the *International Journal of Robust and Nonlinear Control*

# Detail of Convective matrix evaluation

---

In this appendix, state-derivative expressions are given to detail the convective terms in (2.69). To conserve a general formalism the generalized joint-state variable,  $\mathbf{q} \in \mathbb{R}^{n_q \times 1}$ , defined as  $\mathbf{q} = [q_1 \ \dots \ q_{n_q}]$ , corresponds to the kinematic chain(s) DoF<sup>1</sup>s while  $\mathbf{x}_0 \in \mathbb{R}^{6 \times 1}$ , defined as  $\mathbf{x}_0 = [\theta_{0x} \ \theta_{0y} \ \theta_{0z} \ r_{0x} \ r_{0y} \ r_{0z}]^T$ , corresponds to the 6-DoFs of the base.

## A.1 Base-derivative of inertia matrices

In this section the following terms are detailed:

$$\left\{ \begin{array}{l} \mathbf{d}_0 = -\frac{1}{2} \frac{\partial}{\partial \mathbf{x}_0} \left( \mathbf{t}_0^T \mathbf{M}_0 + \dot{\mathbf{q}} \mathbf{M}_{0q}^T + \dot{\boldsymbol{\eta}} \mathbf{M}_{0\eta}^T \right) \quad (\text{A.1a}) \\ \mathbf{d}_{0q} = -\frac{1}{2} \frac{\partial}{\partial \mathbf{x}_0} \left( \dot{\mathbf{q}}^T \mathbf{M}_q + \mathbf{t}_0^T \mathbf{M}_{0q} \right) \quad (\text{A.1b}) \\ \mathbf{d}_{0\eta} = -\frac{1}{2} \frac{\partial}{\partial \mathbf{x}_0} \left( \mathbf{t}_0^T \mathbf{L}_{\eta p}^T \right) \quad (\text{A.1c}) \end{array} \right.$$

---

<sup>1</sup>Degree of Freedom

which can be developed as:

$$\left\{ \begin{array}{l}
 \mathbf{d}_0 = -\frac{1}{2} \begin{bmatrix}
 \mathbf{t}_0^T \frac{\partial}{\partial \theta_{0x}} (\mathbf{M}_0) + \dot{\mathbf{q}} \frac{\partial}{\partial \theta_{0x}} (\mathbf{M}_{0q}^T) + \dot{\eta} \frac{\partial}{\partial \theta_{0x}} (\mathbf{M}_{0\eta}^T) \\
 \mathbf{t}_0^T \frac{\partial}{\partial \theta_{0y}} (\mathbf{M}_0) + \dot{\mathbf{q}} \frac{\partial}{\partial \theta_{0y}} (\mathbf{M}_{0q}^T) + \dot{\eta} \frac{\partial}{\partial \theta_{0y}} (\mathbf{M}_{0\eta}^T) \\
 \mathbf{t}_0^T \frac{\partial}{\partial \theta_{0z}} (\mathbf{M}_0) + \dot{\mathbf{q}} \frac{\partial}{\partial \theta_{0z}} (\mathbf{M}_{0q}^T) + \dot{\eta} \frac{\partial}{\partial \theta_{0z}} (\mathbf{M}_{0\eta}^T) \\
 \mathbf{t}_0^T \frac{\partial}{\partial r_{0x}} (\mathbf{M}_0) + \dot{\mathbf{q}} \frac{\partial}{\partial r_{0x}} (\mathbf{M}_{0q}^T) + \dot{\eta} \frac{\partial}{\partial r_{0x}} (\mathbf{M}_{0\eta}^T) \\
 \mathbf{t}_0^T \frac{\partial}{\partial r_{0y}} (\mathbf{M}_0) + \dot{\mathbf{q}} \frac{\partial}{\partial r_{0y}} (\mathbf{M}_{0q}^T) + \dot{\eta} \frac{\partial}{\partial r_{0y}} (\mathbf{M}_{0\eta}^T) \\
 \mathbf{t}_0^T \frac{\partial}{\partial r_{0z}} (\mathbf{M}_0) + \dot{\mathbf{q}} \frac{\partial}{\partial r_{0z}} (\mathbf{M}_{0q}^T) + \dot{\eta} \frac{\partial}{\partial r_{0z}} (\mathbf{M}_{0\eta}^T)
 \end{bmatrix} \quad (\text{A.2a}) \\
 \\
 \mathbf{d}_{0q} = -\frac{1}{2} \begin{bmatrix}
 \dot{\mathbf{q}}^T \frac{\partial}{\partial \theta_{0x}} (\mathbf{M}_q) + \mathbf{t}_0^T \frac{\partial}{\partial \theta_{0x}} (\mathbf{M}_{0q}) \\
 \dot{\mathbf{q}}^T \frac{\partial}{\partial \theta_{0y}} (\mathbf{M}_q) + \mathbf{t}_0^T \frac{\partial}{\partial \theta_{0y}} (\mathbf{M}_{0q}) \\
 \dot{\mathbf{q}}^T \frac{\partial}{\partial \theta_{0z}} (\mathbf{M}_q) + \mathbf{t}_0^T \frac{\partial}{\partial \theta_{0z}} (\mathbf{M}_{0q}) \\
 \dot{\mathbf{q}}^T \frac{\partial}{\partial r_{0x}} (\mathbf{M}_q) + \mathbf{t}_0^T \frac{\partial}{\partial r_{0x}} (\mathbf{M}_{0q}) \\
 \dot{\mathbf{q}}^T \frac{\partial}{\partial r_{0z}} (\mathbf{M}_q) + \mathbf{t}_0^T \frac{\partial}{\partial r_{0y}} (\mathbf{M}_{0q}) \\
 \dot{\mathbf{q}}^T \frac{\partial}{\partial r_{0y}} (\mathbf{M}_q) + \mathbf{t}_0^T \frac{\partial}{\partial r_{0z}} (\mathbf{M}_{0q})
 \end{bmatrix} \quad (\text{A.2b}) \\
 \\
 \mathbf{d}_{0\eta} = -\frac{1}{2} \begin{bmatrix}
 \mathbf{t}_0^T \frac{\partial}{\partial \theta_{0x}} (\mathbf{L}_{\eta p}^T) \\
 \mathbf{t}_0^T \frac{\partial}{\partial \theta_{0y}} (\mathbf{L}_{\eta p}^T) \\
 \mathbf{t}_0^T \frac{\partial}{\partial \theta_{0z}} (\mathbf{L}_{\eta p}^T) \\
 \mathbf{t}_0^T \frac{\partial}{\partial r_{0x}} (\mathbf{L}_{\eta p}^T) \\
 \mathbf{t}_0^T \frac{\partial}{\partial r_{0y}} (\mathbf{L}_{\eta p}^T) \\
 \mathbf{t}_0^T \frac{\partial}{\partial r_{0z}} (\mathbf{L}_{\eta p}^T)
 \end{bmatrix} \quad (\text{A.2c})
 \end{array} \right.$$

With the expression of the inertia matrices (2.67) the time-derivative in function of  $x_{0l}$

( $l \in [1, 6]$ ) are given by:

$$\left\{ \begin{aligned} \frac{\partial}{\partial x_{0_l}} (\mathbf{M}_0) &= \begin{bmatrix} \frac{\partial}{\partial x_{0_l}} (\mathcal{I}_0) & \mathbf{0}_3 \\ \mathbf{0}_3 & \mathbf{0}_3 \end{bmatrix} + \sum_{i=1}^{n_q} \frac{\partial}{\partial x_{0_l}} (\mathbf{B}_{i0}^T) \begin{bmatrix} \mathcal{I}_i & \mathbf{0}_3 \\ \mathbf{0}_3 & m_i \mathbf{I}_3 \end{bmatrix} \mathbf{B}_{i0} \\ &+ \sum_{i=1}^{n_q} \mathbf{B}_{i0}^T \begin{bmatrix} \frac{\partial}{\partial x_{0_l}} (\mathcal{I}_i) & \mathbf{0}_3 \\ \mathbf{0}_3 & \mathbf{0}_3 \end{bmatrix} \mathbf{B}_{i0} + \sum_{i=1}^{n_q} \mathbf{B}_{i0}^T \begin{bmatrix} \mathcal{I}_i & \mathbf{0}_3 \\ \mathbf{0}_3 & m_i \mathbf{I}_3 \end{bmatrix} \frac{\partial}{\partial x_{0_l}} (\mathbf{B}_{i0}) \end{aligned} \right. \quad (\text{A.3a})$$

$$\left\{ \begin{aligned} &+ \frac{\partial}{\partial x_{0_l}} \left( \sum_{i=1}^{n_p} \mathbf{B}_{P_{f_i}0}^T \begin{bmatrix} \mathcal{I}_i & \mathbf{0}_3 \\ \mathbf{0}_3 & m_i \mathbf{I}_3 \end{bmatrix} \mathbf{B}_{P_{f_i}0} \right) \\ \frac{\partial}{\partial x_{0_l}} (\mathbf{M}_{0q}) &= \sum_{i=1}^{n_q} \frac{\partial}{\partial x_{0_l}} (\mathbf{B}_{i0}^T) \begin{bmatrix} \mathcal{I}_i & \mathbf{0}_3 \\ \mathbf{0}_3 & m_i \mathbf{I}_3 \end{bmatrix} \mathbf{J}_{m_i} + \sum_{i=1}^{n_q} \mathbf{B}_{i0}^T \begin{bmatrix} \frac{\partial}{\partial x_{0_l}} (\mathcal{I}_i) & \mathbf{0}_3 \\ \mathbf{0}_3 & \mathbf{0}_3 \end{bmatrix} \mathbf{J}_{m_i} \\ &+ \sum_{i=1}^{n_q} \mathbf{B}_{i0}^T \begin{bmatrix} \mathcal{I}_i & \mathbf{0}_3 \\ \mathbf{0}_3 & m_i \mathbf{I}_3 \end{bmatrix} \frac{\partial}{\partial x_{0_l}} (\mathbf{J}_{m_i}) \end{aligned} \right. \quad (\text{A.3b})$$

$$\left\{ \begin{aligned} \frac{\partial}{\partial x_{0_l}} (\mathbf{M}_q) &= \sum_{i=1}^{n_q} \frac{\partial}{\partial x_{0_l}} (\mathbf{J}_{m_i}^T) \begin{bmatrix} \mathcal{I}_i & \mathbf{0}_3 \\ \mathbf{0}_3 & m_i \mathbf{I}_3 \end{bmatrix} \mathbf{J}_{m_i} + \sum_{i=1}^{n_q} \mathbf{J}_{m_i}^T \begin{bmatrix} \frac{\partial}{\partial x_{0_l}} (\mathcal{I}_i) & \mathbf{0}_3 \\ \mathbf{0}_3 & \mathbf{0}_3 \end{bmatrix} \mathbf{J}_{m_i} \\ &+ \sum_{i=1}^{n_q} \mathbf{J}_{m_i}^T \begin{bmatrix} \mathcal{I}_i & \mathbf{0}_3 \\ \mathbf{0}_3 & m_i \mathbf{I}_3 \end{bmatrix} \frac{\partial}{\partial x_{0_l}} (\mathbf{J}_{m_i}) \end{aligned} \right. \quad (\text{A.3c})$$

**Inertia derivatives expressions:** The inertia matrices  $\mathcal{I}_0$  and  $\mathcal{I}_i$  are expressed in the inertial frame  $\mathcal{R}_{ine}^2$  as given by (2.10). With (2.8) and (2.9), one can detail the recursive expressions as:

$$\left\{ \begin{aligned} \mathcal{I}_0 &= \mathbf{R}_{\mathcal{A}_0} \mathcal{I}_{\mathcal{S}_0} \mathbf{R}_{\mathcal{A}_0}^T & (\text{A.4a}) \\ \mathcal{I}_i &= \mathbf{R}_{\mathcal{A}_0} \prod_{j=1}^i \mathbf{R}_{\mathcal{A}_j} \mathcal{I}_{\mathcal{S}_i} \left( \mathbf{R}_{\mathcal{A}_0} \prod_{j=1}^i \mathbf{R}_{\mathcal{A}_j} \right)^T & (\text{A.4b}) \end{aligned} \right.$$

This allows to expressed the following derivatives:

$$\left\{ \begin{aligned} \frac{\partial}{\partial x_{0_i}} (\mathcal{I}_0) &= \frac{\partial}{\partial x_{0_i}} (\mathbf{R}_{\mathcal{A}_0}) \mathcal{I}_{\mathcal{S}_0} \mathbf{R}_{\mathcal{A}_0}^T + \mathbf{R}_{\mathcal{A}_0} \mathcal{I}_{\mathcal{S}_0} \frac{\partial}{\partial x_{0_i}} (\mathbf{R}_{\mathcal{A}_0}^T) & (\text{A.5a}) \end{aligned} \right.$$

$$\left\{ \begin{aligned} \frac{\partial}{\partial x_{0_i}} (\mathcal{I}_i) &= \frac{\partial}{\partial x_{0_i}} (\mathbf{R}_{\mathcal{A}_0}) \prod_{j=1}^i \mathbf{R}_{\mathcal{A}_j} \mathcal{I}_{\mathcal{S}_i} \left( \prod_{j=1}^i \mathbf{R}_{\mathcal{A}_j} \right)^T \mathbf{R}_{\mathcal{A}_0}^T \\ &+ \mathbf{R}_{\mathcal{A}_0} \prod_{j=1}^i \mathbf{R}_{\mathcal{A}_j} \mathcal{I}_{\mathcal{S}_i} \left( \prod_{j=1}^i \mathbf{R}_{\mathcal{A}_j} \right)^T \frac{\partial}{\partial x_{0_i}} (\mathbf{R}_{\mathcal{A}_0}^T) \end{aligned} \right. \quad (\text{A.5b})$$

---

<sup>2</sup>Inertial frame

Therefore, the inertia derivative in function of a base state is reduced to the derivation of the rotation matrix  $\mathbf{R}_{\mathcal{A}_0}$ . This leads to  $\frac{\partial}{\partial r_{0x}}(\mathbf{R}_{\mathcal{A}_0}) = \frac{\partial}{\partial r_{0y}}(\mathbf{R}_{\mathcal{A}_0}) = \frac{\partial}{\partial r_{0z}}(\mathbf{R}_{\mathcal{A}_0}) = \mathbf{0}_3$  and with the Euler Angles rotation order given in (2.7) the derivative in function of the base attitude are:

$$\left\{ \begin{array}{l} \frac{\partial}{\partial \theta_{0x}}(\mathbf{R}_{\mathcal{A}_0}) = \\ \left[ \begin{array}{cc} 0 & c(\theta_{0z})s(\theta_{0y})c(\theta_{0x}) + s(\theta_{0z})s(\theta_{0x}) & -c(\theta_{0z})s(\theta_{0y})s(\theta_{0x}) \\ 0 & c(\theta_{0z})c(\theta_{0x}) + s(\theta_{0z})s(\theta_{0y})c(\theta_{0x}) & -c(\theta_{0z})c(\theta_{0x}) - s(\theta_{0z})s(\theta_{0y})s(\theta_{0x}) \\ 0 & c(\theta_{0y})c(\theta_{0x}) & -c(\theta_{0y})s(\theta_{0x}) \end{array} \right] \\ \frac{\partial}{\partial \theta_{0y}}(\mathbf{R}_{\mathcal{A}_0}) = \left[ \begin{array}{ccc} -c(\theta_{0z})s(\theta_{0y}) & c(\theta_{0z})c(\theta_{0y})s(\theta_{0x}) & s(\theta_{0z})c(\theta_{0y}) + c(\theta_{0z})c(\theta_{0y})c(\theta_{0x}) \\ -s(\theta_{0z})s(\theta_{0y}) & s(\theta_{0z})c(\theta_{0y})s(\theta_{0x}) & s(\theta_{0z})c(\theta_{0y})c(\theta_{0x}) \\ -c(\theta_{0y}) & -s(\theta_{0y})s(\theta_{0x}) & -s(\theta_{0y})c(\theta_{0x}) \end{array} \right] \\ \frac{\partial}{\partial \theta_{0z}}(\mathbf{R}_{\mathcal{A}_0}) = \\ \left[ \begin{array}{ccc} -s(\theta_{0z})c(\theta_{0y}) & -s(\theta_{0z})s(\theta_{0y})s(\theta_{0x}) - c(\theta_{0z})c(\theta_{0x}) & c(\theta_{0z})s(\theta_{0y}) - s(\theta_{0z})s(\theta_{0y})c(\theta_{0x}) \\ c(\theta_{0z})c(\theta_{0y}) & -s(\theta_{0z})s(\theta_{0x}) + c(\theta_{0z})s(\theta_{0y})s(\theta_{0x}) & s(\theta_{0z})s(\theta_{0x}) + c(\theta_{0z})s(\theta_{0y})c(\theta_{0x}) \\ 0 & 0 & 0 \end{array} \right] \end{array} \right.$$

with  $c(x)$  and  $s(x)$  respectively corresponding to  $\cos(x)$  and  $\sin(x)$ .

**$\mathbf{B}_{i0}$  derivative expression:** Considering  $\mathbf{r}_{\mathcal{S}_i}$  with  $i \in [1, n_q]$ , the matrix  $\mathbf{B}_{i0}$  (2.15) only depends on the position of the solid  $\mathcal{S}_i$  in the inertial frame. Thus,  $\frac{\partial}{\partial r_{0x}}(\mathbf{B}_{i0}) = \frac{\partial}{\partial \theta_{0y}}(\mathbf{B}_{i0}) =$

$\frac{\partial}{\partial \theta_{0z}}(\mathbf{B}_{i0}) = \mathbf{0}_3$  and:

$$\frac{\partial}{\partial r_{0x}}(\mathbf{B}_{i0}) = \begin{bmatrix} \mathbf{0}_3 & \mathbf{0}_3 \\ \begin{bmatrix} 0 & 0 & 0 \\ 0 & 0 & -1 \\ 0 & 1 & 0 \end{bmatrix} & \mathbf{0}_3 \end{bmatrix} \quad (\text{A.7a})$$

$$\frac{\partial}{\partial r_{0x}}(\mathbf{B}_{i0}) = \begin{bmatrix} \mathbf{0}_3 & \mathbf{0}_3 \\ \begin{bmatrix} 0 & 0 & 1 \\ 0 & 0 & 0 \\ -1 & 0 & 0 \end{bmatrix} & \mathbf{0}_3 \end{bmatrix} \quad (\text{A.7b})$$

$$\frac{\partial}{\partial r_{0x}}(\mathbf{B}_{i0}) = \begin{bmatrix} \mathbf{0}_3 & \mathbf{0}_3 \\ \begin{bmatrix} 0 & 1 & 0 \\ -1 & 0 & 0 \\ 0 & 0 & 0 \end{bmatrix} & \mathbf{0}_3 \end{bmatrix} \quad (\text{A.7c})$$

**$\mathbf{J}_{m_i}$  derivative expression:** With (2.18), the expression of the Jacobian matrix  $\mathbf{J}_{m_i}$  is given  $\forall i \in [1, n_q]$  by:

$$\mathbf{J}_{m_i} = \left[ \mathbf{B}_{i1} \mathbf{p}_{m_1} \quad \dots \quad \mathbf{B}_{i(i-1)} \mathbf{p}_{m_{i-1}} \quad \mathbf{p}_{m_i} \mathbf{0}_{6 \times (n_q - 1)} \right] \quad (\text{A.8})$$

As only  $\mathbf{p}_{m_l}$  ( $l \in [1, i]$ ) depends on the base state,  $\frac{\partial}{\partial x_{0_i}} (\mathbf{B}_{il}) = \mathbf{0}_6$  and thus:

$$\frac{\partial}{\partial x_{0_i}} (\mathbf{J}_{m_i}) = \left[ \mathbf{B}_{i1} \frac{\partial}{\partial x_{0_i}} (\mathbf{p}_{m_1}) \quad \dots \quad \mathbf{B}_{i(i-1)} \frac{\partial}{\partial x_{0_i}} (\mathbf{p}_{m_{i-1}}) \quad \frac{\partial}{\partial x_{0_i}} (\mathbf{p}_{m_i}) \quad \mathbf{0}_{6 \times (n_q - i)} \right] \quad (\text{A.9})$$

Then two cases are considered, either the  $\mathcal{S}_l$  and  $\mathcal{S}_i$  are in the same kinematic chain or not. If they are, then:

$$\frac{\partial}{\partial x_{0_i}} (\mathbf{p}_{m_l}) = \left[ \begin{array}{c} \frac{\partial}{\partial x_{0_i}} (\mathbf{k}_l) \\ \frac{\partial}{\partial x_{0_i}} (\mathbf{k}_l^\times) (\mathbf{r}_{\mathcal{S}_i} - \mathbf{r}_{\mathcal{A}_l}) \end{array} \right] \quad (\text{A.10})$$

and if not:

$$\frac{\partial}{\partial x_{0_i}} (\mathbf{p}_{m_l}) = \left[ \begin{array}{c} \mathbf{0}_{3 \times 1} \\ \frac{\partial}{\partial x_{0_i}} (\mathbf{k}_l) \end{array} \right] \quad (\text{A.11})$$

With the recursive expression of  $\mathbf{k}_l$  (2.9), its derivative expression is given by:

$$\frac{\partial}{\partial x_{0_i}} (\mathbf{k}_l) = \frac{\partial}{\partial x_{0_i}} (\mathbf{R}_{\mathcal{A}_0}) \prod_{j=1}^l \mathbf{R}_{\mathcal{A}_j} \begin{bmatrix} 0 \\ 0 \\ 1 \end{bmatrix} \quad (\text{A.12})$$

with the detail of  $\frac{\partial}{\partial x_{0_i}} (\mathbf{R}_{\mathcal{A}_0})$  given in the previous section.

## A.2 Joint-derivative of inertia matrices

In this section the following terms are detailed:

$$\left\{ \mathbf{d}_{q0} = -\frac{1}{2} \frac{\partial}{\partial \mathbf{q}} (\mathbf{t}_0^T \mathbf{M}_0 + \dot{\mathbf{q}} \mathbf{M}_{0q}^T) \right. \quad (\text{A.13a})$$

$$\left. \mathbf{d}_q = -\frac{1}{2} \frac{\partial}{\partial \mathbf{q}} (\dot{\mathbf{q}}^T \mathbf{M}_q + \mathbf{t}_0^T \mathbf{M}_{0q}) \right. \quad (\text{A.13b})$$



Both convective terms can be developed as:

$$\mathbf{d}_{q0} = -\frac{1}{2} \begin{bmatrix} \mathbf{t}_0^T \frac{\partial}{\partial \mathbf{q}_1} (\mathbf{M}_0) + \dot{\mathbf{q}} \frac{\partial}{\partial q_1} (\mathbf{M}_{0q}^T) \\ \vdots \\ \mathbf{t}_0^T \frac{\partial}{\partial q_{n_q}} (\mathbf{M}_0) + \dot{\mathbf{q}} \frac{\partial}{\partial q_{n_q}} (\mathbf{M}_{0q}^T) \end{bmatrix} \quad (\text{A.14a})$$

$$\mathbf{d}_q = -\frac{1}{2} \begin{bmatrix} \dot{\mathbf{q}}^T \frac{\partial}{\partial q_1} (\mathbf{M}_q) + \mathbf{t}_0^T \frac{\partial}{\partial q_1} (\mathbf{M}_{0q}) \\ \vdots \\ \dot{\mathbf{q}}^T \frac{\partial}{\partial q_{n_q}} (\mathbf{M}_q) + \mathbf{t}_0^T \frac{\partial}{\partial q_{n_q}} (\mathbf{M}_{0q}) \end{bmatrix} \quad (\text{A.14b})$$

where,  $\forall l \in [1, n_q]$ :

$$\begin{aligned} \frac{\partial}{\partial q_l} (\mathbf{M}_0) &= \sum_{i=1}^{n_q} \frac{\partial}{\partial q_l} (\mathbf{B}_{i0}^T) \begin{bmatrix} \mathcal{I}_i & \mathbf{0}_3 \\ \mathbf{0}_3 & m_i \mathbf{I}_3 \end{bmatrix} \mathbf{B}_{i0} + \sum_{i=1}^{n_q} \mathbf{B}_{i0}^T \begin{bmatrix} \frac{\partial}{\partial q_l} (\mathcal{I}_i) & \mathbf{0}_3 \\ \mathbf{0}_3 & \mathbf{0}_3 \end{bmatrix} \mathbf{B}_{i0} \\ &+ \sum_{i=1}^{n_q} \mathbf{B}_{i0}^T \begin{bmatrix} \mathcal{I}_i & \mathbf{0}_3 \\ \mathbf{0}_3 & m_i \mathbf{I}_3 \end{bmatrix} \frac{\partial}{\partial q_l} (\mathbf{B}_{i0}) \\ &+ \frac{\partial}{\partial q_l} \left( \sum_{i=1}^{n_p} \mathbf{B}_{P_{f_i}0}^T \begin{bmatrix} \mathcal{I}_i & \mathbf{0}_3 \\ \mathbf{0}_3 & m_i \mathbf{I}_3 \end{bmatrix} \mathbf{B}_{P_{f_i}0} \right) \end{aligned} \quad (\text{A.15a})$$

$$\begin{aligned} \frac{\partial}{\partial q_l} (\mathbf{M}_{0q}) &= \sum_{i=1}^{n_q} \frac{\partial}{\partial q_l} (\mathbf{B}_{i0}^T) \begin{bmatrix} \mathcal{I}_i & \mathbf{0}_3 \\ \mathbf{0}_3 & m_i \mathbf{I}_3 \end{bmatrix} \mathbf{J}_{m_i} + \sum_{i=1}^{n_q} \mathbf{B}_{i0}^T \begin{bmatrix} \frac{\partial}{\partial q_l} (\mathcal{I}_i) & \mathbf{0}_3 \\ \mathbf{0}_3 & \mathbf{0}_3 \end{bmatrix} \mathbf{J}_{m_i} \\ &+ \sum_{i=1}^{n_q} \mathbf{B}_{i0}^T \begin{bmatrix} \mathcal{I}_i & \mathbf{0}_3 \\ \mathbf{0}_3 & m_i \mathbf{I}_3 \end{bmatrix} \frac{\partial}{\partial q_l} (\mathbf{J}_{m_i}) \end{aligned} \quad (\text{A.15b})$$

$$\begin{aligned} \frac{\partial}{\partial q_l} (\mathbf{M}_q) &= \sum_{i=1}^{n_q} \frac{\partial}{\partial q_l} (\mathbf{J}_{m_i}^T) \begin{bmatrix} \mathcal{I}_i & \mathbf{0}_3 \\ \mathbf{0}_3 & m_i \mathbf{I}_3 \end{bmatrix} \mathbf{J}_{m_i} + \sum_{i=1}^{n_q} \mathbf{J}_{m_i}^T \begin{bmatrix} \frac{\partial}{\partial q_l} (\mathcal{I}_i) & \mathbf{0}_3 \\ \mathbf{0}_3 & \mathbf{0}_3 \end{bmatrix} \mathbf{J}_{m_i} \\ &+ \sum_{i=1}^{n_q} \mathbf{J}_{m_i}^T \begin{bmatrix} \mathcal{I}_i & \mathbf{0}_3 \\ \mathbf{0}_3 & m_i \mathbf{I}_3 \end{bmatrix} \frac{\partial}{\partial q_l} (\mathbf{J}_{m_i}) \end{aligned} \quad (\text{A.15c})$$

In order to maintain the generality, the transformation matrix  $\mathbf{T}_{\mathcal{A}_i, \mathcal{R}_{ine}}$  is differentiated with the recursive relation (2.8) re-written with (2.3)  $\forall l, i \in [1, n_q]$  as:

$$\mathbf{T}_{\mathcal{A}_i, \mathcal{R}_{ine}} = \mathbf{T}_{\mathcal{A}_{l-1}, \mathcal{R}_{ine}} \begin{bmatrix} c(\theta_l) & -c(\alpha_l)s(\theta_l) & s(\alpha_l)s(\theta_l) & a_l c(\theta_l) \\ s(\theta_l) & c(\theta_l)c(\alpha_l) & -c(\theta_l)s(\alpha_l) & a_l s(\theta_l) \\ 0 & s(\alpha_l) & c(\alpha_l) & d_l \\ 0 & 0 & 0 & 1 \end{bmatrix} \prod_{j=l+1}^i \mathbf{T}_{\mathcal{A}_{j-1}, \mathcal{A}_j} \quad (\text{A.16})$$

According to the nature of the joints, the differentiation of  $\mathbf{T}_{\mathcal{A}_i, \mathcal{R}_{ine}}$  according to  $q_l \forall l \in [1, i]$

and  $\forall i \in [1, n_q]$  is given by:

- If the  $l^{th}$  joint is prismatic, then:

$$\frac{\partial}{\partial \mathbf{q}_l} (\mathbf{T}_{\mathcal{A}_i, \mathcal{R}_{ine}}) = \mathbf{T}_{\mathcal{A}_{l-1}, \mathcal{R}_{ine}} \begin{bmatrix} 0 & 0 & 0 & 0 \\ 0 & 0 & 0 & 0 \\ 0 & 0 & 0 & 1 \\ 0 & 0 & 0 & 0 \end{bmatrix} \prod_{j=l+1}^i \mathbf{T}_{\mathcal{A}_{j-1}, \mathcal{A}_j} \quad (\text{A.17})$$

- If the  $l^{th}$  joint is revolute then  $\forall l \in [1, i]$ :

$$\begin{aligned} & \frac{\partial}{\partial \mathbf{q}_l} (\mathbf{T}_{\mathcal{A}_i, \mathcal{R}_{ine}}) \\ &= \mathbf{T}_{\mathcal{A}_{l-1}, \mathcal{R}_{ine}} \begin{bmatrix} -s(q_l) & -c(\alpha_l)c(q_l) & s(\alpha_l)c(q_l) & -a_l s(q_l) \\ c(q_l) & -s(q_l)c(\alpha_l) & -s(q_l)s(\alpha_l) & a_l c(q_l) \\ 0 & 0 & 0 & 0 \\ 0 & 0 & 0 & 0 \end{bmatrix} \prod_{j=l+1}^i \mathbf{T}_{\mathcal{A}_{j-1}, \mathcal{A}_j} \end{aligned} \quad (\text{A.18})$$

If  $l > i$ :

$$\frac{\partial}{\partial \mathbf{q}_l} (\mathbf{T}_{\mathcal{A}_i, \mathcal{R}_{ine}}) = \mathbf{0}_4 \quad (\text{A.19})$$

Thus,  $\forall l \in [1, n_q]$ :

$$\frac{\partial}{\partial \mathbf{q}_l} (\mathbf{T}_{\mathcal{A}_i, \mathcal{R}_{ine}}) = \begin{bmatrix} \frac{\partial \mathbf{R}_{\mathcal{A}_i, \mathcal{R}_{ine}}}{\partial \mathbf{q}_l} & \frac{\partial \mathbf{r}_{\mathcal{A}_i}}{\partial \mathbf{q}_l} \\ \mathbf{0}_{1 \times 3} & 0 \end{bmatrix} \quad (\text{A.20})$$

With (2.8), the differentiation of  $\mathbf{T}_{\mathcal{S}_i, \mathcal{R}_{ine}}$  is given by:

$$\frac{\partial}{\partial \mathbf{q}_l} (\mathbf{T}_{\mathcal{S}_i, \mathcal{R}_{ine}}) = \frac{\partial}{\partial \mathbf{q}_l} (\mathbf{T}_{\mathcal{A}_i, \mathcal{R}_{ine}}) \mathbf{T}_{\mathcal{A}_i, \mathcal{S}_i} + \mathbf{T}_{\mathcal{A}_i, \mathcal{R}_{ine}} \frac{\partial}{\partial \mathbf{q}_l} (\mathbf{T}_{\mathcal{A}_i, \mathcal{S}_i}) \quad (\text{A.21})$$

where:

$$\begin{aligned} \frac{\partial}{\partial \mathbf{q}_l} (\mathbf{T}_{\mathcal{A}_i, \mathcal{S}_i}) &= \frac{\partial}{\partial \mathbf{q}_l} \left( \begin{bmatrix} \mathbf{R}_{\mathcal{A}_i} & (\mathbf{r}_{\mathcal{S}_i} - \mathbf{r}_{\mathcal{A}_i}) \\ \mathbf{0}_{1 \times 3} & 1 \end{bmatrix} \right) \\ &= \begin{bmatrix} \frac{\partial}{\partial \mathbf{q}_l} (\mathbf{R}_{\mathcal{A}_i}) & \frac{\partial}{\partial \mathbf{q}_l} ((\mathbf{r}_{\mathcal{S}_i} - \mathbf{r}_{\mathcal{A}_i})) \\ \mathbf{0}_{1 \times 3} & 0 \end{bmatrix} \end{aligned} \quad (\text{A.22})$$

without detailing the differentiation of the matrix  $\mathbf{T}_{\mathcal{A}_i, \mathcal{S}_i}$  depends on the nature of joints and can be expressed as:

$$\frac{\partial}{\partial \mathbf{q}_l} (\mathbf{T}_{\mathcal{S}_i, \mathcal{R}_{ine}}) = \begin{bmatrix} \frac{\partial}{\partial \mathbf{q}_l} (\mathbf{R}_{\mathcal{S}_i, \mathcal{R}_{ine}}) & \frac{\partial}{\partial \mathbf{q}_l} (\mathbf{r}_{\mathcal{S}_i}) \\ \mathbf{0}_{3 \times 1} & 0 \end{bmatrix} \quad (\text{A.23})$$

**Inertia derivatives expressions:** With the recursive expression of inertias expressed in  $\mathcal{R}_{ine}$  (A.4), the derivatives in function of  $q_l \forall l \in [1, n_q]$  are given by:

$$\begin{aligned} \frac{\partial}{\partial q_l} (\mathcal{I}_i) &= \mathbf{R}_{\mathcal{A}_0} \frac{\partial}{\partial q_l} \left( \prod_{j=1}^i \mathbf{R}_{\mathcal{A}_j} \right) \mathcal{I}_{\mathcal{S}_i} \left( \prod_{j=1}^i \mathbf{R}_{\mathcal{A}_j} \right)^T \mathbf{R}_{\mathcal{A}_0}^T \\ &+ \mathbf{R}_{\mathcal{A}_0} \prod_{j=1}^i \mathbf{R}_{\mathcal{A}_j} \mathcal{I}_{\mathcal{S}_i} \frac{\partial}{\partial q_l} \left( \left( \prod_{j=1}^i \mathbf{R}_{\mathcal{A}_j} \right)^T \right) \mathbf{R}_{\mathcal{A}_0}^T \end{aligned} \quad (\text{A.24})$$

with the differentiation of  $\prod_{j=1}^i \mathbf{R}_{\mathcal{A}_j}$  previously detailed to obtain (A.20).

**$\mathbf{B}_{i0}$  derivatives expression:**

$$\mathbf{B}_{i0} = \begin{bmatrix} \mathbf{0}_3 & \mathbf{0}_3 \\ \left( \frac{\partial (\mathbf{r}_{\mathcal{S}_i} - \mathbf{r}_{\mathcal{S}_0})}{\partial \mathbf{q}_l} \right)^\times & \mathbf{0}_{3 \times 1} \end{bmatrix} = \begin{bmatrix} \mathbf{0}_3 & \mathbf{0}_3 \\ \left( \frac{\partial \mathbf{r}_{\mathcal{S}_i}}{\partial \mathbf{q}_l} \right)^\times & \mathbf{0}_{3 \times 1} \end{bmatrix} \quad (\text{A.25})$$

with the differentiation of  $\mathbf{r}_{\mathcal{S}_i}$  previously detailed to obtain (A.23).

**$\mathbf{J}_{m_i}$  derivatives expression:** The Jacobian matrix  $\mathbf{J}_{m_i}$  (A.8) is differentiated  $\forall l, i \in [1, n_q]$  as:

$$\frac{\partial}{\partial q_l} (\mathbf{J}_{m_i}) = \left[ \frac{\partial}{\partial q_l} (\mathbf{B}_{i1} \mathbf{p}_{m_1}) \quad \dots \quad \frac{\partial}{\partial q_l} (\mathbf{B}_{i(i-1)} \mathbf{p}_{m_{i-1}}) \quad \frac{\partial}{\partial q_l} (\mathbf{p}_{m_i}) \quad \mathbf{0}_{6 \times (n_q - i)} \right] \quad (\text{A.26})$$

First the joint orientation vector,  $\mathbf{k}_k$ , (2.9) is differentiate  $\forall k \in [1, i]$  with (A.20) as:

$$\frac{\partial}{\partial q_l} (\mathbf{k}_k) = \frac{\partial}{\partial q_l} (\mathbf{R}_{\mathcal{A}_i, \mathcal{R}_{ine}}) \begin{bmatrix} 0 \\ 0 \\ 1 \end{bmatrix} \quad (\text{A.27})$$

According to the nature of the joint  $\mathcal{A}_k$  with  $\forall k \in [1, i]$ :

- If  $\mathcal{A}_k$  is prismatic:

$$\frac{\partial}{\partial q_l} (\mathbf{B}_{ik} \mathbf{p}_{m_k}) = \begin{bmatrix} \mathbf{0}_3 \\ \frac{\partial}{\partial q_l} (\mathbf{k}_k) \end{bmatrix} \quad (\text{A.28})$$

- If  $\mathcal{A}_k$  is revolute:

$$\frac{\partial}{\partial q_l} (\mathbf{B}_{ik} \mathbf{p}_{m_k}) = \left[ \begin{array}{c} \frac{\partial}{\partial q_l} \left( (\mathbf{r}_{S_i} - \mathbf{r}_{S_k})^\times \right) \mathbf{k}_k + (\mathbf{r}_{S_i} - \mathbf{r}_{S_k})^\times \frac{\partial}{\partial q_l} (\mathbf{k}_k) + \frac{\partial}{\partial q_l} (\mathbf{k}_k^\times) (\mathbf{r}_{S_i} - \mathbf{r}_{A_k}) + \mathbf{k}_k^\times \frac{\partial}{\partial q_l} ((\mathbf{r}_{S_i} - \mathbf{r}_{A_k})) \end{array} \right] \quad (\text{A.29})$$



# Simple SMS<sup>1</sup> study case

The SMS studied to validate the our proposed tools and control methods is a reduced version of the PULSAR telescope with less DoF<sup>2</sup>s and less elements as one can visualized with figure B.1. In this section, with the help of the urdf file used by the simulation tools detailed in 2.4, the physical properties of the different elements are detailed. Consequently, this section help one to reproduce or develop SMS XML description for an usage of out proposed tools.

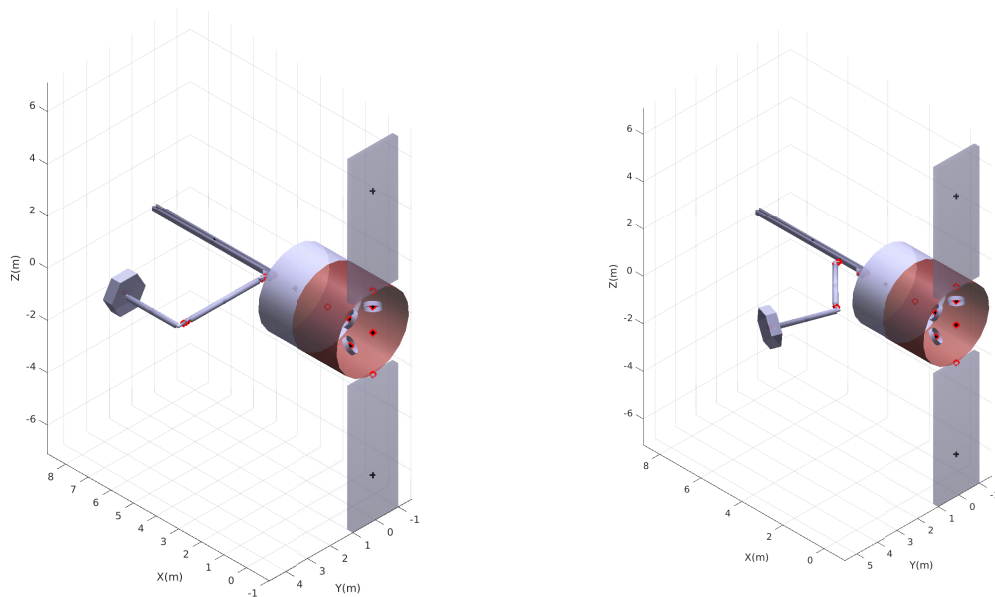


Figure B.1 – Two configurations of the simple SMS used for illustrations

The spacecraft base is a cylinder exhibiting a 1.6m radius and 2m length for a total of 1960kg.

<sup>1</sup>Space Manipulator System

<sup>2</sup>Degree of Freedom

```
<!--Spacecraft-->
<link name="Spacecraft">
  <inertial>
    <origin rpy="0 0 0" xyz="0 0 0"/>
    <mass value="1960"/>
    <inertia ixx="3345" ixy="0" ixz="0" iyy="2202" iyz="0" izz="2202"/>
  </inertial>
  <visual>
    <origin xyz="0.1 0 0" rpy="0 -1.57075 0"/>
    <geometry>
      <cylinder length="2" radius="1.6"/>
    </geometry>
    <material name="Orange"/>
  </visual>
  <stiffness name="rigid"/>
</link>
```

For each body, a parent and a child body are defined with the joint formalism.

```
<!-- Joint to Payload -->
<joint name="Spacecraft_Payload" type="fixed">
  <parent link="Spacecraft"/>
  <child link="Payload"/>
  <origin xyz="1.1 0 0" rpy="0 0 0" />
  <axis xyz="1 0 0"/>
</joint>

<!--Payload-->
<link name="Payload">
  <inertial>
    <origin xyz="1.45 0 0"/>
    <mass value="1440"/>
    <inertia ixx="2458" ixy="0" ixz="0" iyy="1499" iyz="0" izz="1499"/>
  </inertial>
  <visual>
    <origin xyz="0.75 0 0" rpy="0 -1.57075 0"/>
    <geometry>
      <cylinder length="1.5" radius="1.6"/>
    </geometry>
    <material name="Blue"/>
  </visual>
  <stiffness name="rigid"/>
</link>
```

For a flexible element, all the physical properties (dampings, stiffness and natural frequency) are defined additionally to the matrix of the participation factors (L in the XML<sup>3</sup>).

---

<sup>3</sup>eXtensible Markup Language



```

<!-- Joint to Left Solar Panel -->
<joint name="Spacecraft_Left_Panel" type="fixed">
  <parent link="Spacecraft"/>
  <child link="Left_Panel"/>
  <origin xyz="-0.9 0 -1.6" rpy="3.1416 0 0"/>
  <axis xyz="1 0 0"/>
</joint>

<!-- Left Solar Panel-->
<link name="Left_Panel">
  <inertial>
    <origin rpy="0 0 0" xyz="0.001 0.001 3.8447"/>
    <mass value="61"/>
    <inertia ixx="17" ixy="0" ixz="0" iyy="1250" iyz="0" izz="1233"/>
  </inertial>
  <visual>
    <origin rpy="0 0 0" xyz="0 0 2.75"/>
    <geometry>
    <box size="0.25 2 5.5"/>
    </geometry>
    <material name="Blue"/>
  </visual>
  <stiffness name="flexible">
    <mode_number value="5"/>
    <mode_1 pulse="0.16*2*pi" L="-6.4 0 0 0 -35 0" damp="0.005"/>
    <mode_2 pulse="0.70*2*pi" L="0 -6.7 0 35.4 0 0" damp="0.005"/>
    <mode_3 pulse="1.08*2*pi" L="-0.1 -0.1 0 0.3 0 3.8" damp="0.005"/>
    <mode_4 pulse="1.21*2*pi" L="-3.2 0 0 0 -3 -0.01" damp="0.005"/>
    <mode_5 pulse="3.05*2*pi" L="2.3 0 -0.3 0 1.3 0" damp="0.005"/>
  </stiffness>
</link>

```

And similarly for the right panel.

Each reaction-wheel are similar, only the rotating axis differs.

```
<!--joint Spacecraft to Reaction Wheel 1 -->
<joint name="Spacecraft_to_RW1" type="revolute">
  <parent link="Spacecraft" />
  <child link="RW1"/>
  <origin xyz="-0.4 -0.5 0.5" rpy="35.2644*pi/180 pi/4 0" />
  <axis xyz="0 0 1"/>
  <limit effort="1000.0" lower="0" upper="0" velocity="0"/>
</joint>

<!-- Reaction Wheel 1 -->
<link name="RW1" >
  <inertial>
    <origin rpy ="0 0 0" xyz="0 0 0.0" />
    <mass value="4"/>
    <inertia ixx="0.065" ixy="0" ixz="0" iyy="0.065" iyz="0"
      izz="0.1322"/>
  </inertial>
  <visual>
    <origin rpy="0 0 0" xyz="0 0 0"/>
    <geometry>
      <cylinder length="0.16" radius="0.31" />
    </geometry>
    <material name="Grey"/>
  </visual>
  <stiffness name="rigid"/>
</link>
```

Then the detail of the manipulator is given body by body as follow:

```
<!--joint between {parent} and link_0-->
<joint name="Spacecraft_rail_joint" type="fixed">
<origin rpy="-1.57075 0 0" xyz="3.5 0 0"/>
<parent link="Spacecraft"/>
<child link="rail_link_0"/>
</joint>

<link name="rail_link_0">
<inertial>
<origin rpy="0 0 0" xyz="2.65 0 0"/>
<mass value="234.09894105"/>
<inertia ixx="0.001" ixy="0" ixz="0" iyy="0.001" iyz="0" izz="0.001"/>
</inertial>
<visual>
<origin rpy="0 0 0" xyz="0 0 0"/>
<geometry>
<mesh filename="meshes_dISAS/rail/rail_base.dae"/>
</geometry>
<material name="Grey"/>
</visual>
<stiffness name="rigid"/>
</link>
```

```
<!-- joint between link_0 and link_1 -->
<joint name="rail_joint_1" type="prismatic">
<parent link="rail_link_0"/>
<child link="rail_link_1"/>
<origin rpy="0 0 0" xyz="0.15 0 0.15"/>
<axis xyz="1 0 0"/>
</joint>
<link name="rail_link_1">
<inertial>
<origin rpy="0 0 0" xyz="0 0 0"/>
<mass value="15.90105894"/>
<inertia ixx="0.001" ixy="0" ixz="0" iyy="0.001" iyz="0" izz="0.001"/>
</inertial>
<visual>
<origin rpy="0 0 0" xyz="0 0 0"/>
<geometry>
<mesh filename="meshes_dISAS/rail/rail_slot.dae"/>
</geometry>
<material name="Grey"/>
</visual>
<stiffness name="rigid"/>
</link>

<!--joint between {parent} and link_0-->
<joint name="rail_link_1_arm_joint" type="fixed">
<origin rpy="0 0 0" xyz="0 0 0.05"/>
<parent link="rail_link_1"/>
<child link="arm_link_0"/>
</joint>
<link name="arm_link_0">
<inertial>
<origin rpy="0 0 0" xyz="0 0 0.0318"/>
<mass value="7"/>
<inertia ixx="0.01" ixy="0" ixz="0" iyy="0.01" iyz="0" izz="0.08"/>
</inertial>
<visual>
<origin rpy="0 0 0" xyz="0 0 0"/>
<geometry>
<mesh filename="meshes_dISAS/arm/link_0.dae"/>
</geometry>
<material name="Grey"/>
</visual>
<stiffness name="rigid"/>
</link>
```

```
<!-- joint between link_0 and link_1 -->
<joint name="arm_joint_1" type="revolute">
<parent link="arm_link_0"/>
<child link="arm_link_1"/>
<origin rpy="0 0 0" xyz="0 0 0.0635"/>
<axis xyz="0 0 1"/>
</joint>
<link name="arm_link_1">
<inertial>
<origin rpy="0 0 0" xyz="0 0 0.0888"/>
<mass value="7"/>
<inertia ixx="0.021" ixy="0" ixz="0" iyy="0.021" iyz="0" izz="0.01"/>
</inertial>
<visual>
<origin rpy="0 0 0" xyz="0 0 0"/>
<geometry>
<mesh filename="meshes_dISAS/arm/link_1.dae"/>
</geometry>
<material name="Grey"/>
</visual>
<stiffness name="rigid"/>
</link>
```

```
<!-- joint between link_1 and link_2 | 1_T_2 -->
<joint name="arm_joint_2" type="revolute">
<parent link="arm_link_1"/>
<child link="arm_link_2"/>
<origin rpy="-1.57079632679 0 0" xyz="0 0 0.112"/>
<axis xyz="0 0 1"/>
</joint>
<link name="arm_link_2">
<inertial>
<origin rpy="0 0 0" xyz="0 -1.6810 0"/>
<mass value="27"/>
<inertia ixx="51.3" ixy="0" ixz="0" iyy="0.15" iyz="0" izz="51.3"/>
</inertial>
<visual>
<origin rpy="1.57079632679 0 -1.57079632679" xyz="0 0 0"/>
<geometry>
<mesh filename="meshes_dISAS/arm/link_2.dae"/>
</geometry>
<material name="Grey"/>
</visual>
<stiffness name="rigid"/>
</link>
```

```
<!-- joint between link_2 and link_3 | 2_T_3 -->  
<joint name="arm_joint_3" type="revolute">  
<parent link="arm_link_2"/>  
<child link="arm_link_3"/>  
<origin rpy="0 0 3.14159265359" xyz="0 -3.36198 0"/>  
<axis xyz="0 0 1"/>  
</joint>  
<link name="arm_link_3">  
<inertial>  
<origin rpy="0 0 0" xyz="0 0.0237 0"/>  
<mass value="7"/>  
<inertia ixx="0.021" ixy="0" ixz="0" iyy="0.01" iyz="0" izz="0.021"/>  
</inertial>  
<visual>  
<origin rpy="1.57079632679 0 0" xyz="0 0 0"/>  
<geometry>  
<mesh filename="meshes_dISAS/arm/link_3.dae"/>  
</geometry>  
<material name="Grey"/>  
</visual>  
<stiffness name="rigid"/>  
</link>
```

```
<!-- joint between link_3 and link_4 | 3_T_4 -->
<joint name="arm_joint_4" type="revolute">
<parent link="arm_link_3"/>
<child link="arm_link_4"/>
<origin rpy="1.57079632679 0 0" xyz="0 0.1125 0"/>
<axis xyz="0 0 1"/>
</joint>
<link name="arm_link_4">
<inertial>
<origin rpy="0 0 0" xyz="-1.1910 0 -0.2"/>
<mass value="18"/>
<inertia ixx="0.14" ixy="0" ixz="0" iyy="15.7" iyz="0" izz="15.7"/>
</inertial>
<visual>
<origin rpy="0 0 3.14159265359" xyz="0 0 0"/>
<geometry>
<mesh filename="meshes_dISAS/arm/link_4.dae"/>
</geometry>
<material name="Grey"/>
</visual>
<stiffness name="rigid"/>
</link>
```



```
<!-- last joint -->
<joint name="dlsaffe_joint_ee" type="fixed">
<parent link="arm_link_4"/>
<child link="dlsaffe_link_ee"/>
<origin xyz="-2.5 0 -0.13" rpy="0 0 0"/>
</joint>

<link name="dlsaffe_link_ee">
<inertial>
<origin xyz="0 0 0" rpy="0 0 0"/>
<mass value="0"/>
<inertia ixx="0" ixy="0" ixz="0" iyy="0" iyz="0" izz="0" />
</inertial>
<visual>
<origin xyz="0.05 0.05 0.05" rpy="0 0 0"/>
<geometry>
<box size="0.1 0.1 0.1"/>
</geometry>
<material name="Grey"/>
</visual>
<stiffness name="rigid"/>
</link>
```

```
<!-- End-effector Mass -->
<joint name="dlsaffe_joint_ee_tuile" type="fixed">
<parent link="dlsaffe_link_ee"/>
<child link="dlsaffe_link_ee_tuile"/>
<origin xyz="0 0 0" rpy="0 0 0"/>
</joint>

<link name="dlsaffe_link_ee_tuile">
<inertial>
<origin xyz="0 0 0" rpy="0 0 0"/>
<mass value="150"/>
<inertia ixx="6" ixy="0" ixz="0" iyy="6" iyz="0" izz="6" />
</inertial>
<visual>
<origin xyz="0 0 0" rpy="0 -1.570795*2 0"/>
<geometry>
<mesh filename="tile.stl"/>
</geometry>
<material name="Red"/>
</visual>
<stiffness name="rigid"/>
</link>
```



# Bibliography

- [Acq09] Paul Acquatella. “Development of automation & robotics in space exploration”. In: *Proceedings of the AIAA SPACE Conference & Exposition*. Citeseer. 2009, pp. 1–7 (cit. on p. 8).
- [ACT08] Daniel Alazard, Christelle Cumer, and Khalid Tantawi. *Linear dynamic modeling of spacecraft with various flexible appendages and on-board angular momentums*. 2008 (cit. on pp. 17, 19, 20, 31, 60, 64).
- [Agh09a] Farhad Aghili. “Coordination control of a free-flying manipulator and its base attitude to capture and detumble a noncooperative satellite”. In: *2009 IEEE/RSJ International Conference on Intelligent Robots and Systems*. IEEE. 2009, pp. 2365–2372 (cit. on p. 23).
- [Agh09b] Farhad Aghili. “Optimal control of a space manipulator for detumbling of a target satellite”. In: *2009 IEEE international conference on robotics and automation*. IEEE. 2009, pp. 3019–3024 (cit. on pp. 23, 118).
- [Agh20] Farhad Aghili. “Optimal Trajectories and Robot Control for Detumbling a Non-Cooperative Satellite”. In: *Journal of Guidance, Control, and Dynamics* 43.5 (2020), pp. 981–988 (cit. on pp. 23, 118).
- [AL88] Jorge Angeles and Sang Koo Lee. *The formulation of dynamical equations of holonomic mechanical systems using a natural orthogonal complement*. 1988 (cit. on p. 39).
- [Ale+16] Sara Cresto Aleina et al. “Reusable space tug concept and mission”. In: *Acta Astronautica* 128 (2016), pp. 21–32 (cit. on p. 3).
- [Ang+21] Federica Angeletti et al. “End-to-end design of a robust attitude control and vibration suppression system for large space smart structures”. In: *Acta Astronautica* (2021) (cit. on pp. 25, 75).
- [Ata+20] Mohammad Mahdi Ataei et al. “Boundary control design for vibration suppression and attitude control of flexible satellites with multi-section appendages”. In: *Acta Astronautica* 173 (2020), pp. 22–30 (cit. on pp. 25, 75).
- [AVT19] Andrea Antonello, Alfredo Valverde, and Panagiotis Tsiotras. “Dynamics and control of spacecraft manipulators with thrusters and momentum exchange devices”. In: *Journal of Guidance, Control, and Dynamics* 42.1 (2019), pp. 15–29 (cit. on p. 27).
- [AY15] Vladimir S Aslanov and Vadim V Yudinsev. “Dynamics, analytical solutions and choice of parameters for towed space debris with flexible appendages”. In: *Advances in Space Research* 55.2 (2015), pp. 660–667 (cit. on p. 21).
- [Bey+18] Alexander Beyer et al. “Caesar: Space robotics technology for assembly, maintenance, and repair”. In: *Proceedings of the International Astronautical Congress, IAC*. 2018 (cit. on p. 12).

- [BH08] Louis Breger and Jonathan P How. “Safe trajectories for autonomous rendezvous of spacecraft”. In: *Journal of Guidance, Control, and Dynamics* 31.5 (2008), pp. 1478–1489 (cit. on p. 25).
- [BH87] Dae-Sung Bae and Edward J Haug. “A recursive formulation for constrained mechanical system dynamics: Part i. open loop systems”. In: *Journal of Structural Mechanics* 15.3 (1987), pp. 359–382 (cit. on p. 20).
- [Bie+21] Robin Biesbroek et al. “The clearspace-1 mission: Esa and clearspace team up to remove debris”. In: (2021), pp. 1–3 (cit. on pp. 1, 9).
- [Blu+03] William Bluethmann et al. “Robonaut: A robot designed to work with humans in space”. In: *Autonomous robots* 14.2 (2003), pp. 179–197 (cit. on p. 8).
- [Bon18] Christophe Bonnal. “Space debris mitigation & remediation: a general update”. In: *8th JAXA Space Debris Workshop*. 2018 (cit. on pp. 9, 10).
- [Bos+04] Albert B Bosse et al. “SUMO: spacecraft for the universal modification of orbits”. In: *Spacecraft Platforms and Infrastructure*. Vol. 5419. International Society for Optics and Photonics. 2004, pp. 36–46 (cit. on p. 11).
- [Bra+13] Vitali Braun et al. “Active debris removal of multiple priority targets”. In: *Advances in Space Research* 51.9 (2013), pp. 1638–1648 (cit. on p. 9).
- [Bru+10] Siciliano Bruno et al. *Robotics: modelling, planning and control*. 2010 (cit. on p. 17).
- [BS02] Jerzy K Baksalary and George PH Styan. “Generalized inverses of partitioned matrices in Banachiewicz–Schur form”. In: *Linear algebra and its applications* 354.1-3 (2002), pp. 41–47 (cit. on p. 83).
- [Cao+20] Yuteng Cao et al. “Thermal alternation induced vibration analysis of spacecraft with lateral solar arrays in orbit”. In: *Applied Mathematical Modelling* 86 (2020), pp. 166–184 (cit. on pp. 26, 74, 118).
- [Cas11] Marco M Castronuovo. “Active space debris removal: A preliminary mission analysis and design”. In: *Acta Astronautica* 69.9-10 (2011), pp. 848–859 (cit. on p. 9).
- [CC12] ZhongYi Chu and Jing Cui. “Vibration control of maneuvering spacecraft with flexible manipulator using adaptive disturbance rejection filter and command shaping technology”. In: *2012 Sixth International Conference on Internet Computing for Science and Engineering*. IEEE. 2012, pp. 97–101 (cit. on pp. 26, 75).
- [CCS12] ZhongYi Chu, Jing Cui, and FuChun Sun. “Fuzzy adaptive disturbance-observer-based robust tracking control of electrically driven free-floating space manipulator”. In: *IEEE Systems Journal* 8.2 (2012), pp. 343–352 (cit. on pp. 27, 75).
- [Che+00] Wen-Hua Chen et al. “A nonlinear disturbance observer for robotic manipulators”. In: *IEEE Transactions on industrial Electronics* 47.4 (2000), pp. 932–938 (cit. on pp. 124, 125).

- [CLG20] Davide Calzolari, Roberto Lampariello, and Alessandro Massimo Giordano. *Singularity maps of space robots and their application to gradient-based trajectory planning*. 2020 (cit. on p. 85).
- [CLNP17] Olga-Orsalia Christidi-Loumpasefski, Kostas Nanos, and Evangelos Papadopoulos. “On parameter estimation of space manipulator systems using the angular momentum conservation”. In: *2017 IEEE International Conference on Robotics and Automation (ICRA)*. IEEE. 2017, pp. 5453–5458 (cit. on p. 31).
- [Col+18] Pablo Colmenarejo et al. “Methods and outcomes of the COMRADE project-Design of robust Combined control for robotic spacecraft and manipulator in servicing missions: comparison between between Hinf and nonlinear Lyapunov-based approaches”. In: *69th International Astronautical Congress (IAC)*. 2018 (cit. on pp. 3, 119).
- [Col+20] Pablo Colmenarejo et al. “Results of the COMRADE project: combined control for robotic spacecraft and manipulator in servicing missions: active debris removal and re-fuelling”. In: *11th International ESA Conference on Guidance, Navigation & Control Systems*. 2020 (cit. on pp. 10, 23, 26, 75, 76).
- [Cra00] Roy Craig Jr. “Coupling of substructures for dynamic analyses-an overview”. In: *41st structures, structural dynamics, and materials conference and exhibit*. 2000, p. 1573 (cit. on p. 49).
- [CUFA20] Alexander D Crain, Steve Ulrich, and Angel Flores-Abad. “Compliant Spacecraft Capture via a Nonlinear Disturbance Observer-based Impedance Controller”. In: *AIAA Scitech 2020 Forum*. 2020, p. 2079 (cit. on p. 23).
- [Cum+21] Christelle Cumer et al. “MODELLING AND ATTITUDE CONTROL DESIGN FOR AUTONOMOUS IN-ORBIT ASSEMBLY”. In: *ESA GNC 2021*. 2021 (cit. on pp. 65, 76).
- [CYL17] Xibin Cao, Chengfei Yue, and Ming Liu. “Flexible satellite attitude maneuver via constrained torque distribution and active vibration suppression”. In: *Aerospace Science and Technology* 67 (2017), pp. 387–397 (cit. on p. 25).
- [DC14] Qiu-huang Dong and Li Chen. “Impact dynamics analysis of free-floating space manipulator capturing satellite on orbit and robust adaptive compound control algorithm design for suppressing motion”. In: *Applied Mathematics and Mechanics* 35.4 (2014), pp. 413–422 (cit. on p. 118).
- [Did+01] F Didot et al. “The era system: Control architecture and performance results”. In: *Proc. 6th International Symposium on Artificial Intelligence, Robotics and Automation in Space (i-SAIRAS), Montral, Canada*. Citeseer. 2001 (cit. on p. 7).
- [Dif+12] MA Diftler et al. “Robonaut 2—Initial activities on-board the ISS”. In: *2012 IEEE Aerospace Conference*. IEEE. 2012, pp. 1–12 (cit. on p. 8).
- [Dok72] MA Dokainish. *A new approach for plate vibrations: combination of transfer matrix and finite-element technique*. 1972 (cit. on pp. 20, 32, 48).

- [DP93] Steven Dubowsky and Evangelos Papadopoulos. “The kinematics, dynamics, and control of free-flying and free-floating space robotic systems”. In: *IEEE Transactions on robotics and automation* 9.5 (1993), pp. 531–543 (cit. on p. 14).
- [DT91] Steven Dubowsky and Miguel A Torres. “Path planning for space manipulators to minimize spacecraft attitude disturbances”. In: *Proceedings of IEEE International Conference on Robotics and Automation*. Vol. 3. Citeseer. 1991, pp. 2522–2528 (cit. on p. 21).
- [Dub+15] Vincent Dubanchet et al. “Motion planning and control of a space robot to capture a tumbling debris”. In: *Advances in Aerospace Guidance, Navigation and Control*. Springer, 2015, pp. 699–717 (cit. on pp. 23, 118).
- [DY04] Dimitar Nikolaev Dimitrov and Kazuya Yoshida. “Momentum distribution in a space manipulator for facilitating the post-impact control”. In: *2004 IEEE/RSJ international conference on intelligent robots and systems (IROS)(IEEE Cat. No. 04CH37566)*. Vol. 4. IEEE. 2004, pp. 3345–3350 (cit. on p. 22).
- [Ell19] Alex Ellery. “Tutorial review on space manipulators for space debris mitigation”. In: *Robotics* 8.2 (2019), p. 34 (cit. on p. 10).
- [Est+20] Stéphane Estable et al. “Capturing and deorbiting Envisat with an Airbus Spacetug. Results from the ESA e. Deorbit consolidation phase study”. In: *Journal of Space Safety Engineering* 7.1 (2020), pp. 52–66 (cit. on pp. 2, 10).
- [FA+14] Angel Flores-Abad et al. “A review of space robotics technologies for on-orbit servicing”. In: *Progress in aerospace sciences* 68 (2014), pp. 1–26 (cit. on pp. 2, 12, 16–19, 31, 74, 119).
- [FA+20] Angel Flores-Abad et al. “Compliant Force Sensor-less Capture of an Object in Orbit”. In: *IEEE Transactions on Aerospace and Electronic Systems* (2020) (cit. on p. 23).
- [Fau+22] Martin Fauré et al. “ $AH_\infty$  Control Solution for Space Debris Removal Missions Using Robotic Arms: The ESA e. Deorbit Case”. In: *13th UKACC International Conference on Control*. IEEE. 2022 (cit. on p. 23).
- [Fos+95] Carlton L Foster et al. “Solar-array-induced disturbance of the Hubble space telescope pointing system”. In: *Journal of Spacecraft and Rockets* 32.4 (1995), pp. 634–644 (cit. on pp. 19, 25).
- [Fri08] Robert B Friend. “Orbital express program summary and mission overview”. In: *Sensors and Systems for space applications II*. Vol. 6958. International Society for Optics and Photonics. 2008, p. 695803 (cit. on p. 11).
- [FTST06] Tatiana de FPA Taveira, Adriano AG Siqueira, and H Terra. “Adaptive non-linear  $H_\infty$  controllers applied to a free-floating space manipulator”. In: *2006 IEEE Conference on Computer Aided Control System Design, 2006 IEEE International Conference on Control Applications, 2006 IEEE International Symposium on Intelligent Control*. IEEE. 2006, pp. 1476–1481 (cit. on pp. 26, 75, 118).

- [GCAS18] Alessandro M Giordano, Davide Calzolari, and Alin Albu-Schäffer. “Workspace fixation for free-floating space robot operations”. In: *2018 IEEE International Conference on Robotics and Automation (ICRA)*. IEEE. 2018, pp. 889–896 (cit. on pp. 22, 23, 76).
- [Gef+15] Gardell Gefke et al. “Advances in robotic servicing technology development”. In: *AIAA Space 2015 Conference and Exposition*. 2015, p. 4426 (cit. on p. 12).
- [GGAS17] Alessandro M Giordano, Gianluca Garofalo, and Alin Albu-Schäffer. “Momentum dumping for space robots”. In: *2017 IEEE 56th Annual Conference on Decision and Control (CDC)*. IEEE. 2017, pp. 5243–5248 (cit. on pp. 22, 23).
- [Gil+04] R Gillett et al. “A hybrid range imaging system solution for in-flight space shuttle inspection”. In: *Canadian Conference on Electrical and Computer Engineering 2004 (IEEE Cat. No. 04CH37513)*. Vol. 4. IEEE. 2004, pp. 2147–2150 (cit. on p. 12).
- [Gio+16] Alessandro M Giordano et al. “Dynamics and control of a free-floating space robot in presence of nonzero linear and angular momenta”. In: *2016 IEEE 55th Conference on Decision and Control (CDC)*. IEEE. 2016, pp. 7527–7534 (cit. on p. 22).
- [Gio+20] Alessandro M Giordano et al. “Coordination of thrusters, reaction wheels, and arm in orbital robots”. In: *Robotics and Autonomous Systems* 131 (2020), p. 103564 (cit. on pp. 27, 76).
- [Gio+21] Alessandro M Giordano et al. “Compliant floating-base control of space robots”. In: *IEEE Robotics and Automation Letters* 6.4 (2021), pp. 7485–7492 (cit. on p. 169).
- [GLR19] Rabindra A Gangapersaud, Guangjun Liu, and Anton HJ de Ruiter. “Detumbling a non-cooperative space target with model uncertainties using a space manipulator”. In: *Journal of Guidance, Control, and Dynamics* 42.4 (2019), pp. 910–918 (cit. on pp. 23, 118).
- [GOAS19] Alessandro Massimo Giordano, Christian Ott, and Alin Albu-Schäffer. “Coordinated Control of Spacecraft’s Attitude and End-Effector for Space Robots”. In: *IEEE Robotics and Automation Letters* 4.2 (2019), pp. 2108–2115 (cit. on pp. 22, 76).
- [GR10] Alain Girard and Nicolas Roy. *Structural dynamics in industry*. Vol. 7. John Wiley & Sons, 2010 (cit. on pp. 48, 49).
- [Guo+20] Chaoyong Guo et al. “Active control technology for flexible solar array disturbance suppression”. In: *Aerospace Science and Technology* 106 (2020), p. 106148 (cit. on pp. 25, 75).
- [Guy+14] Nicolas Guy et al. “Dynamic modeling and analysis of spacecraft with variable tilt of flexible appendages”. In: *Journal of Dynamic Systems, Measurement, and Control* 136.2 (2014), p. 021020 (cit. on p. 20).



- [HAS19] David Henry, Finn Ankersen, and Luigi Strippoli. “A Class of Unknown Input Observers Under  $H_\infty$  Performance for Fault Diagnosis: Application to the Mars Sample Return Mission”. In: *New Trends in Observer-based Control*. Elsevier, 2019, pp. 225–266 (cit. on p. 20).
- [Hen14] Carl Glen Henshaw. “The darpa phoenix spacecraft servicing program: Overview and plans for risk reduction”. In: *International Symposium on Artificial Intelligence, Robotics and Automation in Space (i-SAIRAS)*. 2014 (cit. on p. 13).
- [Hen+16] David Henry et al. “Model-based FDIR and fault accommodation for a rendezvous mission around the Mars planet: the Mars sample return case”. In: *IFAC-PapersOnLine* 49.5 (2016), pp. 266–271 (cit. on p. 20).
- [Hen+21] David Henry et al. “A 6-DOF sliding mode fault tolerant control solution for in-orbit autonomous rendezvous”. In: *Aerospace Science and Technology* 118 (2021), p. 107050 (cit. on p. 20).
- [HGY19] Wei Hu, Yulong Gao, and Bintang Yang. “Semi-active vibration control of two flexible plates using an innovative joint mechanism”. In: *Mechanical Systems and Signal Processing* 130 (2019), pp. 565–584 (cit. on p. 75).
- [Hil+01] Michael Hiltz et al. *Canadarm: 20 years of mission success through adaptation*. 2001 (cit. on pp. 1, 6).
- [Hin75] Robert Morris Hintz. “Analytical methods in component modal synthesis”. In: *AIAA Journal* 13.8 (1975), pp. 1007–1016 (cit. on p. 20).
- [Hir+13] Daichi Hirano et al. “Vibration suppression control of a space robot with flexible appendage based on simple dynamic model”. In: *2013 IEEE/RSJ International Conference on Intelligent Robots and Systems*. IEEE. 2013, pp. 789–794 (cit. on pp. 3, 20, 25, 32, 75).
- [Hir+14] Daichi Hirano et al. “Simultaneous control for end-point motion and vibration suppression of a space robot based on simple dynamic model”. In: *2014 IEEE International Conference on Robotics and Automation (ICRA)*. IEEE. 2014, pp. 6631–6637 (cit. on p. 75).
- [Hir+94] Gerd Hirzinger et al. “ROTEX-the first remotely controlled robot in space”. In: *Proceedings of the 1994 IEEE international conference on robotics and automation*. IEEE. 1994, pp. 2604–2611 (cit. on p. 13).
- [HLF94] Gerd Hirzinger, Klaus Landzettel, and Ch Fagerer. “Telerobotics with large time delays-the ROTEX experience”. In: *Proceedings of IEEE/RSJ International Conference on Intelligent Robots and Systems (IROS'94)*. Vol. 1. IEEE. 1994, pp. 571–578 (cit. on p. 14).
- [HM05] Qinglei Hu and Guangfu Ma. “Vibration suppression of flexible spacecraft during attitude maneuvers”. In: *Journal of guidance, control, and dynamics* 28.2 (2005), pp. 377–380 (cit. on pp. 25, 75).
- [HW18] Jingchen Hu and Tianshu Wang. “Minimum base attitude disturbance planning for a space robot during target capture”. In: *Journal of Mechanisms and Robotics* 10.5 (2018), p. 051002 (cit. on pp. 24, 74, 118).

- [HZ16] Quan Hu and Jingrui Zhang. “Attitude control and vibration suppression for flexible spacecraft using control moment gyroscopes”. In: *Journal of Aerospace Engineering* 29.1 (2016), p. 04015027 (cit. on pp. 25, 75).
- [Imb79] Jean-François Imbert. *Analyse des structures par éléments finis*. 1979 (cit. on p. 20).
- [Jan+15] Marko Jankovic et al. “Robotic System for Active Debris Removal: Requirements, State-of-the-art and Concept Architecture of the Rendezvous and Capture (RVC) Control System”. In: *5th CEAS Air & Space Conference Proceedings. CEAS, Delft, the Netherlands*. 2015 (cit. on p. 9).
- [Jia+17] Shiyuan Jia et al. “Maneuver and active vibration suppression of free-flying space robot”. In: *IEEE Transactions on Aerospace and Electronic systems* 54.3 (2017), pp. 1115–1134 (cit. on pp. 26, 75).
- [Jin+17] Ming-He Jin et al. “Reaction torque control of redundant free-floating space robot”. In: *International Journal of Automation and Computing* 14.3 (2017), pp. 295–306 (cit. on p. 22).
- [JL21] Haoran Ji and Dongxu Li. “A novel nonlinear finite element method for structural dynamic modeling of spacecraft under large deformation”. In: *Thin-Walled Structures* 165 (2021), p. 107926 (cit. on pp. 20, 32).
- [KCP78] Donald J Kessler and Burton G Cour-Palais. “Collision frequency of artificial satellites: The creation of a debris belt”. In: *Journal of Geophysical Research: Space Physics* 83.A6 (1978), pp. 2637–2646 (cit. on p. 8).
- [KH88] Sung-Soo Kim and Edward J Haug. “A recursive formulation for flexible multi-body dynamics, Part I: open-loop systems”. In: *Computer Methods in Applied Mechanics and Engineering* 71.3 (1988), pp. 293–314 (cit. on p. 20).
- [KK86] Wisama Khalil and J Kleinfinger. “A new geometric notation for open and closed-loop robots”. In: *Proceedings. 1986 IEEE International Conference on Robotics and Automation*. Vol. 3. IEEE. 1986, pp. 1174–1179 (cit. on p. 33).
- [Kra+21a] Sofiane Kraïem et al. “Control of rotation-floating space robots with flexible appendages for on-orbit servicing”. In: *2021 European Control Conference (ECC)*. IEEE. 2021, pp. 249–254 (cit. on p. 116).
- [Kra+21b] Sofiane Kraïem et al. “Robust control of rotation-floating space robots with flexible appendages for on-orbit servicing”. In: *IFAC-PapersOnLine* 54.20 (2021), pp. 134–140 (cit. on p. 116).
- [Kug+17] Justin Kugler et al. “Applications for the archinaut in space manufacturing and assembly capability”. In: *AIAA SPACE and Astronautics Forum and Exposition*. 2017, p. 5365 (cit. on p. 12).
- [Kum+15] Kartik Kumar et al. “Agora: Mission to demonstrate technologies to actively remove Ariane rocket bodies”. In: *Proceedings of the International Astronautical Congress, Jerusalem, Israel*. Vol. 6. 2015, p. 6 (cit. on p. 9).

- [KY97] Ralf Koeppel and Tsueno Yoshikawa. “Dynamic manipulability analysis of compliant motion”. In: *Proceedings of the 1997 IEEE/RSJ International Conference on Intelligent Robot and Systems. Innovative Robotics for Real-World Applications. IROS’97*. Vol. 3. IEEE. 1997, pp. 1472–1478 (cit. on p. 85).
- [Lam10] Roberto Lampariello. “Motion planning for the on-orbit grasping of a non-cooperative target satellite with collision avoidance”. In: *i-SAIRAS 2010* (2010) (cit. on p. 25).
- [Lar+02] Patten Laryssa et al. “International space station robotics: a comparative study of ERA, JEMRMS and MSS”. In: *7th ESA Workshop on Advanced Space Technologies for Robotics and Automation*. 2002, pp. 19–21 (cit. on p. 89).
- [Lew+12] Hugh G Lewis et al. “Synergy of debris mitigation and removal”. In: *Acta Astronautica* 81.1 (2012), pp. 62–68 (cit. on p. 9).
- [Li+19a] Ke Li et al. “Assembly dynamics of a large space modular satellite antenna”. In: *Mechanism and Machine Theory* 142 (2019), p. 103601 (cit. on pp. 12, 74).
- [Li+19b] Wei-Jie Li et al. “On-orbit service (OOS) of spacecraft: A review of engineering developments”. In: *Progress in Aerospace Sciences* 108 (2019), pp. 32–120 (cit. on pp. 10, 12, 14, 74, 75).
- [Lik72] Peter W Likins. “Finite element appendage equations for hybrid coordinate dynamic analysis”. In: *International Journal of Solids and Structures* 8.5 (1972), pp. 709–731 (cit. on pp. 20, 48).
- [Liu+18] Yu Liu et al. “Modeling and observer-based vibration control of a flexible spacecraft with external disturbances”. In: *IEEE Transactions on Industrial Electronics* 66.11 (2018), pp. 8648–8658 (cit. on pp. 20, 32).
- [LLW13] Zhenyu Li, Hong Liu, and Bin Wang. “Motion planning and coordination control of space robot using methods of calculated momentum”. In: *2013 IEEE International Conference on Robotics and Biomimetics (ROBIO)*. IEEE. 2013, pp. 1151–1156 (cit. on p. 27).
- [LLZ87] Richard W Longman, Robert E Lindbergt, and Michael F Zedd. “Satellite-mounted robot manipulators—New kinematics and reaction moment compensation”. In: *The International Journal of Robotics Research* 6.3 (1987), pp. 87–103 (cit. on p. 21).
- [LLZ93] Robert E Lindberg, Richard W Longman, and Michael F Zedd. “Kinematic and dynamic properties of an elbow manipulator mounted on a satellite”. In: *Space Robotics: Dynamics and Control*. Springer, 1993, pp. 1–25 (cit. on p. 16).
- [Lof04] Johan Lofberg. “YALMIP: A toolbox for modeling and optimization in MATLAB”. In: *IEEE international conference on robotics and automation (IEEE Cat. No. 04CH37508)*. IEEE. 2004, pp. 284–289 (cit. on pp. 106, 140).
- [Lon90] Richard W Longman. “The kinetics and workspace of a satellite-mounted robot”. In: *The Journal of the Astronautical Sciences* 38.4 (1990), pp. 423–440 (cit. on p. 17).

- [LP60] F Leckie and E Pestel. “Transfer-matrix fundamentals”. In: *International Journal of Mechanical Sciences* 2.3 (1960), pp. 137–167 (cit. on pp. 20, 32).
- [Luo+18] Jianjun Luo et al. “Robust inertia-free attitude takeover control of postcapture combined spacecraft with guaranteed prescribed performance”. In: *ISA transactions* 74 (2018), pp. 28–44 (cit. on p. 118).
- [LXB97] Bin Liang, Yangsheng Xu, and Marcel Bergerman. “Dynamically equivalent manipulator for space manipulator system. 1”. In: 4 (1997), pp. 2765–2770 (cit. on pp. 18, 31).
- [LXB98] Bin Liang, Yangsheng Xu, and Marcel Bergerman. *Mapping a space manipulator to a dynamically equivalent manipulator*. 1998 (cit. on p. 18).
- [LY20] Jiayuan Lu and Haitao Yang. “Trajectory Planning of Satellite Base Attitude Disturbance Optimization for Space Robot”. In: *2020 3rd International Conference on Control and Robots (ICCR)*. IEEE. 2020, pp. 85–89 (cit. on pp. 24, 74).
- [Lyn+07] Craig Lyn et al. “Computer vision systems for robotic servicing of the Hubble Space Telescope”. In: *AIAA SPACE 2007 Conference & Exposition*. 2007, p. 6259 (cit. on p. 6).
- [Mel+15] Pamela Melroy et al. “DARPA phoenix satlets: Progress towards satellite cellularization”. In: *AIAA SPACE 2015 Conference and Exposition*. 2015, p. 4487 (cit. on p. 13).
- [Men+17] Deshan Meng et al. “Space robots with flexible appendages: dynamic modeling, coupling measurement, and vibration suppression”. In: *Journal of Sound and Vibration* 396 (2017), pp. 30–50 (cit. on pp. 3, 20, 26, 74, 75).
- [Men+18] Deshan Meng et al. “Vibration suppression control of free-floating space robots with flexible appendages for autonomous target capturing”. In: *Acta Astronautica* 151 (2018), pp. 904–918 (cit. on pp. 3, 21, 26, 75).
- [MK19] C Priyant Mark and Surekha Kamath. “Review of active space debris removal methods”. In: *Space Policy* 47 (2019), pp. 194–206 (cit. on p. 9).
- [MM07] Juan Ignacio Mulero-Martinez. “Uniform bounds of the coriolis/centripetal matrix of serial robot manipulators”. In: *IEEE Transactions on Robotics* 23.5 (2007), pp. 1083–1089 (cit. on p. 131).
- [Moh+13] Alireza Mohammadi et al. “Nonlinear disturbance observer design for robotic manipulators”. In: *Control Engineering Practice* 21.3 (2013), pp. 253–267 (cit. on pp. 124, 125, 128).
- [MP98] S Ali A Moosavian and Evangelos Papadopoulos. “On the kinematics of multiple manipulator space free-flyers and their computation”. In: *Journal of Robotic Systems* 15.4 (1998), pp. 207–216 (cit. on p. 19).
- [Nen+99] Dragomir N Nenchev et al. “Reaction null-space control of flexible structure mounted manipulator systems”. In: *IEEE Transactions on Robotics and Automation* 15.6 (1999), pp. 1011–1023 (cit. on pp. 18, 21, 74).

- [NHS11] Thai-Chau Nguyen-Huynh and Inna Sharf. “Adaptive reactionless motion for space manipulator when capturing an unknown tumbling target”. In: *2011 IEEE international conference on robotics and automation*. IEEE. 2011, pp. 4202–4207 (cit. on pp. 23, 118).
- [NM90] Yoshihiko Nakamura and Ranjan Mukherjee. “Nonholonomic path planning of space robots via bi-directional approach”. In: *Proceedings., IEEE International Conference on Robotics and Automation*. IEEE. 1990, pp. 1764–1769 (cit. on pp. 17, 18, 83).
- [NP11] Kostas Nanos and Evangelos Papadopoulos. “On the use of free-floating space robots in the presence of angular momentum”. In: *Intelligent Service Robotics* 4.1 (2011), pp. 3–15 (cit. on p. 22).
- [NP15] Kostas Nanos and Evangelos Papadopoulos. “Avoiding dynamic singularities in Cartesian motions of free-floating manipulators”. In: *IEEE Transactions on Aerospace and Electronic Systems* 51.3 (2015), pp. 2305–2318 (cit. on pp. 24, 84).
- [NP17] Kostas Nanos and Evangelos G Papadopoulos. “On the dynamics and control of free-floating space manipulator systems in the presence of angular momentum”. In: *Frontiers in Robotics and AI* 4 (2017), p. 26 (cit. on p. 22).
- [NUY92] Dragomir Nenchev, Yoji Umetani, and Kazuya Yoshida. “Analysis of a redundant free-flying spacecraft/manipulator system”. In: *IEEE Transactions on Robotics and Automation* 8.1 (1992), pp. 1–6 (cit. on p. 84).
- [NY00] Yoshihiko Nakamura and Katsu Yamane. “Dynamics computation of structure-varying kinematic chains and its application to human figures”. In: *IEEE Transactions on Robotics and Automation* 16.2 (2000), pp. 124–134 (cit. on p. 19).
- [NY06] Hiroki Nakanishi and Kazuya Yoshida. “Impedance control for free-flying space robots-basic equations and applications”. In: *2006 IEEE/RSJ international conference on intelligent robots and systems*. IEEE. 2006, pp. 3137–3142 (cit. on pp. 22, 23, 74, 118).
- [NYU96] DN Nenchev, K Yoshida, and Masaru Uchiyama. “Reaction null-space based control of flexible structure mounted manipulator systems”. In: *Proceedings of 35th IEEE Conference on Decision and Control*. Vol. 4. IEEE. 1996, pp. 4118–4123 (cit. on pp. 21, 88).
- [Oda00] Mitsushige Oda. “Experiences and lessons learned from the ETS-VII robot satellite”. In: *Proceedings 2000 ICRA. Millennium Conference. IEEE International Conference on Robotics and Automation. Symposia Proceedings (Cat. No. 00CH37065)*. Vol. 1. IEEE. 2000, pp. 914–919 (cit. on pp. 1, 9).
- [ONY10] Tomohisa Oki, Hiroki Nakanishi, and Kazuya Yoshida. “Time-optimal manipulator control for management of angular momentum distribution during the capture of a tumbling target”. In: *Advanced Robotics* 24.3 (2010), pp. 441–466 (cit. on p. 87).

- [PA06] C Pittet and D Arzelier. “Demeter: A benchmark for robust analysis and control of the attitude of flexible micro satellites”. In: *IFAC Proceedings Volumes* 39.9 (2006), pp. 661–666 (cit. on p. 88).
- [Pap+21] Evangelos Papadopoulos et al. “Robotic manipulation and capture in space: A survey”. In: *Frontiers in Robotics and AI* (2021), p. 228 (cit. on p. 169).
- [Pap92] Evangelos G Papadopoulos. “Path Planning For Space Manipulators Exhibiting Nonholonomic Behavior.” In: *IROS*. 1992, pp. 669–675 (cit. on p. 24).
- [Par+93] Osman Parlaktuna et al. “Jacobian control for space manipulator”. In: *Robotics and autonomous systems* 11.1 (1993), pp. 35–44 (cit. on p. 21).
- [Pas87] Madeleine Pascal. “Dynamics analysis of a system of hinge-connected flexible bodies”. In: *Celestial mechanics* 41.1 (1987), pp. 253–274 (cit. on p. 20).
- [PD93] Evangelos Papadopoulos and Steven Dubowsky. *Dynamic singularities in free-floating space manipulators*. 1993 (cit. on pp. 17, 84).
- [Pen02] Luis F Penin. “Teleoperation with time delay-a survey and its use in space robotics”. In: *Technical Report of National Aerospace Laboratory* (2002) (cit. on pp. 1, 14).
- [PG15] A Pisculli and P Gasbarri. “A minimum state multibody/FEM approach for modeling flexible orbiting space systems”. In: *Acta Astronautica* 110 (2015), pp. 324–340 (cit. on p. 74).
- [PJ18] Danielle Piskorz and Karen L Jones. “On-orbit assembly of space assets: A path to affordable and adaptable space infrastructure”. In: *The Aerospace Corporation* (2018) (cit. on pp. 12, 13).
- [PMK12] Antoine Petit, Eric Marchand, and Keyvan Kanani. “Tracking complex targets for space rendezvous and debris removal applications”. In: *2012 IEEE/RSJ International Conference on Intelligent Robots and Systems*. IEEE. 2012, pp. 4483–4488 (cit. on p. 2).
- [PO04] Osman Parlaktuna and Metin Ozkan. “Adaptive control of free-floating space manipulators using dynamically equivalent manipulator model”. In: *Robotics and Autonomous Systems* 46.3 (2004), pp. 185–193 (cit. on p. 21).
- [PTN05] Evangelos Papadopoulos, Ioannis Tortopidis, and Kostas Nanos. “Smooth planning for free-floating space robots using polynomials”. In: *Proceedings of the 2005 IEEE International Conference on Robotics and Automation*. IEEE. 2005, pp. 4272–4277 (cit. on pp. 24, 74).
- [QWY19] Jianzhong Qiao, Hao Wu, and Xiang Yu. “High-precision attitude tracking control of space manipulator system under multiple disturbances”. In: *IEEE Transactions on Systems, Man, and Cybernetics: Systems* (2019) (cit. on pp. 26, 75, 118).
- [Rei+11] D Reintsema et al. “DEOS-the in-flight technology demonstration of german’s robotics approach to dispose malfunctioned satellites”. In: *ESA 11th Symposium on Advanced Space Technologies in Robotics and Automation, ESTEC, Netherlands*. 2011 (cit. on p. 10).

- [RGL18] Wolfgang Rackl, Jens Gerstmann, and Roberto Lampariello. “Analysis of liquid fuel sloshing on free-floating robot dynamics under low-gravity condition”. In: *2018 IEEE Aerospace Conference*. IEEE. 2018, pp. 1–12 (cit. on pp. 26, 75).
- [RKS19] Mathieu Rognant, Sofiane Kraiem, and Jurek Sasiadek. “Kinematic Indices of rotation-floating space robots for on-orbit servicing”. In: *IFTToMM World Congress on Mechanism and Machine Science*. Springer. 2019, pp. 3107–3116 (cit. on p. 82).
- [Rog+19] Mathieu Rognant et al. “Autonomous assembly of large structures in space: a technology review”. In: *EUCASS 2019*. 2019 (cit. on pp. 12, 82, 133).
- [RSS16] Tomasz Rybus, Karol Seweryn, and Jurek Z Sasiadek. “Trajectory optimization of space manipulator with non-zero angular momentum during orbital capture maneuver”. In: *AIAA Guidance, Navigation, and Control Conference*. 2016, p. 0885 (cit. on p. 3).
- [RSS17] Tomasz Rybus, Karol Seweryn, and Jurek Z Sasiadek. “Control system for free-floating space manipulator based on nonlinear model predictive control (NMPC)”. In: *Journal of Intelligent & Robotic Systems* 85.3-4 (2017), pp. 491–509 (cit. on pp. 3, 24, 74).
- [RTD11] CR Rocha, CP Tonetto, and Altamir Dias. “A comparison between the Denavit–Hartenberg and the screw-based methods used in kinematic modeling of robot manipulators”. In: *Robotics and Computer-Integrated Manufacturing* 27.4 (2011), pp. 723–728 (cit. on p. 33).
- [RZZ14] Xiaoting Rui, Jianshu Zhang, and Qinbo Zhou. “Automatic deduction theorem of overall transfer equation of multibody system”. In: *Advances in Mechanical Engineering* 6 (2014), p. 378047 (cit. on pp. 20, 32).
- [SA08] Moussa Sylla and Botouoni Asseke. “Dynamics of a rotating flexible and symmetric spacecraft using impedance matrix in terms of the flexible appendages cantilever modes”. In: *Multibody System Dynamics* 19.4 (2008), pp. 345–364 (cit. on pp. 20, 32).
- [Sak99] Yoshiyuki Sakawa. “Trajectory planning of a free-flying robot by using the optimal control”. In: *Optimal Control Applications and Methods* 20.5 (1999), pp. 235–248 (cit. on p. 22).
- [Sal+05] Christian Sallaberger et al. “Robotic technologies for space exploration at MDA”. In: *The 8th International Symposium on Artificial Intelligence, Robotics and Automation in Space. Munich*. 2005 (cit. on p. 6).
- [San+18] Francesco Sanfedino et al. “Finite element based N-Port model for preliminary design of multibody systems”. In: *Journal of Sound and Vibration* 415 (2018), pp. 128–146 (cit. on pp. 20, 32, 48, 49).
- [SB08] Karol Seweryn and Marek Banaszekiewicz. “Optimization of the trajectory of a general free-flying manipulator during the rendezvous maneuver”. In: *AIAA Guidance, Navigation and Control Conference and Exhibit*. 2008, p. 7273 (cit. on p. 21).

- [SGG16] Minghe Shan, Jian Guo, and Eberhard Gill. “Review and comparison of active space debris capturing and removal methods”. In: *Progress in Aerospace Sciences* 80 (2016), pp. 18–32 (cit. on p. 9).
- [SGM20] Angelo Stolfi, Paolo Gasbarri, and Arun K Misra. “A two-arm flexible space manipulator system for post-grasping manipulation operations of a passive target object”. In: *Acta Astronautica* 175 (2020), pp. 66–78 (cit. on p. 169).
- [SGS18] A Stolfi, P Gasbarri, and M Sabatini. “A parametric analysis of a controlled deployable space manipulator for capturing a non-cooperative flexible satellite”. In: *Acta Astronautica* 148 (2018), pp. 317–326 (cit. on p. 169).
- [Sha+21] Xiangyu Shao et al. “Nonsingular terminal sliding mode control for free-floating space manipulator with disturbance”. In: *Acta Astronautica* 181 (2021), pp. 396–404 (cit. on p. 24).
- [Sic+09] Bruno Siciliano et al. “Mobile robots”. In: *Robotics: Modelling, Planning and Control* (2009), pp. 469–521 (cit. on p. 17).
- [SKK16] Lingling Shi, Jayantha Katupitiya, and Nathan Kinkaid. “A robust attitude controller for a spacecraft equipped with a robotic manipulator”. In: *2016 American Control Conference (ACC)*. IEEE. 2016, pp. 4966–4971 (cit. on p. 27).
- [SS19] Asma Seddaoui and Chakravarthini M Saaj. “Combined nonlinear  $H_\infty$  controller for a controlled-floating space robot”. In: *Journal of Guidance, Control, and Dynamics* 42.8 (2019), pp. 1878–1885 (cit. on pp. 24, 118).
- [Sta+01] Peter J Staritz et al. “Skyworker: a robot for assembly, inspection and maintenance of large scale orbital facilities”. In: *Proceedings 2001 ICRA. IEEE International Conference on Robotics and Automation (Cat. No. 01CH37164)*. Vol. 4. IEEE. 2001, pp. 4180–4185 (cit. on p. 12).
- [SW01] Naoki Sato and Yasufumi Wakabayashi. “JEMRMS design features and topics from testing”. In: *6th International symposium on artificial intelligence, robotics and automation in space (iSAIRAS), Quebec*. Vol. 214. 2001 (cit. on p. 8).
- [Tat98] Joseph N Tatarewicz. “The hubble space telescope servicing mission”. In: *From engineering science to big science: The NACA and NASA Collier Trophy research project winners* (1998), p. 365 (cit. on pp. 1, 10).
- [UY87] Yoji Umetani and Kazuya Yoshida. “Continuous path control of space manipulators mounted on OMV”. In: *Acta Astronautica* 15.12 (1987), pp. 981–986 (cit. on p. 21).
- [UY89] Yoji Umetani and Kazuya Yoshida. “Resolved motion rate control of space manipulators with generalized Jacobian matrix”. In: *IEEE Transactions on robotics and automation* 5.3 (1989), pp. 303–314 (cit. on pp. 14, 18, 21, 31).
- [VD87] Z Vafa and Steven Dubowsky. “On the dynamics of manipulators in space using the virtual manipulator approach”. In: 4 (1987), pp. 579–585 (cit. on pp. 17, 18, 31).



- [VL+16] Josep Virgili-Llop et al. “Spacecraft robotics toolkit: an open-source simulator for spacecraft robotic arm dynamic modeling and control”. In: *6th International Conference on Astrodynamics Tools and Techniques*. 2016 (cit. on pp. 31, 40, 57).
- [VL+18] Josep Virgili-Llop et al. *SPART: an open-source modeling and control toolkit for mobile-base robotic multibody systems with kinematic tree topologies*. <https://github.com/NPS-SRL/SPART>. 2018 (cit. on p. 58).
- [Wan+18a] Mingming Wang et al. “Detumbling strategy and coordination control of kinematically redundant space robot after capturing a tumbling target”. In: *Non-linear Dynamics* 92.3 (2018), pp. 1023–1043 (cit. on p. 23).
- [Wan+18b] Mingming Wang et al. “Optimal trajectory planning of free-floating space manipulator using differential evolution algorithm”. In: *Advances in Space Research* 61.6 (2018), pp. 1525–1536 (cit. on p. 24).
- [Wil+18] Markus Wilde et al. “Equations of motion of free-floating spacecraft-manipulator systems: an engineer’s tutorial”. In: *Frontiers in Robotics and AI* 5 (2018), p. 41 (cit. on pp. 3, 14–16, 31, 41, 44, 47, 60, 61, 82).
- [Wit07] Jens Wittenburg. *Dynamics of multibody systems*. Springer Science & Business Media, 2007 (cit. on p. 16).
- [Wu+18a] Hao Wu et al. “Robust Anti-Disturbance Coordination Control for Space Manipulator Systems with Multiple Disturbances”. In: *2018 37th Chinese Control Conference (CCC)*. IEEE. 2018, pp. 2601–2606 (cit. on p. 3).
- [Wu+18b] Yunhua Wu et al. “Attitude control for on-orbit servicing spacecraft using hybrid actuator”. In: *Advances in Space Research* 61.6 (2018), pp. 1600–1616 (cit. on pp. 27, 76).
- [XK12] Yangsheng Xu and Takeo Kanade. *Space robotics: dynamics and control*. Vol. 188. Springer Science & Business Media, 2012 (cit. on p. 16).
- [XLW20] Ruonan Xu, Jianjun Luo, and Mingming Wang. “Kinematic and dynamic manipulability analysis for free-floating space robots with closed chain constraints”. In: *Robotics and Autonomous Systems* 130 (2020), p. 103548 (cit. on p. 85).
- [Xu+13] Shuanfeng Xu et al. “Adaptive reactionless motion control for free-floating space manipulators with uncertain kinematics and dynamics”. In: *IFAC Proceedings Volumes* 46.20 (2013), pp. 646–653 (cit. on p. 21).
- [Xu+14] Wenfu Xu et al. “Dynamics modeling and analysis of a flexible-base space robot for capturing large flexible spacecraft”. In: *Multibody System Dynamics* 32.3 (2014), pp. 357–401 (cit. on p. 20).
- [Xu+16] Wenfu Xu et al. “Hybrid modeling and analysis method for dynamic coupling of space robots”. In: *IEEE Transactions on Aerospace and Electronic Systems* 52.1 (2016), pp. 85–98 (cit. on p. 86).
- [Xu+94] Yangsheng Xu et al. “Control system of the self-mobile space manipulator”. In: *IEEE Transactions on Control Systems Technology* 2.3 (1994), pp. 207–219 (cit. on p. 12).

- [Yan+19] Guocai Yang et al. “A robust and adaptive control method for flexible-joint manipulator capturing a tumbling satellite”. In: *IEEE Access* 7 (2019), pp. 159971–159985 (cit. on pp. 24, 74).
- [YDH19] Xin Ye, Zheng-Hong Dong, and Jia-Cai Hong. “Research on Adaptive Reaction Null Space Planning and Control Strategy Based on VFF–RLS and SSADE–ELM Algorithm for Free-Floating Space Robot”. In: *Electronics* 8.10 (2019), p. 1111 (cit. on pp. 24, 74).
- [YGC19] Zhang-Wei Yu, Ming-Zhou Gao, and Guo-Ping Cai. “Active control of a 6-DOF space robot with flexible panels using singular perturbation method”. In: *The Journal of the Astronautical Sciences* 66.1 (2019), pp. 83–99 (cit. on p. 26).
- [Yos+04] Kazuya Yoshida et al. “Dynamics, control and impedance matching for robotic capture of a non-cooperative satellite”. In: *advanced robotics* 18.2 (2004), pp. 175–198 (cit. on pp. 23, 118).
- [Yos84] Tsuneo Yoshikawa. “Analysys and control of robot manipulators with redundancy. Robotic Research”. In: *The First International Symposium, 1984* (1984), pp. 735–747 (cit. on p. 85).
- [Yos85] Tsuneo Yoshikawa. “Dynamic manipulability of robot manipulators”. In: *Transactions of the Society of Instrument and Control Engineers* 21.9 (1985), pp. 970–975 (cit. on p. 85).
- [Yu+16] Jie-xin Yu et al. “Element-by-element model updating of large-scale structures based on component mode synthesis method”. In: *Journal of Sound and Vibration* 362 (2016), pp. 72–84 (cit. on p. 20).
- [ZCG17] Chenxing Zhong, Zhiyong Chen, and Yu Guo. “Attitude control for flexible spacecraft with disturbance rejection”. In: *IEEE Transactions on Aerospace and Electronic Systems* 53.1 (2017), pp. 101–110 (cit. on p. 19).
- [ZFY08] Chu Zhongyi, Sun Fuchun, and Cui Jing. “Disturbance observer-based robust control of free-floating space manipulators”. In: *IEEE Systems journal* 2.1 (2008), pp. 114–119 (cit. on pp. 26, 75).
- [Zha+15] Fuhai Zhang et al. “Robust adaptive control of a free-floating space robot system in Cartesian space”. In: *International Journal of Advanced Robotic Systems* 12.11 (2015), p. 157 (cit. on pp. 26, 118).
- [Zha+17] Bo Zhang et al. “Coordinated stabilization for space robot after capturing a noncooperative target with large inertia”. In: *Acta Astronautica* 134 (2017), pp. 75–84 (cit. on p. 22).
- [Zha+20] Qi Zhang et al. “Pre-impact Trajectory Planning of Nonredundant Free-Floating Space Manipulator”. In: *2020 5th International Conference on Automation, Control and Robotics Engineering (CACRE)*. IEEE. 2020, pp. 58–65 (cit. on pp. 24, 118).
- [ZLW19] Yiqun Zhou, Jianjun Luo, and Mingming Wang. “Dynamic coupling analysis of multi-arm space robot”. In: *Acta Astronautica* 160 (2019), pp. 583–593 (cit. on p. 22).

- 
- [ZLW20] PengYuan Zhao, JinGuo Liu, and ChenChen Wu. “Survey on research and development of on-orbit active debris removal methods”. In: *Science China Technological Sciences* 63.11 (2020), pp. 2188–2210 (cit. on p. 1).
- [ZM10] Payam Zarafshan and S Ali A Moosavian. “Manipulation control of a space robot with flexible solar panels”. In: *2010 IEEE/ASME International Conference on Advanced Intelligent Mechatronics*. IEEE. 2010, pp. 1099–1104 (cit. on p. 19).
- [ZMP16] Payam Zarafshan, S Ali A Moosavian, and Evangelos G Papadopoulos. “Adaptive hybrid suppression control of space free-flying robots with flexible appendages.” In: *Robotica* 34.7 (2016), pp. 1464–1485 (cit. on p. 75).
- [ZZZ17] Zhi-Gang Zhou, Yong-An Zhang, and Di Zhou. “Robust prescribed performance tracking control for free-floating space manipulators with kinematic and dynamic uncertainty”. In: *Aerospace Science and Technology* 71 (2017), pp. 568–579 (cit. on p. 27).

